Experimental and Theoretical Studies of Ultrasound Computed Tomography

by

J R Jago, BSc, MSc

Thesis submitted in part fulfilment of the requirements
for the Degree of Doctor of Philosophy in the Faculty
of Medicine, University of Newcastle upon Tyne

September 1993

ABSTRACT

The poor lateral resolution and qualitative nature of conventional real-time B-scanning has prompted interest in techniques in which a wide aperture is synthesised by measuring ultrasound over 180 or 360 degrees. This thesis investigates one group of such techniques known as Ultrasound Computed Tomography (UCT).

After a brief introduction to conventional ultrasound imaging and the principles of Computed Tomography, a comprehensive review of the literature on UCT is presented. Consideration is made of the assumptions and limitations inherent in these techniques and the consequences for their practical application. It is concluded that combined reflection and transmission UCT offers the best promise for the realisation of high quality images of soft tissue.

The potential resolution of conventional B-scanning is compared, theoretically, with that of UCT by consideration of point spread functions derived from linear imaging models. The assumptions required for the derivation of these models, and the consequences for other aspects of image quality of their failure, are explored in detail.

The design and construction is described of a prototype system to perform reflection UCT using a commercial linear array rotated in a water bath. Results are presented of studies on phantoms and on soft tissues. The limitations of this system are analyzed, and ways of improving the images, with consequences for the development of another system, discussed.

The use of acoustic speed images, obtained from transmission UCT, to compensate for artifacts in the equivalent reflection UCT images is explored theoretically. The design and construction of a system for combined reflection and transmission UCT imaging, again based on linear arrays, is described. Results are presented of acoustic speed images, and of acoustic speed compensation of reflection images, of phantoms and in-vitro targets.

Using conclusions drawn from the two systems already investigated, suggestions are made for the design of an optimum clinically acceptable system for UCT imaging of suitably accessible soft tissues such as the breast.

ACKNOWLEDGEMENTS

I would like to thank the many members of the Northern Regional Medical Physics Department who have assisted and encouraged me in this work. In particular I would like to thank my supervisor Dr TA Whittingham for his support and guidance, Mr E Horsefield for the mechanical construction of both UCT systems and other equipment, Dr P Lowe for advice on the design of the UCT systems, and Mr J Panchen, Mr I Palmer, Mr J Wallace and Mr G Mitchell for their assistance in the construction of some of the electronics.

Many thanks also to Paul Rutherford, Lionel Whitham and Frank Burns at Batwatch for reproducing the grey scale images.

I am pleased to acknowledge that part of this work was supported by a grant from the Regional Research Committee of the Northern Regional Health Authority.

Finally I would especially like to thank my wife, Jill, without whose continual support and encouragement this thesis would not have been completed.

CONTENTS

1 Background and Aims

1.1 Introduction

The work described in this thesis involves a theoretical and practical investigation into the use of ultrasonic imaging techniques which have developed from the established concepts of Computed Tomography. Ultrasound is defined as sound waves whose frequency is greater than the human audio range of about 20 to 20,000 Hertz. In medical imaging the frequencies normally used are in the range 1MHz to 10MHz, although more recent applications (such as intra-luminal imaging and the imaging of the skin) may use higher frequencies of up to 50MHz. Since it was first used in the 1950's in cardiology, ultrasound has found increasingly widespread applications in the medical field, both for diagnosis and treatment. Ultrasound is now routinely used in obstetrics, paediatrics, cardiology, the abdomen, the breast, the eye and virtually the entire vascular system. The main reasons for the success of ultrasound as a diagnostic tool are: (1) it is generally considered to be safe for the patient and operator - to date there has been no confirmed evidence of harmful effects from ultrasound at diagnostic power levels, (2) the equipment is relatively cheap when compared to some other diagnostic imaging modalities - depending on the application, prices range from a few thousand pounds to about one hundred thousand, (3) ultrasound can provide information about both structure and function. Examples are real-time B-scanning for imaging of the texture and structure of organs, M-mode scanning for the visualisation of rapidly moving structures such as the heart valves, Colour Doppler Imaging for qualitative mapping of blood flow, and continuous-wave and pulsed Doppler for quantitative measurements of blood flow. This thesis is concerned solely with imaging, the most widely used technique of which is known as real-time B-scanning.

In general the use of ultrasound is limited to soft tissues not obscured by gas or bone. Real-time B-scanning also has some additional limitations of its own, essentially relating to the quality of the images produced and the degree of operator interaction required (see 1.2). As a result ultrasound has probably still not realised its full potential for medical imaging. The possibility of developing new techniques or improving existing ones which will overcome some of these limitations is the main justification for this work. It may thus be possible to solve some of the clinical problems which have already been identified, such as the need for more quantitative information for improved characterisation of tissues and better resolution for earlier detection of tumours, and also to generate new clinical applications not yet realised.

One class of techniques which shows considerable theoretical promise is that of Ultrasound Computerised Tomography (UCT), and the study of these techniques forms the subject of this thesis. Strictly speaking, the term Ultrasound Computed Tomography refers to any technique in which ultrasonic information is used to generate a single slice, or tomogram, of a target using computational methods. Conventional real-time B-scan imaging, which is inherently tomographic, is therefore encompassed by this general definition. In the context of this thesis, ultrasound CT refers only to those techniques in which ultrasonic information is acquired over a large range of directions about a constant centre of rotation.

This first chapter offers a brief introduction to the conventional methods of ultrasonic imaging mentioned above, and a discussion of their principles and limitations. This is followed by an introduction to the techniques of UCT, and a general statement of the aims of this study.

1.2 Conventional ultrasonic imaging

The most widely used technique for imaging is the real-time pulse-echo B-scan mode. In this mode ultrasonic pulses are transmitted into the subject by a transducer in direct contact (via coupling gel) with the skin. The returning echoes arising from reflections at interfaces between regions of different acoustic impedance, and from backscatter from small inhomogeneities in acoustic impedance, are subsequently received by the same transducer. A commonly used form of transducer is the real-time linear array shown in Figure 1.1. A linear array is made up of multiple transmit/receive transducer elements which are pulsed, in groups, in a predefined sequence. Each group of elements generates an individual echo-train (called a scan line) corresponding to reflections within a region having the width of the ultrasound beam. The amplitude of the demodulated echoes (ie their envelope) as a function of time (which is interpreted as depth since the acoustic speed is assumed to be constant) are displayed for the many adjacent scan lines to form a two-dimensional slice of the internal structure. In linear array B-scanning the scan

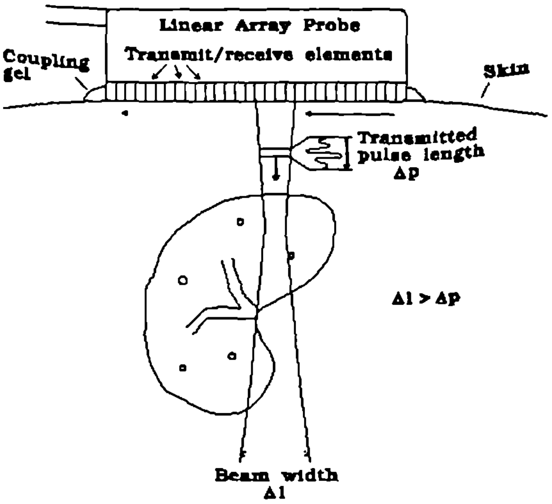

Figure 1.1 Principles of conventional real-time B-scanning

lines are parallel. Hence B-scan images are intrinsically tomographic without the need for additional computer processing. The operator can move the transducer to obtain different slices though the tissue, or hold the transducer stationary to obtain sequential images in real-time and hence display moving structures.

However, in addition to its many attractive features conventional pulse-echo B-scanning possesses the following limitations:-

a. The interactive nature of the scanning procedure requires that the operator should be sufficiently experienced to both produce the images and to interpret them at the time of the scan.

b. The images have poor resolution, in comparison with those from X-ray devices for example. In particular, image resolution lateral to the scanning direction is limited by the ultrasound beam width (typically 3 to 4 mm for a 3 MHz probe). Axial resolution, limited by the length of the ultrasound pulse (typically 1 mm at 3 MHz), is much better.

c. The images possess significant artifacts. For example:
    i. Many interfaces between tissues behave as specular reflectors of ultrasound, and can be properly visualised only when they are perpendicular to the scanning beam.
    ii. The images possess a spatially random noise component known as speckle, due to the partially-coherent nature of the imaging process, which can obscure small details.
    iii. The ultrasound beam is assumed to propagate in a straight line at constant speed. In practice any changes in acoustic speed between different tissues will lead to image degradation and reduced resolution.

d. The images describe the structure of tissue interfaces and indicate the texture of tissues but do not directly yield quantitative information about bulk tissue.

These limitations have restricted the range of applications available to ultrasonic imaging. The lack of quantitative information about tissue characteristics, and the artifactual appearance of ultrasonic images sometimes make it difficult to be totally objective about clinical findings. Consequently operators require long training in order to gain an acceptable level of confidence. The resolution of ultrasonic imaging at the frequencies generally used in the abdomen and breast (3 to 5 MHz) is not sufficient to unambiguously resolve small lesions or calcifications (of less than 2 to 3 mm diameter). These factors have generally made ultrasonic imaging unsuitable as a mass screening modality for the early detection of cancer, particularly in the breast where acoustic speed related artifacts are most troublesome.

1.3 Compound scanning

Many of the limitations of real-time B-scanning discussed above arise because measurements of backscattered ultrasound are obtained only over a relatively narrow angle defined by the size of the receiving aperture. The use of a limited aperture restricts both the potential resolution of the imaging technique and, in the case of specularly reflecting interfaces, the ability to visualise the interface at all. A technique which allows backscatter measurements to be obtained over an effectively much greater angle (and equivalently a wider aperture) has been around from the early days of ultrasonic imaging, and is known as compound scanning. This is a method in which a single element transducer is used to manually scan the target region from a large number of directions in the same scan plane (Figure 1.2), a technique now referred to as "static" B-scanning.

A large range of view directions is achieved by both rocking the transducer and moving it across the skin surface, the spatial position and angle of the transducer being monitored at all times by the scanner hardware. The scan line echo data from each direction is added to form a compound image, using the positional information to define the direction and position of each scan line on the image plane. Since all targets within the object are viewed from multiple directions, specularly reflecting interfaces are more fully visualised. Speckle is also reduced because the echoes obtained from different directions possess largely independent speckle information which is summed incoherently, thus tending to "average out" the contributions due to speckle.

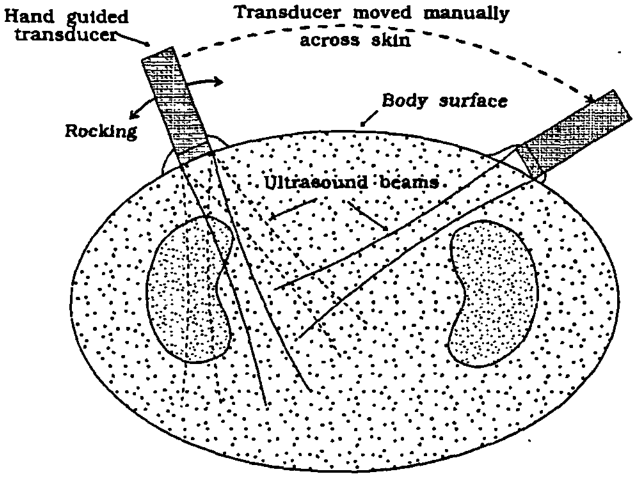

Figure 1.2 Principles of compound scanning

One major disadvantage of compounding is that the potential for real-time imaging is lost. Also many of the limitations of all B-mode scanning techniques still hold. For example, artifacts arising due to any departures from the assumption of a constant speed of sound are likely to be more prominent in compound scans than in conventional B-scans. This is because echoes arising from any particular point in the target will traverse many different regions of the target before reaching the receiver, and will not superimpose correctly if the acoustic speed is variable. In addition, any movement of the patient during the relatively long time required to perform the scan will also result in mis-registration of echoes. These factors together mean that the improvement in resolution that might occur from compounding is frequently not achieved in practice.

1.4 Ultrasound computed tomography

Many approaches to ultrasound CT have been developed over the past twenty years, but most of them may be grouped into three categories depending on the type of measurements made and the assumptions used to reconstruct the images. These techniques will be discussed in detail in Chapter 3, but are introduced briefly here.

The requirement, common to all ultrasound CT techniques, for an ultrasonic transducer to rotate freely about the object (ideally through 360 degrees) in a water-bath, obviously restricts the techniques to the imaging of superficial or easily accessible targets such as the breast in particular, but also potentially the neck, scrotum, limbs, neonate and infant. Most of the in-vivo work to date has concentrated on imaging of the female breast, in view of the lack of bone or gas barriers to ultrasound and its potential for breast cancer screening.

1.4.1 Reflection-mode ultrasound computed tomography

A scanning technique closely related to manual compound scanning is one in which the transducer is rotated automatically around the target, in a water-bath, and about a constant centre of rotation. All the advantages of compound scanning are preserved, while in addition the individual lines of backscattered echo data bear a simple geometric relationship to each other and computer processing may therefore be applied efficiently. Furthermore the automatic nature of the scanning procedure means that it is independent of the operator and allows retrospective reporting of scans. It was first noted by Johnson and co-workers (Johnson et al 1977), and later by others, that this procedure for acquiring ultrasonic backscatter (or reflectivity) data is similar to the procedure used in X-ray computed tomography for acquiring X-ray attenuation data. Consequently it was realised that similar processing algorithms might be used to reconstruct the ultrasonic data into a high quality image, and this technique came to be known as reflection-mode ultrasound computed tomography (or reflection-mode UCT).

1.4.2 Transmission-mode ultrasound computed *tomography*

Another technique which applies the principles of CT to ultrasonic imaging was already established when reflection UCT was first proposed. As the name implies, transmission-mode UCT is involved with measurements of ultrasonic pulses which have been transmitted through an object and as such is more directly analogous to X-ray CT than is reflection UCT. Interest in the technique arose from the desire for more quantitative information about bulk tissue than was available from pulse-echo imaging.

In transmission-mode UCT two transducers are required, one to transmit the ultrasonic pulses and another on the opposite side of the object to receive them. Measurements on the transmitted pulses are made at many lateral positions with respect to the object by laterally translating both transducers in unison, thus forming one projection. Many projections are obtained at angular increments by rotating the whole scanning gantry around the object. There are essentially two kinds of measurement that can be made on these pulses. One possibility is to compare the amplitude of the pulses when they leave the transmitter to their amplitude when they are received, and then use CT methods (e.g. Greenleaf *et al*, 1974) to reconstruct an image representing the distribution of ultrasonic attenuation coefficient. The other possibility is to measure the time it takes for the pulses to travel between the transmitter and receiver. These time-of-flight (TOF) measurements can then be used (e.g. Greenleaf *et al*, 1975) to reconstruct an image of acoustic speed distribution within the object.

1.4.3 *Diffraction tomography*

The simplifying assumptions inherent in conventional UCT techniques, in particular the neglect of diffraction effects, result in the images possessing considerably poorer resolution than the theoretical diffraction limit. In an effort to achieve the ultimate 'diffraction limited' resolution some workers (e.g. Mueller et al, 1978) have attempted to model more accurately the physical mechanisms of image formation. They generally start by solving approximately the wave-equation for an acoustic wave in a medium of varying compressibility, density, or both. Most methods assume that the object is insonated with continuous plane waves, the scattered waves being detected by a transducer scanning a plane located beyond the object. An image is reconstructed by measuring the phase and amplitude of the scattered waves at each point on the receiver plane for many frequencies and/or directions of insonification, and inverting the equations to solve for the spatially varying acoustic parameters. From these parameters acoustic speed and attenuation distributions can usually be derived. These methods have come to be known as Diffraction Tomography or Inverse Scattering Tomography.

1.5 Aims

Although much research has been carried out concerning the application of computed tomography techniques to ultrasonic imaging, this research has not had a large impact on clinical scanning and it was felt that further effort was justified to realise the full potential of the techniques. Consequently this work has been undertaken to study, both in theory and by experiment, these techniques with a view to developing practical systems based on relatively simple and cheap equipment. The main aims of this research can therefore be summarised as follows:-

1) To perform a comprehensive review of the literature on all methods of ultrasound computed tomography.

2) To carry out a theoretical comparison of the methods which appear to offer the most potential for high quality imaging of soft tissue. This comparison should consider the assumptions required for the validity of the methods, the practical limitations imposed by the assumptions, and the consequences of failure of the assumptions for image quality.

3) To develop practical systems to investigate further the UCT methods described previously.

4) To report the results of these investigations from images of phantoms, in-vitro tissues and in-vivo subjects, and discuss any advantages of the UCT techniques over conventional scanning techniques as well as any limitations.

2 Principles of Computed Tomography

2.1 Introduction

Although this thesis is not the place for a comprehensive description of the techniques of Computed Tomography, in order to understand the principles of ultrasound CT and its limitations an overview of the essential aspects of CT in its more familiar application with X-rays is required. For more in-depth discussion into CT and more rigorous mathematical proofs, see for example Gordon and Herman (1974).

Tomographic imaging may be described as a procedure which produces 2-dimensional images of some 3-dimensional quantity from sets of 1-dimensional measurements. Computed Tomography, being the application of computers to tomographic reconstruction, is a relatively recent development. The basic principles of tomographic imaging have been known for a considerable time, with some of the earliest implementations, dating back to the early 1920s, relying on photographic methods of reconstruction. These early methods suffered from several limitations. A particularly severe one was that the desired image slice always suffered some contamination from adjacent slices. With the development of digital computers "true" tomographic imaging became possible, and the technique soon found application in many diverse areas including electron microscopy, radio astronomy, and medical imaging. The first commercial X-ray CT scanner became available in 1971, and X-ray CT has since become a valuable diagnostic tool.

2.2 Geometry and data acquisition

As suggested in the previous section, an ideal tomogram is simply an image of a thin (ideally infinitely thin) slice through an object, where no information from out of the plane of the slice is included in the image. In X-ray CT, a tomogram is produced by using a narrow beam of X-rays to irradiate a thin slice of an object from many directions in the plane of the slice. The simplest arrangement for X-ray CT (Figure 2.1) involves a single finely collimated X-ray source on one side of the object, and a collimated detector on the other side which measures the X-ray intensity transmitted through the object. Assuming that the X-ray beam is infinitely thin and travels in a straight line between the source and the detector (a valid assumption for X-rays within the body), then the intensity $I_\phi(u)$, measured at position u, is related to the intensity $I_\phi^0(u)$ at the source by the equation

$$I_\phi(u) \quad = \quad I_\phi^0(u) \;.\; \exp\left[-\int_A^B \mu(x',y')\; dv'\right]$$

where μ(x,y) is the two-dimensional distribution of linear attenuation coefficient within the object, and x= ucosϕ - vsinϕ, y = usinϕ + vcosϕ. Hence I_ϕ(u) represents the *line-integral* of the attenuation coefficient along the path AB. The source-detector pair is stepped linearly across the target, and measurements of X-ray intensity are recorded at each position u. The set of these measurements is one *projection* p_ϕ, defined by the equation

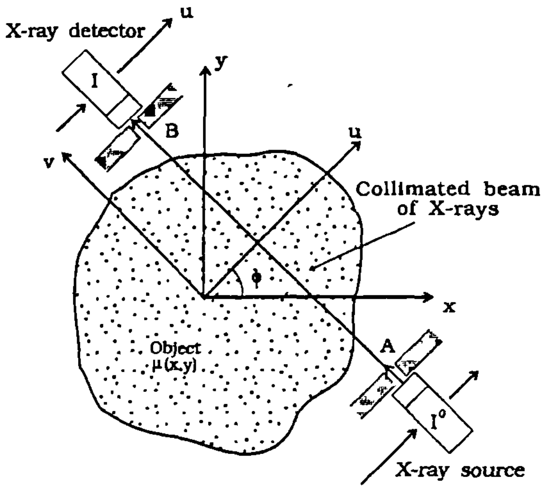

Figure 2.1 Geometry of X-ray CT

$$p_\phi(u) \quad = \quad -\ln\left[\frac{I_\phi(u)}{I_\phi^0(u)}\right] \quad = \quad \int_A^B \mu(x',y')dv' \qquad (2.1)$$

This equation can be written

$$p_\phi(u) \quad = \quad \int_{-\infty}^{\infty}\int_{-\infty}^{\infty} \mu(x',y')\, f(u-u',v-v')\; du'\; dv'$$

where f(u,v) is a two-dimensional function, representing a uniform, infinitesimally thin line along the u = u′ direction which picks out the path AB given by u′ = xcosϕ + ysinϕ.

$$ie \quad f(u,v) \quad = \quad A \;.\; \delta(u)$$

where A is a constant and δ is the Dirac-delta function. Dropping the constant A, equation (2.1) can be recognised as a 2-dimensional convolution between the object distribution μ(x,y) and the function δ(u) which picks out values of μ(x,y) along the set of lines given by u = xcosϕ + ysinϕ.

$$p_\phi(u) \quad = \quad \int_{-\infty}^{\infty}\int_{-\infty}^{\infty} \mu(x',y')\; \delta(x\cos\phi \;+\; y\sin\phi \;-\; u')\; du'\; dv'$$

or

$$p_\phi(u) \quad = \quad \mu(x,y) \ * \ * \ \delta(u) \qquad (2.2)$$

where ** denotes a 2-dimensional convolution.

Many projections at different angles ϕ are acquired by rotating the gantry around the target, until projections have been acquired over at least 180 degrees. Equation (2.2) expresses the linear relationship between the target function $\mu(x,y)$ and the measured projection data p_ϕ. The reconstruction problem is to unscramble the projection information, ie to invert equation (2.1), and present the solutions as quantitative values of attenuation coefficient for each element (or pixel) in a two-dimensional array. This array of pixels is then the reconstructed image of the object slice.

2.3 Image reconstruction from projections

An analytical solution to the reconstruction problem was originally discovered in 1917 by Radon. Equation (2.2) expressed in a slightly different form is often known as Radon's transform. He proved that any two-dimensional object can be reconstructed uniquely from an infinite set of its projections (for details of the solution see Herman and Rowland, 1973). The practical problems associated with applying Radon's analytical solution directly are that (i) only a finite number of projections can be measured, (ii) real measurements are not exact line-integrals since they are contaminated by the beam width, scatter, electronic noise, etc, and (iii) Radon's analytical formula does not generate an efficient algorithm for implementation on a computer.

Various algorithms for the reconstruction of an object from its projections have been developed which are more amenable to implementation on a computer. These methods can be divided into essentially three distinct groups; Fourier domain methods, transform methods and iterative methods.

2.3.1 Fourier domain methods

The first practical use of a Fourier domain solution to the reconstruction problem was reported by De Rosier and Klug (1968), who obtained 3-D reconstructions of bacteria from 2-D electron micrographs. A good mathematical description of the method has been given by Crowther et al (1970).

The basis of the method is the so called *central section theorem*. This states that the 1-D Fourier Transform of a projection of an object, obtained at an angle ϕ, is identical to a line at an angle ϕ through the origin of the 2-D Fourier Transform of the object. To appreciate this, consider a projection $p_0(u)$ obtained at an angle $\phi = 0$ (ie u = x, v = y),

$$ie \quad p_0(x) = \int_{-\infty}^{\infty}\int_{-\infty}^{\infty} \mu(x',y')\, \delta(x-x')\, dx'\, dy'$$

$$\therefore \quad p_0(x) = \int_{-\infty}^{\infty} \mu(x,y')\, dy' \tag{2.3}$$

The 1-D Fourier Transform of the projection is given by

$$P_0(X) = \int_{-\infty}^{\infty} p_0(x) \exp(-i2\pi Xx)\, dx$$

where X is the spatial frequency component equivalent to x. Hence from (2.3)

$$P_0(X) = \int_{-\infty}^{\infty}\int_{-\infty}^{\infty} \mu(x,y) \exp(-i2\pi Xx)\, dx\, dy \tag{2.4}$$

The 2-D Fourier Transform of the object distribution (in this case X-ray attenuation coefficients) is

$$M(X,Y) = \int_{-\infty}^{\infty}\int_{-\infty}^{\infty} \mu(x,y) \exp[-i2\pi(Xx + Yy)]\, dx\, dy$$

Comparing this equation to (2.4) it can be seen that $P_0(\omega_x)$ is equivalent to a line Y = 0 through the origin of M(X,Y), ie along the X-axis.

$$ie \quad P_0(X) = M(X,0)$$

Expressed in polar co-ordinates with the radial frequency component R, we have at $\phi = 0$

$$P_0(R) = M(R,0)$$

This result can be generalised for a projection at any angle ϕ, since the choice of reference axes is arbitrary

$$ie \quad P_\phi(R) = M(R,\phi) \tag{2.5}$$

This is shown graphically in Figure 2.2. Clearly, given an infinite set of projections covering angles of ϕ from 0 to 180 degrees, the 2-D Fourier Transform $M(R,\phi)$ of the object function will be completely determined for all (R,ϕ), the object itself then being given exactly by its inverse *polar* Fourier Transform $\mu(r,\phi)$. In practice only a finite set of noisy projections will be available and $M(R,\phi)$, and hence $\mu(r,\phi)$, will not be obtained exactly. Moreover the maximum frequency content in the image will be limited by the finite width *w* of the X-ray beam (ie the width of the X-ray detector) to some value R_{max},

$$\text{ie} \quad M(R,\phi) = 0 \quad \text{for} \quad |R| > R_{max}$$

where $R_{max} = 1/w$

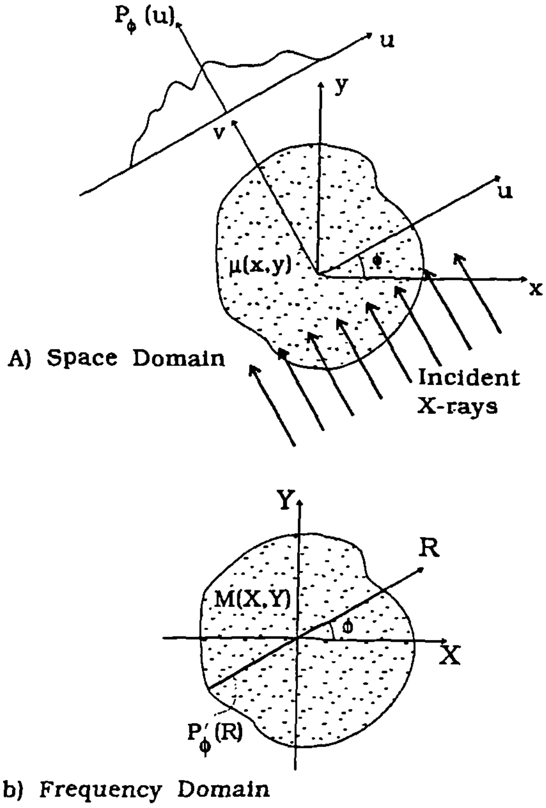

A) Space Domain

b) Frequency Domain

Figure 2.2 Principles of central-section theorem

Sampling theory then dictates that only a finite set of projections is required to completely determine the image to a limited resolution (of *w*/2). The sampling requirements for CT will be dealt with further in section 2.4.

There remains a problem with the practical implementation of the Fourier method. Polar co-ordinate Fourier Transforms are extremely time consuming compared to the fast algorithms which have been developed for cartesian co-ordinate transforms. It would also be preferable to obtain values of the object function $\mu(x,y)$ in cartesian co-ordinates, for example for display purposes. Hence values for $M(X,Y)$ must be interpolated from the values of $M(R,\phi)$. Much research effort has been directed towards finding efficient algorithms to perform this interpolation (see for example Crowther et al, 1970), but generally the algorithms which introduce minimal errors into the reconstruction also require considerable computation time.

2.3.2 Transform methods

These methods are an attempt to approximate a discrete version of the inverse Radon transform. There are two possible approaches which are essentially equivalent but differ in their implementation.

Back-projection with post-filtering

This is probably the easiest reconstruction method to understand, and consequently was one of the first to be applied (Kuhl DE and Edwards RQ, 1963). In this method, also known as the 'summation method', the value of $\mu(x,y)$ at any point (x,y) is estimated by summing all the line-integrals of the rays that have passed through that point in the object. Alternatively, one can imagine each projection being 'dragged' across the image matrix in the same direction along which the projection was obtained. This is shown in Figure 2.3 for four projections of two point targets. The back-projection operation may be expressed mathematically by

$$\mu_B(x,y) = \int_0^{\pi} p_\phi(u)\, d\phi \qquad (2.6)$$

where $\mu_B(x,y)$ represents the image obtained by back-projecting an infinite number of projections. In practice there will only be a finite set of projections and hence the integration of (2.6) should be replaced by a discrete summation. However, the continued use of integrals does not affect the generality of the solutions, provided that sufficient projections are obtained to satisfy the sampling requirements (see Section 2.4).

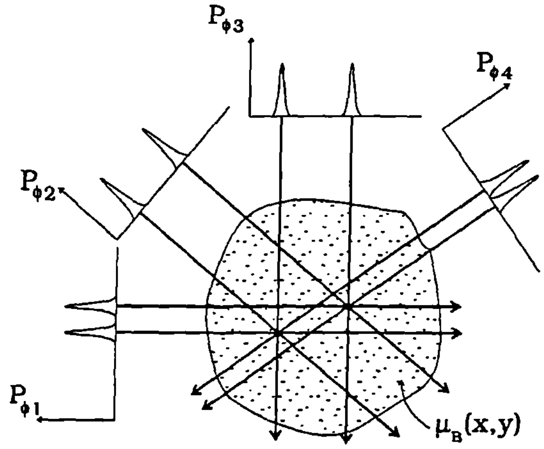

Figure 2.3 Principles of back-projection

Combining equations (2.2) and (2.6) gives,

$$\mu_B(x,y) = \int_0^{\pi} [\mu(x,y) * * \delta(u)]\, d\phi$$

$$\therefore \quad \mu_B(x,y) = \mu(x,y) * * \int_0^{\pi} \delta(u)\, d\phi$$

since $\mu(x,y)$ is not a function of ϕ. But $\int \delta(u)\, d\phi$ is simply the rotation of the line, $x\cos\phi + y\sin\phi$

= 0, about the origin, ie

$$\int_0^\pi \delta(u)\, d\phi = \frac{1}{r}$$

$$\therefore \quad \mu_B(x,y) = \mu(x,y) ** \left[\frac{1}{r}\right] \qquad (2.7)$$

where r is the distance from the origin. Hence the image $\mu_B(x,y)$ formed by simple back-projection is the object $\mu(x,y)$ convolved with the function 1/r. This effect can be seen in Figure 2.3, where point targets in the object appear as "stars" in the back-projected image.

Using the convolution theorem equation (2.7) may be expressed in the frequency domain as

$$M_B(X,Y) = M(X,Y) \,.\, G(R)$$

where G(R) is the Fourier Transform of (1/r)

$$ie \quad G(R) = \frac{1}{|R|}$$

Hence, in principle, it should be possible (e.g. Cho et al, 1974) to reconstruct an image $M'(X,Y)$ of the 'true' object spectrum $M(X,Y)$ by multiplying the back-projected spectrum by an *inverse* filter F(R) of the form

$$F(R) = \frac{1}{G(R)} = |R|$$

$$ie \quad M'(X,Y) = M_B(X,Y) \,.\, |R| \qquad (2.8)$$

The reconstructed image $\mu'(x,y)$ is then given by the inverse Fourier Transform of $M'(X,Y)$. Unfortunately, even though the projection data will be zero outside some limits related to the size of the object, the back-projected image μ_B will never reach zero within finite limits because (1/r) is non-zero everywhere. Hence taking a Fourier Transform on a finite grid will inevitably result in truncation and hence distortion in the reconstruction. In the limit $r \rightarrow \infty$ then $\mu_B \rightarrow 0$, so that a finite grid could be used outside which μ_B would be negligible. However, the additional computational expense of calculating a 2-D Fourier Transform on a grid considerably larger than the required reconstruction size makes this approach unattractive.

Filtered back-projection

An alternative approach to filtering the image after back-projection is to filter each projection before back-projection (Bracewell and Riddle, 1967). Consider the object function $\mu(x,y)$ expressed in terms of its polar Fourier Transform $M(R,\phi)$

$$\mu(x,y) = \int_0^{\pi} \int_{-\infty}^{\infty} M(R,\phi)\ |R|\ \exp[i2\pi R(x\cos\phi + y\sin\phi)]\ dR\ d\phi$$

$$\text{Let} \quad p'_\phi(u) = \int_{-\infty}^{\infty} M(R,\phi)\ |R|\ \exp(i2\pi Ru)\ dR \tag{2.9}$$

where $u = x\cos\phi + y\sin\phi$, as before

$$\text{Then} \quad \mu(x,y) = \int_0^{\pi} p'_\phi(u)\ d\phi \tag{2.10}$$

Equation (2.10) is recognisable as the back-projection operation of (2.6), except this time it is $p'_\phi(u)$ being back-projected instead of $p_\phi(u)$. Now consider equation (2.9). Taking the inverse Fourier Transform of both sides, and using the convolution theorem, it can be shown that

$$\int_{-\infty}^{\infty} p'_\phi(u)\ \exp(i2\pi Ru)\ du = P'_\phi(R) = M(R,\phi)\ .\ |R|$$

But from the central-slice theorem (equation (2.4)), the Fourier Transform of the projection, $P_\phi(R)$, is a line through the origin of $M(R,\phi)$ at an angle ϕ,

$$ie \quad M(R,\phi) = P_\phi(R)$$

$$\therefore \quad P'_\phi(R) = P_\phi(R)\ .\ |R| \tag{2.11}$$

Hence $p'_\phi(u)$ can be thought of as a filtered version of $p_\phi(u)$. This filtering can be carried out either in the frequency domain by multiplying $P_\phi(R)$ by $|R|$ as in equation (2.11), or in the space domain by convolving $p_\phi(u)$ with the Fourier Transform $\rho(u)$ of $|R|$.

$$ie \quad p_\phi^{\prime}(u) \quad = \quad p_\phi(u) \, * \, \rho(u)$$

$$where \quad \rho(u) \quad = \quad \int_{-\infty}^{\infty} |R| \; \exp(i2\pi Ru) \; du$$

To reconstruct the final image, all that now needs to be done is to backproject the filtered projections as in (2.10).

Since the projection data is band-limited by the measuring system both in the space and frequency domains (see section 2.4), the function $|R|$ may be truncated above some value R_{max}. In fact this is essential otherwise noise in the projections, which will dominate the signal at high frequencies, will be amplified by the large value of $|R|$. Various truncated versions F(R) of the function $|R|$ have been suggested. One possibility is a sharp truncation

$$\begin{aligned} ie \quad F(R) &= |R| \qquad for \ |R| < R_{max} \\ F(R) &= 0 \qquad for \ |R| \geq R_{max} \end{aligned}$$

as in Figure 2.4a. Its Fourier transform generates the well known space domain filter of Bracewell and Riddle (1967) shown in Figure 2.4b. The filter has a considerable spread in the space domain, and hence the discrete form (Ramachandran and Lakshminarayanan, 1971) requires a large array which makes the convolution very time consuming. Also, the sharp truncation in the frequency domain tends to introduce 'ringing' artifacts into the reconstructed image. The discrete filter of Shepp and Logan (1974), defined in the frequency domain by

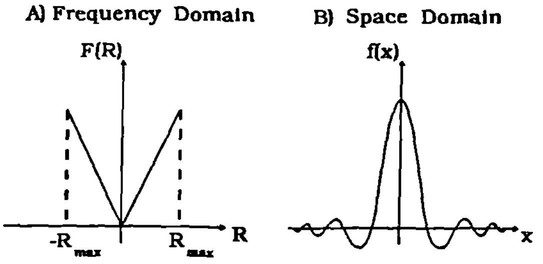

Figure 2.4 Filter of Ramachandran and Lakshminarayanan (1971)

$$F(R) \quad = \quad \left| \left[\frac{2R_{max}}{\pi}\right] \sin\left[\frac{\pi R}{2R_{max}}\right] \right| sinc^2\left[\frac{\pi R}{2R_{max}}\right]$$

$$\text{where} \quad sinc^2(\theta) = \left[\frac{\sin\theta}{\theta}\right]^2$$

is shown in Figure 2.5. This filter falls-off much more quickly in the space domain than does the 'Ram-Lak' filter.

Another advantage of the band-limited nature of the projections is that, unlike filtering the image after back-projection, the Fourier Transforms or convolutions may be performed over reasonable array limits without truncation occurring.

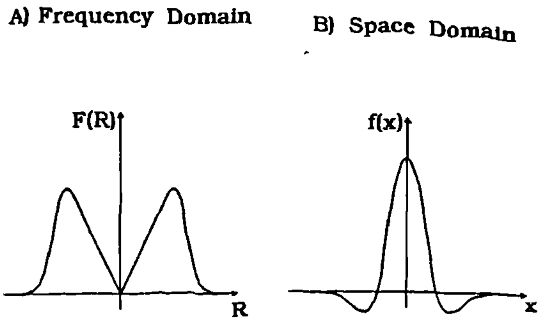

Figure 2.5 Filter of Shepp and Logan (1974)

2.3.3 Iterative methods

Another way of looking at the CT reconstruction problem is to consider each equation defining a projection (ie equation 2.2) as one of a set of N*M simultaneous equations, where N is the number of view directions and hence projections obtained and M is the number of measurements in each projection. It is not possible, in general, to solve these simultaneous equations for the unknown image quantities u(x,y) using conventional direct means (ie matrix inversion) because they may be either underdetermined or overdetermined, and are usually inconsistent due to measurement uncertainties and noise. The alternative methods for solving these equations are generally iterative in nature. Since these methods have rarely been applied to ultrasound CT they will be discussed only briefly here.

The earliest and best known of the iterative methods is the Algebraic Reconstruction Technique (ART), described first by Gordon et al (1970). The method begins with an initial guess of the image (often set all pixel values to an "average" value) and then repeatedly modifies the pixel values, according to the differences between the measured projection data and the projection data calculated from the previous iteration of the reconstructed image. The process is halted when the difference between pixel values of successive iterations (or between the calculated and true projection data) falls below some defined level. The way in which the projection data is used to modify the pixel values of the next iteration varies between implementations. In additive ART, the value of a pixel $\mu(i,j)$ in the q^{th} iteration is changed from its value in the previous iteration according to the formula

$$\mu_{ij}^{q} = \mu_{ij}^{q-1} + \frac{p_{\phi}(u) - p_{\phi}^{q-1}(u)}{N_{\phi}(u)}$$

where $p_{\phi}(u)$ is the measured projection at angle ϕ and $p_{\phi}^{q-1}(u)$ is the equivalent projection calculated from the q-1th iteration. $N_{\phi}(u)$ is the number of pixels lying along the path $u = x\cos\phi + y\sin\phi$. For multiplicative ART the formula is

$$\mu_{ij}^{q} = \left[\frac{p_{\phi}(u)}{p_{\phi}^{q-1}(u)}\right] \mu_{ij}^{q-1}$$

These operations are repeated for every projection to complete one iteration. Other iterative methods exist which change the pixel values at each iteration using data from all the projections simultaneously. One such method (Gilbert 1972) is appropriately called the Simultaneous Iterative Reconstruction Technique (SIRT).

The main advantage of these iterative methods over Fourier based methods is that it is possible to introduce additional information about the object into the reconstruction process. For example, the reconstructed values may be constrained after each iteration to be positive since a negative X-ray attenuation coefficient is physically meaningless. Despite these potential advantages these methods are now rarely used in X-ray CT because they tend to require a great deal of processing time. However, they have been shown (Gordan and Herman, 1974) to be useful in situations where the projection data is particularly noisy or inconsistent, or when the data is under-determined (e.g. if there are insufficient projections to satisfy the ideal sampling requirements, see next section).

2.4 Sampling requirements for computed tomography

In computed tomography, as in all sampled systems, the measured data must be sampled sufficiently finely to allow all frequency components in the data to be represented unambiguously, ie to prevent aliasing. The Shannon sampling theorem states that, for a band-limited function with a maximum frequency component f_{max}, aliasing will not occur if the sampling interval (s) satisfies the condition $s \leq 1/(2.f_{max})$. This also has consequences for the number N_p of projections required to reconstruct an image.

Assuming that the X-ray detector width is w, then the maximum spatial frequency that can be present in the projections, and hence in the reconstructed image, is given approximately by

$$f_{max} = \frac{1}{w} \tag{2.12}$$

Hence the sampling interval, or distance between each detector position, along a profile should satisfy

$$s \leq \frac{w}{2}$$

For an object diameter of D, the number of samples per projection will be

$$N_s = \frac{D}{s}$$

$$\therefore \quad N_s \geq \frac{2D}{w} \tag{2.13}$$

It would make sense to choose the size of the pixels Δp in the reconstructed image to equal the potential resolution, such that

$$\Delta p = s = \frac{w}{2}$$

It is helpful to now consider the situation in the frequency domain. Figure 2.6 represents the 2-dimensional Fourier Transform (F.T.) of object space. As mentioned in 2.3.1, it can be shown that the 1-D F.T. of the projection of an object, obtained at an angle θ, is identical to a line at θ through the origin of the 2-D F.T. of the object. This line extends from $-f_{max}$ to $+f_{max}$ as given by equation (2.12). The frequency resolution Δf within this line is the reciprocal of the distance over which projection data has been obtained,

$$ie \quad \Delta f = \frac{1}{D}$$

As already stated, many projections are required to fully reconstruct the object, each projection providing a unique line in frequency space. These lines should be spaced so that the maximum distance between them in frequency space does not exceed the frequency resolution of the projections Δf. This results in an angle between projections, $\Delta\theta$, given by

$$\Delta\theta = \frac{1}{D f_{\max}} = \frac{w}{D}$$

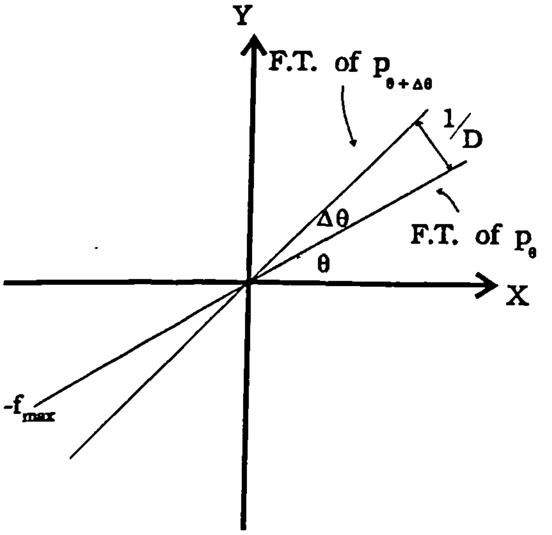

Figure 2.6 CT sampling requirements

It can be seen from Figure 2.6 that, theoretically, projections need only be obtained over a total angle of 180° (or pi radians) to fully reconstruct the object. This implies a total number of projections N_p of

$$N_p = \frac{\pi}{\Delta\theta} = \frac{\pi D}{w} = \frac{\pi D}{2\Delta p} \qquad (2.14)$$

3 Literature Review

3.1 Introduction

Ultrasound CT should strictly refer to any technique where ultrasonic information from many directions is combined into a single image via computational means, but has largely come to refer only to techniques where algorithms similar or identical to those used in X-ray Computed Tomography have been applied. Ultrasound CT techniques may be further sub-divided, according to the kind of measurements and/or assumptions that are made, into reflection, transmission or diffraction UCT. A great deal of research into ultrasound CT has been carried out over the last 18 years. An attempt to describe all this work in detail would not be appropriate, and hence this literature review will concentrate only on research which has presented significant advances or typified particular techniques.

Although reflection UCT was not the earliest application of CT to ultrasonic imaging (although similar in concept, compound scanning is not really a CT technique because no fixed geometry is imposed and in general no computer processing is applied), this technique will be discussed first because it is the one for which it is easiest to see the connection with conventional ultrasonic imaging. Subsequently the various UCT techniques involving measurements of transmitted ultrasound will be discussed. The two quantities most usually reconstructed from these transmission measurements are the acoustic speed and attenuation distributions. No attempt has been made to implement a practical diffraction tomography system in the work described in this presentation. However, it was considered worthwhile to present a brief review of the published research into this technique because an understanding of why diffraction tomography has so far failed to generate impressive images of real tissue is necessary in order to justify its exclusion from this research project.

Since the objective of this literature review is to determine which of the various UCT techniques were most appropriate for further investigation in this study, this chapter will conclude by summarising the relative advantages and disadvantages of these techniques.

3.2 Reflection-mode ultrasound computed tomography

As suggested in chapter 1, the techniques of reflection ultrasound CT developed out of the need to overcome some of the limitations and artifacts inherent to the conventional and already well established reflectivity imaging technique known as real-time B-scanning. Although an introduction to the basic concepts of reflection-mode UCT will be given here, a detailed theoretical analysis will be presented in Chapter 4.

3.2.1 Broad-beam methods

Probably the simplest approach conceptually to reflection-mode UCT, adopted first by Wade et al (1978), assumes that a wide aperture (greater than the object's largest dimension) transducer acts as transmitter and receiver of a short acoustic pulse (Figure 3.1a). As in conventional pulse-echo imaging, echoes return to the transducer from interfaces and scatterers within the object. Assuming that plane waves are incident on the object and the acoustic speed is constant, echoes from scatterers at a given range will arrive at the same time at the receiver and their sum will appear as the output voltage. This sum can then be considered as the integral of the object reflectivity at that particular range and across the whole width of the target, unlike B-scanning where only a small portion of the target is interrogated by each scan line beam. Consequently the output signal as a function of time following transmission can be considered as a 1-D projection of the object reflectivity as a function of range. Thus one difference to X-ray CT is that the projection of the object is parallel to the direction of propagation of the ultrasound beam, rather than perpendicular as is the case in X-ray CT.

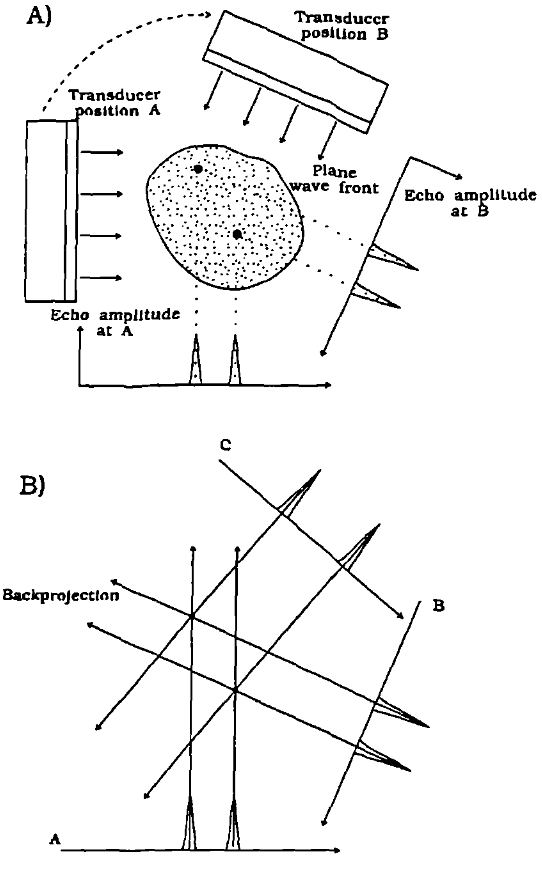

Figure 3.1 Broad-beam reflection UCT using wide single-element transducers (Wade 1978).

Wade et al proposed that by rotating the transducer around the object to obtain projections at many angles, and backprojecting the projection data across image space according to the techniques of Computed Tomography (Figure 3.1b), it should be possible to reconstruct a 2-dimensional image of the object reflectivity showing ideally isotropic resolution determined by the length of the ultrasonic pulse. Since the standard CT process of backprojection has an inherent blurring (or low-pass filtering) effect on the reconstructed image (see 2.3.2), similar filters to those used in X-ray CT (eg a Shepp-Logan filter) must be applied to the data in order to achieve the best possible resolution.

Wade and co-workers suggested that departures from this simple model of reflectivity image formation, caused for example by attenuation of the pulses as they propagate to and from the scatterers within the object, might not be too serious because of the averaging affect of the multiple projections. In their experimental set-up a large diameter transducer, designed to produce a nearly uniform beam, was rotated around brass cylinders in water. Images were reconstructed using Shepp-Logan filtered backprojection. Various artifacts were observed in the images, such as incomplete cylinder boundaries and boundary distortion, largely due to the high reflectivity of brass in water. This caused shadowing of the back half of each cylinder by the front half, and in some projections the shadowing of parts of cylinders by other cylinders - effects not accounted for in their model.

The concepts of reflection UCT were developed further by Norton and Linzer (1979) who derived a theoretical method for reconstructing 2-D reflectivity images obtained with a circular array of point transducers completely surrounding the object to be imaged (Figure 3.2a). Each transducer is excited independently one after the other. They assumed that (a) the object can be modelled as a collection of isotropic weakly scattering point targets, so that the energy propagating through the object is much greater than the backscattered energy (this is known as the Born approximation and is discussed more fully in section 3.4); (b) the acoustic speed is constant; and (c) attenuation can be compensated for. Accepting these assumptions they showed that the reflectivity reconstruction problem reduces, for every transducer in the array, to backprojection along concentric circular arcs centred on each transducer of the raw (ie not envelope detected) rf signal recorded by that transducer (Figure 3.2b). The backprojection is along circular rather than straight paths (as was the case for a wide transducer generating plane-waves) because the small transducers generate a divergent spherical wave. They also showed that the system point spread function (PSF) is limited only by the bandwidth, and does not depend on the size of the array since the imaging aperture is always 360° and there is effectively no far-field requirement. However no experimental results were presented.

Note that any variation in the object or in the ultrasound field in the direction perpendicular to the scan plane has been ignored in all the methods discussed so far. In other words, all methods have assumed that the object may be considered as a 2-dimensional distribution of reflectivity (or backscatter) coefficient. In a later paper (Norton and Linzer 1981) extended their theory to three dimensions, and drew more closely the similarity between their approach to reflection UCT and the arguably more fundamental approach of diffraction tomography (see 3.4). They proposed that the fundamental acoustic parameter actually reconstructed from rf backscatter measurements is a simple function of the compressibility and density of the medium, although there is some disagreement as to whether specular reflection is encompassed by this model.

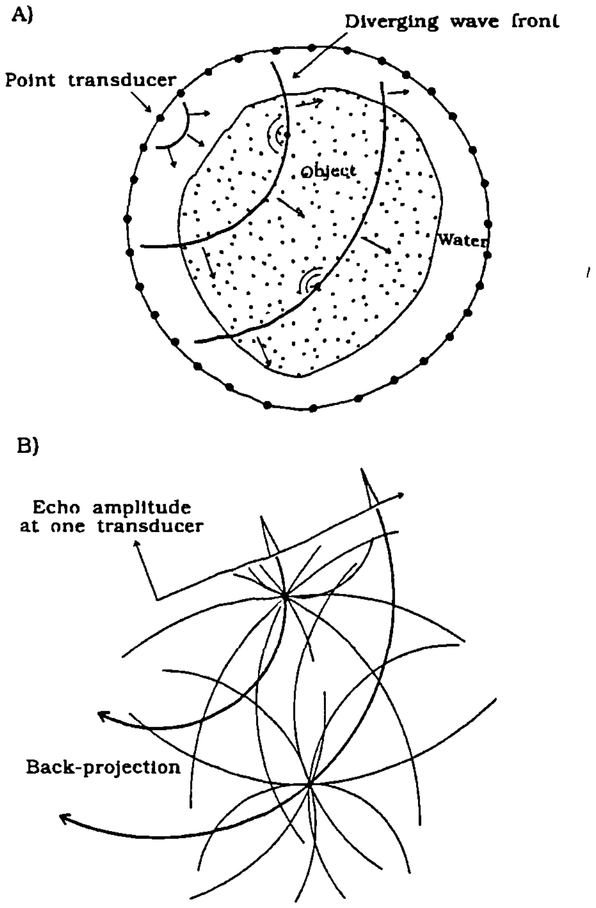

Figure 3.2 Reflection UCT using a circular array of transducers (Norton and Linzer 1979).

It has already been noted that compensation for the attenuation losses of the ultrasound pulses as they propagate through the object is necessary for an accurate reconstruction of acoustic reflectivity. This compensation has normally been achieved using a time (and therefore depth) dependent amplification of the received echoes called time-gain compensation (TGC). The problem with TGC is that in its conventional application it assumes that the attenuation varies identically with depth for all possible acoustic pulse-echo paths through the object. A method for correcting the attenuation losses more accurately than can be achieved by TGC was proposed by Duck and Hill (1979). Their method relies on the possibility of reconstructing, using CT techniques, both the attenuation and reflectivity distributions of an object section solely from measurements of backscattered ultrasound. By assuming that attenuation and scattering are independent and isotropic, and neglecting the frequency dependence of attenuation, they derived an iterative solution to this problem that was similar to the Arithmetic Reconstruction Techniques (ART) used in transmission CT. Results were presented for simulated circular targets of uniform scattering but varying attenuation, which showed good accuracy in the reconstructed attenuation after six iterations. Results from a lamb kidney in-vitro using a laterally scanned 5MHz transducer, with 10 scans obtained at 36° intervals, were less encouraging. Some structure was apparent in the backscatter image, but very little in the attenuation image.

3.2.2 Narrow-beam methods

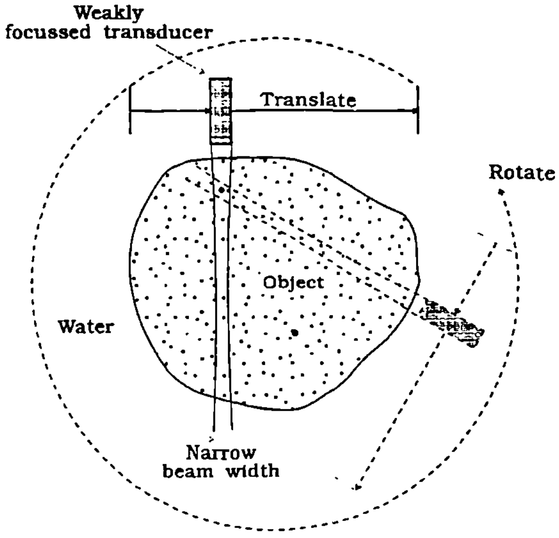

Figure 3.3 Narrow-beam reflection UCT using single-element transducers (Maderlechner et al 1980).

Also amongst the earliest researchers to report results from real tissue in-vitro were Maderlechner et al (1980). They appear to have been the first to attempt to impose better resolution on the reflectivity images by the use of narrow beams, rather than using the wide-beam approaches of Wade et al and Norton and Linzer. Accordingly, they scanned a narrow weakly focused single element transducer laterally across, followed by rotation around, the object to be imaged (Figure 3.3). They compared methods of reconstructing acoustic reflectivity based on a) synthesising a broad plane-wave by averaging the data from the lateral transducer positions to form a single reflectivity projection, and then using a reconstruction algorithm similar to that of Wade et al, and b) a method which preserved the separate information from each transducer position, effectively generating conventional B-scans of the object at each viewing angle which were then summed to form a single image. Method (b) can be thought of as a sophisticated form of compound scanning in which the measurement geometry is fixed and digital filtering can be applied. Slightly modified forms of the CT reconstruction filter are required to allow for the fact that backprojection of each reflectivity measurement now longer occurs across the whole image. Maderlechner' group considered method (b) most likely to provide the superior images because the lateral information from each B-scan is preserved. To obtain the reflectivity data a 10mm diameter transducer generating 2MHz pulses of 0.6mm length (in water) was mechanically scanned in the lateral direction by a stepper motor, with the object resting on a turntable also under the control of a stepper motor. Using a human hair as a target they showed that the potential resolution of the method when the B-scans were combined simply by summation was 0.6 mm (ie this was the full width at half max of the image of the hair). When Shepp-Logan filtering was applied before summation the FWHM was reduced to 0.3mm. They also obtained reconstructions of acoustic reflectivity in a sponge phantom and an in-vitro pig heart, and demonstrated relatively good isotropic resolution and reduced artifact in these images compared to conventional B-mode images.

One of the problems of using a mechanically scanned single element transducer to generate the reflectivity projections is the time taken to acquire the data. Hiller and Ermert (1980, 1982) were the first to attempt to reduce scan times by the use of a linear array (Figure 3.4) where the lateral scanning is achieved electronically without the need for any mechanical movement, but because of limitations in their mechanical rotation system they could still only achieve a minimum acquisition time (for 120 projections) of two minutes. In common with Maderlechner et al they also compared alternative methods of reconstructing the pulse-echo data based on either (a) discarding or (b) preserving the lateral information available from each B-scan. They pointed out that method (b) is less dependent on the assumptions, such as isotropic scattering and compensateable attenuation, required for reflection CT and has a higher immunity to measurement errors. They also suggested that fewer angular transducer positions would be required using method (b) compared to method (a) (ie 45 compared to 120), because of the greater amount of information obtained at each angle.

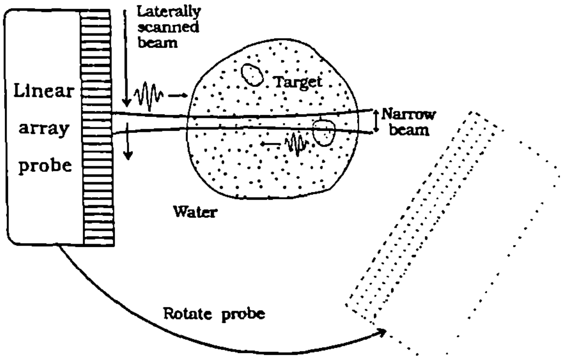

Figure 3.4 Narrow-beam reflection UCT using linear arrays (Hiller and Ermert 1980).

The experimental apparatus of Hiller and Ermert consisted of one or two commercially available 2.3MHz 54-element linear arrays mounted on a turntable, and submerged in a water tank. Only the central 32 elements of the array were used, thus allowing 32 lateral positions (or scan lines) for each angular position. Reconstructions, using both methods (a) and (b) with a modified Shepp-Logan filter, were obtained of a ring of 0.6mm diameter steel needles. Both UCT methods demonstrated considerable improvement over an individual B-scan, with an isotropic resolution of better than 2mm. Another target consisting of an irregularly shaped piece of PVC, to provide specularly reflecting surfaces, demonstrated more clearly differences between conventional B-scanning and the two UCT methods. In the individual B-scan only a very small portion of the PVC surface was visible, ie that part of the surface that was perpendicular to the scanning beam, whereas in both UCT images the surface was complete. However 'streak' artifacts were much more evident in the image obtained by method (a) because the specular reflections violate the assumption of isotropic scattering, whereas method (b) was much less sensitive to this assumption.

Hiller and Ermert also appear to have been the first to present in-vivo results for reflection UCT, initially of the human foreman (Hiller and Ermert 1980) but later in the female breast (Hiller and Ermert 1982), although Carson et al (1981) had already presented reflection images of the breast in-vivo (although not incorporating CT filtering) along with transmission UCT images, and had shown that the two UCT techniques give unique and almost independent information on tissue structure (see 3.3.4). Hiller and Ermert (1982) also presented results of transmission UCT measurements, but using linear arrays for both reflection and transmission measurements rather than single element transducers. Reflection, attenuation and acoustic speed images were shown of a dog testicle in-vitro, and of a human testicle and breast in-vivo.

Friedrich et al (1982) investigated some of the factors likely to influence the quality of reflection UCT images. They investigated the affects of the choice of the particular tomographic filter and the scanning geometry (number of scan angles and total scan angles) used, and considered the affects of pulse-length, beam-width and registration accuracy. It had already been established by other workers that the resolution of reflection UCT images was limited by the pulse length. However, Friedrich and co-workers pointed out that beam width is also important in so much as it determines the thickness of the scan plane. Registration and refraction errors due to the assumptions of a known and constant acoustic speed, and consequently straight-path propagation, were thought to be the most likely causes of image degradation. Mis-registration due to mechanical inaccuracies in the scanning apparatus was also recognised as a possible problem. They suggested that mis-registration problems could be minimised by limiting the information used from each B-scan to that corresponding to the half of the object nearest the transducer. This approach was possible because they had also shown that a 180° total scan was sufficient and that scanning through 360° achieved no significant improvement in image quality. Although some quite good images of in-vitro breasts were presented, in common with all previous studies the scan times were unacceptably long for a clinical system.

Limited angle reflection UCT was also considered by Roehrlein and Ermert (1985) and Ermert and Roehrlein (1986), with the intention of applying the technique to targets for which 360° access is not possible, such as the neck (ie thyroid) and upper legs. They realised that for scan angles of less than 180° the reflection image PSF no longer has rotational symmetry, i.e. the resolution is not isotropic. However they showed that isotropic resolution can be achieved by post-processing with appropriate 2-dimensional inverse filtering. For in-vivo experimental investigations a special applicator was built to hold either a 3.5MHz linear array (for thyroids, legs and breast), or a 5MHz linear array (for testicles). A study of 70 patients, using scan angles of 155°, suggested that limited angle reflection UCT is feasible, particularly for thyroids.

Roehrlein and Ermert (1986) also considered the appearance of speckle in reflection UCT images. They showed that for reflection UCT images obtained by simple summation (ie no filtering) of totally uncorrelated B-scans, the mean speckle amplitude (expressed as the ratio between the standard deviation of the B-scan amplitude and its mean value throughout the image) is reduced by the square root of the number of B-scans in the summation. The speckle size of the summation image was found to lie between the axial and lateral components of the speckle size of an individual B-scan. Tomographic filtering of the summation images, which is normally performed to improve resolution in line with the conventional CT approach, was found to reduce the speckle size down to the axial component of the B-scan speckle, but only at the expense of an increase in the mean speckle amplitude up to that found originally in the B-scan.

3.2.3 Reflection UCT with acoustic speed compensation

It has already been suggested that mis-registration of the superimposed B-scans, due to acoustic speed variations within the object, may be the main cause of artifact and limitation on resolution in reflection UCT images. Although many workers have suggested combining simultaneous acquisition of reflection and transmission data (eg Carson et al 1981 and Hiller and Ermert 1982, see above), others have also proposed using reconstructions of acoustic speed distributions to correct registration errors in reflection images. As early as 1973 Jellins and Kossoff (1973) had shown improvements in basic compound B-scan images of the breast using very simple acoustic speed corrections based on a trial-and-error approach. Greenleaf et al (1975) were apparently the first to propose the use of transmission UCT generated acoustic speed images to improve unfiltered reflection UCT images. They used a single element 5MHz transducer which was mechanically scanned in a fan beam for both reflection and transmission data (Greenleaf et al 1977). They scanned a phantom consisting of a string held rigidly near to a rubber finger cot filled with saline having an acoustic speed 5% higher than the surrounding water. The uncorrected reflection images showed blurring of the string towards the finger cot, whereas in the acoustic speed corrected reflection image the string was in much sharper focus.

The first to apply acoustic speed correction to more demanding targets were Kim et al (1984), who demonstrated some improvement in Shepp-Logan filtered reflection UCT images of dog hearts in-vitro using mechanically scanned 2.25MHz transducers. However, as had been the case with Greenleaf et al (1977) straight-path propagation was assumed and hence no correction was made for lateral registration errors due to refraction of the ultrasound beam. Bartelt (1988) developed a method for reconstructing independent images of reflectivity, acoustic speed, attenuation and scattering directivity from measurements of reflected ultrasound alone. Six 3.5MHz linear arrays were arranged in a ring to reduce scan times, and the whole ring was rotated (up to 60 degrees) around the object to be imaged. Directivity estimates were obtained by selecting, for every point in the object, the two azimuthaly adjacent scans which encompassed the peak backscattered signal from that point, and calculating the rate of change of the backscattered signal with angle. Acoustic speed and attenuation estimates were made by comparing overlapping A-scan lines obtained from opposite directions. For acoustic speed the A-scans were cross-correlated, the maximum of the cross-correlation function providing an estimate of the average acoustic speed along the line of the A-scans. The acoustic speed values obtained along many lines and from many directions were then reconstructed into an image of acoustic speed using conventional CT algorithms. The main problem was attenuation of the echoes in the A-scan signals which reduced the accuracy of the cross-correlation function and tended to bias the acoustic speed estimates. For attenuation imaging they calculated the average amplitude difference of opposite A-scans. However, this provided only a qualitative estimate of attenuation. Reflection UCT images of a phantom structure, having regions of different acoustic speed, and of a human forearm were subjected to acoustic speed correction. Probably because of the relatively poor quality of the acoustic speed images only small improvements in resolution were evident in the corrected reflection images.

3.2.4 Reflection UCT with RF data

The only researchers, apart from the early work of Norton and Linzer (1979), to have used the raw rf echo signal in their reconstruction of reflection UCT images have been Herment et al (1989a and 1989b). Others workers have generally considered only demodulated (ie envelope detected) signals. Demodulation is a non-linear operation and thus strictly invalidates the concept of linear summation inherently assumed in CT techniques (see 4.3.1.3). Herment et al compared various methods of reflection UCT in terms of resolution, signal-to-noise (or signal-to-speckle) ratio and computing time. They consider both a broad beam method (Herment et al 1989a) and a narrow beam method using a mechanically scanned single element transducer (Herment et al 1989b). For both methods, they considered the affects of varying the order in which the following stages of image reconstruction were applied:- (i) deconvolution of the rf point spread function to widen the signal band-width, (ii) envelope detection to conform to the conventional mode of presentation of B-scan images, (iii) backprojection for CT image reconstruction, and (iv) tomographic filtering to restore the high spatial frequencies attenuated by the backprojection process.

They found that the conventional CT method (envelope detection followed by backprojection and tomographic filtering, with no deconvolution stage) resulted in a factor of 4 improvement in resolution compared to the lateral resolution of a simple B-scan. Including a deconvolution stage resulted in a further factor of 3 improvement in resolution over the conventional CT method. Resolution was even better when both deconvolution and tomographic filtering were performed before envelope detection. However deconvolution was found to degrade the signal-to-noise ratio compared to conventional CT, although this effect was not quantified. In terms of computing time, all methods were found to be very similar. Herment et al also pointed out that the ultimate resolution is only achievable when the acoustic speed is absolutely constant throughout the object - a situation unlikely to occur in practice. They thus proposed that their method may be best suited to the study of superficial structures, such as the carotid arteries, where there is likely to be less opportunity for acoustic speed variations to degrade the echo data.

A further practical disadvantage of using rf data for reconstruction is that it requires high geometrical accuracy in the measurement apparatus (better than wavelength/10, or 50 μm for 3MHz ultrasound), and hence the technique is probably restricted to data acquisition configurations where no mechanical movement of the transducers is required, such as is the case for a circular array.

3.3 Transmission-mode ultrasound computed tomography

The earliest published research into transmission UCT was performed in the early 70s by Greenleaf and co-workers at the Mayo Foundation in Rochester, USA. They were the first to suggest the possibility of applying the by then well known techniques of Computed Tomography to the reconstruction of acoustic attenuation (Greenleaf et al 1974) from measurements of the amplitude of transmitted pulses. Their scanning apparatus consisted of two (one to transmit and one to receive) 5 MHz single element transducers arranged on opposite sides of the target being scanned (Figure 3.5a). The transmitting transducer was pulsed, and the total transmitted energy was calculated as the log of the squared and integrated pulse from the receiver. The application of CT techniques is valid if it can be assumed that the transmitted energy, measured at many lateral positions in a fixed direction (ie a projection, Figure 3.5b) by mechanically translating both transducers, is simply and linearly related to the 2-dimensional distribution of attenuation coefficient within the object (see also 2.2). Although they realised that this assumption was not strictly valid for ultrasound in human tissues because of reflection and refraction, they still felt that the approach was worth attempting. Images of the acoustic attenuation distribution were reconstructed onto a 64*64 matrix using a standard CT technique known as the Arithmetic Reconstruction Technique (see 2.3.3). Results were presented for simple phantoms and a canine heart in-vitro. The images showed recognisable structure, but with thickened boundaries between structures and poor quantitative accuracy. Despite these artifacts, which they decided were probably due to refraction, they felt that the technique showed some promise.

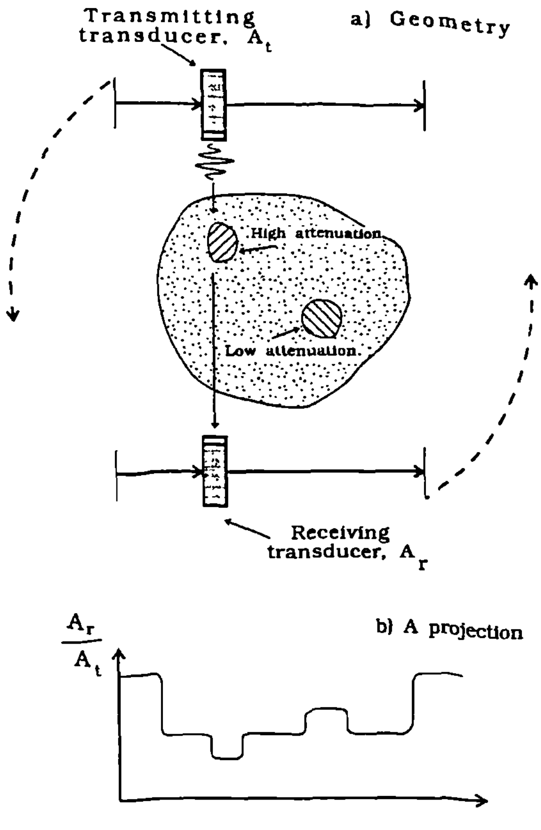

Figure 3.5 Principles of transmission UCT

Later, the same group (Greenleaf et al 1975) also suggested reconstructing acoustic speed distributions from measurements of the time of flight of acoustic pulses through tissue. They used basically the same equipment used for attenuation imaging to reconstruct acoustic speed distributions for various tissues in-vitro. Pulse time-of-flight (TOF) was measured by detecting the point when the pulse first rises above the noise level in the signals. Images of acoustic speed distribution were obtained from excised canine hearts, and comparisons with photographs of the sliced heart were quite encouraging. Images obtained from post-mastectomy breasts showed more artifacts, but it was still possible to distinguish between areas of fatty (low acoustic speed) and connective (high acoustic speed) tissue. By comparing images of acoustic speed and attenuation obtained from the same target, they showed that these images represent nearly independent parameters.

Greenleaf's group argued that the major cause of the artifacts in both their attenuation and acoustic speed reconstructions was due to refraction. Refraction of the ultrasound beam results in violation of the assumption that the ultrasound travels in a straight line between transmitter and receiver, an assumption inherent in the standard CT reconstruction technique. This may result in either under- or over-estimation of the parameter being measured for the projection data, with consequent inconsistencies in the projection data and "streak" artifacts in the reconstructed image, as well as violation of the basic CT principle that the measured projection is linearly related to the true geometrical projection of the object. Attempts have been made by several researchers to develop reconstruction algorithms which do not rely so strongly upon the assumption of straight line propagation. These approaches will be discussed in a later section (3.3.3), but for now the consequences of violation of this assumption within the standard straight line reconstruction technique will be discussed, both in terms of measurement requirements and image artifacts.

In a later paper Greenleaf et al (1978) identified theoretically the underlying assumptions required for straight line propagation when the ultrasound wave may be modelled by the time-independent Helmholtz equation. They argued that when diffraction may be ignored (ie $\lambda \to 0$), and the relative refractive index varies by less than 10% (ie acoustic speed everywhere in target is similar to acoustic speed in surrounding medium so that refraction is relatively minimal), then the projection measurements required for attenuation CT and acoustic speed CT can be based simply on the amplitude ratios and phase differences respectively of incident and transmitted waves (note that rather than measuring incident waves it is more usual in practise to measure waves transmitted with, and without, the target present). Whether these conditions hold sufficiently in soft tissues is an important question that will be discussed in Chapter 4.

Greenleaf et al pointed out that, not only does refraction violate the straight line assumption of the reconstruction algorithm, but in the case of attenuation measurements may also result in some of the ultrasound energy missing the receiver and hence the attenuation being overestimated. Since attenuation will also be overestimated if any of the ultrasound is reflected from interfaces within or at the boundaries of the target, they concluded that attenuation images produced from transmission UCT measurements are more likely to be prone to artifacts and also less quantitative than acoustic speed images. The main reason for this is that the basic measurements required for acoustic speed CT are of the times of flight (TOF) of the ultrasonic pulses propagating across the target. As pointed out by Greenleaf et al (1975) and later by Glover and Sharp (1977) pulse TOF, unlike pulse amplitude, should be largely unaffected by reflection of some of the energy within the pulse.

Since the requirements differ for the measurement of basic projection data for attenuation and acoustic speed reconstructions, the problems associated with these measurements and the affects on image artifacts will be discussed separately. For a good review of the early work in transmission ultrasound CT, see for example Wade (1979).

3.3.1 Measurement requirements for attenuation CT

Greenleaf and co-workers (Greenleaf et al 1978) and other groups (eg Carson and Scherzinger 1979, Miller et al 1979) have recognised that the undesirable contributions to attenuation from parameters that are independent of frequency, such as specular reflection and to a lesser extent refraction, may be minimised by reconstructing the frequency dependence of attenuation rather than the attenuation coefficient itself. This approach is only valid if the frequency dependence of attenuation may be assumed to be linear, an assumption that appears to be roughly true in most soft tissues at the frequencies used (Duck 1990). This technique obviously requires measurements at a range of frequencies, either by multiple experiments at different frequencies, or more usually by measurements on broad band pulses.

In another approach, the Carson group (Carson and Scherzinger 1979) showed experimentally that large receivers (19mm) give better results for attenuation measurements on female breasts in-vivo because there is less chance of a refracted beam missing the receiver. However, one disadvantage of using large receivers for breast imaging is that it becomes difficult to image sections close to the chest wall.

The Carson group also identified another source of error in attenuation measurements, that is phase cancellation at the receiver. The phenomenon results from the fact that conventional piezo-electric transducers are sensitive to the instantaneous amplitude (and hence phase) of the incident ultrasound pressure wave. If the ultrasound wave front becomes distorted as it propagates through the target, either by refraction or diffraction or more likely both, then phase cancellation will occur across the receiver aperture resulting in an overestimation of attenuation. Another way of looking at this is to recognise that conventional transducers have a very peaked directivity pattern, so that they are only sensitive to waves that impinge upon them at angles close to the perpendicular. This problem is particularly severe for the large aperture transducers favoured for attenuation measurements. The Carson group suggested a method to overcome this problem by using a large array of small transducer elements as a receiver. Being considerably smaller than the total aperture size, each element has quite a broad directivity pattern. By rectifying the signal from each element before summation and so eliminating the possibility of cancellation, the array is sensitive to wave components impinging at glancing angles, such as those waves which have been bent by refraction. In a later paper (Chenevert et al 1984) the same group showed significant improvements in attenuation images of a breast phantom using a scanned 0.25mm hydrophone to synthesise a 5cm diameter 40-element array, compared to a 19mm diameter single element receiver. However, some expected loss of resolution which is itself due to the broadened directivity pattern was also observed.

Another way of overcoming the problem of phase cancellation at the receiver is to use a transducer that is inherently insensitive to phase. Such an approach, using an acoustoelectric transducer, was proposed by Miller and co-workers (Miller et al 1979). These transducers are sensitive to the instantaneous intensity of the ultrasound wave, and have a broad directivity pattern. They compared acoustoelectric receivers with conventional piezoelectric receivers for attenuation imaging of dog myocardium in-vitro. The images obtained using the acoustoelectric receivers appeared to be more consistent, with less artifact at the edges of the targets where refraction is greatest. The same transducer was used for imaging the frequency dependence of attenuation in dog kidneys in-vitro, with even better results. The inevitable consequence of using such a transducer is again that some reduction in potential resolution must be accepted.

In a later paper (Klepper et al 1981), the same group went further by exploring theoretically the likely magnitudes of the affects of phase cancellation, refraction, and also the variation of beam width with frequency (ie diffraction) on attenuation measurements. They proposed a method of correcting for the beam width variations of the transmitting transducer by measuring its directivity pattern for various frequencies, and then applying appropriate filters to the measured attenuation data. They also discussed another potential cause of artifacts in attenuation images that had not previously been identified. It is well known that some tissues, such as muscle fibre, exhibit an attenuation coefficient that itself has some angle dependence. This anisotropy is not allowed for in the CT reconstruction process and hence these tissues will be reconstructed with an "average" attenuation coefficient. From experimental results in dog myocardium they show that the affects of anisotropy are significant. They also found that although high attenuation correlates well with infarct in the heart muscle, the attenuation values were not good quantitatively even when using acoustoelectric receivers and beam width correction, probably because of anisotropy. Brandenburger et al (1981) performed a more detailed theoretical analysis of anisotropy. They showed that anisotropy can be intrinsic (eg muscle fibres) or extrinsic (refraction and reflection are both angle dependent), and concluded from a simulation study that anisotropy can be a major cause of inaccuracy in attenuation reconstructions.

Farrell (1981) argued that one problem with using the frequency dependence of attenuation as the reconstructed parameter was that, because a range of frequencies was required (the larger the range the better the accuracy), the technique would be limited to targets of relatively low attenuation since high frequencies would be attenuated too strongly. He proposed an alternative method for reducing refraction and phase cancellation effects which required knowledge of the acoustic speed distribution of the target. Initially TOF measurements are used to reconstruct the acoustic speed distribution as in conventional acoustic speed CT. This distribution is then used to calculate simulated amplitude projections by ray tracing. These projections represent the amplitude measurements that would be obtained for a target with this acoustic speed distribution but with no attenuation, so that any amplitude losses are due solely to refraction and phase cancellation affects. These calculated projections are then used to correct the actual measured projections before reconstruction of the attenuation image. Good results were obtained with simulated data from circularly symmetrical targets, but the quality of the images is clearly very dependent on the ability to obtain accurate acoustic speed images. In addition, the method takes no account of reflection or diffraction losses unlike the frequency dependence methods.

The basic attenuation measurements made by the majority of the researchers discussed up to now was of the ratios of the peak amplitude or total energy of pulses transmitted with and without the target present. Dines and Kak (1979) proposed an alternative method of measuring the integrated attenuation that should be less affected by refraction and reflection. They showed theoretically that assuming the ultrasonic pulses may be represented by Gaussian functions, that non-linear propagation may be neglected, and that the frequency dependence of attenuation in soft tissue is approximately linear, then the integrated attenuation along the path between the transmitter and receiver is proportional to the difference in centre frequency between the with target and the without target pulses. Since it is the spectrum of the transmitted pulse that determines the measured attenuation value, and not the absolute amplitude of the pulse, the method should still provide a reasonable estimate of integrated attenuation even if some of the energy of the pulse fails to reach the receiver because of refraction or reflection. Some improvements in image quality over the conventional peak amplitude method were demonstrated for excised dog hearts.

Crawford and Kak (1982) showed through computer simulation that, irrespective of the measurement technique used (ie frequency shift or amplitude ratio), the attenuation images are degraded partly by what they call "multipath". Multipath refers to the multiple ray paths which connect the transmitter to the receiver in any complex target. The interference of these multiple pulses at the receiver causes a scalloping of the received power spectrum (equivalent to speckle in B-mode images). They proposed two methods to reduce the affects of multipath; homorphic signal processing of the received spectrum to estimate the integrated attenuation for just one of the rays, or median filtering of the measured projections to remove the glitches caused by multipath. They found that both methods were successful in improving attenuation images of an ATS labs Tissue Equivalent phantom, and of a breast phantom.

3.3.2 Measurement requirements for acoustic speed CT

The projection data required for the reconstruction of an acoustic speed image are usually calculated by subtracting the reference "water-path" time-of-flight (TOF) measured with the target absent to the TOF measured with the target in place. Most of the early researchers into acoustic speed CT (eg Greenleaf's group, Glover's group, and Carson's group) measured TOF using the so called leading-edge or earliest-arrival-time method. As the name of this method implies, the pulse is assumed to have arrived when its leading edge rises above some (usually fixed) threshold level. Because of refraction, there will be many possible paths linking the transmitter to the receiver (Crawford and Kak 1982). However, when the refractive index varies by less than 10% the first pulse to arrive is likely (Greenleaf et al 1978) to be the pulse that has travelled the shortest (ie straightest) path, which is also the path assumed by the standard reconstruction algorithm. Hence when using this detection method, refraction will also tend to have less affect on acoustic speed reconstructions than on attenuation ones. Using this method, Glover and Sharp (1977) demonstrated high quantitative and geometrical accuracy for an acoustic speed image of four fingers of a rubber glove filled with fluids of known acoustic speeds, where the maximum deviation in acoustic speed of any of the fluids from the surrounding medium (water) was less than 7%.

Despite its apparent success in the reconstruction of simple targets with small acoustic speed variations, some problems with the use of the earliest arrival time method have been recognised. Greenleaf et al (1978) noted that small regions of low acoustic speed imbedded within regions of higher speed may not be detected or their size may be underestimated since, because of the finite beam width, pulses traversing such regions may appear after pulses traversing the surrounding areas. Similarly the size of regions with a higher speed of sound than their surroundings will tend to be overestimated since the region will be detected even if it intersects only a small portion of the ultrasonic beam. This affect could be minimised by using as small a receiving transducer as possible in order to reduce the number of possible paths, and accepting the consequent reduction in sensitivity. Note that the requirement for a small receiver is opposite to that found in attenuation CT.

Carson and Scherzinger (1979) also commented on the importance of using a small receiver transducer since they had observed that this helped generate a fast rise time, which can also be understood in terms of a reduction in the range of paths and hence arrival times of pulses. They also observed that the measured TOF appears to be artificially high when the pulse is strongly attenuated, because the received signal crosses the fixed threshold slightly later. This phenomenon was also described by Crawford and Kak (1982) who called it "time-walk". Crawford and Kak also identified another possibility, which they called "time-hop", when the attenuation is so severe that the first cycle of the received pulse (or half-cycle for rectified pulses) fails to cross the fixed threshold. In this case the TOF will be overestimated by one or more wave periods, depending upon the degree of attenuation. These problems can be partly overcome by allowing the received pulses to heavily saturate the receiver amplifier, or by having some form of automatic gain on the amplifier.

A rather more serious limitation of the earliest arrival time method was pointed out by McKinnon and Bates (1980). They showed theoretically that in most media regions exist which will never be crossed, because of refraction, by pulses which have propagated for the shortest time between transmitter and receiver, irrespective of the size or position of the transmitter and receiver. Hence attempting to use a very small receiver may simply result in no ultrasonic energy reaching the receiver, a situation which had already been observed in attenuation CT (see 2.3.1).

The effects of both refraction and diffraction on ultrasonic time-of-flight measurements were investigated experimentally by Greenleaf et al (1981). Simple objects, consisting of finger cots filled with various liquids of differing acoustic speeds, were insonated with a near plane wave pulse from a large area transmitter. The transmitted pulse was measured by a linearly scanned 2mm receiver. They observed that the edges of the finger cot give rise to a diffracted wave, the divergence of which depends only on the geometry of the situation and not on the acoustic speed of the liquid in the finger cot. The degree of refraction however is, as expected, strongly affected by the acoustic speed within the finger cot. These results also demonstrated clearly why the size of objects, with higher or lower acoustic speeds than their surroundings, are over or under estimated respectively when using the earliest arrival time method for CT reconstruction.

In an attempt to overcome some of the problems of the earliest arrival time method for measuring TOF projections, some researchers have proposed alternative methods. Chenevert et al (1984) suggested a method based on calculation of the cross-correlation between the reference water-path pulse and the target propagated pulses. Conceptually, the cross-correlation process uses the reference pulse as a template whose TOF is adjusted until it best matches the target propagated pulse. Even when there are multiple paths through the target between transmitter and receiver, the cross-correlation TOF is determined by the largest component in the received signal fitting the shape of the template. Hence the sizes of high and low speed regions should be reconstructed more accurately than when using the earliest arrival time method. Chenevert et al showed considerable qualitative improvements in acoustic speed images of a breast phantom and a breast in-vivo, but the average acoustic speed in the breast phantom was still different from the "true" value by nearly 1%. They postulated that this was due to frequency dependent attenuation, and interference between multiple propagation paths, which distorted the shape of the target propagated pulses so that they were no longer able to match accurately with the reference pulse.

3.3.3 Alternative reconstruction algorithms

It has already been mentioned that probably the main cause of artifacts in both attenuation and acoustic speed images obtained from transmission ultrasound CT is refraction of the ultrasound pulse from the straight line path between transmitter and receiver. In the previous two sections some techniques have been described which attempt to minimise the consequences of refraction by constraining or processing the measurements themselves - ie such that only the energy that has travelled as closely as possible to the straight line path is recorded - and then reconstructing the image assuming ideal straight line propagation. In a slightly different approach Norton and Linzer (1982) derived 2^{nd} order corrections for refraction that were calculated from an acoustic speed image reconstructed using a conventional straight path method. These corrections were applied to the TOF measurements, which were then used for a subsequent improved straight path reconstruction of the acoustic speed. They also derived perturbation corrections for phase cancelation and beam displacement errors in attenuation imaging. When compared to conventional straight path reconstructions of simulated circularly symmetric targets, these methods showed considerable improvements in geometrical and quantitative accuracy.

Other researchers have adopted a different approach in which they have attempted to reconstruct an image by calculating the curved paths that the refracted ultrasonic pulses had actually travelled. As early as 1975, Greenleaf et al (1975) suggested that the problem of refraction artifacts in acoustic speed images might be overcome by an iterative reconstruction algorithm which takes an acoustic speed image reconstructed assuming straight line propagation as a first iteration, and then obtains subsequent improved acoustic speed images by calculating the refracted (ie curved) ray-paths from the previous iteration. Apparently the first to implement such a method was Schomberg (1978), who developed an extension of the conventional iterative Arithmetic Reconstruction Technique (ART) by combination with the principles of geometric optics. The method was tested with computer simulated data of a female breast. A reconstruction of the acoustic speed distribution obtained with the new method appeared to be superior when compared with a reconstruction obtained with a conventional straight line technique.

One of the problems with the method of Schomberg is the need to calculate the curved ray paths in a medium encompassing both discrete interfaces and continuously varying acoustic speed, the values of which are only known at discrete intervals on a matrix so that the direct application of Snell's Law is not possible. This problem has been considered by, amongst others, Smith et al (1980) who showed that the differential form of Snell's Law can be applied when the acoustic speed image has been smoothed. The technique was tested with three different types of acoustic speed image for which theoretical ray paths were known for comparison. They found that there was a trade-off between lateral displacement error, which increased with greater smoothing, and angular displacement error which were reduced with smoothing.

It was not until 1990 that an iterative ray tracing approach to refraction correction was implemented with experimentally acquired projection data. Andersen (1990) applied ray tracing with a Simultaneous Algebraic Reconstruction Technique (SART) to experimental time of flight data from an ATS gelatine phantom. The TOF was measured using the first arrival method. Reconstructions of the acoustic speed distribution of the phantom using their technique showed finer resolution and more accurate representation of the sizes of regions compared to reconstructions obtained with a conventional straight line technique. The authors pointed out however that their technique still relied on the assumption that only a single propagation path links the transmitter and receiver, ie the path of the first pulse to arrive. Multiple paths, and the consequent interference of the multiple pulses at the receiver, were not accounted for.

3.3.4 Applications and clinical trials

One of the main requirements for transmission UCT is that it must be possible to access the target of interest over a full 360° angle. This obviously limits the range of soft tissues to which the technique may practically be applied. One of the most promising applications of the technique was thought by many workers to be the female breast, because it is an accessible soft tissue with complex structure for which a viable non-invasive alternative, or adjunct, to X-ray examination would be useful. The first acoustic speed images of breasts in-vivo were presented by Glover (1977), who reported results from 5 asymptomatic volunteers and 15 patients with known gross breast pathologies. Despite the limitation of long scan times (about 10 min per slice), which resulted in inevitable movement and 'streak' artifacts in the images, some encouraging results were obtained. He showed that, for the normals, the young firm breasts exhibited much higher average acoustic speed than older fatty breasts. Malignant lesions in the generally older symptomatic patients also presented a higher acoustic speed than the surrounding tissue, although there was considerable overlap between these values and the parenchyma and mammary tissue of the young normal breasts. The malignant and benign lesions were differentiable in all cases, although it was accepted that the number of patients studied was too small to make firm conclusions.

The first attenuation reconstructions of breasts in-vivo were presented by Carson and Scherzinger (1979). Image slices were shown of the breast of a women with palpable fibrocystic disease. The known position of the cystic region appeared to correlate well with regions of low attenuation in the images. Attenuation and acoustic speed images of the breast of a women with a papillary carcinoma (confirmed post-mastectomy) were presented for comparison. The carcinoma appeared to exhibit both higher attenuation and higher speed of sound than the surrounding normal tissue. When they compared transmission UCT images of another breast with images from a conventional pulse-echo real time scanner, they found that the acoustic speed images appeared to demonstrate the distributions of major tissue type better than did the attenuation images.

In a later paper (Carson et al 1981) the same group obtained simultaneously both transmission UCT (attenuation and acoustic speed) and reflection UCT images of in-vivo breasts, using mechanically scanned single-element 3.5MHz transducers. They argued that the two techniques provide essentially unique information about tissue structure and composition, and therefore have complementary roles. They found that, whilst the reflection images were of a high quality from young dense breasts, they were much poorer in fatty breasts where the acoustic speed images appeared to provide the better diagnostic information.

The potential role for transmission ultrasound CT in routine breast examination was elaborated by Greenleaf et al (1980). They identified four situations for which ultrasound CT might be indicated; 1) in young women in whom X-ray mammography is contraindicated, 2) for pre-mammographic screening of all women, 3) in women in whom the results of X-ray mammograms are ambiguous, and 4) for temporal surveillance of lesions in patients in whom multiple X-ray examinations is contraindicated. They showed examples of some early breast acoustic speed images obtained with their system. They also showed some results of applying automatic pattern recognition methods to the acoustic speed images which correlated quite well with lesions identified by histology and X-ray mammography.

The first extensive clinical trial of transmission UCT was carried out by Greenleaf and Bahn (1981) who obtained over 1000 images of acoustic speed and attenuation from approximately 150 patients, of whom 30 had biopsy proven cancer. From these results they were able to identify various characteristics of the images which appeared to correlate well with particular tissue type or pathology. Normal young breasts were characterised by a relatively homogeneous zone of low speed (1400-1450ms^{-1}) and low attenuation just beneath the skin, with the parenchyma showing a reticulated pattern with intermediate acoustic speed and attenuation. Cysts showed relatively low attenuation, and speed (1500-1520ms^{-1}) within the range of water at body temperature. The attenuation of solid lesions was not a good indicator, since this could be low relative to surrounding tissue in young dense breasts, but relatively increased in older fatty breasts. However solid lesions generally showed high absolute speed ($>$ 1465ms^{-1}) as well as relatively increased speed compared to the surrounding tissue. Thus it was concluded that acoustic speed was better than attenuation as an indicator of malignant lesions.

In a more recent study the same group (Schreiman et al 1984) looked at 78 patients with palpable and/or mammographically evident lesions. Since the absolute values of acoustic speed and attenuation for normal tissues had been shown by previous studies to vary considerably between women, they decided to concentrate on relative values, ie the difference in speed or attenuation between normal and suspicious areas within a given breast. Their apparatus consisted of four pairs of single element transducers, allowing the simultaneous acquisition of data for four adjacent coronal slices of the breast. Typically 8 slices were obtained, requiring 5 minutes in total. As well as visual analysis of the images based on criteria already partially established in earlier studies, computer-aided analysis was performed. For each patient, the image slice or slices that were most likely to contain the lesion were selected manually. The computer algorithm then calculated the average and standard deviation of the acoustic speed and attenuation within the boundaries of the breast. Then an area of 3 x 3 pixels with the highest average acoustic speed was located, and the average and standard deviation of the speed and attenuation within this "suspicious" region was calculated. Equivalent values of these 8 parameters were also calculated for a "control" slice, usually from the contralateral breast. These 16 parameters were then used, in conjunction with the pathological diagnoses, to derive discriminant functions for the prediction of carcinoma. The purely visual analysis was found to be quite unreliable, showing in particular a rather low sensitivity of 62.5%, with a specificity of 63.2% (c.f. 92.5% and 34.2% respectively for X-ray mammography with the same patient group). Computer-aided analysis of the UCT images improved the sensitivity to 82.5% (with a specificity of 60.5%), which although encouraging was still significantly below the value for mammography.

Similar results were obtained by Scherzinger et al (1989), who applied quantitative discriminant analysis techniques to acoustic speed and attenuation data from 40 patients with unequivocal clinical diagnoses. They also found that relative acoustic speed and attenuation values gave the best results, achieving a sensitivity of 83% and specificity of 86% in discriminating between cancer and solid benign lesions or cysts. However, they found that their results were not so good in young breasts, where the average acoustic speed is higher. They concluded that transmission UCT in its present form is unlikely to assume a major role in breast cancer detection and diagnosis. However UCT has been shown to add additional information to that obtainable from pulse echo ultrasound, and they proposed that a combined UCT and pulse echo scanner might be the best way forward if one could be constructed that was sufficiently convenient in patient scanning and of sufficiently low cost.

Other potential in-vivo targets other than the breast have been investigated by a limited number of workers. Carson and Scherzinger (1979) were the first to demonstrate that attenuation UCT was possible in sections containing bone when they showed images of an admittedly limited quality of a leg of lamb. Dines et al (1981) looked at the feasibility of using UCT for the diagnosis of intracranial abnormalities. They scanned an infant cadaver head with 5 MHz ultrasound and an adult cadaver head with 750 kHz ultrasound. Initially both acoustic speed and attenuation reconstructions were attempted, but they found that pulse distortion and multipath interference, especially at the skull-brain interfaces, had a particularly severe affect on the time of flight measurements. The attenuation images obtained showed some correlation of general anatomical features with X-ray CT images, especially in the infant head, which they felt warranted further investigation. They noted however more severe artifacts on slices obtained close to the base of the skull, or its vertex, because of the increased amount of bone and its curvature within the scan plane.

3.4 Diffraction tomography

Most of the published work in ultrasound CT, as described in the preceding sections, has been based upon algorithms that had been developed initially for X-ray CT. As such these algorithms are based on assumptions that are valid for X-rays, such as the wavelength of the interrogating radiation being much less than the minimum scatterer size (hence no diffraction) and negligible refraction, with the result that the measured transmitted quantity (ie X-ray intensity) can be considered as a simple geometric projection of the object. As will be discussed fully in a later section (4.2), these assumptions are far less applicable to ultrasonic imaging where the wavelengths are much longer (typically 0.5mm to 1mm) and the acoustic speed may vary by up to 10% in soft tissue alone. The presence of significant diffraction and refraction in the interaction of ultrasound with soft tissue has been shown to cause significant artifacts to arise in UCT images reconstructed using conventional CT algorithms. Although some workers have attempted to overcome the problems of refraction by iterative curved-path algorithms (see 3.3.3), these algorithms assume that the curved paths may be calculated using the principles of geometric optics, and hence still ignore diffraction.

Various researchers have attempted to develop methods for ultrasound CT that include diffraction effects, some of which are described here under the general term of diffraction tomography. The methods generally involve the derivation of analytical solutions to the (usually simplified) wave equation for an incident ultrasonic wave propagating in a scattering medium. The scattering medium is often modelled as small fluctuations about a mean value of one or more acoustic parameters, such as acoustic speed or refractive index (or more fundamentally, compressibility and density). Thus these methods take a quite different approach to reflection and transmission UCT, in that they attempt to model the processes by which the scattered waves are produced from interaction between the incident waves and the object, rather than to model the image forming process itself. The problem in diffraction CT is to reconstruct, by inversion of the wave equation, the distribution of the acoustic parameter from sufficient measurements of the scattered waves, typically with a recording aperture located beyond the scattering medium. Sufficient measurements are obtained by varying the direction of illumination (or equivalently the orientation of the object) and/or its frequency. Unfortunately the wave equation cannot normally be inverted without resorting to various simplifying assumptions, and it is the constraints imposed on the experimental method by these assumptions that ultimately limits the usefulness of diffraction CT and probably explains why so few experimental results have been presented.

Probably the first to apply inverse scattering solutions to the problem of ultrasonic imaging were Mueller et al (1978) and Johnson et al (1978). Two quite different approaches were taken by these two groups, in particular Mueller's group used a narrow-band (ie single frequency) approach while Johnson's used broad-band illumination. Subsequent to the publication of this work, other researchers have tended to adopt one or other of these approaches and these will therefore be reviewed separately.

3.4.1 Narrow band methods

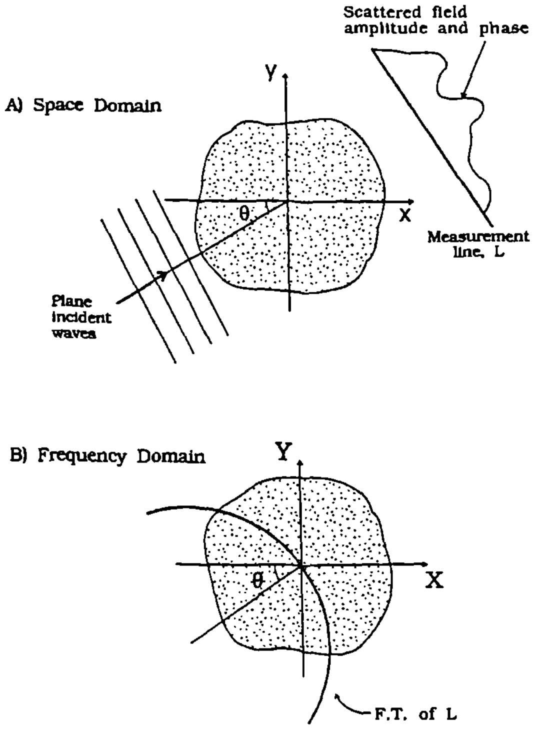

Figure 3.6 Principles of diffraction tomography

Mueller et al (1978) modelled the unknown object as a continuous distribution of varying refractive index. They used a single frequency (ie continuous wave) derivation of the Helmholtz wave equation, and solved the inverse problem of determining the refractive index distribution from measurements of the scattered wave with the assumptions: (1) that the refractive index variations are small thus allowing a first order perturbation (Born) approximation, (2) plane waves are incident on the object, and (3) density variation and attenuation may be neglected. They showed that the 1D FT of the scattered field, measured at points along a line at a given angle with respect to the object (Figure 3.6a), represents an arc (at the same angle) of the 2D FT of the object distribution (Figure 3.6b). Note that this is somewhat different to the standard CT formulation where the 1-D FT of the projection represents a straight line in the frequency space of the object. By measuring the scattered field at many angles with respect to the object (either by rotating the object or the direction of the incident field), they showed that it was possible to reconstruct the object in the frequency domain by interpolation. A 2-dimensional inverse FT then provided the object distribution. However reconstructions of simulated cylindrical inhomogeneities demonstrated that the perturbation approximation breaks down when the refractive index variation is too large.

In a later paper (Mueller et al 1979) they compared the relative merits of the Born approximation and another, similar, first order approximation known as Rytov's approximation. They argued that both are probably equally valid within the constraints they had assumed for the object. They also showed that the Rytov approximation formally reduces to the ray-tracing (ie geometric optics) approach of transmission UCT for the case of a severely band-limited object - ie one for which 1 / (ultrasonic wavelength) is much greater than maximum spatial frequency present, or in other words when the wavelength is much less than the minimum scale of the scatterers. Ball et al (1980) also used the Rytov approximation to derive inverse solutions for both a plane wave source and a spherical wave source, but in this case no results were presented.

Vezzetti and Aks (1979) drew a distinction between the problem of determining the scattered field when the scatterer and incident wave is known - which they called the direct problem, and the problem of determining the scatterer when the incident and scattered fields are known - the inverse problem. They argued that, while the direct problem may have a unique solution under very general conditions, the inverse problem only has a unique solution under quite restrictive conditions which may be impossible to achieve in practice. Inevitably, in order to obtain a practical inverse solution the direct problem must be simplified. The Born approximation is one such example of a simplification of the direct problem that has a simple inverse solution. They explored the conditions for validity of the Born approximation. Theoretically, in order to apply the Born approximation to the Helmholtz equation the following assumptions must be made: weak reflection; weak scattering and absorption; weak refraction; the phase of the assumed scattered wave must not differ from phase of the true wave by more than wavelength/2 - this is likely to be violated at high frequencies. Using simulated data for simple targets (such as a sphere) which possess an exact analytical solution for comparison, they determined the accuracy of the Born approximation for objects of various degrees of refractive index contrast. They showed that, as expected, the approximation breaks down at high spatial frequencies, particularly for high contrast objects. They also looked at the effects of scattering angle on the accuracy of the reconstructions, and found that the best results were obtained for angles other than near 180° (backscatter) or near 0° (forward scatter) - the scattering angles most commonly used for diffraction tomography experiments. To overcome some of the problems of the Born approximation due to the restrictive assumptions required, they proposed an iterative procedure whereby an initial reconstruction of the refractive index is obtained by the standard Born method, while subsequent reconstructions are obtained by approximating the field inside the scatterer by the incident field whose phase has been modified by the local refractive index (obtained from the previous reconstruction). Using this method they demonstrated improved reconstructions of a simulated spherical target.

Modifications to the simple Helmholtz equation to allow for density (as well as compressibility) fluctuations were introduced as early as 1980 by Mueller (1980). He used a perturbation method to derive an inhomogeneous wave equation, under both Born and Rytov approximations, but an inverse solution was not presented. Much later Robinson and Greenleaf (1986) demonstrated by simulation and experiment that density fluctuations can probably be justifiably neglected in soft tissues. In this paper they also explored the general validity of the time-independent Helmholtz equation itself - ie the direct problem for ultrasound diffraction tomography. They argued that the following assumptions must be made for the wave equation to be valid; (i) wave propagation must be linear, (ii) scattering must be isotropic, (iii) absorption per wavelength must be small enough to allow its effects to be assigned solely to the imaginary part of the refractive index, and (iv) the scattering object must be unable to support shear stress. They proposed that (iii) and (iv) are probably valid in soft tissue, but that non-linear propagation and anisotropy have been clearly demonstrated (see also 3.3.1). To test their arguments the scattered fields from cylinders with various scattering properties were determined both by simulation and from actual experimental measurements. Cylinders were chosen because, within the assumptions discussed above, an exact solution for the scattered wave is known to exist. The experimental conditions were such that non-linear propagation and anisotropy could be neglected. It was observed, as previously by Anderson and Adams (1982), that the main problem with the experimental requirements was obtaining a plane incident wave. Simulation and experiment were shown to agree closely, hence validating the assumptions required for solution of the direct problem.

Having established that the scattered field calculated from the homogeneous Helmholtz equation agreed well with measured data, Robinson and Greenleaf used this simulated (ie noise free) data from cylinders to test reconstruction algorithms based on either the Born or Rytov approximations. The real part of the reconstructed refractive index was assumed to represent the distribution of acoustic speed, and the imaginary part the distribution of acoustic absorption. They showed that both the Born and the Rytov methods produce more accurate reconstructions than a conventional "straight path" CT algorithm applied to the same data, although they pointed out that one would normally use localised (ie narrow) beams for UCT rather than plane waves. The Rytov reconstructions appeared to offer the best geometrical and quantitative accuracy (except at the cylinder boundary), particularly in objects where the acoustic speed variations were large. The Born reconstructions in this case tended to show considerable cross-talk between real (speed) and imaginary (absorption) parts. However problems did arise with the Rytov approximation when the object exhibited high absorption (10 dB/cm at 1 MHz). In this case the reconstructed values of speed and absorption fluctuated wildly, while the Born reconstruction was marginally more recognisable. It was suggested that this might be because the phase unwrapping, required for the Rytov method, was performed incorrectly. They concluded that the future of diffraction tomography may lie with alternative higher order iterative techniques.

Devaney (1982) developed a space domain approach for the reconstruction of an object distribution. They pointed out that with the conventional method (eg Mueller et al 1978, see above) the image must first be formed in the spatial frequency domain by interpolation of the measured data (representing arcs in frequency space) onto the square grid required for the inverse 2-D FFT, a process which is inherently prone to noise and also requires extreme accuracy in the registration of data from different angles. They proposed an alternative algorithm which they called filtered backpropagation, based on the Born or Rytov approximations and plane-wave insonification but not requiring any frequency domain representation. Backpropagation essentially involves assigning secondary sources to the measurement plane according to the amplitude of the measured scattered wave and its normal gradient. Waves from these secondary sources are then computationally propagated back through image space while being modified by a depth dependent filter. They showed that their filtered backpropagation algorithm is completely analogous to the filtered backprojection algorithm of conventional transmission UCT, and that it reduces exactly to the filtered backprojection algorithm when the wavelength is allowed to approach zero. In a later paper (Devaney and Beylkin 1984) the theory was extended to include reconstruction algorithms for transmitters and/or receivers positioned on arbitrary surfaces enclosing the object. Rouseff et al (1988) proposed a modified form of the plane wave backpropagation algorithm that did not require the time consuming step of calculating the backpropagated field from every view direction for every point in the image. They showed that provided the ultrasound wavelength is significantly smaller than the minimum spatial scale of the object, then the backpropagated field is a simple geometric projection of the scatterer in the plane normal to the plane wave illumination. Hence the object can be reconstructed from the field calculated at this plane by standard filtered backprojection techniques.

In an attempt to overcome the practical problem of mechanical accuracy in transducer positioning Witten et al (1988) discussed a conceptual diffraction tomography system which utilised a fixed, circular configuration of transmitters and receivers. This approach would also allow the problems of phase jitter due to movement induced vibrations in the transducers to be eliminated, and scan times to be reduced hence minimising patient movement artifacts. The reconstruction algorithm was based on the typical single frequency, constant density and Born approximation approach, with solutions derived especially for the circular geometry. The algorithm was tested using synthetically generated data from discs possessing different acoustic speeds imbedded in a larger disc. They also proposed a method for generating separate images of compressibility and density by collecting data at two different frequencies. They appear, as yet, not to have published results from a practical implementation of the circular array system described.

3.4.2 Broad band methods

One probable advantage of using broad-band illumination instead of narrow-band (or CW) sources is that the time dependence of the measured scattered waves should provide additional information to that obtained by simply varying the spatial position of the measurements. Also, broad-band pulses are easier to generate than CW illumination because of problems with reverberation and multiple-scattering effects. Having realised these potential advantages, several researchers have derived solutions to the inverse scattering problem for the case of broad-band illumination.

Johnson et al (1978) assumed that the object could be represented by an unknown distribution of independent, isotropic point scatterers. The value of the ultrasound field at each scatterer was assumed to be given by the unperturbed incident field - the essence of the Born approximation. Making these assumptions for the interaction of the incident wave with the object, the problem of finding the locations of the point scatterers from measurements of scattered waves at many angles (ideally over a full 360°) has an exact analytical solution. Equivalent results are obtained if the scattered waves are measured at many angles about a fixed object, or if the object is rotated within a fixed measurement geometry. The solution of the equivalent discrete form by an iterative matrix inversion technique (similar to ART in conventional CT) was shown to be easier when the incident wave was taken to be an impulse (ie a very broad bandwidth pulse). A solution was also found for the case where the model was extended to include attenuation. The algorithm was tested with a simulated noise-free distribution of 6 point scatterers, and assuming that the sources and receivers were coincident - ie only backscattered waves were considered. Thus the data is identical to that acquired in broad-beam reflection UCT, and they compared their results to a backprojection reconstruction method (described in 3.2) which they called synthetic focusing. They suggested that the iterative ART-like method may be more suitable than backprojection when non-enclosing (ie less than 360°) apertures must be used.

Norton and Linzer (1981) obtained a 3-dimensional solution for the distribution of ultrasonic reflectivity from measurements of backscattered waves only. The incident waves were generated by broad-band spherical wave (ie point) sources distributed on a 2-dimensional (plane, spherical or cylindrical) surface. They showed that as long as the scattering is weak enough for the Born approximation to apply, absorption is neglected, and only backscattering is considered, then the mathematics of the inverse scattering problem are greatly simplified and solutions can be obtained that do not rely on the measurements being made in the far-field. This represented a great advantage over many previous methods, since the far-field requirement implies large imaging distances which may be impractical in a clinically acceptable system.

The solutions derived by Norton and Linzer make use of the fact that measurements made (as a function of time) at each source-receiver may be regarded, assuming a constant (to first order, ie Born approx.) acoustic speed for the scattering medium, as equivalent to surface integrals of the reflectivity of the medium over concentric spherical surfaces (with radius varying as a linear function of time) centred at the source-receiver point. Note that this formulation is very similar to that assumed by Norton and Linzer, and others, for reflection UCT (see 3.2), where the 2-dimensional reflectivity distribution is reconstructed by filtered backprojection and summation along circular arcs. Norton and Linzer showed that the 3-dimensional reflectivity distribution can also be reconstructed by backprojection and summation, but this time over spherical surfaces and without the need for additional filtering. The $(1/r)^2$ filtering normally required for 3-dimensional CT reconstruction (c.f. $1/r$ filtering for 2-D CT) is not required in this case because it is already provided by the $(\text{frequency})^2$ dependence of scattering obtained with the Born approximation. The main limitation of the method is that no allowance is made for variation of the acoustic speed within the object. Any such variations would mean that the integration could no longer be assumed to be over perfectly spherical surfaces.

In a later paper Norton (1983) showed theoretically that the use of broad-band plane-wave insonification allowed separate images of density and compressibility to be obtained. Two large area rectangular transducers were required, one to provide the incident plane waves and to measure the backscattered waves, and another placed at a fixed angle (typically 90°) with respect to the source to act solely as a receiver for waves scattered through this angle. To obtain sufficient measurements for reconstruction, both transducers are rotated together through 180° about the scattering object. The basic principle of their reconstruction method is that far-field scattering from an infinitesimal density variation is known to be dipole-like, whereas scattering from a compressibility variation is monopole-like. Using large area transducers allows the measurements to be obtained in the near-field because wave components that have only been scattered through a known angle can be selected. For example, assuming weak (ie Born) scattering and no absorption, measurements at a scattering angle of 90° will not include any contributions from density scatterers, whereas measurements of backscattered waves will include equal contributions from density and compressibility scatterers. Combination of these two measurements allows the contributions to be separated. The method again assumes that the incident plane wave is not significantly distorted by acoustic speed variations within the scattering medium, and unfortunately no experimental results were presented.

3.4.3 Experimental results

Of the few early researchers into diffraction CT to present experimental results from real targets were Adams and Anderson (1980). Their method was based on measurements of backscattered continuous waves at points along a line in the Fresnel region of the object, where the object was modelled as a 2-dimensional collection of independent, isotropic point scatterers. Derivation of the reconstruction algorithm followed a different line to that of Mueller's group, the main differences being due to the spherical wave insonification and near-field measurements of Adams and Anderson. Also, the reconstruction was performed directly in the space-domain by backpropagation and deconvolution in a method similar to that of Devaney (1982). Images of limited quality obtained with 1 MHz insonification were presented of an object consisting of four metal rods in water.

Rather more encouraging results were obtained by the same group (Anderson and Adams 1982) using a more conventional approach with forward scatter measurements. The object was modelled this time by a 3-dimensional distribution of varying compressibility, with as usual constant density and negligible attenuation assumed. Measurements of the scattered waves were made over a (ideally infinite) plane located beyond the scattering object. A reconstruction algorithm was developed, based on the Born approximation and implemented in the space domain by backpropagation and deconvolution. Similarly to most of the diffraction CT techniques, plane wave insonification was assumed. This is difficult to achieve experimentally, and so the actual incident wave was measured first without the object present and the measured scattered data normalised according. Quite impressive images were presented of 1mm wires in water using 5 MHz ultrasound, were a resolution of about 2mm was apparently achieved. A block of reticulated polyurethane foam containing imbedded holes and wires was also imaged, this time with 1 MHz ultrasound to reduce attenuation. Separate images reconstructed from amplitude and phase measurements demonstrated considerable structure, and they suggested that the phase image may represent the attenuation distribution of the object (ie assuming a complex compressibility).

Sponheim and Johansen (1991) used a fixed, 4 MHz, 20 cm wide rectangular source transducer, and rotated the object. The receiving hydrophone, located beyond the object, was scanned laterally at a distance of 78 mm from the centre of the object. All measurements were corrected, for differences between the actual illuminating field and the plane wave assumed by the reconstruction algorithm, by measuring the field without the object present. The signal from the hydrophone was separated into real and imaginary parts to allow separate reconstructions of acoustic speed and attenuation. Image reconstruction was by backpropagation as described by Devaney (1982). Images obtained of acrylic and brass rods and rubber tubes were not very impressive, especially in terms of the quantitative accuracy of the acoustic speed images. It was suggested that the main problems were due to the scattering being too strong (due to failure of the Born approximation), and the requirement that the mechanical apparatus should be accurate to fractions of a wavelength (ie tens of μm).

Several groups have compared reconstructions obtained with diffraction tomography methods to those obtained with the conventional "straight-path" transmission UCT methods. Jones and Meng (1988) constructed a gelatine phantom containing regions in which the acoustic speed was known *a priori* to an accuracy of ± 2 ms^{-1}. They compared the quantitative accuracy of acoustic speed reconstructions obtained using the following methods; standard transmission UCT using straight-path backprojection, UCT with iterative ray-tracing (see 3.3.3), and a backpropagation method of diffraction tomography using the Rytov approximation. The ray-tracing approach appeared to give the most accurate results, the average error in acoustic speed being just less than 0.15% compared to about 0.20% for both of the other methods, but also took approximately five times as long to compute.

Robinson and Greenleaf (1989) used a tissue mimicking breast phantom and compared a Fourier-domain (Born) diffraction method to straight path UCT (both attenuation and acoustic speed), taking particular care to avoid experimental measurement errors such as mechanical mis-registration and imperfections in the transmitting and receiving transducers. Despite the fact that the Born approximation was clearly violated, evidenced by measured phase shifts in the incident wave of more than pi radians, the real and imaginary parts of the diffraction tomogram appeared to show better resolution and less artifact than either of the UCT images. However, because of the violation of the Born approximation and the consequent "cross-talk" between the real and imaginary parts of the diffraction image, no quantitative information about speed or absorption was available from the diffraction reconstructions.

3.5 A comparison of ultrasound CT methods

It is clear from this review that a great deal of research has already been conducted into ultrasound CT, and that there are many possible approaches requiring different measurement apparatus and providing different information about soft tissue. In order to establish which of these techniques would benefit most from further investigation, it is useful to summarise this review by comparing the techniques in terms of their main advantages and disadvantages.

1) Reflection UCT

Advantages

* The technique is similar in principle to the well established technique of compounding and is thus relatively easy to understand.
* Various approaches are possible which require different assumptions and different measurement apparatus, but in general the requirements for a practical system are not insurmountable and in most cases conventional B-scan imaging equipment can be used.
* The technique is based on backscatter (pulse-echo) measurements where the potential resolution is limited mainly by the ultrasound pulse length. Since the pulse length is typically a third or a quarter of the beam width, the potential resolution is better than for the transmission UCT methods.

Disadvantages

Reflection UCT, based as it is upon pulse-echo measurements, suffers from some of the limitations of conventional B-scan imaging, although they generally have a less serious affect on image quality. These limitations are:-

- The images are not inherently quantitative because of attenuation and non-linear processing of the back-scattered data.
- The technique takes no account of diffraction, so that the images are degraded by speckle (see next chapter).
- Specular reflection is also not accounted for but, particularly in the case of the narrow-beam methods, this may not detract severely from image quality since all interfaces should be visualised.
- The acoustic speed within the target is assumed to be known and constant. The effects of any failure of this assumption are even more serious for reflection UCT images than they are for B-scan images.

2) Transmission CT

Advantages

- This is very similar in principle to X-ray CT so the same or similar reconstruction algorithms can be used.
- The assumptions required do not place particularly severe constraints on the design of practical systems.
- The image quality obtained is not so dependent on the validity of the assumptions as it is for diffraction CT, mainly because some resolution is effectively imposed on the images by the use of narrow interrogating ultrasound beams (ie similar to collimation in X-ray and radioisotope imaging). More fundamentally, transmission (and reflection) UCT uses relatively large transmitter and receiver apertures and focusing to impose directivity, whereas diffraction CT uses broad plane waves and point receivers with no inherent directivity.
- In appropriate situations (eg low attenuation and acoustic speed variations) the images, particularly of acoustic speed, can show reasonably good quantitative accuracy.

Disadvantages

- The image quality does deteriorate markedly in the presence of significant refraction, due to the failure of the straight path assumption.
- The technique takes no account of diffraction. This assumption is particularly limiting for attenuation imaging.
- The resolution is ultimately limited by the width of the ultrasound beams, which is in general

several times the pulse length and an order of magnitude larger than the wavelength.

3) Diffraction CT

Advantages

- Diffraction CT can be considered the most "fundamental" approach in that it is based upon a theoretical model that makes the fewest assumptions about the interaction of ultrasound with tissue.
- In principle, diffraction limited resolution (ie limited only by the wavelength) can be achieved since diffraction is accounted for.
- The technique is also potentially quantitative, with the possibility of imaging truly fundamental tissue properties such as density and compressibility.

Disadvantages

- The image quality in diffraction CT is very sensitive to the accuracy of the few assumptions that are made, due mainly to the necessity of using the exact phase of scattered waves in the reconstruction. Some of these assumptions may not be valid even in soft tissues, resulting in phase distortion of the waves. For example the Born approximation, which underlies virtually all of the techniques, assumes low scattering which will not be valid in the presence of any specular reflectors, and in most approaches attenuation is ignored which is clearly not valid.
- These techniques also place the most stringent requirements on the measurement apparatus since plane-wave assumptions are usually inherent in the model and very accurate recording of phase information is required.
- Even when reasonable experimental results for soft tissue structure have been achieved (eg Robinson and Greenleaf 1989), the images are not quantitative due to violation of the assumptions.
- Further theoretical work is still required to establish the most suitable model for the interaction of ultrasound with soft tissue.

In conclusion, previous research has shown that, of the UCT techniques, reflection UCT can generate images of soft tissue which show the best resolution and fewest artifacts. However variations in the acoustic speed in the target have been shown to seriously reduce image quality. Transmission

UCT has potential, but will probably never achieve the accuracy and precision required for diagnosis. Although diffraction CT has the potential for the best resolution of all, the techniques developed so far place virtually impossible demands on the apparatus and practical results have in general been disappointing. Consequently it was decided that this project would concentrate on developing systems for reflection and transmission UCT to investigate whether these techniques can be improved.

4 A Theoretical Analysis of Ultrasound Computed Tomography

4.1 Introduction

The primary objective of this Chapter is to explore the theoretical basis of those UCT techniques discussed in Chapter 3 which appeared to show the most promise, namely reflection and transmission UCT. In particular an attempt will be made to compare with conventional B-scanning the quality of the images generated by these techniques. One of the most important aspects of image quality is spatial resolution. Assuming that the image formation processes are linear, then the resolution can be compared, for any target, by considering the image produced by a single point target - known as the point spread function (psf). It will be shown in 4.3 that, by making certain assumptions whose validity will be discussed fully, the image formation process is approximately linear for B-scanning, for reflection UCT and for transmission UCT, thus allowing expressions for the psfs to be derived.

A comparison of these psfs, and a discussion of the consequences for the potential resolution of the ultrasound imaging techniques, will be presented in section 4.4. Optical transfer functions, the Fourier Transform of the psf, are also discussed because in some cases they give a deeper insight into the relative advantages and limitations of the imaging techniques considered here.

Comparing ultrasound imaging techniques solely in terms of spatial resolution is insufficient. One reason for this is that any measure of spatial resolution is affected by the level of noise in the images. Also, another important aspect of image quality is contrast resolution - ie the ability to discriminate between two regions solely on the basis of their mean backscatter level. Contrast resolution will also be affected by noise in the images. Other aspects of image quality, which may have an influence on both spatial and contrast resolution, include various image artifacts which arise from failure of some of the assumptions used in deriving the linear image formation models (required for the derivation of psfs). All of these other factors determining relative image quality will be discussed in section 4.5.

We start by deriving fundamental equations describing the propagation of ultrasound waves in soft tissues.

4.2 Ultrasound propagation in soft tissue

Ultrasonic imaging, whether it be pulse-echo B-scanning or the various forms of ultrasound CT, represents an attempt to form a map of some property of a medium from measurements of ultrasonic waves which have propagated through and interacted with that medium. Thus to discover which properties of the medium can be imaged, an understanding of the ways that an ultrasound wave interacts with the medium and equations to describe this interaction are required.

Various assumptions are generally made to obtain a tractable solution for an ultrasound wave propagating in a soft tissue medium. The most important of these are the following:-

(a) It is normally assumed that shear waves may be neglected, an assumption that is probable valid since at diagnostic frequencies shear waves are known to be very strongly attenuated by soft tissue (Duck 1990).

(b) Absorption affects may be separated and propagation considered to be lossless, at least initially. Such an assumption is acceptable when deriving equations for the scattering of ultrasound provided that the absorption per wavelength is negligible, because the effects of absorption can then be assigned solely to the imaginary part of the refractive index (Robinson and Greenleaf 1986). Since the wavelength of 3MHz ultrasound in soft tissue is about 0.5mm with an absorption over this distance of typically less than 1.5%, this assumption appears to be valid. Absorption can then be introduced later as a simple modification to the equations.

(c) The neglect of absorption, and the additional assumption of small amplitude waves, also allows for the derivation of linear equations. Justifying this assumption is a little more difficult, since for example non-linear affects are known to occur in water due to the different propagation speeds of the compression and rarefaction phases of the wave. This effect causes a 'steepening' of the wave front, with energy being transferred into higher frequency harmonics of the wave. Fortunately the frequency dependence of attenuation in soft tissues serves to inhibit non-linear propagation, so that this assumption can probably be retained in most practical situations with which we will be concerned.

With these assumption in mind it is possible (Morse and Ingard 1968) to derive an expression for an ultrasound wave $P(\underline{r})$ propagating in a medium of uniform density ρ_0 and compressibility κ_0, imbedded in which is an inhomogeneity R of density $\rho(\underline{r})$ and compressibility $\kappa(\underline{r})$ which will act as a source of scattered waves (Figure 4.1). The following equation is valid both inside and outside R

$$\nabla^2 P(\underline{r}) - \frac{1}{c_0^2}\frac{\partial^2 P(\underline{r})}{\partial t^2} = \frac{\gamma_\kappa(\underline{r})}{c_0^2}\frac{\partial^2 P(\underline{r})}{\partial t^2} + \nabla.[\gamma_\rho(\underline{r}).\nabla P(\underline{r})] \qquad (4.1)$$

where γ_ρ and γ_κ are the fractional changes in density and compressibility between the inhomogeneity and the surrounding medium,

$$\gamma_\rho(\underline{r}) = \frac{\rho(\underline{r})-\rho_0}{\rho_0}, \qquad \gamma_\kappa(\underline{r}) = \frac{\kappa(\underline{r})-\kappa_0}{\kappa_0}$$

and $c_o^2 = 1/\rho_0\kappa_0$ is the propagation speed of the wave in the surrounding medium.

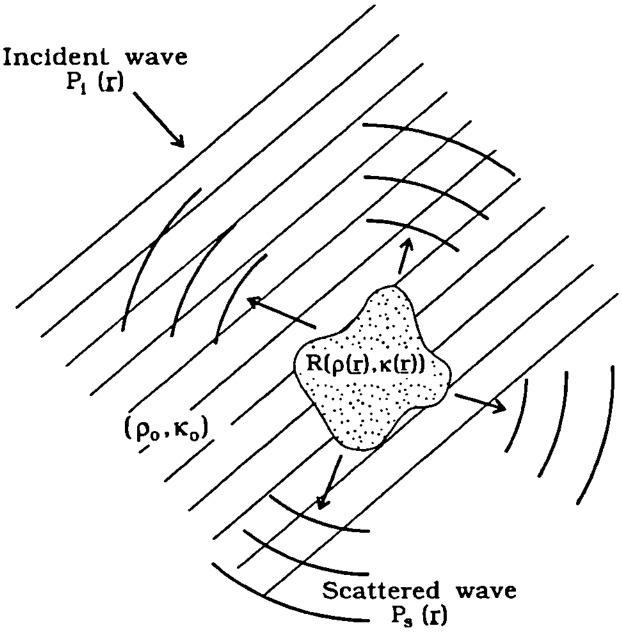

Figure 4.1 Scattering from an inhomogeneity

This equation can be further simplified by the additional assumption that the density variations may be ignored or are negligible. This assumption has been investigated by Robinson and Greenleaf (1986) who found that in most soft tissues compressibility variations are much more significant than density variations and therefore dominate scattering. In this case equation 4.1 simplifies to

$$\nabla^2 P(\underline{r}) - \frac{1}{c_0^2}\frac{\partial^2 P(\underline{r})}{\partial t^2} = \frac{\gamma_\kappa(\underline{r})}{c_0^2}\frac{\partial^2 P(\underline{r})}{\partial t^2}$$

Consider a single frequency (continuous wave) solution.

$$ie \quad P(\underline{r},t) = P(\underline{r})\, e^{i\omega t}$$

$$\nabla^2 P(\underline{r}) + k_0^2 P(\underline{r}) = -k_0^2\, \gamma_\kappa(\underline{r})\, P(\underline{r}) \tag{4.2}$$

$$\text{where} \quad k_0^2 = \frac{\omega^2}{c_0^2}$$

As shown in Figure 4.1, the total pressure field P($\underline{r}$) at any point $\underline{r}$ is the sum of the incident field $P_i(\underline{r})$ and the scattered field $P_s(\underline{r})$

$$\text{ie} \quad P(\underline{r}) = P_i(\underline{r}) + P_s(\underline{r}) \tag{4.3}$$

Since the incident field P_i must satisfy the homogeneous Helmholtz equation

$$\nabla^2 P_i(\underline{r}) + k_0^2\, P_i(\underline{r}) = 0$$

equation (4.2) becomes

$$\nabla^2 P(\underline{r}) + k_0^2 P(\underline{r}) = -k_0^2\, \gamma_\kappa(\underline{r}) \left[P_i(\underline{r}) + P_s(\underline{r})\right]$$

This equation can be converted into integral form using (Morse and Ingard 1968) the Green's function for free space, with the result

$$P_s(\underline{r}) = \frac{k_0^2}{4\pi} \int_{V'} \left[P_i(\underline{r}') + P_s(\underline{r}')\right] \gamma_\kappa(\underline{r}')\, \frac{e^{ik_0|\underline{r}-\underline{r}'|}}{|\underline{r}-\underline{r}'|}\, dV' \tag{4.4}$$

If it is further assumed that the scattering is weak (the well known Born approximation) so that the field within the scatterer is dominated by the incident field

$$\text{ie} \quad P_s(\underline{r}) \ll P_i(\underline{r})$$

then equation (4.4) may be simplified to

$$P_s(\underline{r}) = \frac{k_0^2}{4\pi} \int_{V'} P_i(\underline{r}')\, \gamma_\kappa(\underline{r}')\, \frac{e^{ik_0|\underline{r}-\underline{r}'|}}{|\underline{r}-\underline{r}'|}\, dV' \tag{4.5}$$

This single frequency solution shows that, when irradiated by an incident field $P_i(\underline{r})$, each inhomogeneity gives rise to a scattered wave which radiates spherically outward with a field amplitude proportional to $k_o^2 P_i \gamma_\kappa$. The total scattered field is then just the coherent sum of the scattered waves from all the inhomogeneities within the object. Multiple frequency (ie pulsed field) solutions can also be derived by linear summation of the single frequency solutions. This basic equation will now be used in deriving image formation models and point spread functions for each of the ultrasonic imaging techniques of interest here.

4.3 Derivation of point spread functions

Using equation (4.5) as a starting point, linear image formation processes will be derived for B-scanning and for UCT which will eventually lead to linear equations for their respective point spread functions.

4.3.1 B-scan point spread function

4.3.1.1 Introduction

The first stage in deriving a point spread function for conventional B-scan imaging is to construct a suitable model for how such an image is formed. For the point spread function to have meaning, the model must obey the principles of linear superposition - ie it must be a linear model. It will be shown that, within certain limits, such a model can be derived for B-scanning.

4.3.1.2 Linear model for B-scan imaging

All 2-dimensional B-scan images, whether formed by a linear array or a mechanically moved single-element transducer, are composed of a set of lines of ultrasonic echo data known as scan lines. In the particular case of linear arrays these scan lines are parallel. Each scan line represents a plot of echo (ie back-scatter) amplitude against the go-return time of the pulse for one particular location of the transmitting-receiving transducer aperture. Assuming a constant known acoustic speed in the target, the scan line data may be considered to be a plot of echo amplitude against range from the transducer. Thus in order to characterise a B-scan image, the relationship between a scan line measured from a particular target and the target itself must be defined.

Equation (4.5) showed that the scattered wave from a region of varying compressibility is given simply by a linear summation of scattered waves, the scattered wave amplitude being proportional to the incident pressure field $P_i(\underline{r})$. In B-scan imaging the incident pressure wave is typically a short pulse generated by an ultrasound transducer, with the same transducer receiving the backscattered waves (or echoes) and converting the integrated pressure across the surface into an electrical signal A(t). To derive a linear expression relating the received signal to the object, several assumptions, additional to those made in section 4.2, will be made concerning both the transducer and the target (justifications for these will be discussed later in 4.3.1.3):-

a) The compressibility distribution may be represented (as in Figure 4.2) by a 2-dimensional distribution of independent isotropic point scatterers s(x,y). This is known as the discrete scatterer model (Dickinson 1986), and is equivalent to representing each compressibility inhomogeneity (R in Figure 4.1) by a delta function. In this case equation (4.5) represents a linear convolution between the incident field and the scatterer distribution s(x,y). For a B-scan image in which only backscattered waves are detected, s(x,y) can be thought of (Bamber and Dickinson 1980) as the 2-D distribution of acoustic reflectivity.

b) The problem is purely 2-dimensional, ie the ultrasonic beam and target have zero extent out of the x-y plane.

c) Multiple scattering is negligible.

d) Only plane waves are incident on the target distribution, so that all scatterers at the same range from the transducer receive the pulse at the same time. This can be effectively achieved if the targets are all in the far-field (or focal region) of the transducer. This also ensures that the echo wave-fronts from the scatterers are effectively plane waves by the time they are received by the transducer.

e) The intervening medium between the transducer and the scatterers has a uniform speed of sound at all ranges and across the full width of the ultrasonic beam, so that no distortion of the transmitted or echo wave-fronts occurs.

f) No non-linear processing has been applied to the echo data.

g) Attenuation can be neglected.

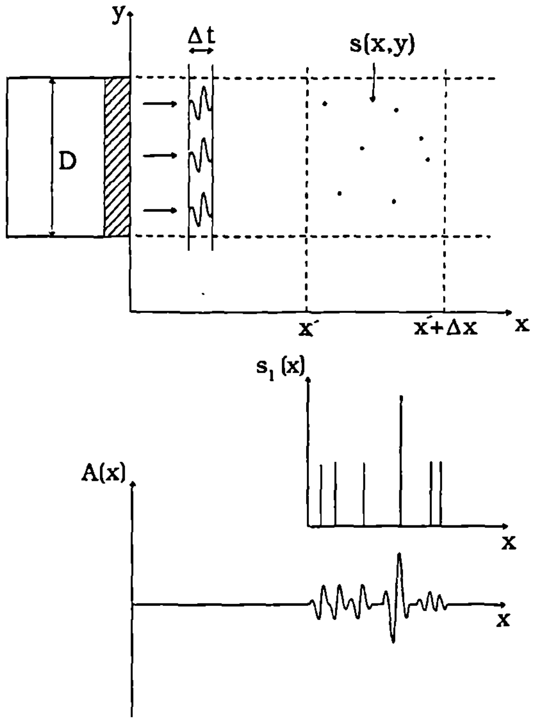

Figure 4.2 The formation of a scan line

Consider the situation represented in Figure 4.2. This shows a wide aperture transducer emitting a short ultrasonic pulse of length (Δt), and receiving echoes from a region of the scattering distribution s(x,y) lying between x and x+Δx, where x = c.t/2, and c and t are the acoustic speed and the go-return time of flight respectively. Note that since the incident field is a plane wave with no variation in the pressure field in the y-direction (ie across the beam), the 2-D object distribution s(x,y) can be represented by its lateral sum (or projection) given by

$$s_l(x) = \int_{-\infty}^{\infty} s(x,y)\ dy \qquad (4.6)$$

If assumptions (a) to (g) hold, and assuming that any modification of the backscattered ultrasound pulse by the electro-mechanical properties of the transducer is also linear, then using equation (4.5) it can be shown (see for example Fatemi and Kak, 1980) that the rf echo signal as a function of range A(x) can be represented by a linear convolution between the rf echo $h_a(x)$ from a single point scatterer and the function s(x,y).

$$ie \quad A(x) = \int_{-\infty}^{\infty} s_l(x') \ .\ h_a(x-x')\ dx'$$

or using (4.6)

$$A(x) = \int_{-\infty}^{\infty} \{ \int_{-\infty}^{\infty} s(x',y)\ dy \}\ h_a(x-x')\ dx' \qquad (4.7)$$

The function $h_a(x)$ takes account of the scaling terms (e.g. k^2 and 1/r) in equation (4.5) as well as the electro-mechanical properties of the transducer, while its extent is determined primarily by the ultrasound pulse length. Although it may be possible to derive an expression for this function (Fatemi and Kak 1980), such an expression is not needed here because $h_a(x)$ can be measured experimentally (see Chapter 5).

Consider now a more realistic situation where the ultrasound beam is not uniform, but rather is represented by the function $h_l(y)$. Equation (4.7) now becomes

$$A(x) = \int_{-\infty}^{\infty} \{ \int_{-\infty}^{\infty} s(x',y)\ .\ h_l(y)\ dy \}\ h_a(x-x')\ dx'$$

In practice the extent of $h_l(y)$ (ie the beam width) is determined by the aperture width *D* and by the degree of focusing imposed in both transmission and reception. An rf B-scan image b(x,y) (Figure 4.3) is simply composed of a set of scan lines obtained at adjacent lateral positions (ie along y). In a linear array these scan lines are obtained by electronic switching of an active sub-group (width *D*)

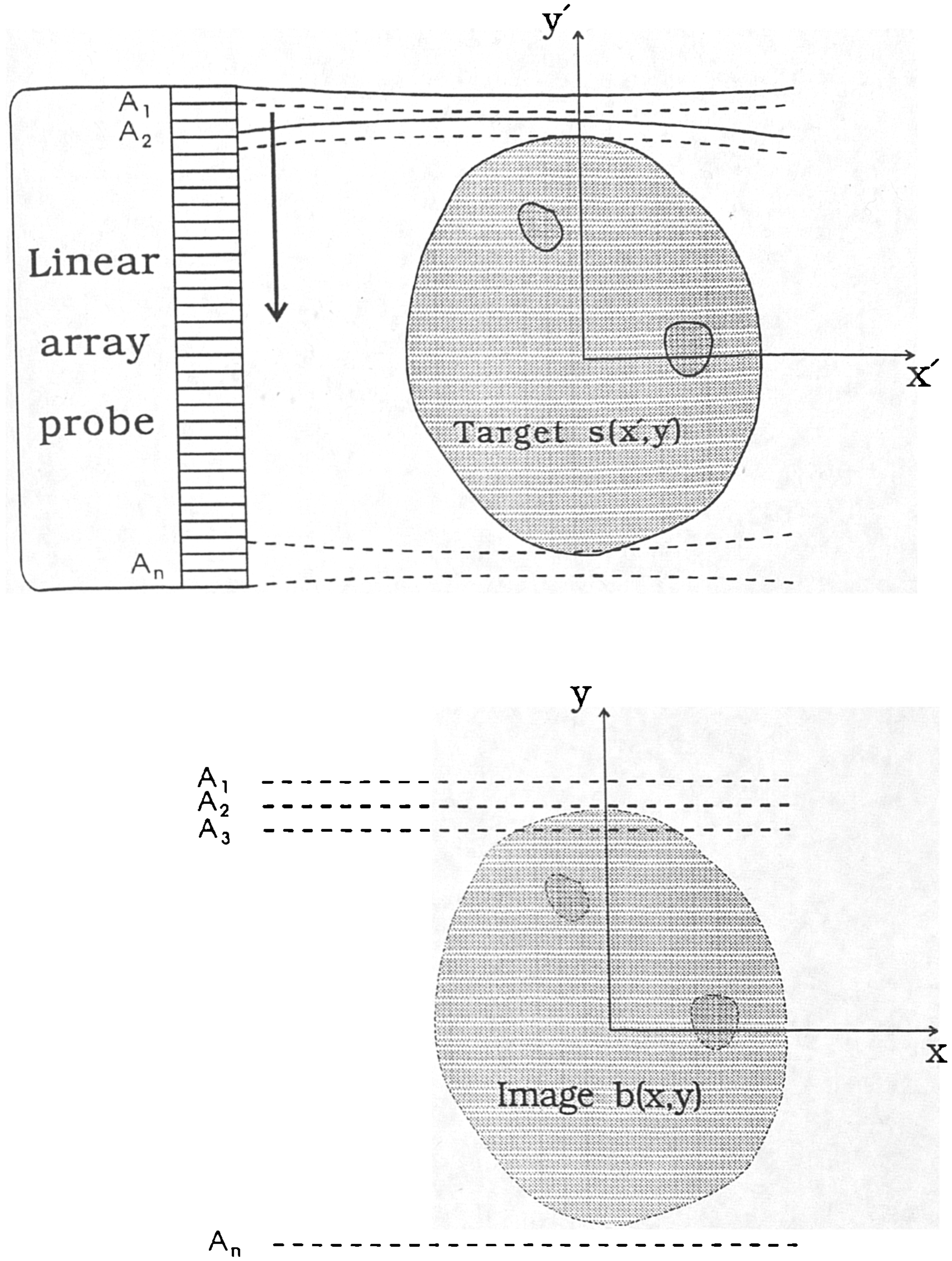

Figure 4.3 The formation of a B-scan image from scan lines

of transducer elements. Assuming that the beam steps are infinitesimally small (in practice sampling considerations would stipulate that a beam stepping of less than half the beam width is sufficient), then b(x,y) is given by

$$b(x,y) \quad = \quad \int_{-\infty}^{\infty}\int_{-\infty}^{\infty} s(x',y').h_l(y-y').h_a(x-x')\ dy'dx'$$

Defining the function h(x,y)

$$h(x,y) \quad = \quad h_a(x)\ .\ h_l(y) \tag{4.8}$$

leaves

$$b(x,y) \quad = \quad \int_{-\infty}^{\infty}\int_{-\infty}^{\infty} s(x',y').h(x-x',y-y')\ dx'dy' \tag{4.9}$$

The function h(x,y) may be thought of as the rf B-scan psf, ie the rf image obtained from a single point scatterer. The functions $h_a(x)$ and $h_l(y)$ are then the axial and lateral components respectively of the psf. Thus it has been shown that an rf B-scan may be represented by a simple 2-dimensional linear convolution between the object function s(x,y) and the rf B-scan psf h(x,y).

$$ie \quad b(x,y) \quad = \quad s(x,y) \ *\ *\ h(x,y)$$

A similar expression can be defined for the spatial frequency domain which relates the frequency content of the image B(X,Y) to the frequency content of the object S(X,Y)

$$B(X,Y) \quad = \quad S(X,Y)\ .\ H(X,Y)$$

where H(X,Y) is called the optical transfer function (OTF) and is given by the Fourier Transform of the point spread function.

4.3.1.3 Validity of the assumptions of the model

Using linear imaging theory, a model has been derived for the formation of a B-scan image which is based on various assumptions. The validity of these assumptions will now be examined for a realistic imaging situation.

a) Object can be represented by point scatterers

This assumption has been explored by various researchers (e.g. Fatemi and Kak 1980, Bamber and Dickinson 1980), who have generated theoretical and computer models of tissue as a collection of randomly positioned independent isotropic point scatterers. The simulated B-scan images thus obtained have shown strong similarities to real B-scan images of human tissue. However these models do not account very well for interfaces between media of different acoustic impedance where the extent of the interface is considerably greater than the wavelength of the interrogating ultrasound. Such interfaces will give rise to specular reflections for which the laws of geometric optics apply - ie the angle of reflection equals the angle of incidence. Hence the scattering is far from isotropic and only those interfaces that are nearly perpendicular to the ultrasound beam will be detected on a B-scan.

b) No ultrasonic beam out of x-y plane

All practical transducers generate a 3-dimensional field, and hence a B-scan image inevitably contains echo information from targets outside of the x-y plane of the scan. This will of course limit the resolution of targets within the scan plane, and is particularly a problem if very strong scatterers or reflectors (such as bone) are located just outside the scan plane. The problem is not so severe if the target contains few strong scatterers (such as a breast), and if the target varies only slowly within the slice thickness (typically 3-4mm) in the direction perpendicular to the scan plane.

c) Multiple scattering

Very little theoretical or experimental work has been done on the importance or otherwise of multiple scattering, but it is thought by most researchers (e.g. Vezzetti and Aks, 1980) to be unimportant because of the relatively weak scattering that is already assumed within the Born approximation.

d) Plane wave insonification

This assumption can only be justified if the target is placed in the distant far-field of an unfocused transducer, or at the focus of a focused transducer. This is not always practical, although with the dynamic focusing available on most modern B-scanners the length of the focal zone may be quite significant. The main consequence of a departure from plane wave insonification is that the lateral beam profile $h_l(y)$ will not be constant with range (x). Hence equation (4.9), which assumes a space-invariant $h_l(y)$, no longer strictly applies although $h_l(y)$ can usually be assumed to change only slowly near the focal region of a focused transducer.

e) Uniform speed of sound

For any realistic tissue target, the speed of sound will not be completely uniform over the extent of the transducer's ultrasonic field. Indeed variations in the acoustic speed within soft tissue from the generally assumed value of 1540 m/s are one of the main causes of artifacts in B-scan images. A varying acoustic speed along the beam axis will mean that the axial component of the psf $h_a(x)$ will be range dependent, because $x = c.t/2$, and may result in targets being misplaced in the B-scan image from their true positions. A varying acoustic speed across the beam will cause distortion of both the transmitted and received ultrasonic wave-fronts, resulting in refraction and further mis-registration as well as de-focussing of the beam. The likely magnitudes of such geometric distortions will be examined in detail in section 6.2.

The distorted wave-fronts will also cause phase cancellation at the receiver, which will manifest itself in the B-scan image as 'speckle-like' fluctuations in echo amplitude (see Abbott and Thurstone 1979 or O'Donnell 1982). The magnitude of these effects, and whether they influence significantly the assumptions of a linear system with a space-invariant psf, obviously depends on the magnitude of the acoustic speed variations. The effects of different degrees of acoustic speed inhomogeneity will be investigated experimentally later in this Thesis (in Chapters 5 and 6).

f) Non-linear processing

The theory put forward so far has assumed that no processing has been applied to the rf scan-line data. In conventional B-scan imaging, a considerable amount of processing is typically applied before the scan-line signals are combined into a B-scan image. In particular, the rf signal is usually envelope detected (or demodulated) to reduce the required digitisation rates and to facilitate display of the image. The signal may also be logarithmically compressed to fit the wide dynamic range of the received echoes into the limited dynamic range of the display device. Both these operations are non-linear, the consequence being that the B-scan image can no longer be represented exactly by a linear superposition of echoes from independent point scatterers. Hence the apparently random fluctuations in echo amplitude, which occur as a result of coherent destructive and constructive interference between the rf echoes of scatterers at slightly different ranges within the pulse envelope, can no longer be modelled by a linear convolution of the scatterers with the psf (as in 4.9). Consequently a demodulated B-scan can not be considered as truly quantitative since the scatterer distribution can not be deconvolved from the backscattered data.

The fluctuations in echo amplitude take on the appearance of a spatially varying "noise" component in the B-scan image, and have become known as speckle. Hence despite the apparent violation of the linear model for B-scan imaging, this model can still be usefully applied provided that speckle is accepted as a noise component which determines the maximum contrast (or dynamic range) of the images with a second-order influence on the resolution.

g) <u>Negligible attenuation</u>

Attenuation can certainly not be neglected in the majority of situations. However, it is common practice in conventional B-scanning for the operator to apply range dependant amplification to the scans, in an attempt to compensate for attenuation. This compensation could be performed more effectively if information were known a-priori about the 2-dimensional distribution of attenuation coefficient within the scan plane.

4.3.2 Reflection UCT point spread function

4.3.2.1 Introduction

The basic concepts of reflection UCT have already been introduced in section 3.2. It was stated there that the pulse-echo signal from a wide-aperture transducer can be thought of as a projection of the reflectivity distribution of the insonified object, the projection being in a direction perpendicular to the direction of propagation of the ultrasonic pulse. This technique will be called the "broad beam" method. The form of the data acquired with this method is analogous to X-ray CT, so that by acquiring projections from many angles it should be possible to reconstruct the object distribution using conventional CT reconstruction techniques. As discussed in Chapter 3, other techniques exist which allow some lateral information, ie perpendicular to the direction of the projection, to be incorporated into the reconstruction. This can be done by laterally scanning a narrow single element transducer, or by using a wide field linear array. These methods will be called the "narrow beam" methods.

It was shown in section 4.3.1 that, within certain limitations, conventional B-scan imaging can be modelled using linear imaging theory. Since reflection UCT simply involves combining scan lines or whole B-scan images from many directions, linear imaging theory can be used for reflection UCT as long as it is remembered that the same assumptions and limitations of the B-scan model still apply.

4.3.2.2 Linear model for reflection UCT

In reflection UCT, as in conventional CT, data is required from many angles around the target. This data is obtained by simply rotating the ultrasound probe through a number of positions around the target and in the same plane, and storing the B-scan data from each position. From Figure 4.4, it can be seen that for a B-scan obtained at an arbitrary angle ϕ, the image co-ordinates (u,v) are related to the object co-ordinates (x,y) by

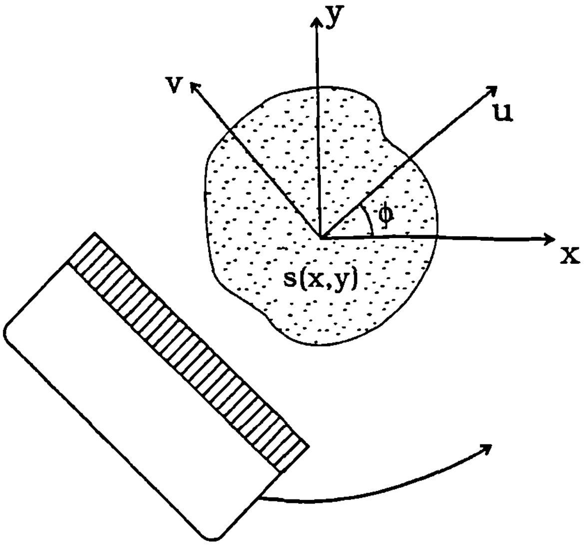

Figure 4.4 Geometry for reflection UCT

$$u = x\cos\phi + y\sin\phi$$

and $$v = y\cos\phi - x\sin\phi$$

Hence from equation (4.9),

$$b_{\phi}(u,v) = s(x,y) ** \{ h_a(u).h_l(v) \} \qquad (4.10)$$

The reconstruction of a reflection UCT image involves processing of the B-scan data in various ways. The two methods considered here are the "broad beam" and "narrow beam" methods.

<u>Broad beam method</u>

The simplest approach involves synthesising broad-beam insonification by averaging (or integrating) each B-scan data laterally to the direction in which the B-scan was taken (ie along v in Figure 4.4). Hence all lateral resolution in the B-scans is lost, and provided that the un-processed rf signals are combined, the data obtained is very similar to that obtained from a wide single element transducer. The main advantage of this approach, as will be shown below, is that the form of the data is now directly analogous to that obtained in conventional CT and hence identical reconstruction algorithms may be used.

Consider again the B-scan image of a point target, ie the B-scan psf h(x,y). The laterally averaged psf $h^*(x,y)$ can be represented as

$$h^*(u,v) \quad = \quad \int_{-\infty}^{\infty} h(u,v)\, dv$$

and using (4.8)

$$h^*(u,v) \quad = \quad h_a(u) \;.\; \int_{-\infty}^{\infty} h_l(v)\, dv$$

Assuming a normalised Gaussian function for the lateral beam profile

$$h_l(v) \quad = \quad \exp\left[\frac{-\pi v^2}{a^2}\right]$$

where a is a constant proportional to the beam width. Clearly

$$\int_{-\infty}^{\infty} \exp\left[\frac{-\pi v^2}{a^2}\right] dv \quad = \quad a$$

Hence the laterally averaged B-scan psf may be represented solely by the axial point response multiplied by a constant scaling factor,

$$h^*(u,v) \quad = \quad a \;.\; h_a(u) \qquad (4.11)$$

Similarly the laterally averaged B-scan OTF is simply the axial component $H_a(X)$ of the B-scan OTF.

To show that image reconstruction in broad beam reflection UCT is directly equivalent to X-ray CT, assume temporarily that the axial B-scan point response $h_a(u)$ can be represented by a delta-function $\delta(u)$, ie a very short pulse (this is equivalent to the initial assumption of an infinitely narrow X-ray beam in 2.2). Then the laterally averaged B-scan psf will be given, from equation (4.11), by

$$h^*(u,v) \quad = \quad a \;.\; \delta(u)$$

and from (4.10) the laterally averaged B-scan b^*_ϕ is now

$$b^*_\phi(u) \quad \propto \quad s(x,y) \;**\; \delta(u)$$

Comparing this equation with equation (2.2) it is clear that $b^*_\phi(u)$ can be thought of as a 1-D projection of the object reflectivity s(x,y) along the direction *u*, where the resolution of the projections in this case is limited by the axial component of the B-scan psf, or $h_a(u)$. Hence in principle any of the algorithms presented in section 2.3 may be used to reconstruct an image from many projections b^*_ϕ at different angles ϕ.

Using a simple back-projection approach results in a broad beam reflection UCT image $s_{bb}(x,y)$ given by equation (2.6), ie

$$s_{bb}(x,y) \quad = \quad \int_0^\pi b_\phi^*(u)\, d\phi \quad = \quad s(x,y) \ * * \int_0^\pi h_a(u)\, d\phi$$

and thus a back-projected (but unfiltered) broad beam reflection UCT psf given by

$$h_{bb}(x,y) \quad = \quad \int_0^\pi h_a(u)\, d\phi \tag{4.12}$$

Hence the image $s_{bb}(x,y)$ formed by simple summation (ie no filtering) of laterally averaged B-scans is the object s(x,y) convolved with a rotated and summed axial B-scan psf, $h_{bb}(x,y)$. Equation (4.12) can be expressed in the frequency domain as

$$S_{bb}(X,Y) \quad = \quad S(X,Y)\ .\ H_{bb}(X,Y)$$

where

$$H_{bb}(X,Y) \quad = \quad \int_0^\pi H_a(U)\, d\phi$$

Narrow beam method

It is also possible to derive reconstruction algorithms which allow the lateral information in the B-scans to be preserved. This method has various advantages over the broad-beam method, the details of which will be discussed in section 4.4.3.3. The first step in reconstruction is to sum the B-scan images from all directions to form a summation image $s_{nb}(x,y)$. In the limit of an infinite number of B-scans, this is equivalent to an integration with respect to ϕ,

$$s_{nb}(x,y) \quad = \quad \int_0^\pi b_\phi(u,v)\ d\phi \qquad (4.13)$$

This is again clearly similar to the backprojection operation of equation 2.6. Combining (4.13) with (4.10) gives

$$s_{nb}(x,y) \quad = \quad s(x,y) \ * * \int_0^\pi h_a(u).h_l(v)\ d\phi$$

$$or \quad s_{nb}(x,y) \quad = \quad s(x,y) \ * * \ h_{nb}(x,y) \qquad (4.14)$$

where

$$h_{nb}(x,y) \quad = \quad \int_0^\pi h_a(u).h_l(v)\ d\phi \qquad (4.15)$$

The equivalent expressions in the spatial frequency domain are then

$$S_{nb}(X,Y) \quad = \quad S(X,Y)\ .\ H_{nb}(X,Y)$$

where

$$H_{nb}(X,Y) \quad = \quad \int_0^\pi H_a(X).H_l(Y)\ d\phi \qquad (4.16)$$

4.3.2.3 Validity of the assumptions of the model

The derivation of linear models for reflection UCT was dependent upon the same assumptions listed in 4.3.1.2 for B-scanning. However the consequences on image quality of failure of these assumptions are in some cases different.

(a) Use of demodulated data

Most researchers who have used this technique have, for various reasons discussed in detail in section 5.3.1, combined demodulated scan lines rather then the raw rf echo data. Hence speckle cannot be accounted for within this model, just as for conventional B-scanning, and must be considered as an image artifact. However there is good reason (see section 4.5) to expect that speckle will be less of a problem for reflection UCT than it is for B-scanning. The consequences of using demodulated data for the broad beam method specifically are more complicated, because in this case the laterally averaged echo data is not strictly identical to the data that would be obtained from a single element transducer.

b) Constant acoustic speed

Reflection UCT images are likely to be even more adversely affected by acoustic speed variations, as shown by previous studies (see 3.2.3). This is because the technique relies on correct registration (summation) of echoes from all directions through the target. If there are any acoustic speed variations anywhere within the target, the opportunity is greater in reflection UCT for mis-registration and consequent loss of resolution to occur.

4.3.3 Transmission UCT point spread function

4.3.3.1 Introduction

The purpose of this section is to derive a linear theory for transmission UCT using the same formalism and equations as used to describe the backscatter imaging techniques of B-scanning and reflection UCT. Although this analysis will reveal the principles underlying both acoustic speed and attenuation CT, only acoustic speed CT will be explored in any detail because, for the reasons discussed below, only acoustic speed CT has been attempted experimentally in this work.

4.3.3.2 Linear model for transmission UCT

Restating, in differential form, the inhomogeneous Helmholtz equation (4.5) for a field $P(\underline{r}).e^{i\omega t}$ propagating in a uniform medium containing a compressibility inhomogeneity

$$\nabla^2 P(\underline{r}) + k_0^2 P(\underline{r}) \quad = \quad -k_0^2\ \gamma_\kappa(\underline{r})\ P(\underline{r})$$

where

$$\gamma_\kappa(\underline{r}) = \frac{\kappa(\underline{r}) - \kappa_0}{\kappa_0}$$

Rearranging this equation leads to

$$\nabla^2 P(\underline{r}) + k_0^2 \frac{\kappa_r}{\kappa_0} P(\underline{r}) = 0$$

Substituting

$$\kappa_0 = \frac{1}{c_0^2 \rho_0} \quad and \quad \kappa(\underline{r}) = \frac{1}{c(\underline{r})^2 \rho_0}$$

gives

$$\nabla^2 P(\underline{r}) + k_0^2 \frac{c_0^2}{c(\underline{r})^2} P(\underline{r}) = 0$$

It is useful to define a refractive index N, where

$$N^2(\underline{r}) = \frac{c_0^2}{c(\underline{r})^2} \qquad (4.17)$$

Then

$$\nabla^2 P(\underline{r}) + k_0^2 N(\underline{r})^2 P(\underline{r}) = 0 \qquad (4.18)$$

The spatial dependence of the pressure field can be represented by

$$P(\underline{r}) = P_0 \, e^{ik_0\phi(\underline{r})} \qquad (4.19)$$

where $\phi(r)$ is the eikonal, or acoustic path length, function (see for example Born and Wolf, pp 111-115). Substituting equation (4.19) into (4.18) results in

$$\frac{i\nabla^2\phi}{k_0} - \nabla\phi . \nabla\phi + N^2 = 0 \qquad (4.20)$$

Several assumptions additional to those listed in 4.2 must now be made. The most important of these is the assumption that diffraction may be neglected. This is equivalent to allowing the ultrasound wavelength λ to approach zero

$$ie \quad as \quad \lambda \to 0, \quad so \quad k_0 = \frac{2\pi}{\lambda} \to \infty$$

Therefore, by neglecting diffraction, equation (4.20) can be approximated by

$$\nabla\phi.\nabla\phi = N^2 \tag{4.21}$$

Recalling from section 4.2 that the total field equals the incident (ie unperturbed) field plus the scattered (or perturbed) field, then

$$\phi = \phi_0 + \phi_1$$

where ϕ_0 and ϕ_1 are the solutions of (4.21) in the unperturbed and perturbed media respectively. Also let

$$N = N_0 + N_1$$

where N_0 is the refractive index in the unperturbed medium (ie $N_0 = 1$) and N_1 is given by

$$\begin{aligned} N_1(\underline{r}) &= N(\underline{r}) - N_0 \\ &= \frac{c_0}{c(\underline{r})} - 1 = \frac{c_0 - c(\underline{r})}{c(\underline{r})} \end{aligned}$$

Hence equation (4.21) becomes

$$\begin{aligned} \nabla\left(\phi_0 + \phi_1\right) . \nabla\left(\phi_0 + \phi_1\right) &= \left(N_0 + N_1\right)^2 \\ \nabla\phi_0.\nabla\phi_0 + \nabla\phi_1.\nabla\phi_1 + 2\nabla\phi_0.\nabla\phi_1 &= N_0^2 + N_1^2 + 2N_0N_1 \end{aligned} \tag{4.22}$$

From (4.21) the solution for ϕ_0 in the unperturbed medium is given by

$$\nabla\phi_0 . \nabla\phi_0 = N_0^2 = 1$$

Therefore

$$\phi_0(\underline{r}) = \hat{k}_0.\underline{r}$$

where k_0 is a unit vector in the direction of the incident wave. The solution for the incident field is then

$$P_0(\underline{r}) = P_0\, e^{i\underline{k}_0 \cdot \underline{r}}$$

This conforms with the initial assumption of a plane wave propagating along the direction k_0. Substituting these results into equation (4.22), and assuming also that the refractive index perturbations are small, ie $N_1 << N_0$ and hence terms in N_1^2 and $\nabla\phi_1.\nabla\phi_1$ are negligible, gives a solution for the perturbed field

$$\nabla\phi_0 \cdot \nabla\phi_1 = N_0\, N_1$$

and hence

$$\hat{\underline{k}}_0.\nabla\phi_1(\underline{r}) = N_1(\underline{r}) \tag{4.23}$$

Integrating this equation along a path, which must be parallel to k_0, between any two points a and b gives

$$\phi_1(b) - \phi_1(a) = \int_a^b N_1(\underline{r})\, ds \tag{4.24}$$

where ds is the element of length along the path a to b.

If the perturbing medium is attenuating the acoustic speed $c(\underline{r})$, and hence the refractive index $N_1(\underline{r})$ and the eikonal $\phi_1(\underline{r})$, will be complex. It is clear from equation (4.19) that the imaginary part of the eikonal (ϕ_{1I}) is given by

$$\phi_{1I}(\underline{r}) = \frac{1}{k_0} \ln\left[\frac{P_0}{P(\underline{r})}\right]$$

Hence the imaginary parts of ϕ_1 and N_1 in equation (4.24) give a solution for the integrated attenuation between a and b as follows

$$\ln\left[\frac{P(b)}{P(a)}\right] = -k_0 \int_a^b N_{1I}(\underline{r})\, ds \tag{4.25}$$

Similarly, dividing the real parts of equation (4.24) by the acoustic speed c_o in the unperturbed medium, gives (Born and Wolf p.115) the relationship between the time of flight of the ultrasound wave between a and b and the *relative* refractive index $\eta(\underline{r})$

$$TOF[a\rightarrow b] = \int_a^b dt = \frac{\phi_{LR}(b) - \phi_{LR}(a)}{c_0} = \int_a^b \eta(\underline{r})\, ds \qquad (4.26)$$

where

$$\eta(\underline{r}) = \frac{1}{c(\underline{r})} - \frac{1}{c_0}$$

Equations (4.25) and (4.26) form the basis of ultrasound attenuation and acoustic speed CT. The principle assumptions made in deriving these equations will now be reviewed and discussed.

4.3.3.3 Validity of the assumptions of the model

Several new assumptions were made in deriving equation (4.26) from equation (4.5). These were:-

a) That diffraction may be ignored (ie $\lambda \sim 0$). This is acceptable if the ultrasonic source, and all objects within the target, have dimensions which are much greater than the ultrasound wavelength. This assumption is definitely not valid within soft tissue targets which have many structures (such as cells, vessels and muscle fibres) of dimensions near to or less than the wavelength. The consequences of the failure of this assumption are particularly severe for attenuation imaging, where diffraction effects cause loss of signal at the receiver which is interpreted as attenuation. This results in inconsistencies in the projection data and causes loss of accuracy and artifacts in the reconstructed image. The affects on the measurement of pulse TOF, and hence on acoustic speed imaging, are likely to be less severe but will depend critically on the method chosen for determining pulse arrival. An experimental investigation into various methods of measuring pulse TOF has been conducted and will be reported in section 6.5.3.

b) That both incident and transmitted waves are plane waves. Although difficult to achieve exactly, a fair approximation to plane wave insonification can be achieved by placing the target in the focal zone of a weekly focused transducer.

c) That refractive index variations are small. Published measurements of the acoustic speed in various soft tissues (eg Duck 1990) suggest that acoustic speed, and hence refractive index, varies by less than 10%. In soft tissues excluding muscle and fat the variation is probably less than 5%. Whether these variations are acceptable for transmission UCT is best determined experimentally, so further discussion of this topic will be left until the experimental results are reported in Chapter 6.

d) That the path of integration of the refractive index is along the direction of the incident plane wave. This therefore assumes that the ultrasound wave propagates in a straight line between transmitter and receiver, with no refraction. The degree to which this assumption is true is largely determined by the validity of assumption (c). Failure of this assumption is again more severe for attenuation imaging, but may also cause problems in acoustic speed imaging if beams are refracted to such an extent that they miss the receiver completely.

Clearly the quality of attenuation images is likely to be more severely impaired by any failure of these assumptions than are acoustic speed images. This result has been confirmed experimentally by previous workers in transmission UCT (see Chapter 3). Accordingly it was decided that this work should concentrate on acoustic speed imaging, bearing in mind the possibility of using acoustic speed images in combination with reflection UCT images (see 3.2.3 and Chapter 6).

4.3.3.4 Reconstruction of an acoustic speed image

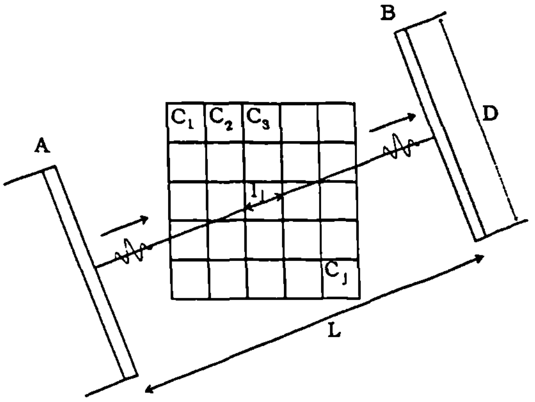

Figure 4.5 Relationship between TOF measurements and image space

For reasons discussed above, it has been decided in this work to concentrate on acoustic speed imaging. It can now be shown that the reconstruction of the acoustic speed distribution within a object may be accomplished using CT methods. Let the object, and image, space be divided into *n*n* elements (or pixels), each assigned the average value of the acoustic speed within that pixel (Figure 4.5). The value assigned to the jth pixel would be c_j. The region outside the reconstruction region has a constant acoustic speed c_w. Let l_j be the length of the path of an ultrasonic pulse as it traverses the jth pixel. The total time T for the pulse to travel from the transmitter (A) to the receiver (B) is given by

$$T = \sum_j \frac{l_j}{c_j} + \frac{L - \sum_j l_j}{c_w}$$

This equation is not yet in a form that can be solved by CT methods, because the parameter to be reconstructed must be zero outside the reconstruction region. To obtain such a parameter it is necessary to measure the time T_w for the pulse to travel the same path with no object present, or in other words, just through the water.

$$ie \quad T_w = \frac{L}{c_w}$$

$$\therefore \quad T - T_w = \sum_j \frac{l_j}{c_j} - \sum_j \frac{l_j}{c_w}$$

$$= \sum_j l_j \left[\frac{1}{c_j} - \frac{1}{c_w} \right]$$

$$\therefore T - T_w = \sum_j l_j \eta_j \tag{4.27}$$

$$where \quad \eta_j = \left[\frac{1}{c_j} - \frac{1}{c_w} \right]$$

is the *relative* refractive index of the jth pixel.

Equation (4.27) is consistent with the more rigorously derived equation (4.26), and meets the criteria for CT reconstruction in that (i) it defines a measurable quantity ($T - T_w$) that is given by the linear summation of the parameter to be reconstructed (η_j) multiplied by a function of length, and (ii) the reconstructed parameter is zero everywhere outside the reconstruction region. Also, note the similarity to the equivalent expression for the ratio of received to transmitted X-ray intensities well known from X-ray CT.

$$-\ln\left[\frac{I}{I_0}\right] = \sum_j l_j \, \mu_j$$

By measuring T - T_w for many parallel rays across the target, a TOF projection (P_ϕ) of the object is formed. By obtaining many projections at different angles enough information can be acquired to reconstruct, using any of the algorithms discussed in Chapter 2, the value of η_j for every pixel in the image. Using a simple back-projection approach results in an acoustic speed image $\eta(x,y)$ given by equation (2.6), ie

$$\eta(x,y) = \int_0^\pi P_\phi(u) \, d\phi \qquad (4.28)$$

Note that the resolution of the projection is determined by the ultrasound beam width, ie by $h_l(u)$. Thus the back-projected (but unfiltered) acoustic speed image psf is given by

$$h_{sos}(x,y) = \int_0^\pi h_l(u) \, d\phi \qquad (4.29)$$

Although the quantity that is actually reconstructed is η_j, if c_w is known it easy to convert these values into the acoustic speed c_j.

4.4 A comparison of B-scan and UCT point spread functions

4.4.1 Introduction

Having shown that the image formation processes leading to conventional B-scan and UCT images may be considered as approximately linear (and accepting that violations of this assumption cause image artifacts), it is now possible to compare the potential spatial resolution of conventional B-scanning, reflection UCT and transmission UCT by considering their respective point spread functions.

4.4.2 B-scan psf

Equation (4.9) defined the B-scan imaging process as a linear convolution between the scatterer distribution s(x,y) and a point spread function h(x,y),

$$b(x,y) \quad = \quad s(x,y) \ * \ * \ h(x,y)$$

Equation (4.9) has an equivalent expression in the spatial frequency domain given by

$$B(X,Y) \quad = \quad S(X,Y) \ . \ H(X,Y) \tag{4.30}$$

where B(X,Y), S(X,Y) and H(X,Y) are the Fourier transforms of b(x,y), s(x,y) and h(x,y) respectively. The B-scan psf can be measured fairly easily by obtaining a B-scan of a very thin wire target orientated perpendicularly to the scan plane (see Chapter 5).

The axial resolution (along the beam axis) of a B-scan image is given by $h_a(x)$ and hence is determined by the length of the transmitted ultrasound pulse. Neglecting the electro-mechanical properties of the transducer in receive and the limited bandwidth of the receiver amplifiers, $h_a(x)$ may be approximated by half the transmitted pulse length since the range x is a function of $c.t/2$, where t is the go-return time of the pulse.

The lateral resolution is given by $h_l(y)$ which is determined by the ultrasound beam-width. In fact it is the pulse-echo beam width that is required, again because of the two-way passage of the acoustic pulse. Since the minimum possible (ie with focusing) beam width at a given point is determined fundamentally by the angle subtended by the transmit-receive aperture at that point, good lateral resolution in B-scan images requires large or enclosing transducer apertures. Unfortunately in real-time B-scanning it is often not beneficial to increase aperture lengths beyond a few centimetres, because in many of the sites of the human body where the technique is applied the superficial areas free of bone or gas (often called acoustic "windows") are relatively small.

It is instructive to consider the situation in the spatial frequency domain. Equation 4.30 shows that the frequency content of the object distribution will be modified by the frequency content of the OTF. Since the OTF is inevitably band-limited by the pulse length, the beam width and by the limited bandwidth of the receiver amplifiers, the B-scan image will not be an accurate representation of the object. Typically, the axial component $H_a(X)$ will have a wider band-width than the lateral component $H_l(Y)$, because the axial pulse length is typically 3 to 4 times shorter than the lateral beam-width. Hence the resolution of a B-scan image is limited primarily by the lateral component of the OTF, which is itself determined by the pulse-echo beam generated by the transducer aperture.

4.4.3 Reflection UCT psf

It has been shown that the resolution of a B-scan image is limited mainly by the lateral component of the OTF, the axial component typically have a much wider band-width. This is why computed tomography techniques involve obtaining data from many directions about an object because, by rotating the B-scan psf, the maximum band-width available (in this case the axial band-width) can be made to extend in all directions. Part of the CT reconstruction process can be thought of as an attempt to restore, as closely as possible, the frequency content of the original object from knowledge of the OTF.

4.4.3.1 Broad-beam method

The broad beam reflection UCT psf was given by equation (4.12) as the axial component $h_a(u)$ of the B-scan psf rotated and summed over 180°,

$$h_{bb}(x,y) = \int_0^{\pi} h_a(u)\, d\phi$$

Note that, unlike the B-scan psf, $h_{bb}(x,y)$ (or its Fourier Transform $H_{bb}(X,Y)$) will have rotational symmetry (see Figure 4.6).

$$ie \quad H_{bb}(X,Y) = H_{bb}(R)$$

where $R = \{ (X)^2 + (Y)^2 \}^{1/2}$

Also, $H_{bb}(R)$ will have a maximum frequency R_{max} equal to the maximum frequency in the axial component $H_a(U)$ of the B-scan OTF. Hence the image $s_{bb}(x,y)$ should be an improvement on an individual B-scan image b(x,y) since it will have a wider overall bandwidth, although it's frequency content will still have been modified from that in the object because, in general, $H_{bb}(R)$ will not have a constant value inside the circle with radius R_{max}. In fact the $H_{bb}(R)$ approaches the exact (1/R) function predicted by CT theory as the axial B-scan psf $h_a(u)$ approaches a delta function. Hence it may be possible to use CT reconstruction filters (such as the Shepp-Logan filter discussed in section 2.3.2) to de-convolve the (1/r) blurring and reduce the reflection UCT psf to closer to the axial B-scan psf.

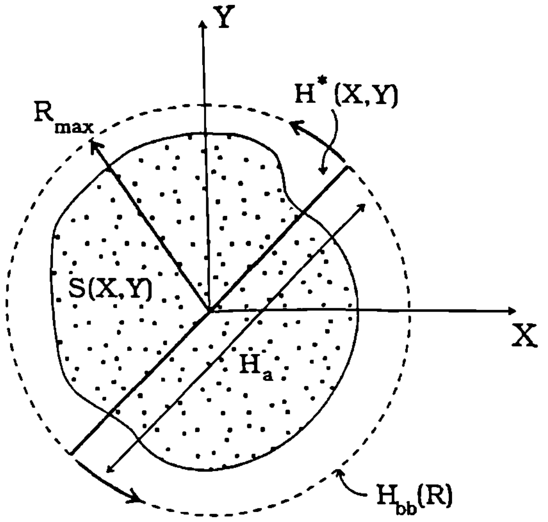

Figure 4.6 OTF for broad-beam reflection UCT

4.4.3.2 Narrow-beam method

The narrow beam reflection UCT psf was given by equation 4.15 as

$$h_{nb}(x,y) = \int_0^{\pi} h_a(u).h_l(v)\ d\phi$$

and the OTF by

$$H_{nb}(X,Y) = \int_0^{\pi} H_a(X).H_l(Y)\ d\phi$$

A possible narrow beam OTF is shown in Figure 4.7. Both the narrow beam psf and the OTF will again have rotational symmetry, and $H_{nb}(R)$ will again have a maximum frequency R_{max} equal to the maximum frequency in the axial component $H_a(U)$ of the B-scan OTF. However $h_{nb}(r)$ is of more limited extent than the broad beam psf $h_{bb}(r)$, because the incorporation of lateral resolution results in a multiplication by the lateral component $h_l(v)$ of the B-scan psf. In the frequency domain, this follows because each B-scan contributes information over a wider frequency range ($H_a(U) \times H_l(V)$) than occurs with the laterally averaged B-scans ($H_a(U) \times \delta(V)$) used for broad beam UCT.

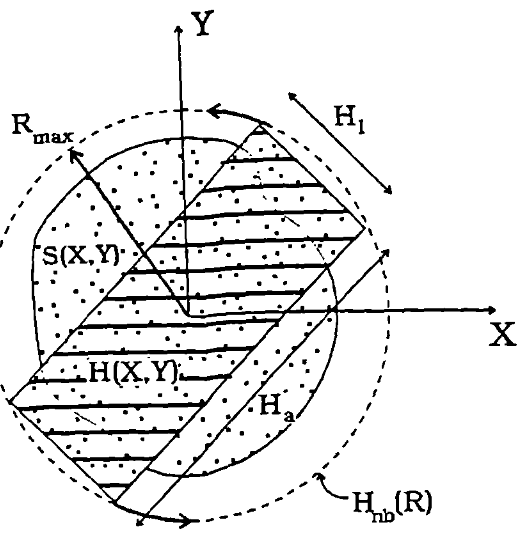

Figure 4.7 OTF for narrow-beam reflection UCT

Even though the form of $H_{nb}(R)$ is quite different to the (1/R) functions found in conventional CT, it might still be possible to restore more closely the original object's frequency content S(X,Y), at least inside the circle $|R| \leq R_{max}$, by the use of an *inverse filter* given most simply by

$$F(R) = \frac{1}{H_{nb}(R)} \quad ; \ |R| < R_{max}$$

$$F(R) = 0 \quad ; \ |R| \geq R_{max}$$

The reconstructed image will then be given (in the frequency domain) by

$$S'(X,Y) = S_{nb}(X,Y) \ . \ F(R)$$

This simple filter has two serious limitations :-

(i) The sharp cut-off at R_{max} induces 'ringing' or oscillations in the filtered image.

(ii) The filter takes no account of noise, which is always present in any real data.

An inverse filter that rolls-off more smoothly and takes account of the noise spectrum of the signal is the well known Wiener filter. Wiener filters are discussed in Appendix I, and experimentally results using them are presented in section 5.5.4.

4.4.3.3 Comparison of broad and narrow-beam methods

The results obtained with these two reconstruction methods would be expected to be somewhat different because of the differing requirements and assumptions of the two methods.

i. Resolution and inverse filtering

It has been shown that the unfiltered narrow beam psf is narrower than the broad beam psf, because the incorporation of lateral resolution restricts the total extent of the psf to that of the lateral B-scan psf. Hence any inverse filtering performed to restore more closely the object's frequency content is likely to be more successful for the narrow beam method, because its OTF falls-off into noise less quickly.

ii. Number of view directions required

It was shown in Section 2.4 that, in order to satisfy sampling requirements, the number of projections (or view directions) N_ϕ required over 180 degrees is given by

$$N_\phi = \frac{\pi D}{2\Delta p} \tag{4.31}$$

where D is the diameter of the reconstruction region (ie the length of the projection) and Δp is the resolution of the projection, which for reflection UCT is the axial resolution given by half the transmitted pulse length.

In a wide-field linear array probe the scanned ultrasound field is typically about 30 times wider than the width of an individual ultrasound beam. For the broad-beam method the projections are across the full width (D) of the ultrasonic field, whereas for the narrow beam method the projections are only across the null-null width of the beam. This suggests that the broad beam method would require about 30 times more view directions than the narrow beam method to satisfy the sampling requirements. This argument is demonstrated graphically by comparing the OTF of a B-scan (Figure 4.7) with the OTF of a laterally averaged B-scan (Figure 4.6). This confirms that many fewer views would be required to adequately sample the object's frequency space using the narrow beam method than using the broad beam method.

4.4.4 Transmission UCT psf

The psf of an acoustic speed image obtained from transmission measurements was given by equation (4.29) as

$$h_{sos}(x,y) = \int_0^\pi h_l(u)\, d\phi$$

Thus the theoretical psf is similar to that obtained for broad-beam reflection UCT (equation 4.12), except that for acoustic speed imaging it is the lateral component of the B-scan psf that determines the limits of the psf instead of the much shorter axial component. Hence the resolution of an acoustic speed image, even after filtering, will inevitably be poorer than for a reflection UCT image.

The number of TOF projection required to reconstruct an acoustic speed image is again given by equation (4.31). The diameter of the reconstruction region is again the width of the ultrasound field D, while the resolution of the projections (Δp in 4.31) is now given by the 6dB beam width (w).

4.5 Other factors influencing B-scan and reflection UCT image quality

In the previous sections it has been shown theoretically that, when compared in terms of their respective point spread functions, reflection UCT images should show better overall spatial resolution than conventional B-scans.

However many assumptions had to be made about the linearity of ultrasound imaging in order that a theory could be derived relating reflection UCT and B-scan psfs. It was shown in sections 4.3.2.3 and 4.3.3.3 that some of these assumptions do not strictly hold, resulting in the appearance of certain artifacts and other characteristic features in the images. Examples of these affects are speckle and specular reflection. It will be argued below that, although both reflection UCT techniques are less severely affected by these artifacts than conventional B-scans, the broad beam method is likely to be more severely affected than is the narrow beam method.

4.5.1 Specular reflection

The appearance of specularly reflecting surfaces is one of the main features of a B-scan image, a typical example being the boundary of an organ such as a kidney. It is observed that the organ boundary is only seen when it is virtually perpendicular to the scanning ultrasound beam axis. Since in a B-scan system ultrasound beams are directed into the target over only a very limited range of angles, determined by the solid angle subtended by the transmitting-receiving aperture, visualisation of organ boundaries is incomplete and this makes interpretation of ultrasound images more difficult.

The reflection UCT techniques involve combining backscatter data from all angles around a target. Hence specularly reflecting surfaces should contribute echoes to at least one view direction and hence should always be visualised on the resultant image. For the broad beam method, a strong echo at one probe direction from a localised surface will 'spread' its contribution across the full width of the image because of the operation of averaging across the field width. With the narrow beam method, however, the contribution will be localised to a single beam width and hence will not significantly contaminate other parts of the image, resulting in better signal to noise.

4.5.2 Speckle and contrast resolution

Speckle arises as a consequence of applying non-linear processing to the echo data. The effect of demodulation is that the interference between scatterers within the same sample volume (ie the pulse length * beam width) can no longer be accounted for, resulting in speckle. In conventional B-scan images speckle actually appears as a roughening or granularisation of what might be expected to be homogeneous areas of an image. It is normally considered as undesirable noise since it can obscure small structural details and hence leads to reduced spatial resolution. Speckle noise also masks the underlying mean backscatter level of the tissues, resulting in a relatively poor signal to noise ratio and hence poor contrast resolution.

The 'granules' or speckle patches have a characteristic size related to the resolution (and hence sample volume) of the scanning system - the better the resolution, the smaller are the speckle patches. On B-scans obtained from very different view angles the conditions for interference between scatterers and hence the speckle patterns observed will be completely different, with the correlation between speckle patterns gradually increasing as the angle between the B-scans gets smaller.

Reflection UCT techniques aim to take advantage of the fact that data obtained from different view angles should have independent speckle components. When the data is combined into a single image the speckle sums randomly, whereas echoes from strong scatterers which are less corrupted by speckle sum linearly, resulting in an effective reduction of the relative mean speckle level and an improved "signal to noise" ratio. A reduction in the speckle noise level should also result in improved contrast resolution.

Clearly the effectiveness of this speckle reduction will depend on the size of the speckle "patches" in the original data. For the broad beam method the effective sample volume is much larger than in the narrow beam method, because the 'beam' now has the full width of the ultrasonic field, making the speckle patches much larger and the reduction in speckle level obtained by summation less significant.

4.6 Conclusions

It has been shown it this section that linear models can be used to describe the processes of image formation for B-scanning, reflection UCT and transmission UCT, and consequently that point spread functions can be derived and subsequently used to compare their potential resolution. However certain characteristic features of the images (such as speckle in B-scans and reflection UCT images), which result from processes for which linear theory is violated (for example the non-linear process of demodulation in B-scanning and reflection UCT), will not be totally accounted for by the psf and must therefore be accepted as second order perturbations or artifacts.

Comparing these techniques on the basis of their predicted point spread functions (or their optical transfer functions) shows that better resolution is expected from reflection UCT than from B-scanning. Reflection UCT methods should also be less affected by most of the artifacts which appear in B-scan images, and in particular they should have a lower mean speckle level and hence better contrast resolution. Of the two reflection UCT methods considered here, the narrow-beam method should have the best resolution and should be the least affected by any residual image artifacts.

Acoustic speed imaging should have fewer artifacts than attenuation imaging because it is less affected by refraction, but even without artifacts the resolution is only likely to be as good as the lateral resolution of a B-scan image.

5 Development of a system for reflection UCT

5.1 Introduction

The results obtained by other researchers into ultrasound CT (Chapter 3), and the theoretical comparison of ultrasound CT techniques undertaken as part of this work (Chapter 4), both suggested that reflection-mode UCT was the technique that was most likely to be able to achieve one of the main objectives of this work - namely to develop a practical scanning system able to produce high quality images of soft tissue, preferably in-vivo. Due to the anticipated technical difficulties of constructing a water-bath scanning system suitable for in-vivo studies, it was decided that a practical investigation into reflection UCT should start with the development of a relatively simple system which would allow initially the imaging of phantoms and in-vitro targets only. Hence in the development of this system the desire for short scanning times, which would be one of the main requirements of a clinical system, has in general been sacrificed in favour of high positional accuracy and thus optimum image quality.

This chapter will describe the main considerations involved in the design and construction of a practical reflection CT system for the study of in-vitro targets. The first stage in this process is to define the requirements of an "ideal" system, and then to establish specifications for a practical system, in terms of its mechanical, electronic and software components, which are realistically achievable within the cost and time constraints. The construction of this system will be described, along with the sequence of events involved in acquiring the experimental data and reconstructing an image.

Various experiments will then be described, which attempt to establish whether the improvements in image quality predicted theoretically (in Chapter 4) are achieved in practice. This chapter will then conclude with a general discussion of the relative advantages and limitations of this reflection-only UCT system, and suggestions for the development of an improved system.

5.2 General requirements

Since this system was intended mainly as a test bed for reflection UCT and not as a clinical scanner, it was possible to design a system which could be built relatively quickly and cheaply, and mostly with materials and expertise already available in the Medical Physics department.

The basic requirement of a system to perform reflection UCT is that pulse-echo information must be obtainable from many directions about a target, with each direction defined by a constant centre of rotation. The need for a constant centre of rotation prohibits direct contact of the ultrasound source with the target, so that the scanning must be performed in a fluid coupling medium such as water. It was decided that this reflection UCT system would be designed to scan in a vertical plane because a prototype scanning tank had already been constructed along these lines, and because it was felt that a vertical plane system would be easier to build. The choice of a vertical scan plane limits the maximum scanning angle to about 180 degrees for any practical target (ie one that can be submerged by only a few centimetres in water), but may allow easier access for some potential in-vivo targets such as the neonatal head.

For reasons discussed fully in section 4.4.3.3, it was decided that a narrow beam approach to reflection UCT would be implemented. Thus an ultrasound transducer was required for the transmission and reception of ultrasound pulses along a narrow beam, with the beam being scanned in a lateral direction to allow pulse-echo measurements to be made at many positions across the full extent of the target. The transducer must also be able to rotate through 180° around the target and about a constant centre of rotation. It should also be possible to move the position of the transducer in a direction perpendicular to the plane of rotation, ie to allow multiple parallel slices to be acquired. This movement however need not be under the control of the computer and can be done manually. An alternative to rotating the transducer around the target is to rotate the target itself. This approach has the side benefit of allowing greater than 180° scanning of the target even with a vertical plane system. However, it was decided that the difficulty of preventing deformation of a soft tissue target rotating rapidly in water and the impracticality of ever scanning in-vivo with this approach outweighed the potential advantages.

A high speed digitiser is required with sufficient memory to store the data required for a single reconstruction. Software is required to control scanning movement, data acquisition, data storage, image reconstruction and image display. A computer is required that is powerful enough to reconstruct the reflection UCT images in a reasonable time. The computer must also be able to display the images to a resolution that as least as good as the inherent resolution of the images.

5.3 Detailed requirements and specifications

The basic requirements outlined above will now be examined in detail, in terms of what would constitute an "ideal" system and in terms of what has been achieved in practice.

For the purposes of ease of specification and design, the scanning system was broken down into several sub-systems (shown schematically in Figure 5.1) which could be designed and constructed separately. These will be described in the following sections.

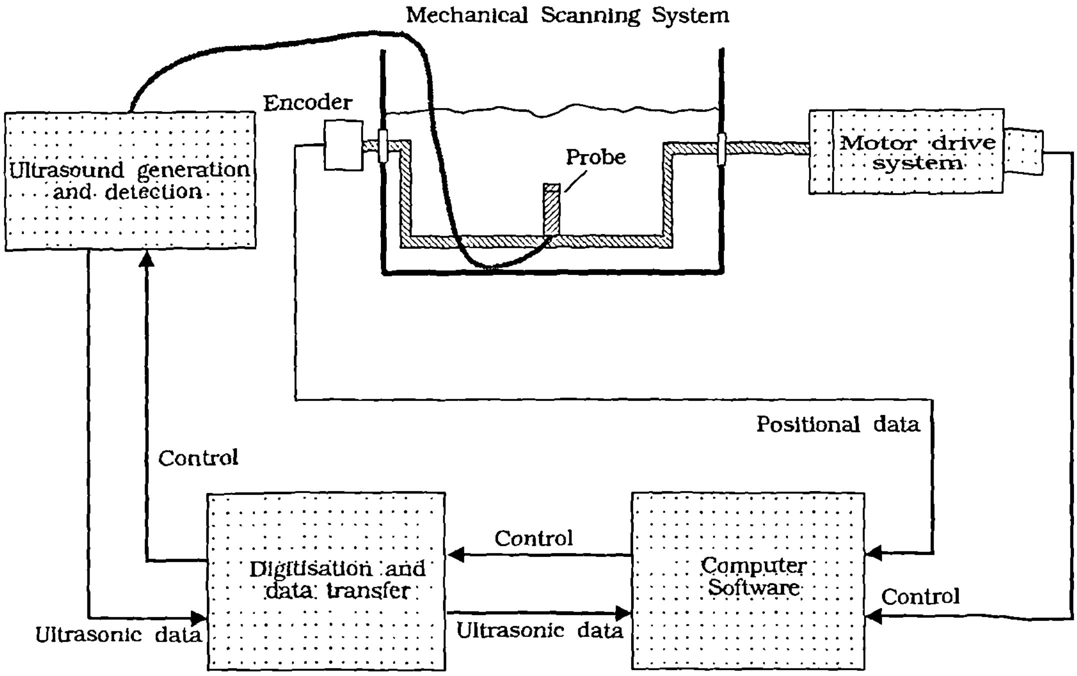

Figure 5.1 Schematic diagram of the reflection-only system.

5.3.1 Ultrasound generation and detection

In order to limit development time and costs, the system for ultrasonic generation and detection was based around a commercial Hitachi EUB-24 linear array scanner (Figure 5.2) which was no longer required for other clinical imaging. The scanner consists of a linear array probe (Figure 5.3) with a nominal 3 MHz centre frequency, plus electronics for ultrasonic signal detection and display. Despite its age (built in 1977), this scanner had the advantage of possessing a wide-field width (10.5 cm) linear array probe. The use of a linear array allows the lateral scanning requirement of narrow beam reflection UCT (see 4.3.2.2) to be performed electronically rather than mechanically,

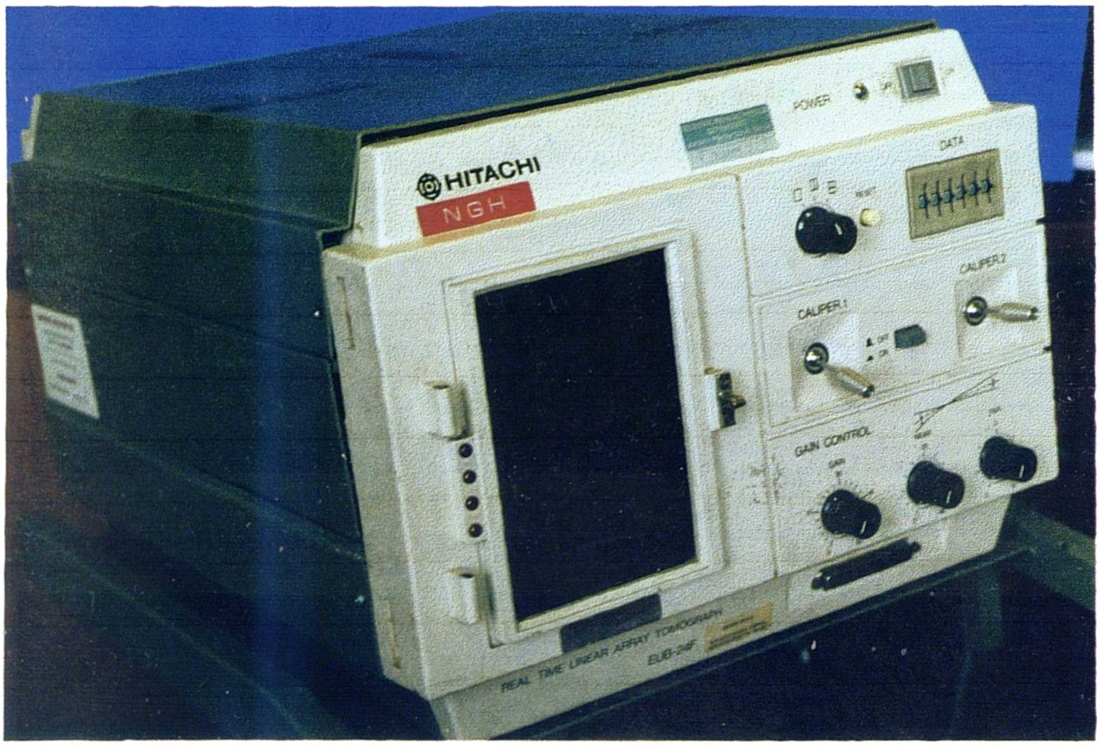

Figure 5.2 The Hitachi EUB-24F scanner used in the UCT systems.

Figure 5.3 The 3 MHz linear array probe of the Hitachi EUB-24.

thus allowing faster scanning times and more importantly higher positional accuracy than could be easily achieved with a single element transducer. The only disadvantage with using a commercial system rather than one specifically designed for reflection-mode CT is that it may not have the ideal characteristics for UCT. These characteristics will now be considered under several headings.

Ultrasound frequency and pulse length

The choice of which ultrasonic frequency to use for reflection UCT is governed as usual by the conflicting requirements of good image resolution and sufficient penetration of ultrasonic energy into the target. It was shown in Chapter 4 that the potential resolution of a reflection UCT system, assuming that the various assumptions (such as constant acoustic speed) are valid, is limited not by the width of the ultrasound beam as in conventional pulse-echo imaging but rather by the length of the ultrasonic pulse. Hence from resolution considerations the best transducer for reflection UCT would be one that emits as short a pulse as possible. However the shorter the pulse the greater the range of frequencies present in the pulse (ie the wider its bandwidth). The transmitter and receiver electronics must then have a wide enough bandwidth to amplify the wide range of frequencies, resulting inevitably in increased noise levels and reduced dynamic range. Primarily for this reason ultrasonic imaging systems rarely use transmitted pulses of fewer than 2 to 3 cycles at the transducer's resonant frequency, so that the length of the pulse is largely determined by the ultrasound wavelength. The best resolution is thus achieved by using the highest possible frequency.

Unfortunately another complicating factor is that the attenuation of ultrasound in soft tissue increases with increasing frequency. Although attenuation can be partially compensated for by depth dependent gain, there comes a point where the received echoes from the far side of an attenuating target may become so small that they are indistinguishable from electronic noise in the receiver. Thus attenuation, along with the limited dynamic range of the receiver electronics, effectively place a limit on either the highest frequency that can be used or on the penetration that can be achieved in any particular target. The preferential attenuation of high frequencies is also another reason why very short pulses (ie less than 2 wavelengths) are impractical, since the higher frequencies in the wide band pulse will be attenuated with increasing range thus decreasing the band width and lengthening the pulse.

For a target of 10 cm diameter (ie compatible with the linear array probes available), and with typical soft tissue attenuation coefficients in the range 0.5 to 1.0 dB/cm/MHz (Duck 1990), an acceptable compromise between resolution and signal-to-noise ratio occurs for pulses of 2 to 3 wavelengths with a resonant frequency in the range from 2 to 3 MHz. In terms of resolution, a 3 MHz pulse of 3 cycles length would imply a total pulse length of 1.5 mm (and a potential pulse-echo resolution of about 0.75 mm) in soft tissue.

The transmitted pulse from the Hitachi's 3 MHz linear array was measured in water using a PVDF hydrophone with an 0.5 mm diameter active element. The pulse obtained approximately at the focus, and its spectrum, are shown in Figures 5.4a and 5.4b respectively. The pulse shows minimal affects from non-linear propagation, probably due to the relatively low transmitted peak negative pulse amplitude of 0.35 MPa at the focus, as measured by the Department's output measurement system (Martin 1986). The pulse has a centre frequency of 3.0 MHz, and a 6dB bandwidth of 1.7 MHz, which is within the range specified above as suitable for breast imaging. The pulse length is also acceptable, being about 1.5 mm and thus giving an axial pulse-echo resolution of approximately 0.75 mm.

Ultrasound beam width

Under ideal circumstances the width of the ultrasound beam should have no affect on the resolution or quality of reflection UCT images. However, as argued in section 4.5.1, the assumptions inherent to the reflection UCT method, such as the neglect of specular reflection, become more unreliable and result in worsening artifacts as the beam width increases. Hence a transducer used for reflection UCT should ideally have as narrow a beam as possible. Narrow beams are traditionally obtained by strong focusing, which results in a narrow beam around the focal range but with wide beam widths both before and after the focus. In the case of reflection UCT a uniformally narrow beam is required ideally throughout the extent of the target. Note that for reflectivity imaging it is the pulse-echo beam width and not simply the transmitted beam width which is relevant. In modern ultrasound systems the pulse-echo beam width is kept narrow by techniques such as dynamic focusing on receive, in which the position of the focal zone is varied dynamically to coincide with the sources of echoes as they arrive at the transducer from greater and greater depths.

A fundamental requirement of CT imaging in general is that each image plane is assumed to be effectively independent from other parallel planes. In ultrasound imaging this is only possible if the width of the ultrasound beam in the direction perpendicular to the scan plane (often called the slice thickness) is infinitely thin, or at least in practice as thin as possible.

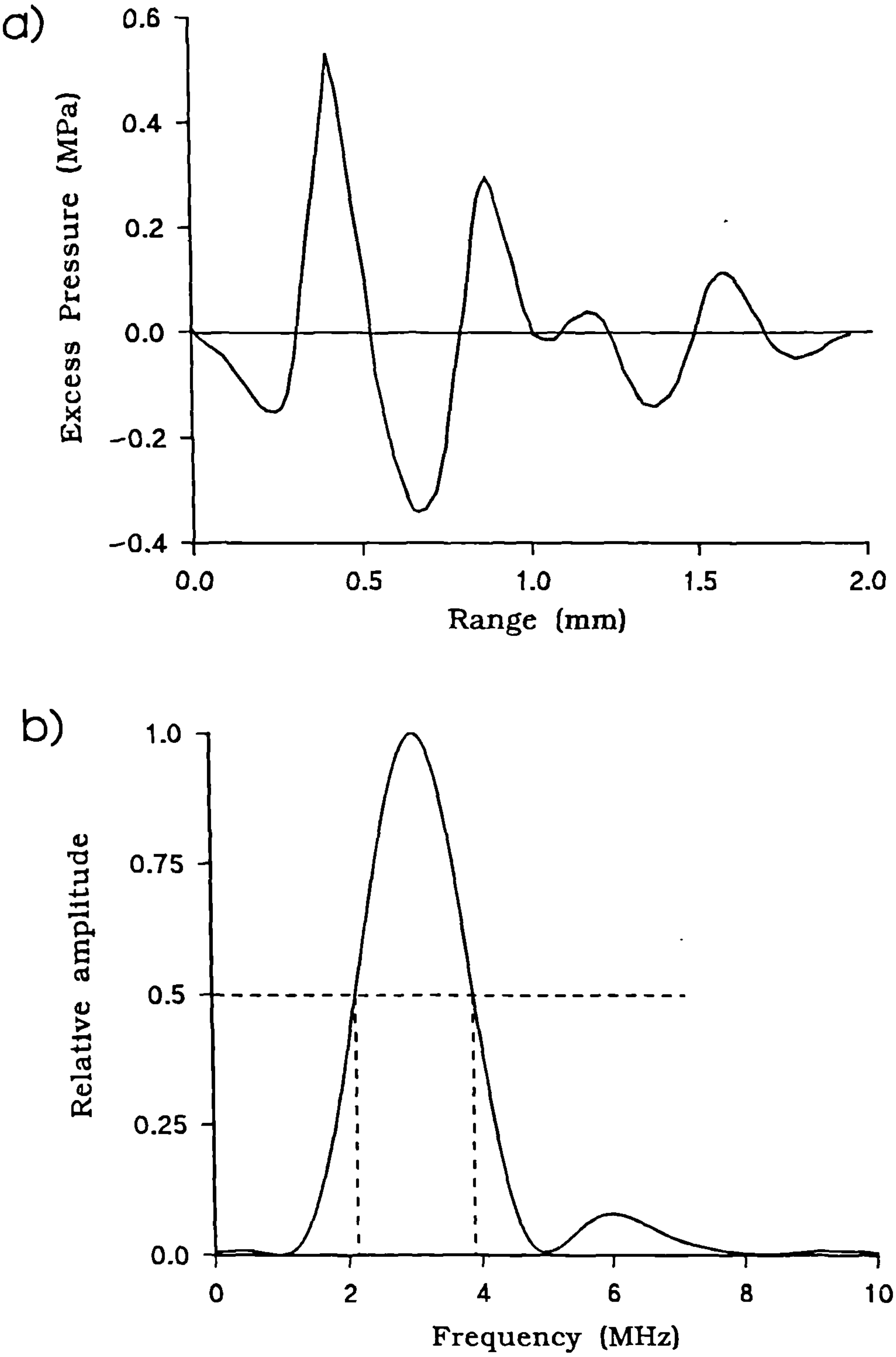

Figure 5.4 Transmitted (a) pulse and (b) spectrum from the Hitachi EUB 24's 3MHz linear array probe.

A pulse-echo beam profile for the Hitachi EUB-24's 3 MHz probe, measured in water using the Department's beam plotting system, is shown in Figure 5.5a. The beam has a pulse-echo focus at about 58 mm from the transducer. In the near-field the beam width converges from a 6 dB beamwidth of 10.0 mm at 2cm from the transducer face to 3.6 mm at the focus. Beyond the focus the beam diverges at an angle of about 1.5 degrees, reaching a 6 dB width of 6.2 mm at a range of 12 cm. Clearly it would be impossible with this probe to maintain a constant beam width over a typical target dimension of about 10 cm (see below), mainly because the Hitachi EUB-24 does not perform dynamic focusing. This consequences of this limitation will become evident in later sections.

Figure 5.5b shows a pulse-echo beam plot obtained with the Hitachi EUB-24's probe rotated through 90 degrees, and hence shows the beam profile perpendicular to the scan plane. The out of plane focus is at about 36 mm, with a minimum 6 dB slice thickness of 4.6 mm and up to 13 mm at 12 cm. Although this slice thickness performance is typical for a linear array of this type, it should be realised that in any image produced with this probe there may be significant contamination from targets located above or below the image plane.

Scanned field width and beam spacing

One of the basic requirements of reflection UCT using narrow beams is that the transmitting/receiving transducer aperture must be scanned laterally across the whole width of the target, with pulse-echo measurements obtained at regular precisely known intervals. From sampling requirements (see 2.4) the interval between measurement positions should be no more than half the 6 dB beam width. The accuracy at which the position of the aperture must be known will be discussed in section 5.3.4.

For this probe the field-width is 10.5 cm, which thus restricts the maximum target diameter to about 10 cm. This target diameter is less than ideal, but since very few commercial linear arrays are available which offer a wider field width, it was decided that this limit would be acceptable for a prototype system. The array is composed of 80 elements at 1.5 mm intervals, and fired in batches of 10 giving an active aperture width of 15 mm and a total of 70 lines per B-scan frame (ie 1.5 mm beam spacing). Thus the beam spacing of 1.5 mm meets the requirements of sampling theory in that it is less than half the beam width at any range. The line period is 278 microseconds, giving a maximum possible imaging range of about 20 cm in water. The field period is 21.8msec, which is therefore the absolute minimum time taken to acquire the pulse-echo data for one B-scan.

a)

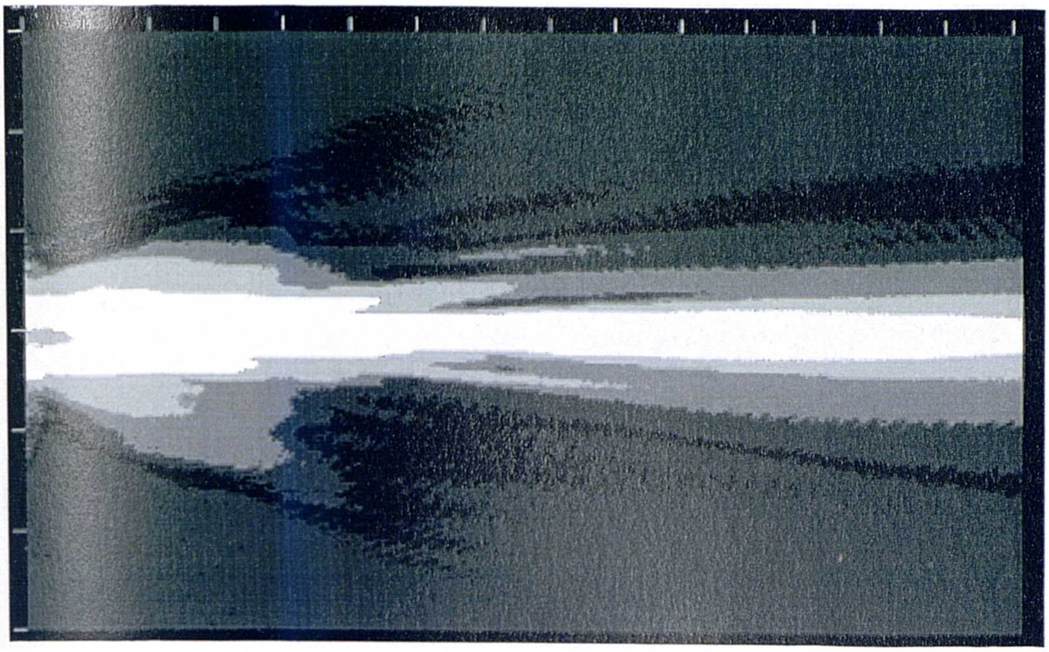

b)

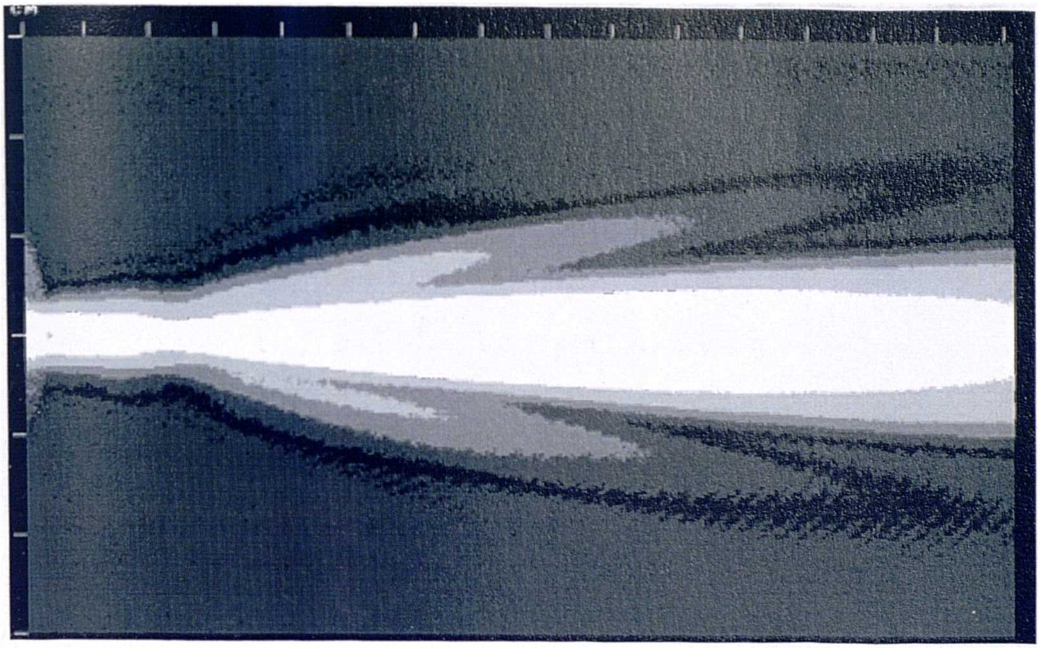

Figure 5.5 **Pulse-echo beam plots of the 3 MHz linear array; a) parallel to the scan plane, and b) perpendicular to the scan plane. Each grey level represents a 6 dB change in echo amplitude.**

Signal processing

An ideal system for reflection UCT would involve no non-linear processes in the measurement system since, as emphasised in Chapter 4, the principles of CT reconstruction are based on linearity and superposition. Hence signal demodulation and non-linear amplification are both undesirable features.

In principle signal demodulation could be avoided by using the raw RF data, but this is often impractical because of:-

a) The high digitisation rates required (ideally > 20 MHz for a 3 MHz pulse with a 1.2 MHz bandwidth).
b) The large amount of storage required because of the high digitisation rates.
c) The very high accuracy required in the positional system to prevent incorrect phase cancelation of signals combined from different transducer angles or positions. To prevent phase cancellation a positional accuracy of better than the ultrasonic wavelength/10 is required, which for 3 MHz implies a positional accuracy of better than 0.05 mm.

Factors b) and c) above have limited the work presented in this thesis to the processing of demodulated signals, although it is hoped that it may be possible to use RF signals at a later date. Strictly speaking, this limitation invalidates the use of the linear equations derived in section 4.3 and 4.4 for B-scan and reflection UCT image formation. However, as argued in section 4.3.1.3 these equations may still be used, provided that we accept that speckle will not be accounted for and that the resolution of the system can never be less than half the pulse length. In practice speckle is much less of a problem in reflection UCT images than in conventional B-scan images, because of the fact that UCT images are composed of many separate B-scans obtained from different angles. Since the B-scans contain essentially independent speckle patterns, the mean speckle level in the combined image will increase by $\sqrt{n}$, where n is the number of B-scans, whereas the echo level of any strong scatterers will, assuming correct registration, increase by n.

In a conventional B-mode pulse-echo system, the RF echo signal is demodulated (or envelope detected) before display. However the demodulated signal from the Hitachi EUB-24 was found to be noisy and a poor representation of the true signal envelope. In addition the EUB-24 performs various other non-linear processing operations on the RF signal, such as automatic gain control (AGC) and edge-enhancement. Consequently it was decided that the RF signal would be extracted from the

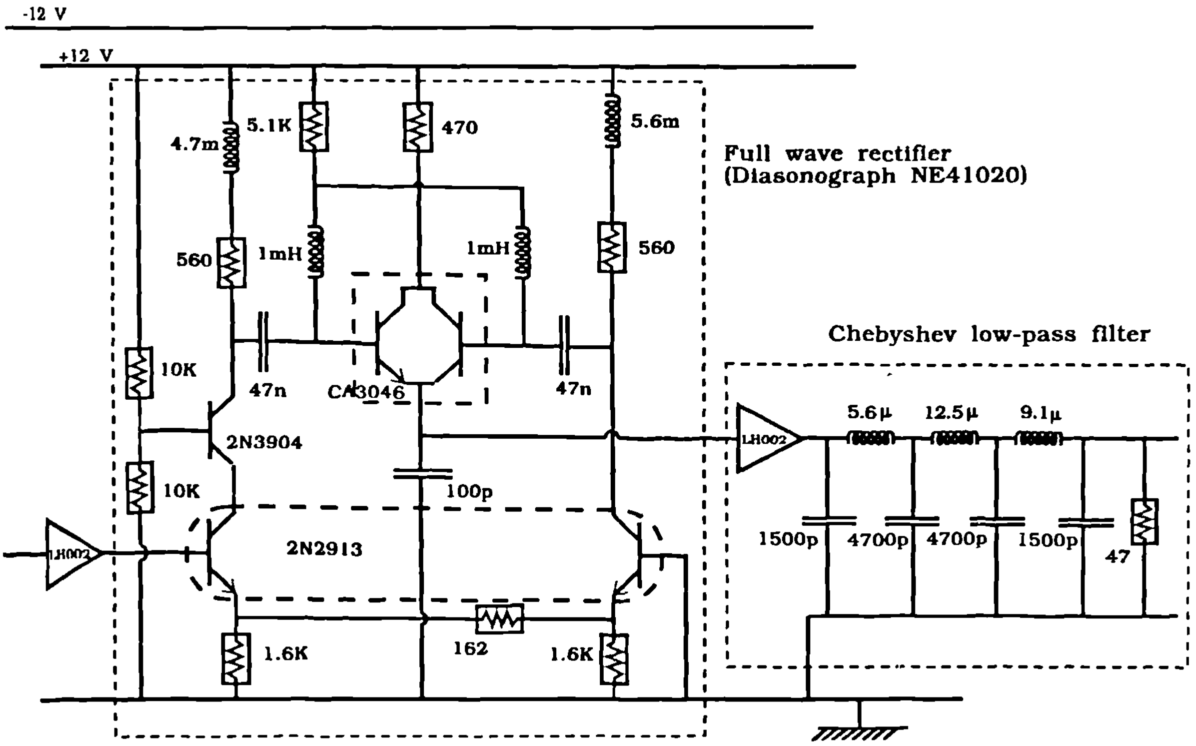

Figure 5.6 **Circuit for signal demodulation, incorporating a full-wave rectifier from a Diasonogaph NE4102A.**

EUB-24 before the demodulation stage and fed into a separate circuit designed specifically to perform low noise demodulation. The full-wave rectifier part of this circuit is a modification to one used in a Diasonograph NE4102A B-mode scanner. The low-pass filter is a 9-pole Chebyshev with a high frequency roll-off at 1.25 MHz, and was designed specifically for this UCT work. The circuit layout is shown in Figure 5.6.

Logarithmic compression is another non-linear processing stage usually present in conventional B-scanning. It will now be shown how this stage can be usefully retained for reflection UCT even though it violates the assumption of linearity. The main reason for performing logarithmic compression on the received signal is that the dynamic range (ie the ratio of the largest to the smallest signal) of the echoes from soft tissue and tissue interfaces may be as high as 50 dB, whereas the dynamic range of a typical 6-bit digitiser used in conventional scan-converters is only 36 dB. Much of the structural information of most interest is contained in the lower level echoes which because of the limited dynamic range of the digitiser can be represented by only a relatively small number of digitised levels. Conversely the echoes from tissue interfaces are relatively large and need not be represented by very many digitised levels to preserve their information. Hence appropriate logarithmic compression of the echo signal is applied to allow the echoes of most interest to be better matched to the available dynamic range of the digitiser.

For this work an 8-bit digitiser (dynamic range is 2^8 or 48 dB) has been used (see below). This obviously reduces the problem, but it is still useful to have as many digitised levels as possible available for the lower level echoes. The problem of non-linearity has been alleviated by restoring the linearity of the digitised data in the computer. This was done by first converting the data into 16-bit numbers to allow a higher dynamic range (96 dB), and then scaling the data with the inverse of the logarithmic compression function.

5.3.2 Digitisation, data transfer and sampling requirements

5.3.2.1 Digitisation rates and dynamic range

The digitisation rates required depend on the maximum frequency content of the signal being digitised. The Nyquist sampling criterion requires that the digitisation rate should be at least twice the highest frequency present in the signal. Since all real signals are inevitably contaminated to some extent by wide band noise, in practice the rate should be higher than this to ensure that all signal frequencies are reproduced with the correct amplitude. It has been decided here to sample at twice the Nyquist frequency, ie at four times the highest frequency in the signal. For demodulated echoes from the 3 MHz probe there should be no significant signal above 1.5 MHz, and so ideally a digitisation rate of at least 6 MHz should be used.

Any digitised signal has a limited dynamic range determined by the number of binary digits (bits) assigned to each digitised sample. As discussed in the previous section, an 8-bit (48 dB) digitiser should be adequate provided that the dynamic range of the echo signal has been logarithmically compressed before digitisation.

The total amount of data required for the reconstruction of a complete reflection UCT image of a single plane will depend on the following factors:-

(1) The number (N_p) of B-scan positions around the target.

(2) The number (l) of beam positions making up each B-scan.

(3) The total pulse-echo time required at each beam position which depends on the diameter (d) of the target being scanned and the average acoustic speed (c) of the target.

(4) The digitisation rate (R).

(5) The dynamic range (D) of the digitiser in bytes (1 byte = 8 bits) per sample.

The formula for the total amount of data required (in bytes) is

$$Number\ of\ bytes \quad = \quad N_p * l * \frac{(2\,d)}{c} * R * D \qquad (5.1)$$

5.3.2.2 Sampling requirements

It was shown in section 4.6.3.3 that, to obtain an adequately sampled reconstruction using the narrow beam method, the number of B-scans required within a total angle of 180° is given by

$$N_p \quad = \quad \frac{\pi\, w}{2\Delta p}$$

where w is the minimum null to null pulse-echo beam width and Δp is half the transmitted pulse length. Hence for this system

$$N_p \quad = \quad \pi \left[\frac{\sim 7\ mm}{1.5\ mm}\right] \quad \simeq \quad 15 \qquad (5.2)$$

It is preferable that the data is acquired and stored as quickly as possible in order to minimise the possibility of target movement during the scan. Hence an ideal system would allow all of the data for one reflection UCT image to be stored in very fast access memory, since the relatively slow transfer of data onto computer disc (for example) would extend the acquisition time.

A Le-Croy 200-MHz 8-bit transient recorder and buffer was used for digitisation of the demodulated pulse-echo signals. The Le-Croy is a fully programmable system with 1 MByte of data storage. Assuming a digitisation rate R of 6.25 MHz, and substituting values for l, d, c and D of 70, 0.105 m, 1540 m/s and 1 respectively, results from (5.1) in a total amount of data for a single reflection UCT image of 893,750 bytes. Hence all of the data for one reconstruction can be stored in the transient recorder's buffer storage.

The transient recorder is interfaced to the computer for control and data transfer via an IEEE high-speed bus. Many features of the system are programmable, including choice of digitisation rates, definition of digitisation windows, choice of pre- and post-trigger samples and selection of amplifier gains and offsets. Criteria for the selection of these parameters will be discussed in section 5.4.3.

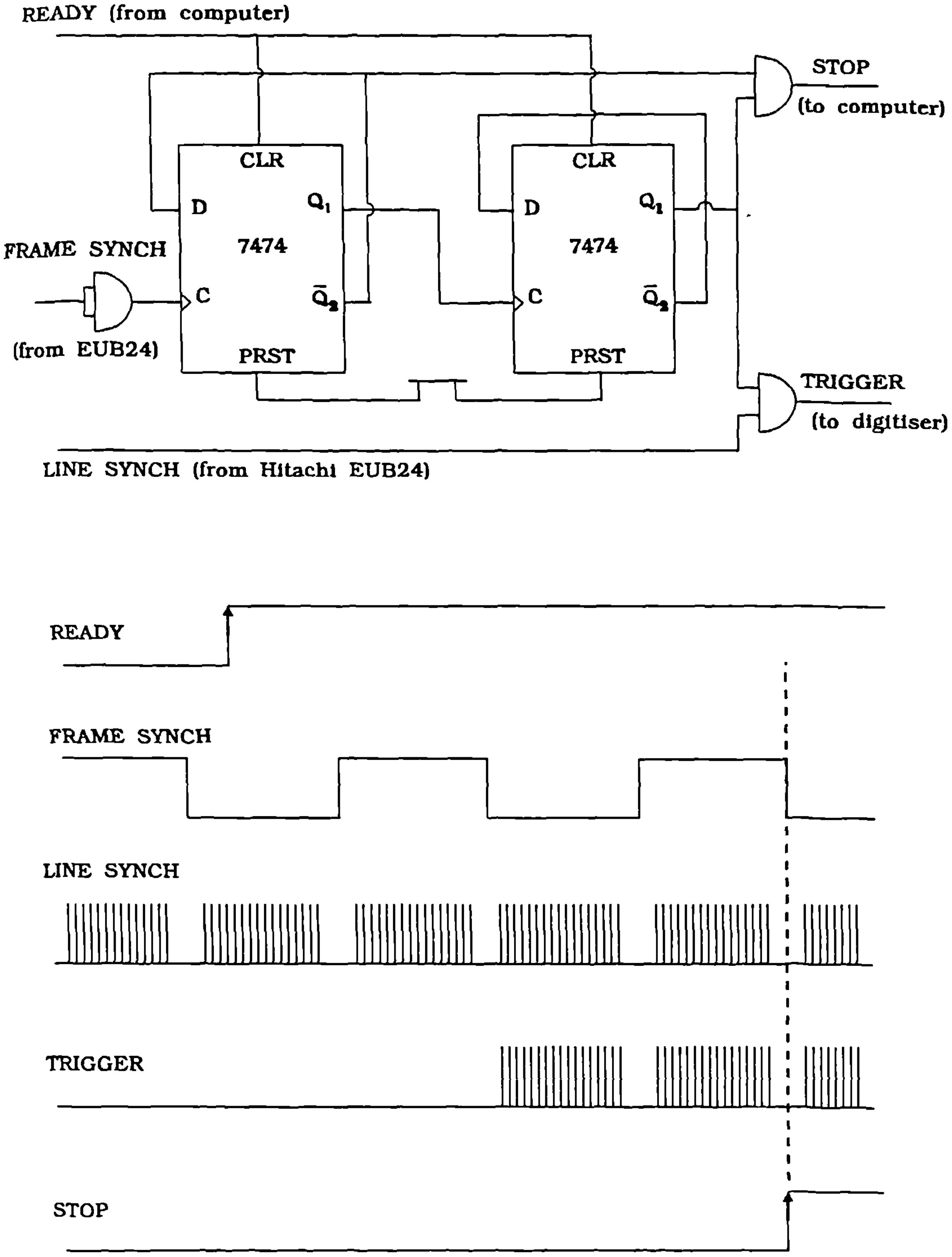

Figure 5.7 Logic circuit and signals for the synchronisation of data capture.

Synchronisation of data capture with the start of one B-scan frame of the linear array, and triggering of the Transient Recorder for digitisation of individual lines within a frame, was achieved via an electronic logic circuit shown in Figure 5.7.

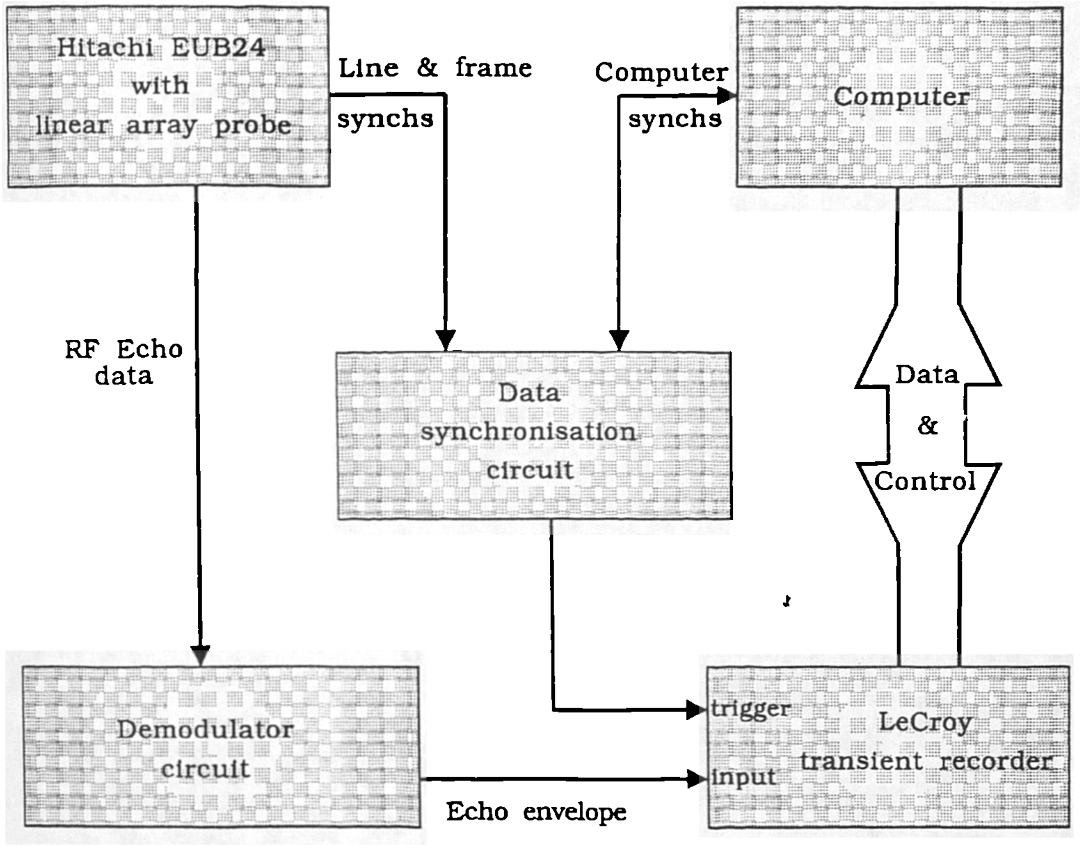

Figure 5.8 **Schematic diagram of the data acquisition system.**

This utilises frame and line synchronisation signals from the EUB-24, and a control signal from the computer, to generate the signals necessary for synchronisation and triggering. The electronic connections between the various components of the complete data acquisition system are shown schematically in Figure 5.8.

5.3.3 Mechanical scanning system

The movements required of the transducer aperture for reflection UCT may be separated into lateral and rotational components. Both lateral and rotational movements should ideally be under the control of a computer for maximum flexibility.

a) Lateral scanning

It has already been mentioned that the transducer aperture must be scanned laterally across the whole width of the target, with pulse-echo measurements being obtained at regular precisely known intervals to generate one B-scan from a given direction. For the positioning system not to be a limiting factor on the potential resolution (ie half the pulse length), it was decided that the position of the aperture during each measurement should be known to an accuracy of better than one-fifth of the pulse length (ie better than 0.3 mm).

Using a linear array probe for reflection UCT greatly simplifies the problem of accurate lateral scanning of the transducer aperture, since in a linear array this scanning is performed electronically by dynamic selection of an active group of transducer elements. The inter-element spacing for this array is 1.5 mm, which can be reasonably expected to be accurate to better than 0.3 mm. Hence the lateral beam positioning should be accurate to better than 0.3 mm. Since no mechanical movement with the inevitable backlash and vibration is required, the time taken to "move" the ultrasound beam to the next position is negligible compared to the time spent at each position (ie the pulse-echo time of the ultrasound pulse).

b) Rotational scanning

Since the lateral B-scans must also be obtained from many directions around the target, obviously a rotational movement of the transducer aperture is required. The positional accuracy of the rotational movement must at least as good as that in the lateral direction, ie better than 0.3 mm, for errors in probe positioning not to compromise the resolution of the reflection UCT image.

Thus a mechanical system was needed to rigidly support the linear array probe, with the freedom to move in a circular arc through 180 degrees in a suitable scanning tank. The full specification for the mechanical components of the system was as follows:-

i The centre of rotation of the probe must be constant to better than 0.3 mm.

ii The probe, once positioned, must remain fixed with a precision of less than 0.3 mm.

iii The system should have as little inertia as possible, consistent with sufficient rigidity, to allow rapid movement of the probe and hence short scanning times.

iv The probe mounting should be as streamlined as possible to minimise any turbulence in the water.

With these specifications in mind, a preliminary design of a probe support was made based on a simple cylindrical arm pivoted at both ends via flat plates and subsequently used in a detailed analysis of stress and strain. This analysis included consideration of a range of realistic scanning sequences (ie number of angular positions, time to complete scan, acceleration and deceleration profiles, etc), so that the expected torques and forces could be calculated. Decisions on materials and material thicknesses could then be made. A diagram of the probe support arm is shown in Figure 5.9.

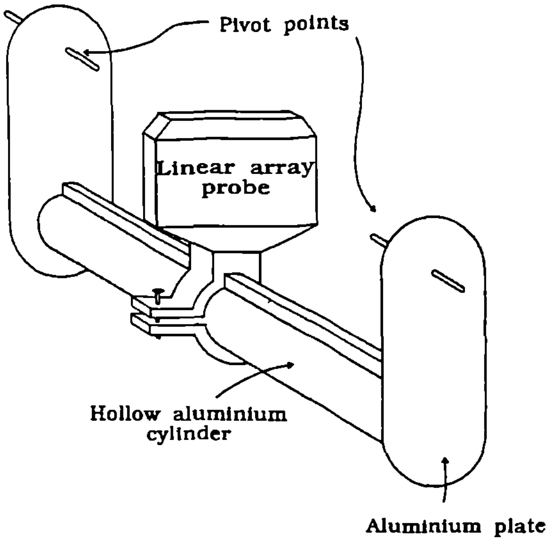

Figure 5.9 Probe support arm.

c) Scanning tank

The scanning tank needed to be large enough to accommodate the full range of probe movement. Since the width of the scanned field was 10.5 cm (see 5.3.1), which defines the upper limit on the size of target that can be imaged, it was decided that a scan diameter of up to 20 cm would be more than adequate for all targets. Allowing for the depth of the probe and support arm (about 15cm), the dimensions of the rectangular scanning tank were set at 70 cm long by 60 cm wide by 40 cm high. The rigidity of the pivot points for the probe support arm was maintained by a strong iron framework outside the tank. Hence the polypropylene walls of the tank only needed to be thick enough to contain the water, and were not required to aid mechanical rigidity. Waterproofing of the probe was achieved by placing the probe, and part of its cable, in a large latex sheath obtained from a commercial supplier. These sheaths are designed specifically for covering ultrasound probes (e.g. transrectal and transvaginal probes) and as such cause minimum perturbation of the ultrasonic beam when used with an ultrasound coupling gel.

The scanning tank was filled with a water/alcohol solution to provide acoustical coupling between the probe and the target. The ethyl alcohol is included to raise the normal speed of sound in the water (about 1480 m/sec at room temperature) to nearer the average speed of sound in soft tissue (1540 m/sec), so as to minimise artifacts which would arise from a difference in acoustic speed between the water and the target. This requires a concentration of about 10% alcohol.

The design of the mechanical system was submitted to the Department's Bioengineering Section for comments and approval. All of the construction of the system, apart from the polypropylene water-tank which was commissioned from a commercial manufacturer according to specifications, was carried out in the Department's Mechanical Workshop.

5.3.4 Motor drive system

A drive system was required to move the probe in a circular arc and position it, quickly and accurately, under the control of a computer. The following specification was produced:-

i To move the probe to any position in a 180 degree arc with a resolution of 0.1 degrees (equivalent to 0.3 mm for a scan radius of 10 cm).

ii To achieve the movement in the minimum time consistent with reasonable cost.

iii To allow full control of the drive profile (ie acceleration rates, deceleration rates, peak speed, etc) from a computer.

Based on the design of the mechanical scanning system (see Section 5.3.4), an analysis was performed of the torque, rotor inertia and maximum speed requirements for a motor, assuming the same scan sequences as considered previously.

Two types of drive system were considered, a) an open-loop stepper-motor system, and b) a closed-loop dc servo-motor system. The main problem with an open-loop system is that it is possible under heavy load to "loose track" of position, ie miss a step, and there is no way of knowing if this has occurred. In a closed-loop system where the position of the load is constantly monitored, any inevitable flexibility or backlash between the drive and the load can be accommodated. Hence a closed-loop servo motor system which met the specifications was purchased from a commercial supplier. The components of this system and their inter-relations are shown in Figure 5.10.

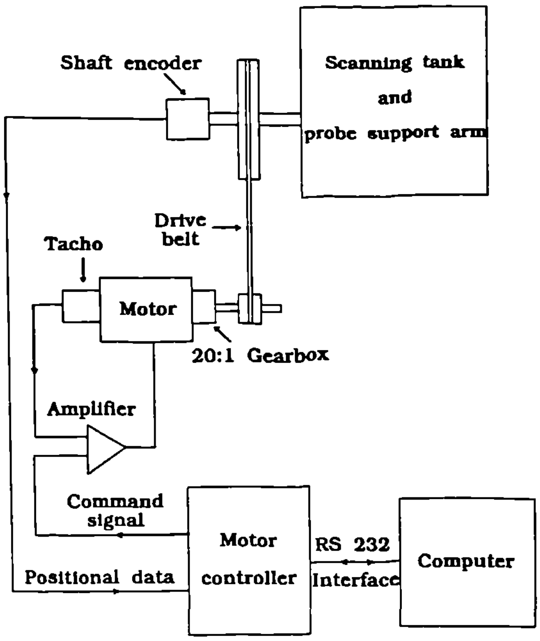

Figure 5.10 Schematic diagram of the motor drive system.

To provide sufficient torque at the load with a servo-motor of reasonable size and cost, a gear ratio of 60:1 was inserted between the motor and the load. This gearing was provided by a 20:1 gearbox attached directly to the motor and a 3:1 toothed belt drive.

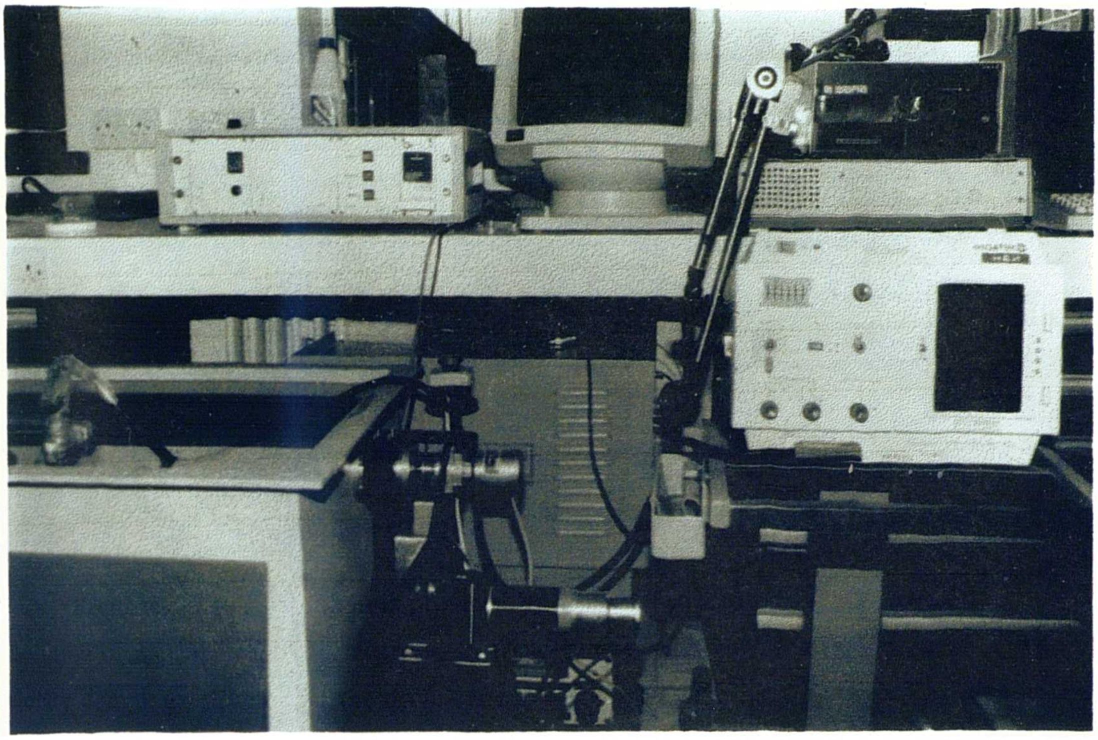

Figure 5.11 **Photograph of the complete reflection-only UCT system.**

Feedback of load position is provided by a 4000 line incremental shaft-encoder, giving a resolution of approximately 0.1 degrees. A tacho-generator provides feedback of motor speed for velocity damping. Control of the drive system is achieved via an RS232 serial link between the computer and an intelligent motor controller. The motor controller accepts ASCII commands to alter the acceleration, deceleration, speed and position of the motor, as well as many other functions. The controller utilises Proportional Integral Derivative Feedforward (P.I.D.F.) control, using four constants which may be varied, either manually or automatically via a software package, to optimise the behaviour and response of the motor for a particular move profile. Particular emphasis may be placed on settling-time, overshoot, disturbance response, or some combination of these. These feedback parameters were varied systematically until a set suitable for the majority of the envisaged scanning profiles was obtained. Figure 5.11 shows a photograph of the complete reflection-mode UCT system.

5.3.5 Software

The software to perform reflection UCT was initially written on a Sage IV micro-computer running the CPM-68K operating system, although this computer was later replaced by a more advanced SUN 386i. Pascal was chosen as the language for the majority of the software, and for the user-interface in particular, because it is modular and hence aids structured design and programming, and it is well supported and thus fairly portable. Some low-level routines that needed to run particularly fast, or needed access to the computer's operating system or peripherals, have been written in 'C' or assembler. The modular nature of both Pascal and 'C' has enabled the software routines to be separated into discrete modules, where all routines within a module share a common purpose. This modular design has been essential in allowing the software development for such a large project (over 6000 lines of code have been generated for this reflection-only UCT system alone) to be efficiently managed. The main modules are:-

"UCT_MOTOR":

Contains routines for defining a scanning sequence and programming the motor controller.

"UCT_ACQUISITION":

Contains routines for data acquisition, including control of data capture, transfer, and storage, and calculation of the centre of rotation of the system (see Section 5.4.2 for details).

"UCT_RECONSTRUCT":

Contains routines for converting the raw scan data to B-scan image format, routines for displaying B-scan images, and routines for reconstructing and displaying reflection UCT images.

"UCT_PROCESS":

Contains routines for reflection UCT image processing, including image rotation, adding, multiplying, scaling, linear translation, log and anti-log transforms, histograms, 1-D and 2-D convolutions and Fast Fourier Transforms, and many others.

With the basic tools outlined above any of the reconstruction techniques discussed in Section 2.3 can be implemented. Some of these techniques, and others, will be explored in the following sections.

5.4 Acquisition of a reflection-mode UCT image

5.4.1 Introduction

The main components of the hardware and software developed to perform reflection UCT in a vertical plane have now been described. The sequence of procedures involved in actually acquiring and reconstructing a reflection CT image are summarised in Figure 5.12. These are:-

a) Measure the centre of rotation of the system. This stage may be omitted if the probe has not been moved since the centre of rotation was last measured.

b) Enter the parameters defining the acquisition of the ultrasonic data, such as number of B-scans, total time for scan, etc.

c) Perform the scan.

d) Reconstruct the reflection UCT image.

e) Display the image.

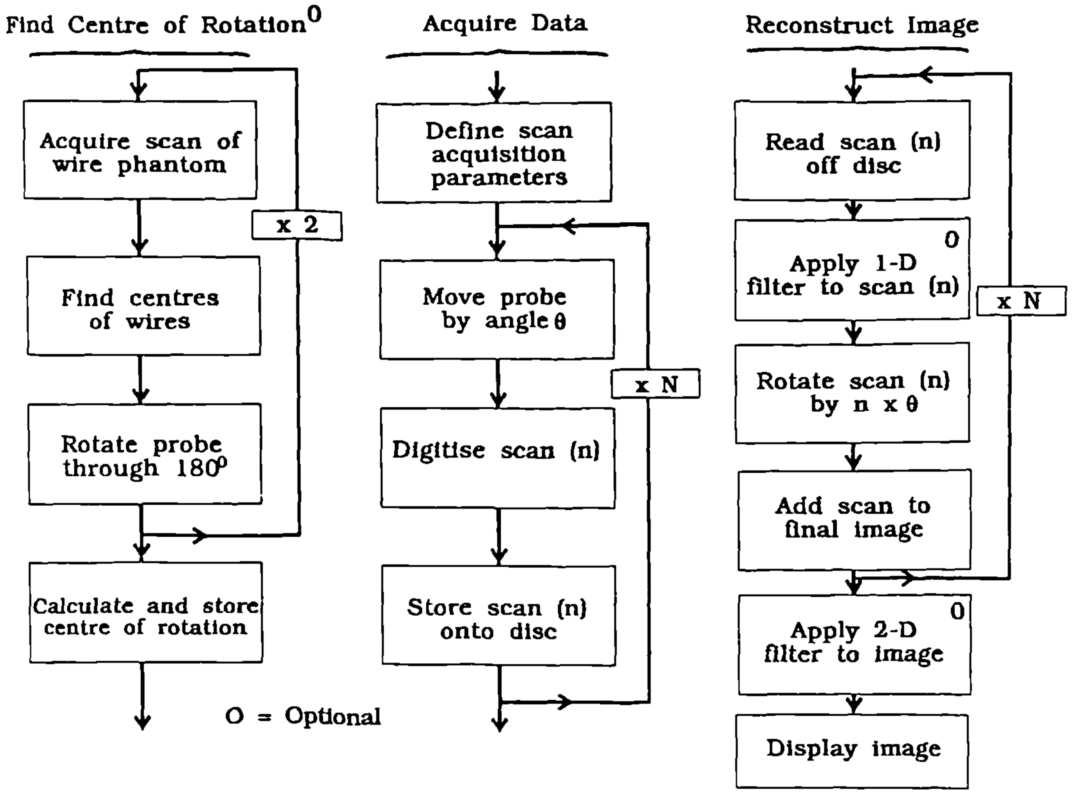

Figure 5.12 Procedures involved in acquiring and reconstructing a reflection UCT image.

These procedures will now be described in detail.

5.4.2 Measurement of the centre of rotation

An essential requirement for any imaging system that involves acquisition of data from many directions around a target, such as reflection UCT, is that the centre of rotation of the system can be determined to an accuracy which is considerably better than the required resolution of the image, and that this centre of rotation remains fixed (to the required accuracy) throughout the full range of movement. For this system, knowledge of the centre of rotation (c.o.r.) is required so that the reflectivity data from each of the B-scans that have been acquired at different angular positions may be correctly rotated and superimposed in the computer. Hence the accuracy of the estimation of the c.o.r. will inevitably limit the ultimate resolution of the reflection UCT image, irrespective of the efficacy of any reconstruction algorithm used. Consequently considerable effort has gone towards ensuring that the c.o.r. can be measured accurately.

There are essentially two distinct approaches by which the c.o.r. can be estimated. One possible method is to estimate the position of the c.o.r. by careful measurements on the mechanical scanning system itself. It was felt that this would be very difficult to achieve to the required accuracy of 0.2 mm, and also very time consuming if the c.o.r. was likely to change between scans, and particularly after removing and replacing the probe. An alternative method involves looking at the images actually produced by the system, using a suitable test object, and attempting to choose a c.o.r. that in some way optimises the image. A method such as this can be implemented in software and hence made to operate automatically, thus allowing the c.o.r. to be re-calculated easily at any time. A method based on this latter approach has been developed and is described below.

Referring to Figure 5.13, consider the B-scan image of a point target P(x,y) in water/alcohol obtained with the probe pointing along the negative y-axis. The distance of the point target from the front face of the probe is x_1, while the distance to one edge of the probe's ultrasonic field is y_1. These distances can be measured quite easily from the B-scan image itself, since both the speed of sound in the water/alcohol and the line spacing of the probe are known. If the probe is rotated by 180 degrees about the unknown centre of rotation (x_c, y_c), so that it now points along the positive y-axis, the equivalent distances become x_2 and y_2 respectively. The centre of rotation, in terms of the axial distance from the probe face and the lateral distance from one end of the probe, may now be estimated from the average (ie effectively the Centre of Gravity) of the co-ordinates $(x_1, y_1; x_2, y_2)$.

The accuracy of this estimate will depend on how accurately the distances $(x_1, y_1; x_2, y_2)$ can be measured, in other words on how accurately the centre of an echo image from a point target can be determined. This accuracy will be of the order of half the pulse length along x (ie about 0.75 mm), and about half the beam width along y (about 2.0 mm). However a second target in the image would give another estimate of the c.o.r., and, assuming that the measurement errors are random, N targets would give N independent estimates which could be averaged to give a more accurate result (accuracy of average using N independent estimates is 1/√N better than accuracy from a single estimate). As many targets can be used as are necessary to achieve the required accuracy in the estimate of the c.o.r., as long as their echoes do not overlap.

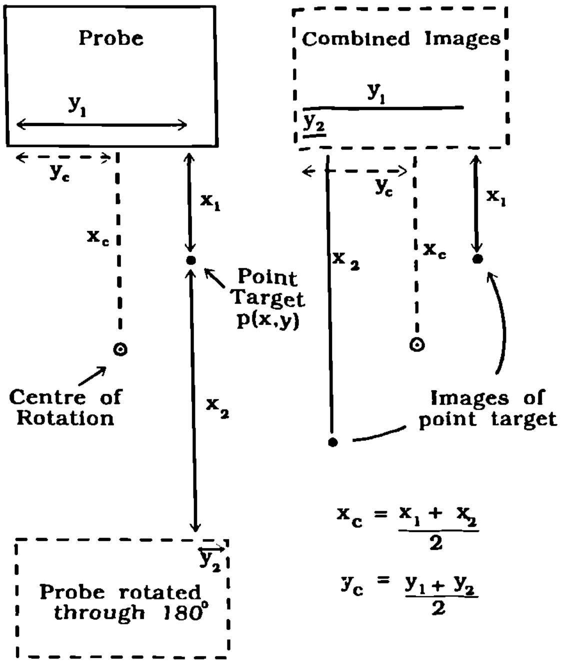

Figure 5.13 **Principle of the method for measuring the centre of rotation.**

A test-object for measurement of the c.o.r. has been constructed (Figure 5.14). It consists of 50 thin (0.2 mm dia.) nylon wires arranged in a rigid lattice. These wires were found, after experiments, to give the shortest echoes consistent with sufficient tensile strength in the wire. Software has been written to automatically search for the centres of the echoes in the two opposite B-scans, and subsequently calculate the c.o.r. The complete process of setting up and measuring the centre of rotation takes about 3 to 5 minutes.

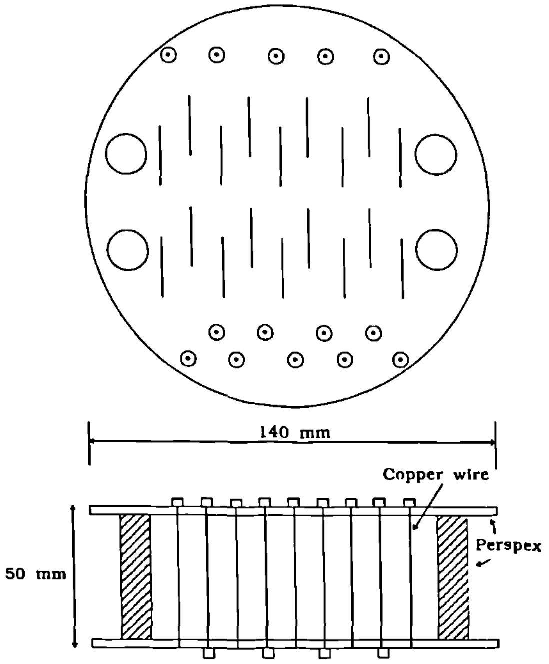

Figure 5.14 **Test-object for measuring the centre of rotation.**

The repeatability of the method has been tested by taking a series of separate measurements of the c.o.r., with the test-object being removed and then replaced in a slightly different position between each measurement. The experiment showed that the measurement is repeatable to less than 0.3 mm, which just about meets the requirements set out in section 5.3.4.

5.4.3 Definition of the acquisition parameters

Once the centre of rotation of the system has been obtained, the operator must define several parameters which will determine how the ultrasonic data will be acquired.

a) <u>Scan parameters:</u>

The operator must first define the scanning geometry in terms of

i. The total scan angle (up to a maximum of 180 degrees).
ii. The number of angular positions of the probe (ie the number of B-scans) required.
iii. The total time for the scan to be completed.

The program written for reflection UCT then calculates the time available to move the probe between positions and, based on the angular displacement profile shown in Figure 5.15 and the known inertias of the complete system, calculates whether the motor can deliver the necessary torque to achieve this. The displacement profile incorporates a 'creep' phase to minimise the possibility of ringing or overshoot in the probe positioning. If there is insufficient torque to deliver the requested move, the operator is asked to re-enter the parameters and to allow a longer time for the move. Although it may seem sensible to always select the shortest possible scan time, this may not be advisable for some targets where turbulence generated in the water by the rapidly moving probe might cause the target to move during the scan. When an acceptable move has been

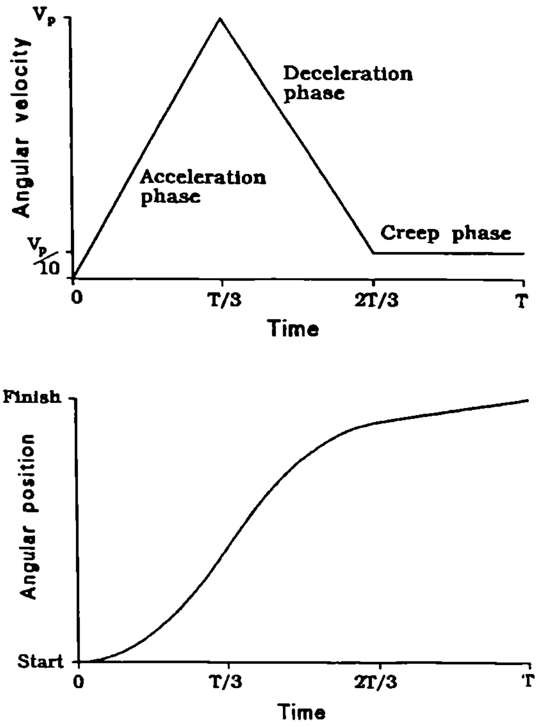

Figure 5.15 **Angular displacement profile for probe movement.**

defined, the software then programs the motor controller with the appropriate acceleration, maximum speed and deceleration information.

b) Data acquisition parameters:

The operator must now choose the parameters which determine how the ultrasonic data will be acquired. These are:-

i. The distance along a scan line where digitisation will start and end, ie defining the target region. This values are converted to the equivalent ultrasonic times-of-flight, assuming that the speed of sound in the water/alcohol solution is known, which are then used to set the digitisation window of the transient recorder.

ii. The digitisation rate, which for demodulated signals is 6.25 MHz.

iii. The maximum amplitude of the received signal. This ensures that the full dynamic range of the digitiser (ie 8 bits = 48 dB) is utilised.

The software will then program the transient recorder accordingly.

c) Receiver gain:

It has already been mentioned in section 5.3.1 that the ultrasonic pulses suffer exponential attenuation as they propagate through the target, thus reducing the amplitude of echoes received from increasing ranges. This attenuation can be at least partially compensated for by a logarithmic receiver gain which varies with time-of-flight and hence range. This feature is often called time gain compensation (TGC) or swept gain. Since a real (ie tissue) target will normally exhibit a spatially varying attenuation coefficient, TGC can only compensate for the "average" attenuation of a target. Also, different targets will present different average degrees of attenuation so that a way of varying the slope of the logarithmic gain is required. Such a control already exists on the Hitachi EUB-24 and so no additional electronics were necessary. This control is adjusted, before acquisition of the reflection UCT data, until the strongest echoes displayed in the real-time B-scan image from the EUB-24 appear to be just below saturation level at all ranges within the target.

5.4.4 Performing the scan

Some care is required in positioning the target within the scan plane. The target should ideally be centred as closely as possible to the centre of rotation of the scanning system. This ensures that outer parts of the target do not extend outside the field of view of the linear array for some probe positions. The target should also be constrained so that any turbulence set up in the water by the rotating probe do not cause appreciable movement. If this is not possible, as for example with an in-vivo subject, the scan is best performed as quickly as the program will allow to minimise involuntary movements of the subject.

Having defined the scan geometry and the data acquisition parameters, the scan acquisition sequence can be initiated. As soon as the data from all the B-scan positions has been digitised and stored by the transient recorder, the data is immediately transferred to the computer and stored onto hard disc. Acquisition of a 15-view scan (ie 15 B-scans) takes a minimum of about 10 seconds.

5.4.5 Reconstruction of the reflection UCT image

The theoretical basis of reconstructing a reflection UCT image has already been discussed in detail in section 4.4.2. Hence this section will merely outline the practical implementation of the main stages.

5.4.5.1 Scan conversion

The first stage of image reconstruction is to convert the ultrasonic data acquired in B-scan format, ie 70 lines of digitised echo data, into the 256 by 256 pixel-image format. For this work this has been accomplished by a software implementation of the linear-array scan-converters used in commercial scanners. In this program linear interpolation, both along and between scan lines, has been used to derive the echo value to be assigned to a given pixel.

5.4.5.2 Backprojection

The process of backprojection involves summing, for each and every pixel in the reconstructed image, the echo amplitudes from corresponding points in each (filtered or un-filtered) B-scan defined by the pixel's location in image space. In practice it is faster to deal with all the data for each B-scan in sequence, which then involves calculating which pixel or pixels should receive data from each digitised sample in the B-scan.

5.4.5.3 Post-processing

As described in Section 4.4.3, knowledge of the point spread function (psf) of the imaging system can be used to further improve the resolution of the simple summation image. There are two possible approaches (see Section 2.3.2):-

a) Summation with post-filtering:

The B-scans are rotated and summed to form the simple summation image, and then a 2-dimensional filter is applied to the final image.

b) Filtered summation:

Each scan-line of every B-scan is filtered with an appropriate 1-dimensional filter function before rotation and summation.

Method (a) has been implemented in this work because it is much faster then method (b) when more than about 4 B-scans are involved. The only potential advantage of method b) is that the filtering may be made depth dependent to account for a depth dependent psf (eg because of varying beam width). However, since there is not, as yet, sufficient information available about the nature of the psf within tissue, and particularly about how it varies with depth, it was not considered worthwhile to implement a depth dependent filter.

The filtering may be performed equivalently in either the space or spatial frequency (ie Fourier) domains, but for an image array size of 256*256 experience has shown that Fourier domain filtering is quicker. Details of the filters used and the results obtained for various targets will be presented in section 5.5.

5.4.6 Displaying the image

The reconstructed images are displayed at 256 by 256 resolution with a 256 level grey-scale look-up table. For the maximum target diameter of 10.5 cm this gives a pixel size of about 0.4 mm, which is about half the axial resolution of a B-scan and hence also about half the potential resolution of a reflection UCT image. Although the raw data in each B-scan is digitised to 256 levels, the processed reflection UCT images typically possess a wider dynamic range than this because they are composed from many summed B-scans and are accordingly represented by 16-bit numbers. Hence routines have been written to re-compress the image data using a selection of linear or logarithmic grey-scale transfer curves, so that the information in the images is better matched to the to the dynamic ranges of the display device and the human visual system. Logarithmic compression is particularly useful for emphasising low-echo regions in the images obtained from real tissues (ie equivalent to the log compression available as standard on conventional B-scanners).

5.5 Results from the vertical plane reflection-only system

5.5.1 Introduction

The primary aim of this practical investigation into reflection UCT was to highlight any advantages, or disadvantages, that reflection UCT has compared to conventional real-time B-scanning. Accordingly reflection UCT images obtained from various different kinds of target will be compared to single B-scan images obtained from the same target, and using the same linear array scanner for data acquisition (ie the Hitachi EUB-24F). This scanner is over 15 years old and has relatively poor dynamic range and penetration, and consequently the B-scan images presented will not be as good as could be obtained from a more modern machine. However, since the same raw ultrasonic data is used to reconstruct both the UCT image and the B-scan image, it seems justifiable to compare the two imaging methods directly. It should be true that any advantages that can be demonstrated for UCT over B-scanning would still apply if more sophisticated equipment (e.g. with a shorter ultrasonic pulse length and better dynamic range and penetration) was used for the data acquisition.

All the UCT images presented here have been acquired with the following conditions:-

i. Only demodulated echo data has been used.
ii. Data has been acquired over a total angle of 180 degrees.
iii. Fifteen views (ie 15 separate B-scans) have been acquired, at angles of 12 degrees between each view, in accordance with the sampling requirements discussed in Section 5.3.2.2.

Various factors must be considered when deciding which targets to scan. It might appear that the best way to compare two imaging techniques is to choose a target whose characteristics (ie geometry, scatterer density, etc) are known exactly. In this way the ability of the imaging techniques to represent the true structure of the target can be compared unambiguously. For ultrasonic imaging, the only targets whose characteristics are likely to be known exactly are those which have been constructed especially for this purpose, ie phantoms. In this study simple arrangements of thin wires in water have been used for the measurement of point spread functions (5.5.2) and to establish the high contrast resolution of the techniques (5.5.3 and 5.5.4). More complicated phantoms of varying scatterer density have been used to assess contrast resolution (5.5.3 and 5.5.4), while phantoms showing varying acoustic speed and attenuation have been used (5.5.5) to assess the presence of imaging artifacts.

The disadvantage of using phantoms to compare imaging techniques, at least those techniques intended ultimately for the imaging of soft tissue in-vivo, is that it is very difficult to construct phantoms which exhibit the complexity and range of structures found in real soft tissues. Since this reflection UCT system was not constructed to be particularly suitable for in-vivo imaging, an acceptable alternative is to image soft tissues in-vitro. Hence results for reflection UCT and B-scan imaging of some animal tissues in-vitro will be presented in section 5.5.6.

It could be argued that the only really worthwhile comparison of two in-vivo imaging techniques is with images obtained in-vivo. Some examples of in-vivo images are presented in section 5.5.7

5.5.2 Measurement of system point spread function

As discussed in Section 4.1, the simplest way of characterising a linear imaging system is through the system's point spread function (psf), or its Fourier Transform the system point transfer function (OTF). Although conventional B-scanning and reflection UCT can only be considered as linear imaging processes within certain restrictions (see 4.3 and 4.4), their respective psfs and OTFs can still show a great deal about the potential spatial resolution of the techniques. In the spatial frequency domain, the OTF shows how the spatial frequency content of the original object will be transformed by the imaging system into the spatial frequency content of the image. In particular, the maximum frequencies present (above noise) in the OTF will reveal what level of detail there will be in the image (ie the effective resolution of the image). Hence measuring the psfs, and then calculating the equivalent OTFs, is one useful way of comparing conventional B-scanning with reflection UCT.

The psf of an imaging system can most simply be measured by obtaining an image of a high contrast point target, ie a single target which is much smaller than the likely resolution of the system. In practice it is usually easier to use a line target orientated perpendicularly to the plane of the scan. Clearly, using such a target tells us nothing about the ability of the imaging system to resolve targets in the direction perpendicular to the scan plane, ie its ability to separate parallel image planes.

5.5.2.1 B-scan point spread function

The B-scan psf was measured by suspending a copper wire of diameter 0.22 mm (ie much less than half the pulse length) in a water bath, with the axis of the wire perpendicular to the scan

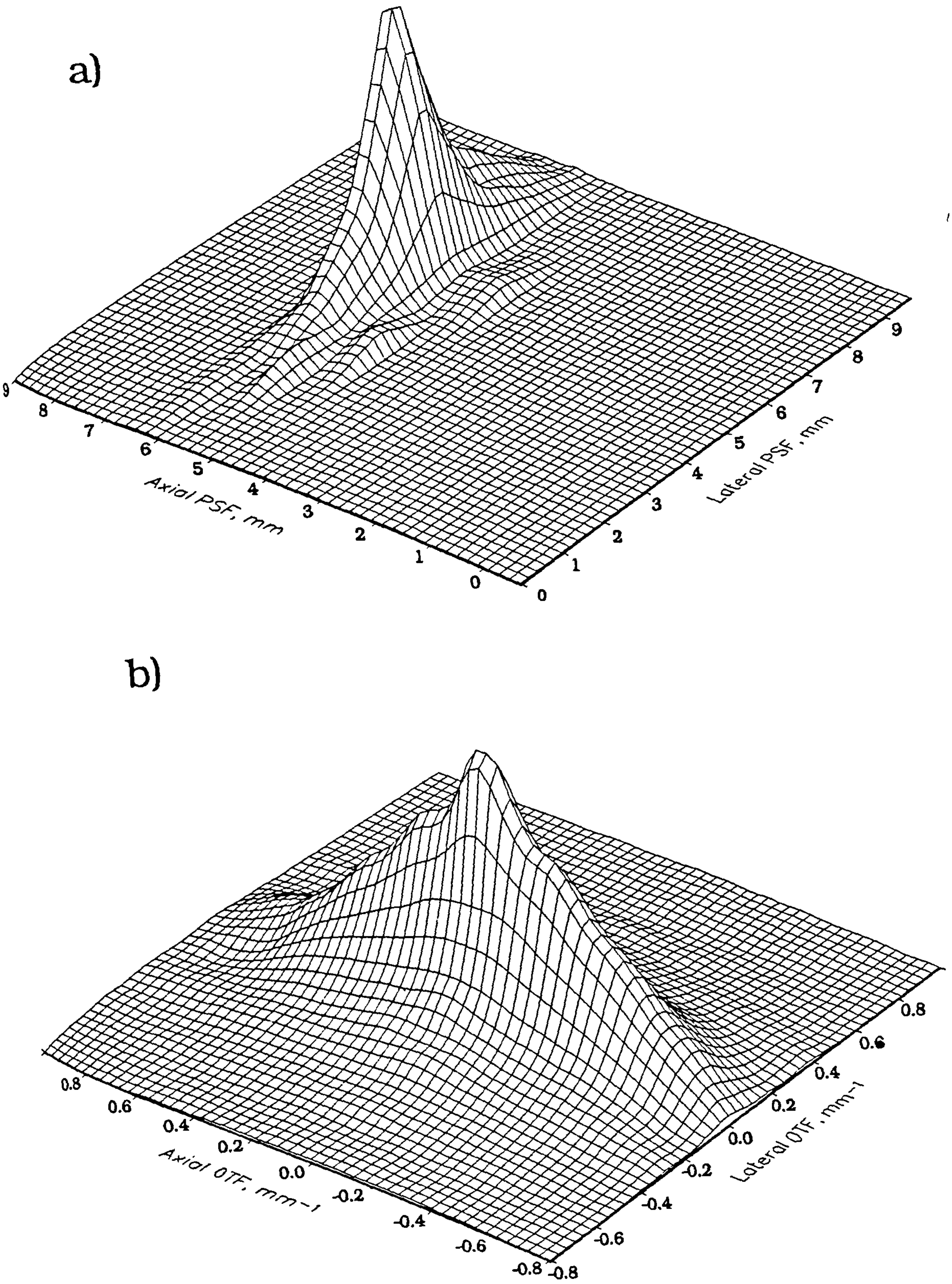

Figure 5.16 Measured B-scan (a) psf and (b) OTF.

plane so that it appears as essentially a point target. The wire was placed as close as possible to the centre of rotation of the reflection UCT system, at a distance of about 65 mm from the front face of the probe, ie near to the pulse-echo focus. To show the extent of the B-scan psf, a 3-D contour plot of the wire image has been plotted in Figure 5.16a. The axial component of the psf (ie $h_a(x)$ in section 4.3.2.2) has a full width at half maximum (FWHM) of about 1.0 mm, and this will correspond to the axial resolution of the B-scan. As expected, this is considerably better than the lateral component, $h_l(y)$, of the psf (ie lateral resolution) with a FWHM of about 2.8 mm. The B-scan OTF, obtained by Fourier transforming the psf, is shown in Figure 5.16b. It is actually displayed here as the modulus of the OTF (ie the spectrum). This clearly shows the wider bandwidth available in the axial as compared to the lateral direction.

5.5.2.2 Reflection UCT point spread function

To measure the psf of the reflection UCT system (ie $h_{ub}(x,y)$ in Section 4.3.3.2), the same wire target was scanned from 15 directions over 180 degrees. The B-scans were combined using simple, un-filtered summation to form a single image. A contour plot of this image (ie the reflection UCT psf) is shown in Figure 5.17a. Notice that the psf is now approximately symmetrical, as expected, indicating nearly isotropic resolution. The FWHM is about 1.6 mm. This value lies between the FWHM of the axial component and the FWHM of the lateral component of the B-scan psf, which is to be expected since, as shown in section 4.4, the reflection UCT psf is basically a rotated version of the B-scan psf. Hence the resolution of an unfiltered UCT image will be a little poorer than the axial resolution of a B-scan image but considerably better than its lateral resolution. The calculated OTF is shown in Figure 5.17b. The OTF is also nearly symmetrical, and again appears to extend to some way between the axial and lateral components of the B-scan OTF.

5.5.3 Potential resolution of reflection UCT and B-scanning

The resolution of an imaging system depends on many factors in addition to the point spread function. In particular, spatial resolution (the ability to discriminate between high contrast targets) and contrast resolution (the ability to discriminate targets of similar contrast) are inter-dependent, and both are affected by the level of noise in the image.

One useful way of representing both spatial and contrast resolution is in a contrast-detail diagram (e.g. Hill et al 1991), which plots the threshold for detectability of targets showing increasing

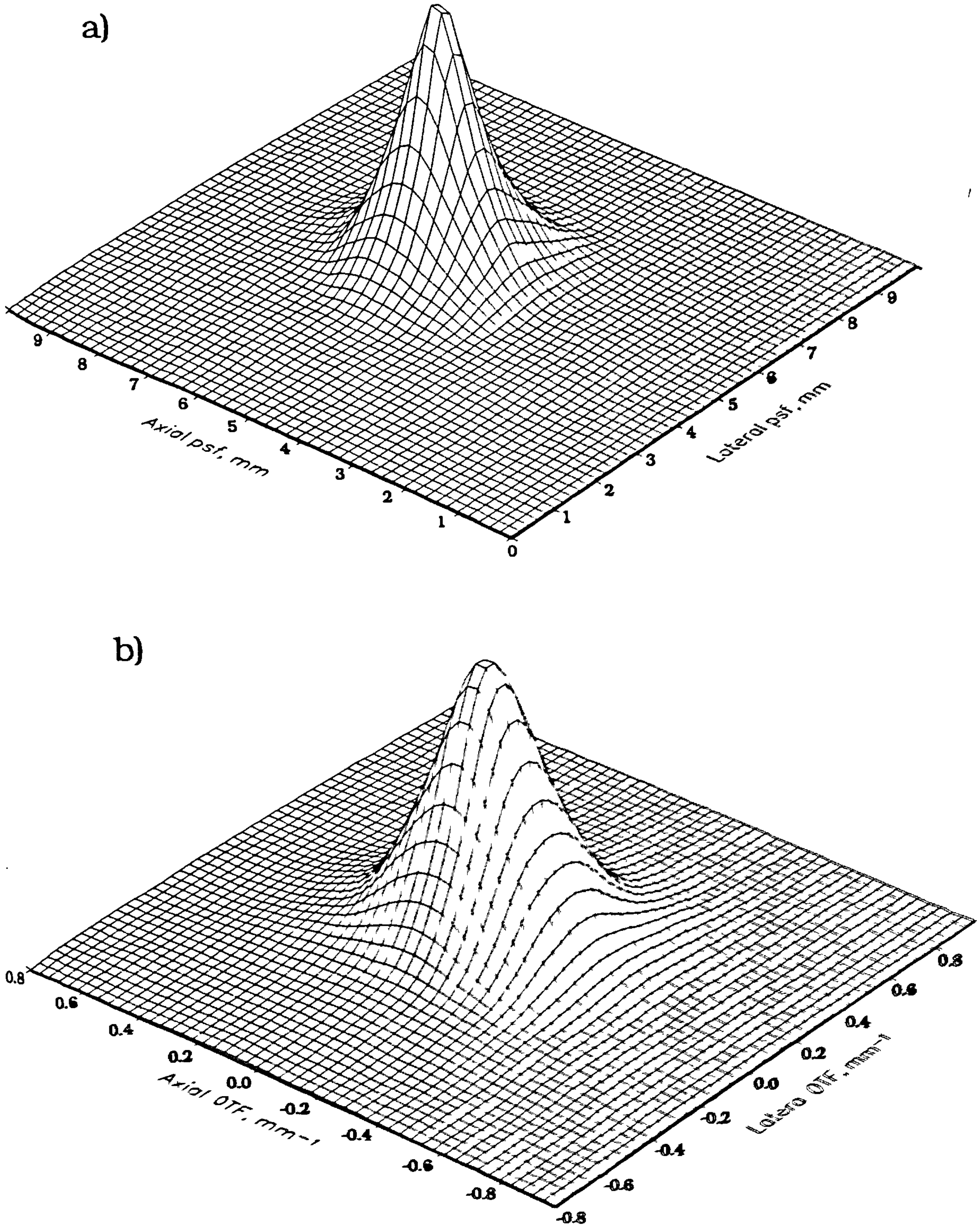

Figure 5.17 Reflection UCT (a) psf and (b) OTF.

size along one axis and increasing contrast (compared to the background noise level) along the other axis. To construct such a diagram requires measurements on a phantom having a wide range of targets of varying size and contrast. Such phantoms have been made for ultrasound (Smith and Lopez 1981), although a recent study (Lopez et al, 1990) suggests that errors associated with their use in comparing the performance of imaging systems are quite high. Another problem is that commercially available versions of this phantom are not suitable for the wide range of scanning angles necessary for reflection UCT. Although some attempts were made to construct a contrast-detail phantom suitable for reflection UCT, severe problems in obtaining predictable contrast levels were encountered and no results are presented here.

Studies using the phantom of Smith and Lopez have established that there are two regions in the contrast-detail relationship for B-scanning; (a) a high contrast region where target detection is primarily determined by the B-scan psf and is relatively insensitive to the contrast, and (b) a low contrast region where detectability is strongly dependent on target contrast. Following this principle, the assessment of comparative resolution for reflection UCT and B-scanning has been divided into high and low contrast situations.

High contrast spatial resolution has been assessed quantitatively using wire targets in water and in tissue equivalent materials. Due to the difficulty in making phantoms (reliably) having regions with small contrast variations, contrast resolution has been assessed qualitatively using a single low-scatter insert in a tissue equivalent material. Despite the limitations of this phantom, it is still useful for a simple comparison of reflection UCT and B-scanning.

Clearly, the construction of a phantom suitable for obtaining a full contrast-detail assessment of reflection UCT would be a useful area for further work.

5.5.3.1 Spatial resolution

On the basis of their measured psfs, reflection UCT would be expected to show improvements compared to B-scanning in the ability to resolve closely spaced targets, at least in the direction perpendicular to the B-scan beam axis. Various experiments have been performed to establish if this is true in practice.

Wires in water

It is instructive to compare conventional B-scanning with reflection UCT imaging in terms of their ability to resolve high contrast targets such as wires in water. Two B-scans were obtained, one with the axis of the beam along the line of the wires (Figure 5.18a) and one with the axis of the beam perpendicular to the wires (Figure 5.18b). The wire spacings are 1 mm, 2 mm, 5 mm, 10 mm and 20 mm respectively. As expected, the axial resolution (about 1 mm) is considerably better than the lateral resolution (between 2 and 5 mm). Figure 5.18c shows the un-filtered reflection UCT image of the wires. Here all but the 1mm separation wires are resolved.

Wires in tissue equivalent material

A more realistic indication of the potential resolution in real tissue is to look at targets imbedded in a medium which exhibits some of the features of real tissues, such as speckle. Hence a tissue equivalent material (TEM) phantom was made, using a mixture of agar, propanol and graphite powder (see Appendix II and Burlew MM et al, 1980), and having an acoustic speed close to that of the surrounding medium (ie 1540 m/s). This generates a B-scan with a general appearance that is very similar to that obtained from real soft tissues. A set of wires was then imbedded in this phantom. The B-scan image is shown in Figure 5.19a. Note the coarse pattern of bright and dark patches in the scattering background. These patches, which are commonly known as speckle, arise from the coherent nature of ultrasonic imaging and cannot be attributed to actual scattering centres in the object (see 4.3.2.3).

The unfiltered reflection UCT image (Figure 5.19b) is a considerable improvement. Note that the mean echo level of the speckle is reduced and the pattern is finer, a result that was predicted theoretically (4.4.3) and is also consistent with results obtained by, amongst others, Roehrlein and Ermert (1986). The reduction in the speckle level also contributes to the significant reduction in the size of the echoes from the wires and hence in potential spatial resolution.

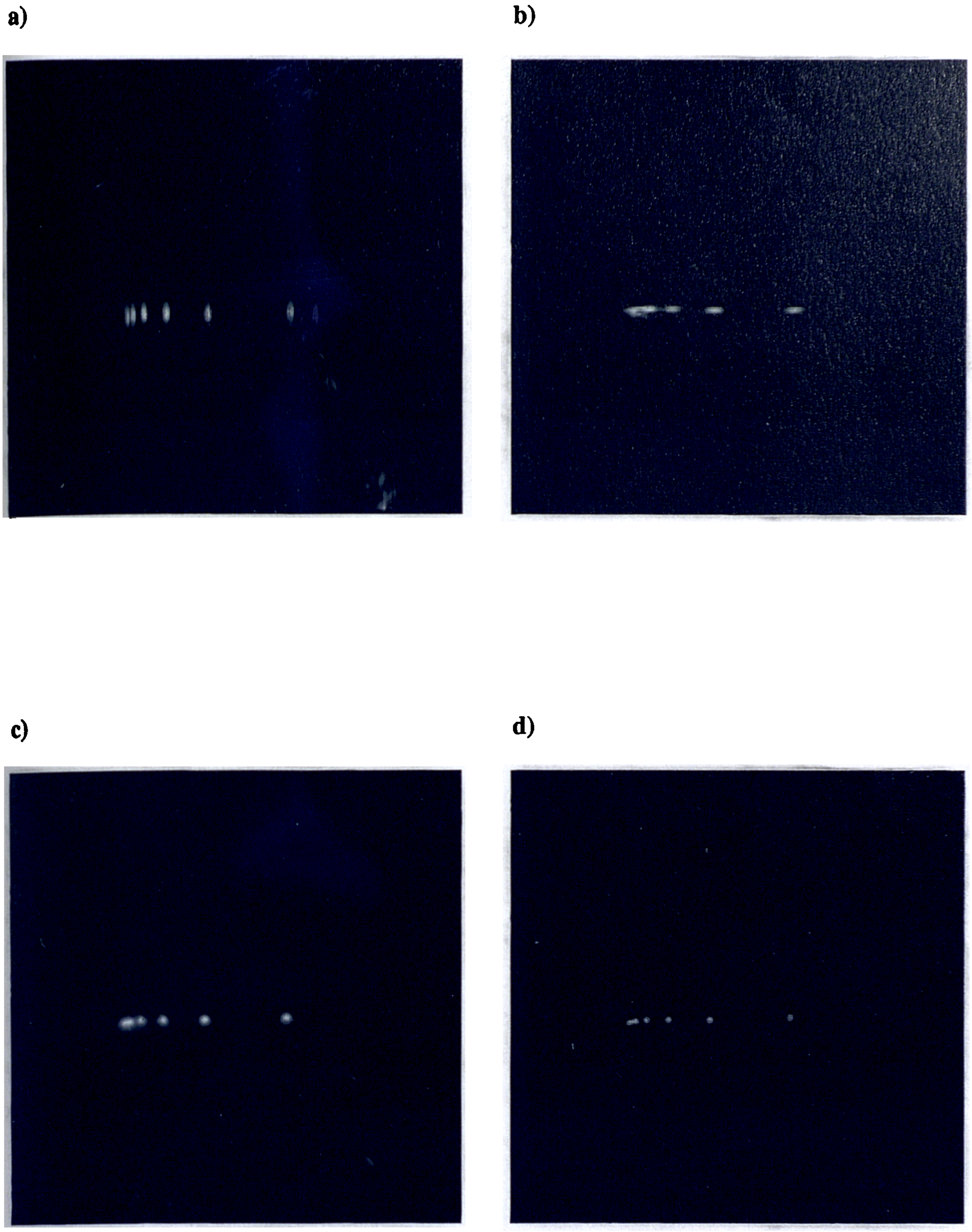

Figure 5.18 Resolution of metal wires in water; a) B-scan with beam axis parallel to wires, b) B-scan with beam access perpendicular to wires, c) unfiltered reflection UCT image and d) Wiener filtered reflection UCT image.

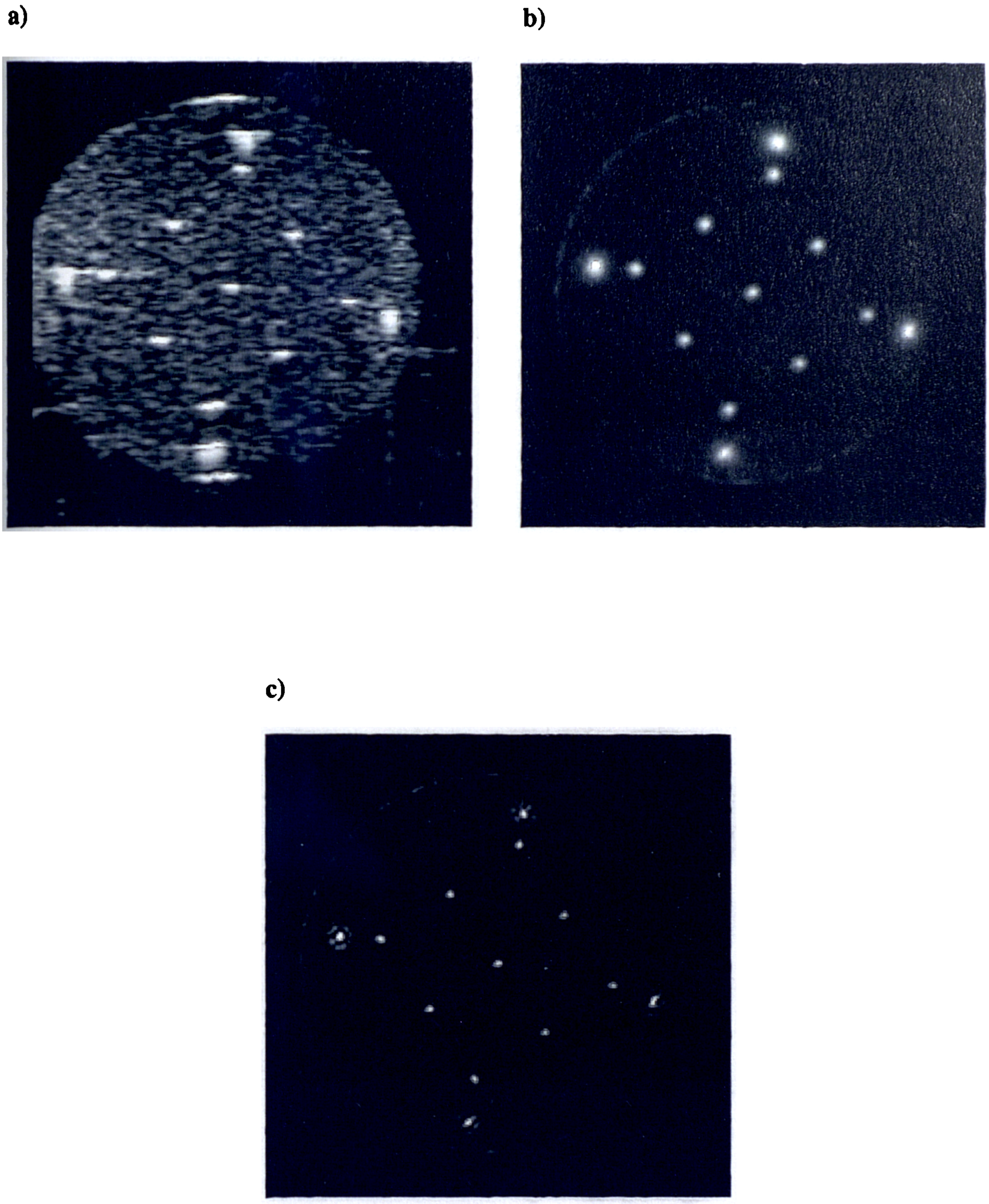

Figure 5.19 Wires in a tissue equivalent material: a) B-scan, b) unfiltered reflection UCT image and c) Wiener filtered reflection UCT image.

5.5.3.2 Contrast resolution

The targets that have been imaged so far are still not very realistic, for example one doesn't often find copper wires in soft tissues! To assess the comparative performance of reflection UCT and B-scanning in a target showing a more realistic level of contrast, a phantom consisting of a region of low scatter amplitude (a hole filled with a water/alcohol solution) embedded in a region of moderate scatter amplitude (the same TEM material as was used in the wire phantom) was constructed. This phantom can be thought of as similar to a fluid filled cyst in the liver, for example. Figure 5.20a shows a single B-scan of such a phantom, again with the ultrasound probe on the left. Note that the boundary of the "cyst" only appears when it is perpendicular to the ultrasound beam axis. In the unfiltered reflection UCT image, shown in Figure 5.20b, the boundary of the cyst is complete, making interpretation of the image easier. The speckle pattern is again much finer and less obtrusive, thus improving the potential contrast resolution when compared to the B-scan.

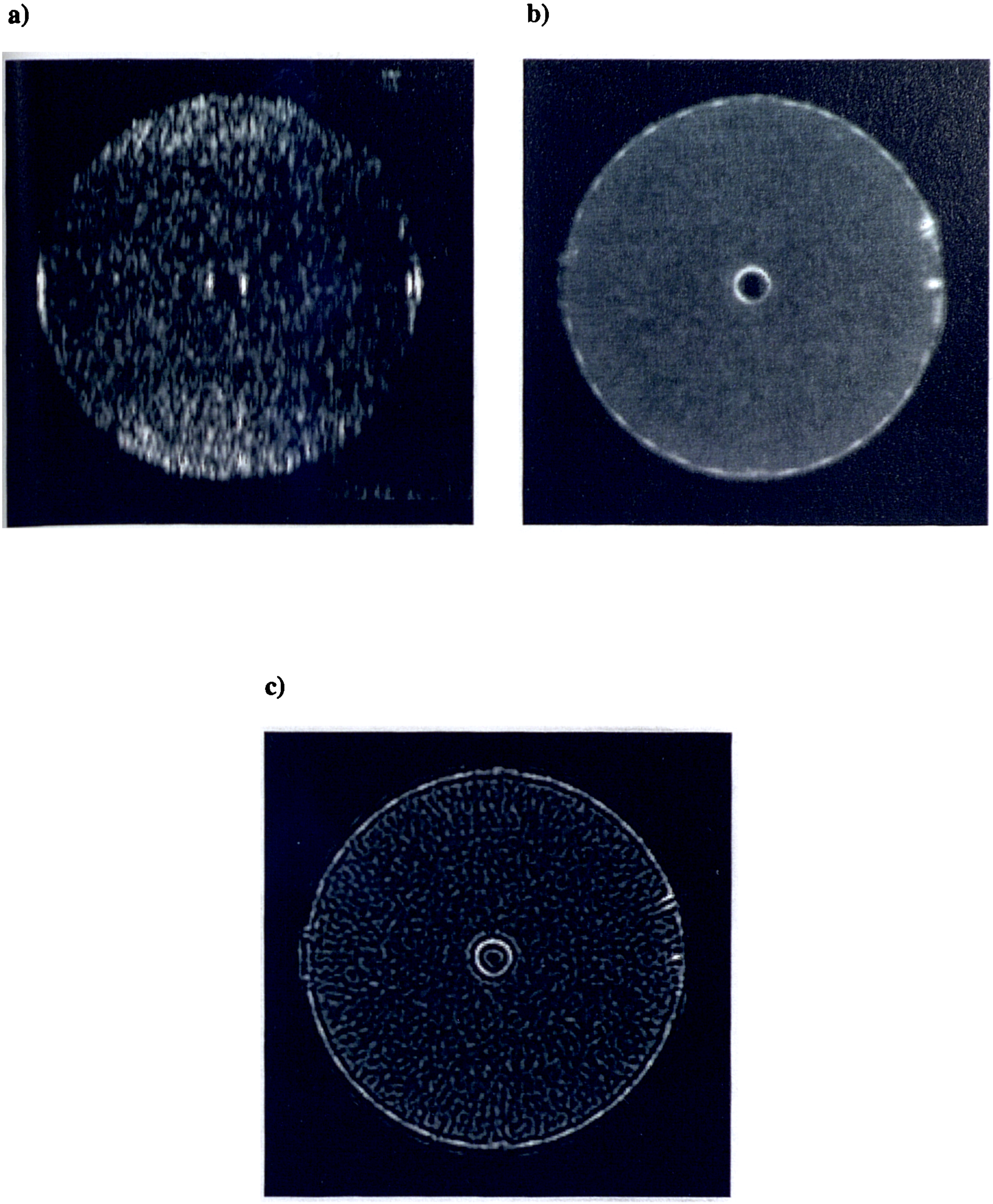

Figure 5.20 Cysts in a tissue equivalent material: a) B-scan, b) unfiltered reflection UCT image and c) Wiener filtered reflection UCT image.

5.5.4 Affects of inverse filtering on reflection UCT images

5.5.4.1 Introduction

The reflection UCT OTF extends, although at reduced amplitudes, right out to the maximum frequencies present in the axial component of the B-scan OTF. By applying a filter such as those discussed in section 4.4.3.2 to the UCT image, the potential appears to be there to achieve the axialresolution of a B-scan image in all directions. A suitable filter would be the Wiener inverse filter described in Appendix I.

The purpose of filtering in CT is to restore in the image the frequency content of the original object as closely as possible, up to the maximum frequency (R_{max}) present in the OTF. Wiener inverse filtering was introduced in section 4.4.3.2 as an alternative to the conventional tomographic filtering of CT images (see 2.3.2), which allows the high frequency roll-off of the filter to be optimised for the particular signal-to-noise characteristics of the OTF of the imaging system. A Wiener inverse filter appropriate to reflection UCT has been calculated from the reflection UCT OTF and is shown in Figure 5.21. It is interesting to see that, at low frequencies, the filter bears a strong resemblance to the filters predicted from CT theory (shown in Figure 2.4).

ie $\quad F(R) \simeq |R|$

It is also important to note that inverse filtering using such a filter is only strictly valid when the psf used to derive it does not depend on position. This filter has been applied to various targets to establish whether this assumption is justified, and whether inverse filtering in reflection UCT in general is worthwhile.

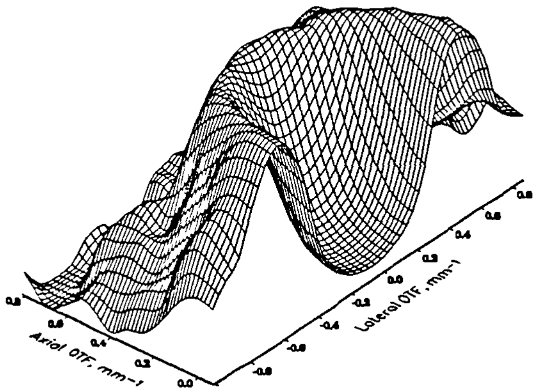

Figure 5.21 Wiener filter derived from reflection UCT psf.

5.5.4.2 High contrast targets

Single wire in water

The simplest test of a Wiener filter is to apply it to the UCT image of a single wire, ie to the psf used originally to derive it. The filtered image is shown in Figures 5.22a and the spectrum in

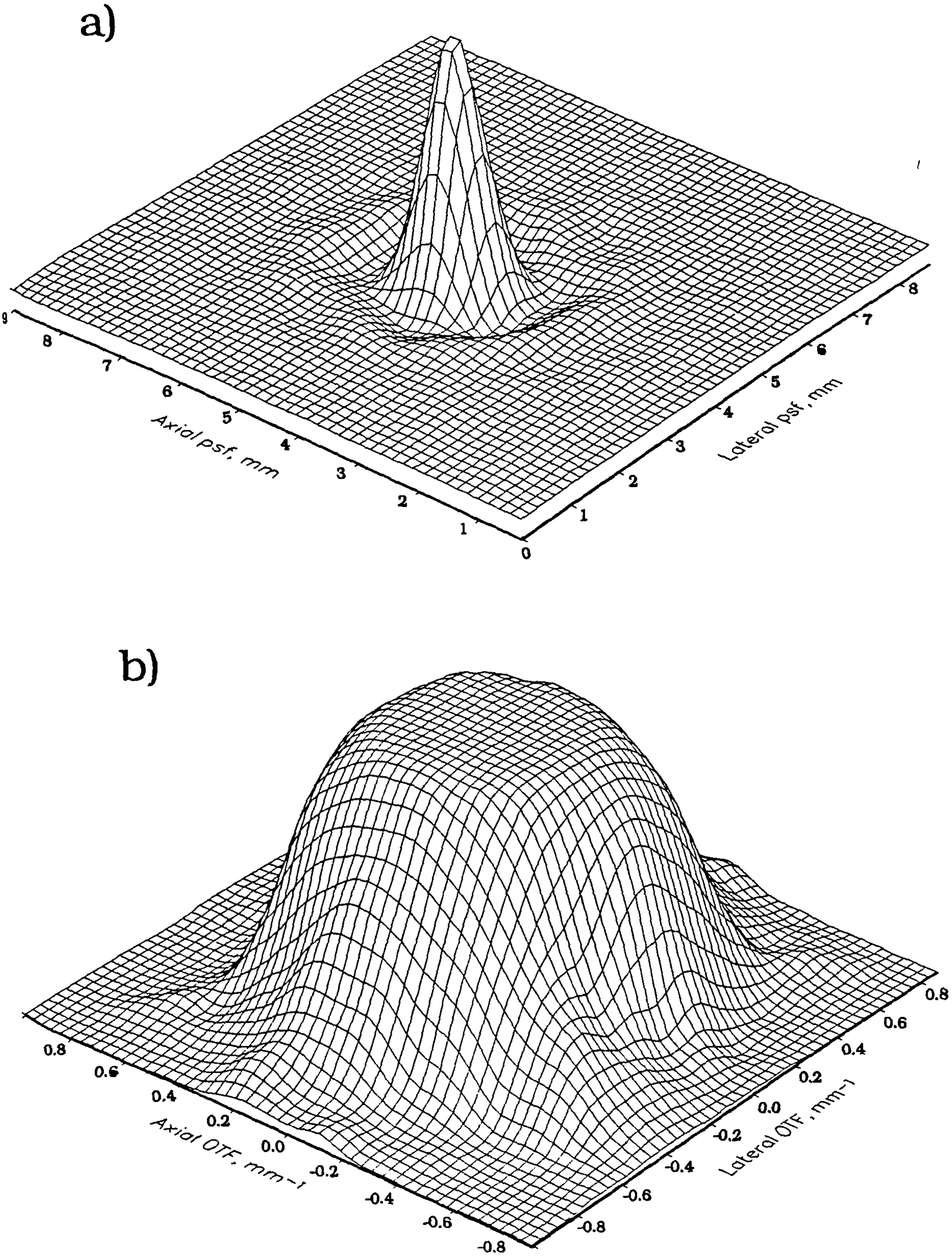

Figure 5.22 Wiener filtered image (a) of a single wire, and (b) its spectrum.

Figure 5.22b. Clearly the FWHM of the image of the point target has been significantly reduced (to about 1mm). In the frequency domain, the spectrum appears broader and more uniform compared to the un-filtered spectrum (Figure 5.17b).

Multiple wires in water

Figure 5.23a shows a B-scan of a set of six copper wires, where the direction of the scan is from above. The four very bright echoes are from steel rods used in the framework and should be ignored. An important point demonstrated in Figure 5.23a is that, contrary to the assumption of a position invariant psf, the beam width and hence the B-scan psf clearly changes with distance from the probe. Figure 5.23b shows the unfiltered reflection UCT image of the same target. The purpose of this target was originally to derive six separate inverse filters, ie one from each of the wire images, in order to take account of the varying beam width. However, it was found that the inverse filters so derived were almost identical, irrespective of the position of the wire in the field of view. This is almost certainly because the pulse length, which is independent of depth (at least to first order), is the dominant factor in the resolution and hence the psf of reflection UCT images. These results indicate that the inverse filter derived above from a single centrally placed wire should be sufficient to deconvolve any set of wire targets. This is borne out by the result, shown in Figure 5.23c, of applying this filter to the original reflection UCT image of the multiple wires.

Figure 5.18d shows the reflection UCT image of the resolution test wires after filtering with the Wiener filter. Now even the 1mm wires are resolved. Clearly for images of wires at least, the resolution of reflection UCT images, already markedly better than the lateral resolution of B-scan images, is significantly improved by inverse Wiener filtering.

Wires in tissue equivalent material

The Wiener filtered image of the wires in the TEM (Figure 5.19) is shown in Figure 5.19c. Although the resolution of the wires is further improved as before, some enhancement of the background speckle can also be seen. It can be postulated that this speckle reinforcement arises because speckle is not accounted for in the linear imaging model, since wave front distortion and non-linear processing imply a space-variant psf and a non-linear system respectively. Inverse filters effectively act as high-pass filters to restore, up to the maximum spatial frequency in the psf, the frequencies present in the original object that have been attenuated by the imaging system. Since the speckle in the reflection UCT image has a wider bandwidth than in a single B-scan, inverse filtering

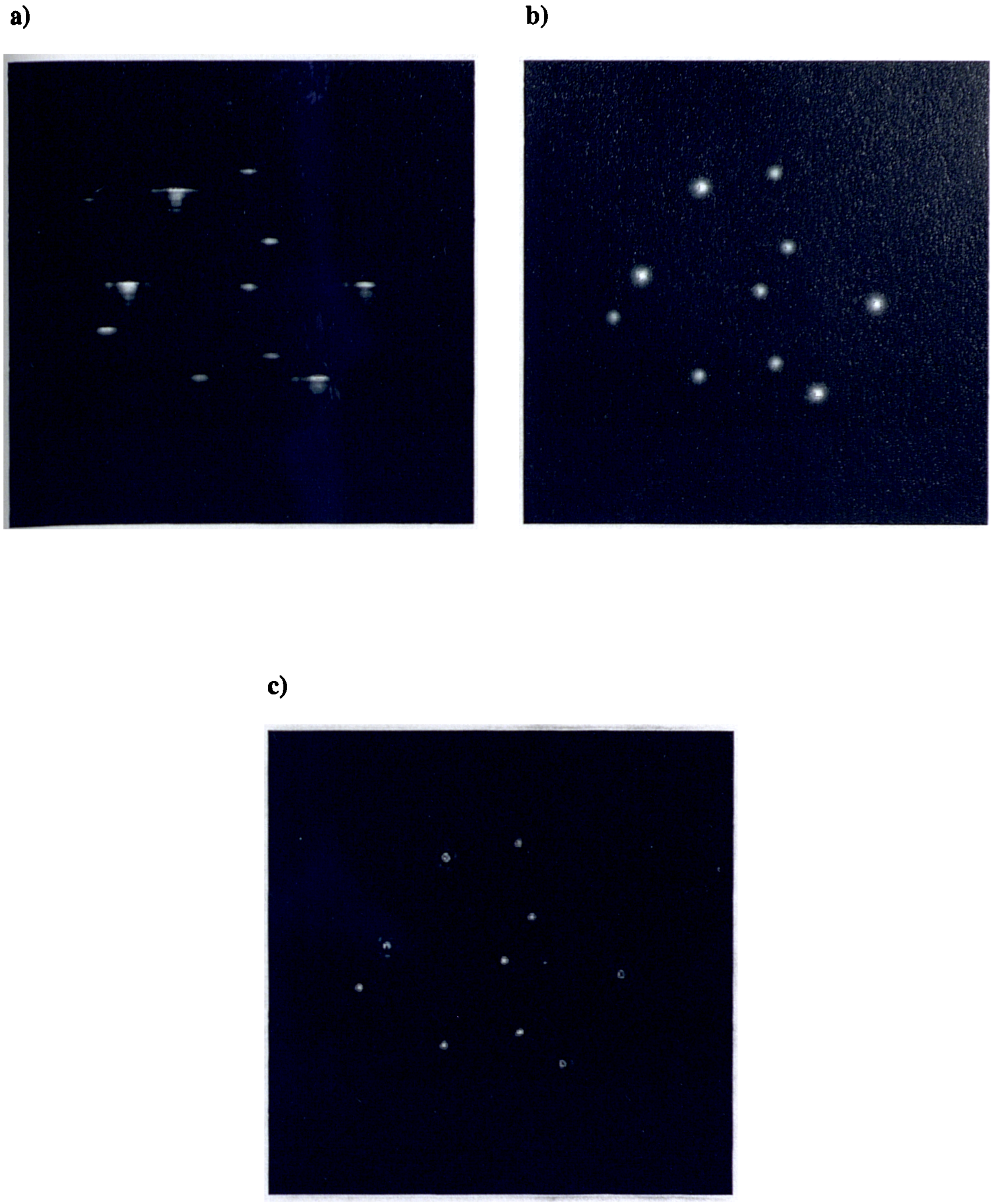

Figure 5.23 Wire test-object to show spatial variation of the psf: a) B-scan, b) unfiltered reflection UCT image and c) Wiener filtered reflection UCT image.

will preferentially boost the high frequency components of the speckle and hence increase the mean speckle level.

5.5.4.3 Low contrast targets

Speckle enhancement as a result of inverse filtering is even more evident on more realistic targets showing less contrast. The Wiener filtered reflection UCT image of the cyst phantom of Figure 5.20 is shown in Figure 5.20c. Although the boundaries of the cyst are now sharper, the speckle has been markedly enhanced. This problem is now more obvious than with the image of the wires imbedded in the TE material because of the much lower contrast between the "cyst" and the TEM, compared to the wires, which are very highly scattering, and the TEM. Speckle enhancement leading to reduced contrast resolution is the main disadvantage of using inverse filtering on reflection UCT images of anything but the simplest targets, and consequently inverse filtering has not been applied to any of the images to be shown subsequently.

5.5.5 Investigations of artifacts in reflection-mode UCT images

It has been established that unfiltered reflection UCT can overcome many of the limitations of B-scanning, showing improved and isotropic resolution, better delineation of specular reflectors and reduced speckle, for relatively simple and "undemanding" targets. However, real tissues may posses regions with high attenuation and varying acoustic speed which could degrade the quality of the reflection UCT images. The likely effects of attenuation and acoustic speed variations on the quality of the reflection UCT images has thus been studied with various phantoms.

5.5.5.1 Artifacts due to attenuation

To investigate how the presence of a relatively small highly attenuating region in a target affects the quality of a reflection UCT image, such a region was inserted into a cyst phantom (Figure 5.24a) by increasing the proportion of graphite scatterer in the attenuating region to produce an attenuation coefficient of approximately 4.5 dB/cm at 3 MHz (ie similar to skeletal muscle, Duck 1990). The single B-scan (Figure 5.24b), with the probe at the top, demonstrates the typical shadowing that this region causes. The cyst at the centre of the phantom is now barely visible. The reflection UCT image of this target (Figure 5.24c) shows a much reduced artifact, presumably because the region in shadow in the single B-scan has received sufficient interrogation from some of

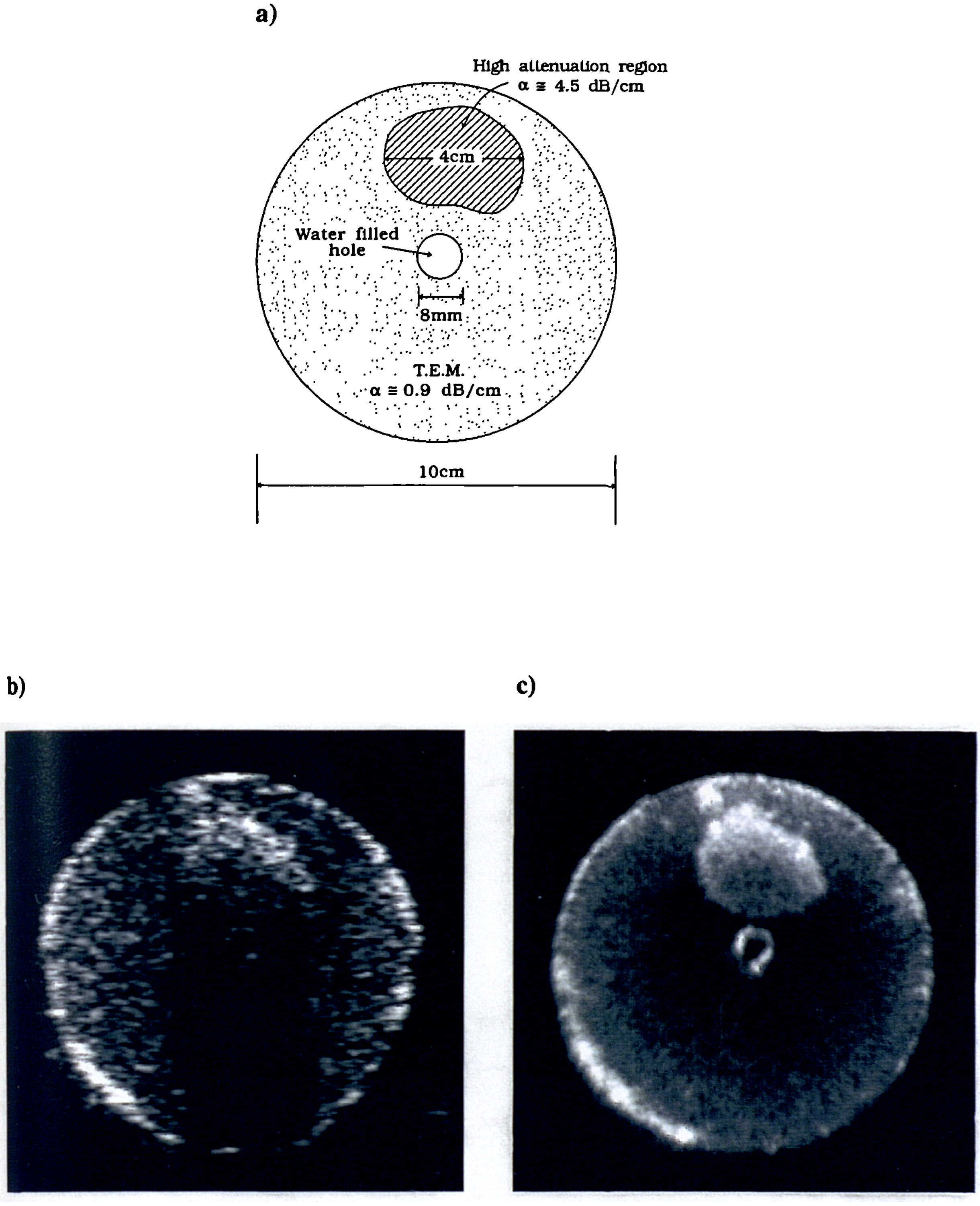

Figure 5.24 A cyst phantom (a) with a high attenuation region; a) B-scan, b) reflection UCT image.

the other B-scan positions contributing to the reflection UCT image. This result is consistent with the observations of other workers (e.g. Freidrich et 1982, and Roehrlein and Ermert 1985), who showed that scanning angles of slightly less than 180° can produce reflection UCT images showing only marginally reduced quality. This suggests that relatively small strongly attenuating regions will not be a major problem in reflection UCT, provided that there is sufficient penetration, at a sufficiently wide range of angles, into all parts of the target.

5.5.5.2 Artifacts due to speed of sound variations

Another possible cause of artifacts in reflection UCT is when the acoustic speed of the target is significantly different from that of the coupling medium. It has already been mentioned that ethyl alcohol is added to the water in the scanning tank so that the speed of sound in the water is close to that in the target being scanned, assuming that the average acoustic speed in the target is about 1540 m/s. However, there is quite a range of average acoustic speed to be found in different types of human tissue (e.g. from about 1430 m/s for a fatty breast, to about 1570 m/s for a dense breast, Duck 1990). It is not easy to reduce the acoustic speed in the water after the chosen quantity of alcohol has been added, since this would require discarding a portion of the water/alcohol solution which is expensive and impractical. Hence the acoustic speed of the water/alcohol is left fixed at 1540 m/sec regardless of the target being scanned. Another potential problem is that the acoustic speed within any particular target may also vary considerably, possibly by 5% or more in breasts (Greenleaf and Bahn, 1981). These two situations will be considered separately.

a) Target With Average Acoustic Speed Different to Coupling Medium

To investigate the consequences for reflection UCT image quality of scanning a target having a uniform but significantly different acoustic speed to that of the coupling medium, a graphite/gel phantom was made without adding propanol. The acoustic speed of this phantom should thus be (Burlew MM et al, 1980) about 1500 m/s. A set of copper wires was inserted into this phantom to act as recognisable scattering targets. The reflection UCT image of this phantom (Figure 5.26a), reconstructed assuming an acoustic speed of 1540 m/s, shows each wire as a crescent instead of the expected point. It can be argued theoretically that these artifacts are due to displacement of echoes, both laterally and axially, in the component B-scan images. To appreciate why this is so refer to Figure 5.25, which shows a point target in a medium of acoustic speed (c_2) being viewed, from many directions, with a probe in a coupling medium of speed (c_1). The information actually obtained from

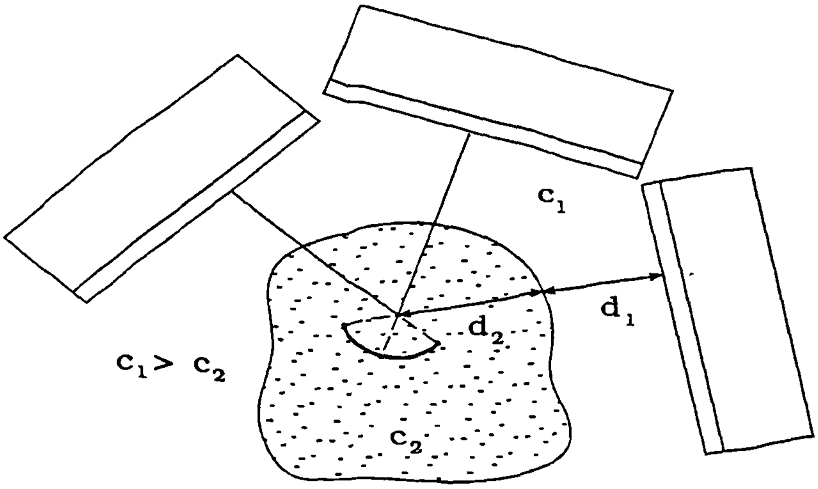

True distance to target $= d_1 + d_2 = t_1 c_1 + t_2 c_2$

Reconstructed distance $= (t_1 + t_2)\, c_1$

Axial displacement error, $d_a = \dfrac{d_2 (c_1 - c_2)}{c_2}$

Figure 5.25 **Blurring artifact caused by a different acoustic speed in target and surrounding medium.**

a B-scan is the time of flight to the target, rather than the actual distance. Hence to display the B-scan image as distances (x) the time of flight (t) must be converted using the relation ($x = t.c/2$). The speed of sound used will normally be that in the coupling medium, ie c_1, because this can be measured very accurately before-hand. However, if $c_1 \neq c_2$ (say $c_1 > c_2$), then the following effects will occur:-

1) The images of the point target will be placed further along the scan lines than they should be, as shown in Figure 5.25. This can be thought of as the axial component (ie along the scan line) of the acoustic speed artifact. When the B-scans are combined into a single image, the echoes from the point target will fail to overlap, ie mis-registration will occur, and the image of the point will be blurred to form the characteristic crescent shape.

2) If the interface between the object and the water is not at right angles to the ultrasonic beam, then refraction of the beam will also occur (this is not shown in Figure 5.25). This will result in the echoes being displaced laterally on the B-scan images, again causing blurring in the combined UCT image.

Simple acoustic speed compensation

If the average acoustic speed in the object can be estimated,either by prior knowledge of the object, or by a trial-and-error approach, then artifacts due to axial mis-registration (ie effect1) can be reduced by applying a filtering algorithm to the B-scan data. This algorithm works as follows:-

(1) For each A-scan line of a B-scan image, starting at the pre-defined starting depth for the scan, progress along the scan line, converting time of flight to distance by assuming a speed of sound of c_1.

(2) As soon as a large echo (above a pre-defined threshold) is detected, assume that this is the start of the object. From this point onwards, convert from time of flight to distance using a speed of sound of c_2.

(3) Repeat this process for all the B-scans comprising the reflection UCT image.

The result of applying such a filter to the B-scan data used in the reconstruction of Figure 5.26a is shown in Figure 5.26b. The images of those wires nearest to the centre of the target now appear as small points. The wires closest to the edge of the target still show some artifact, presumably because the refraction affects, which are not corrected by this algorithm, are more severe for these wires.

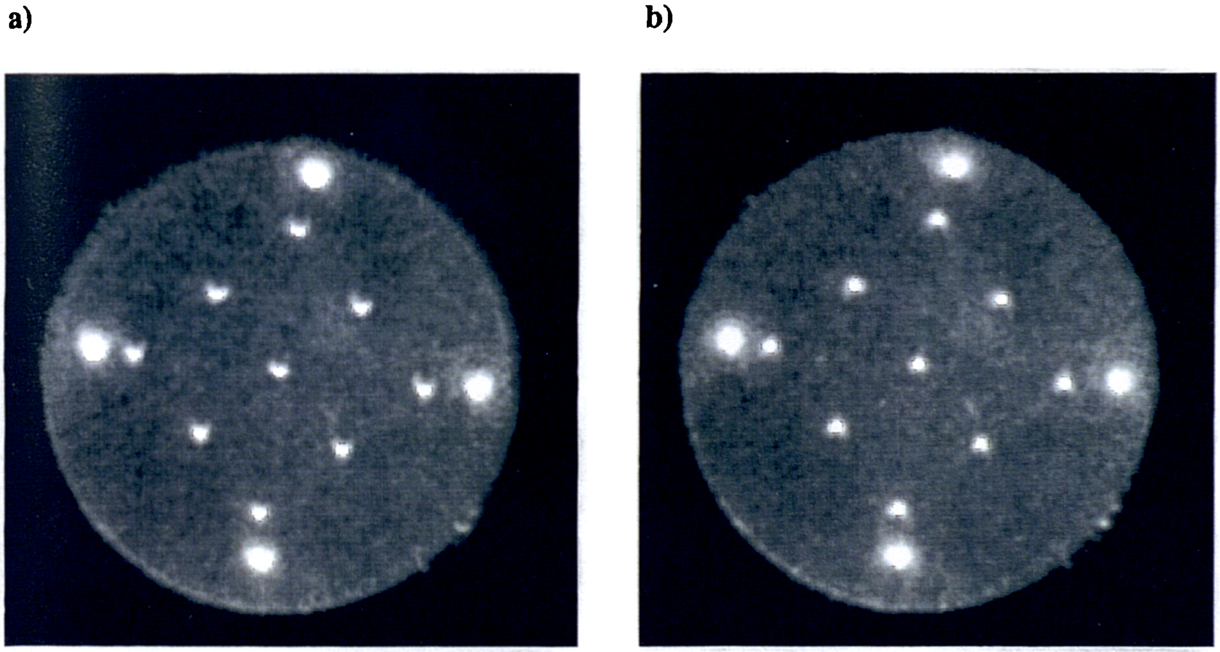

Figure 5.26 **Reflection UCT images showing a) blurring due to different acoustic speed in target and surrounding medium and b) after simple compensation.**

b) Target Showing Significant Acoustic Speed Variation

It has been shown that a simple correction for the difference in average acoustic speed between the target and the coupling medium can have quite a dramatic affect on the quality of the reflection UCT images. However, the algorithm described cannot take account of speed of sound variations within the object itself, or of any refraction effects. To investigate if speed of sound variations within the target would significantly affect the images, a "cyst" phantom was made (Figure 5.27a) with one region having an acoustic speed of approximately 1640 m/s, with the rest of the phantom at about 1540 m/s. In the reflection UCT image (Figure 5.27b), this high acoustic speed region is in the top left corner. Note that the boundaries of the cyst, and the edges of the phantom itself, are very blurred. This is because of incorrect registration of echoes from ultrasound beams which have passed through the high acoustic speed region.

It seems likely that the high acoustic speed region has to be quite large before it has a significant effect on the images. This is because the amount of blurring at any particular point in the reflection UCT image depends on what proportion of beams in the total 180° coverage, reaching the equivalent point in the object, have passed through the high speed region. This is borne out by the phantom shown in Figure 5.28a, where a set of three wires have been inserted at different distances from a high speed region. Note that in the reflection UCT image (Figure 5.28b) only the nearest wire has been significantly blurred, because the angle subtended at the other wires by the edges of the high speed region is quite small.

The only way that the blurring in these images could be removed would be to have some prior knowledge of the distribution of acoustic speed values within the same target sections. This information could then be used to correct the raw data used in the reconstruction of the reflection UCT image. It has already been shown in Section 4.3.3 that this information can in principle be obtained from transmission mode UCT. A system designed to perform combined reflection and transmission UCT for this purpose will be described in Chapter 6.

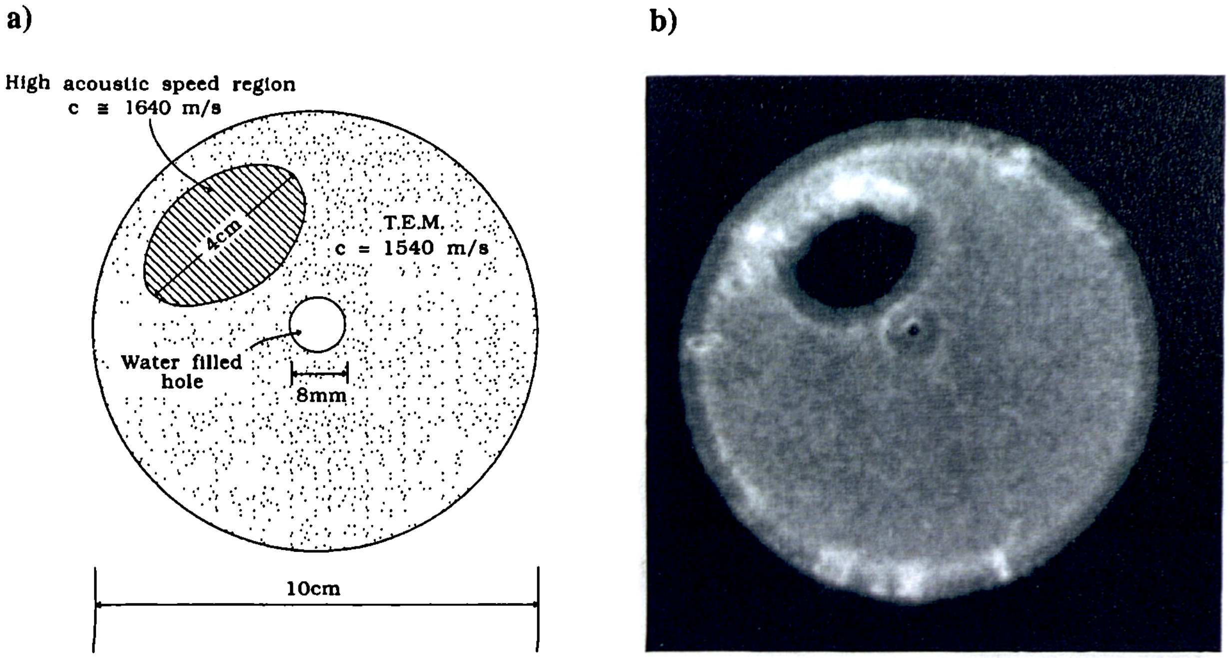

Figure 5.27 Cyst phantom containing a region of high acoustic speed; a) diagram of phantom and b) reflection UCT image.

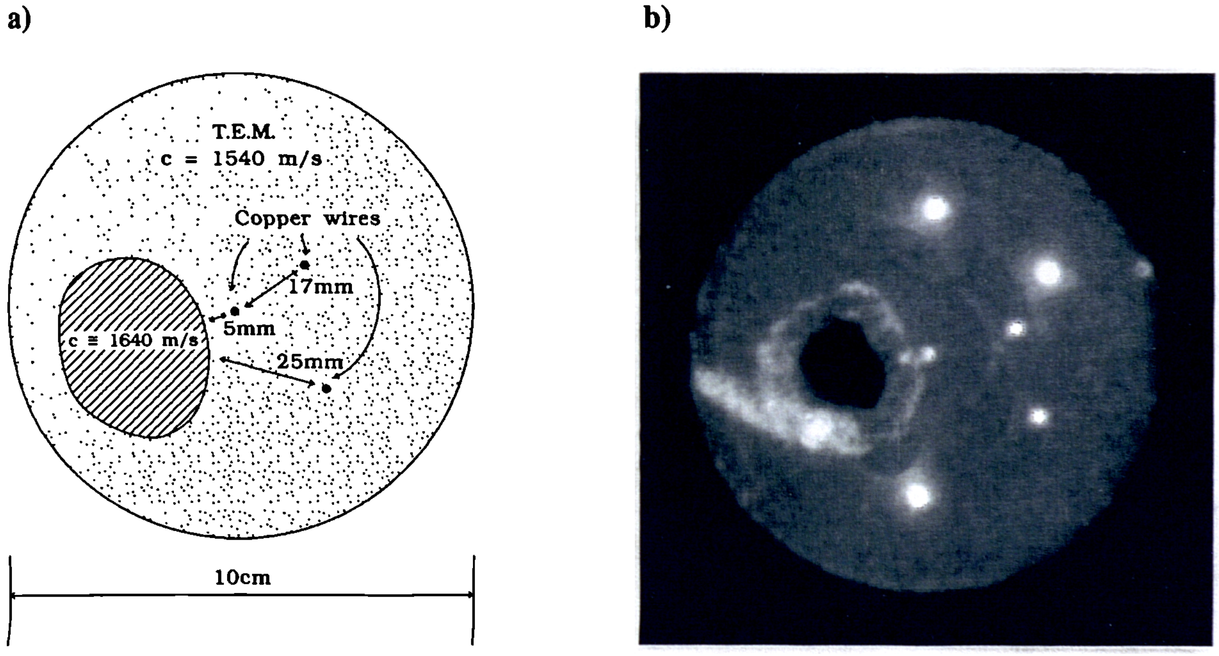

Figure 5.28 Wire phantom containing a region of high acoustic speed; a) diagram of phantom and b) reflection UCT image.

5.5.6 Images of animal tissue in-vitro

The next step is to compare images obtained from real tissue. For this purpose, a fresh bovine kidney was obtained from an abattoir, and placed in a thin plastic bag filled with 6% NaCl in water (speed of sound = 1540 m/sec) so as to prevent contamination of the water in the scanning tank. The B-scan image is shown in Figure 5.29a, where the scan has been obtained from the right. Some features can be recognised, in particular the strongly scattering calyces. However note the poor resolution laterally, specular reflectors such as the organ walls only visible when they are perpendicular to the beam, and shadowing of deep regions by highly attenuating tissues such as the calyces.

Figure 5.29b shows the 180° reflection UCT image of the same target, reconstructed assuming an average acoustic speed in the kidney of 1560 m/s. The organ boundary is now visible from all directions, at least in the lower portion of the kidney. Resolution is much improved and speckle reduced making interpretation of the image much easier, ducts and tubules in the kidney being clearly discernable. However the limited 180 degree coverage with this particular system results in a poor image quality in the upper portion of the kidney. This is probably due to two affects. The most serious is that the ultrasound from some directions cannot penetrate, due to attenuation, to the depths required to reach this region. Hence this region of the image does not contain information over a sufficient fraction of the 180 degrees required for a good reconstruction. The other problem is that the upper region of the kidney is always beyond the focus of the ultrasound beams where the beam width is wider. Hence the resolution, although still dominated by the pulse length, is likely to be slightly poorer than in the lower portion of the kidney.

5.5.7 Images of human organs in-vivo

Although obviously the most realistic situation, obtaining images from tissues in-vivo may be less informative than images of in-vitro tissue or phantoms because it is not possible to establish exactly the internal structure of the target. Also the present vertical plane system, although potentially suitable for a wide range of in-vivo targets such as the breast and the neonatal head, has somewhat limited accessibility as a water-bath system. There are also problems with immobilising the target for the 10 seconds required to complete the scan. Possible solutions to these problems will be considered in Chapter 7.

One possibility that has been investigated experimentally is the human forearm. This is also a good target for reflection UCT because it contains plenty of structure; such as muscle, blood vessels, tendons, ligaments and subcutaneous fat, although the presence of bone is likely to cause some problems. The B-scan image of a male forearm is shown in Figure 5.30a. It appears to contain a great deal of structure, but all of this is again very hard to interpret and there is considerable shadowing from the bones. The reflection UCT image (Figure 5.30b), reconstructed assuming an acoustic speed of 1590 m/s throughout the target, demonstrates clearly all of the advantages of reflection UCT that have been discussed previously. The outlines of the ulna and radius can be seen, as well as muscle fascia, probable blood vessels, and the skin and sub-cutaneous fat layer. The bones are less of a problem than expected because they are small enough to allow visualisation of surrounding structures from sufficient view directions. There is again, however, a problem with insufficient penetration into the top half of the target.

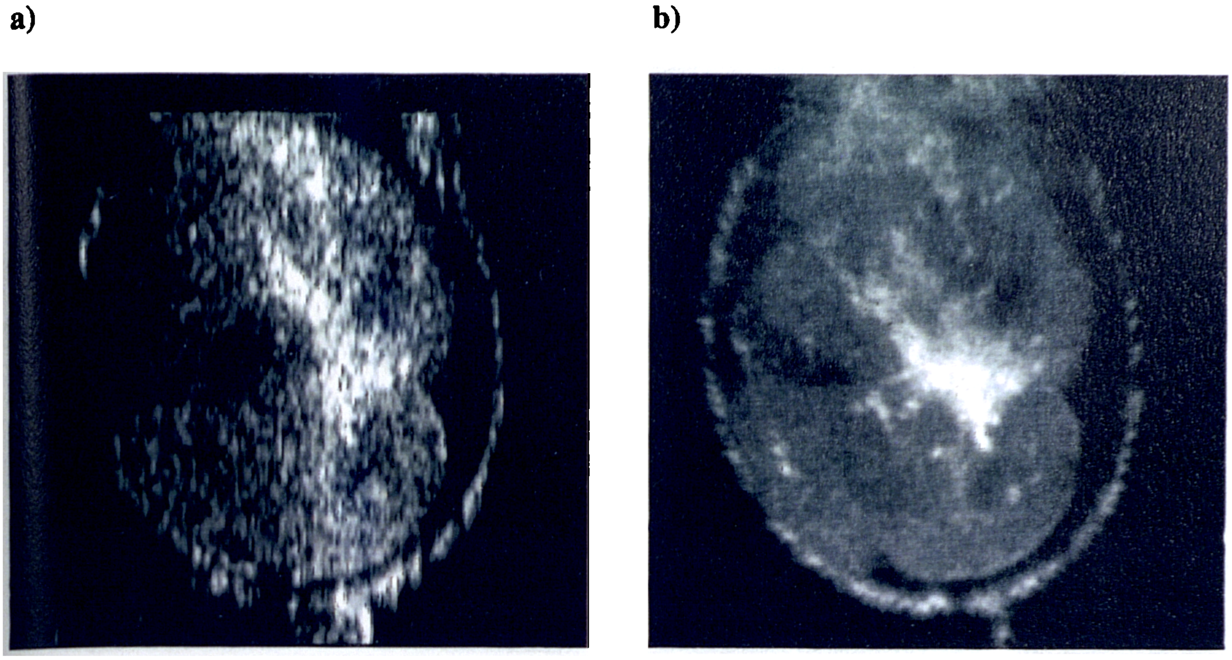

Figure 5.29 Images of an in-vitro bovine kidney; a) B-scan and b) reflection UCT image (reconstructed assuming an average acoustic speed in the kidney of 1560 m/s).

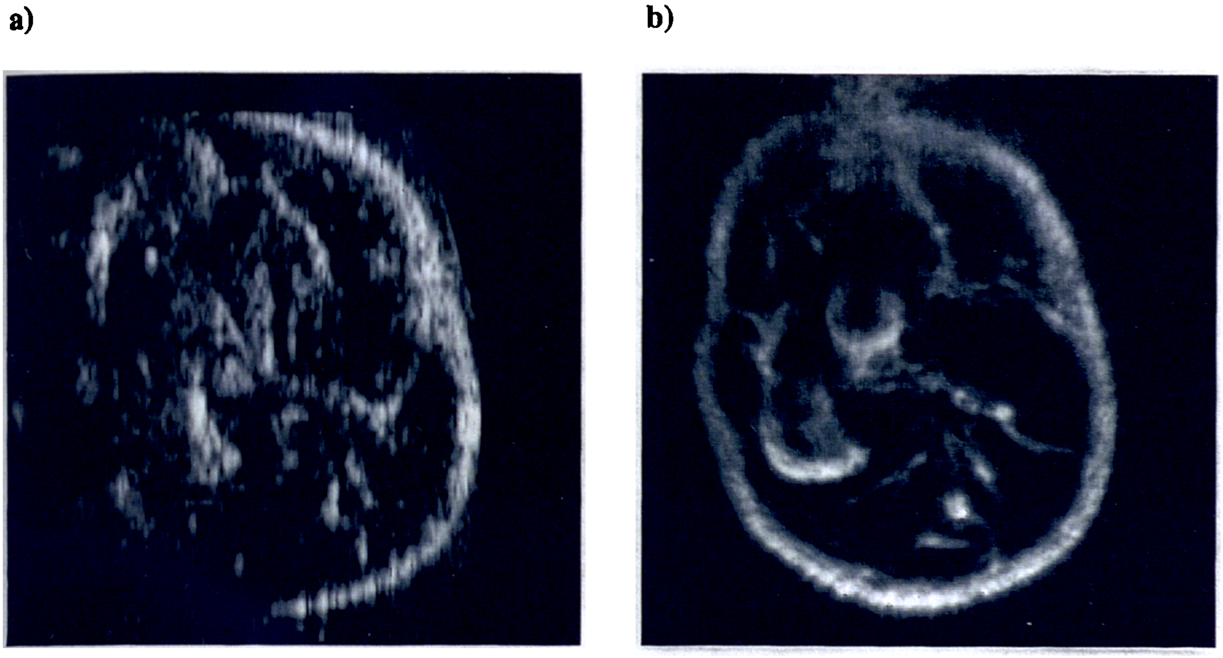

Figure 5.30 Images of an in-vivo human forearm; a) B-scan and b) reflection UCT image (reconstructed assuming an average acoustic speed in the arm of 1590 m/s).

5.6 Discussion of reflection-only system

This chapter has described the design, construction and operation of an ultrasound CT system for narrow beam reflection imaging in a vertical scan plane. This system incorporates a linear array for rapid and precise positioning, as well as algorithms for very accurate calculation of the system's centre of rotation.

Reflection UCT images of phantoms, in-vitro and in-vitro organs have been presented and compared to B-scans of the same targets. These results have been encouraging, the reflection UCT images appearing to show considerably improved spatial and contrast resolution compared to conventional B-scans. High contrast spatial resolution was compared by measuring point spread functions. Unfiltered reflection UCT images were shown to have a psf which, as predicted by the theory presented in Chapter 4, lies between the axial and lateral components of the B-scan psf. This is borne out by images from high contrast targets (wires in water) which show that the resolution of a reflection UCT image (about 1.6mm) lies between the axial resolution (1mm) and the lateral resolution (3mm) of a B-scan image. Resolution in a "real" soft tissue target is harder to quantify because it depends on the contrast of the resolved target compared to its surroundings, ie on the relative scattering strengths. However in real tissue the resolution of a reflection UCT image would be expected to be considerably better than that for a B-scan image due to the higher signal-to-speckle ratio (and hence contrast resolution) of the UCT images.

A Wiener inverse filter derived from a measured reflection UCT point spread function was shown to be effective in improving still further the resolution (to less than 1 mm) of reflection UCT images of high contrast targets. However in more realistic targets, such as TEM phantoms and soft tissues, inverse filtering caused an amplification of the speckle component. This speckle amplification almost certainly arises from the high-pass nature of the inverse filtering operation. Thus for images of real tissue (ie containing speckle), Wiener inverse filtering still improves the spatial resolution for high contrast targets but only at the expense of contrast resolution. It may be possible in the future, with the benefit of higher precision positioning systems and higher data storage capacity, to use the raw RF echo signal rather than the demodulated signal in the reconstruction. Although the contributions to speckle from wavefront distortion will still be present (see 4.3.1.3), speckle in RF images should be much less apparent and hence it may be possible to apply inverse filtering techniques beneficially.

Reflection UCT images also show improvements compared to B-scans in terms of more subjective criteria such as the ease of interpretation of the images, due mainly to the improved delineation of tissue boundaries and reduced speckle. Although the B-scan images presented are from an old scanner and are thus not representative of images obtainable from state-of-the-art equipment, it is expected that the improvements demonstrated by reflection UCT over conventional B-scanning would be preserved when using data from more advanced equipment.

An investigation into the likely causes of artifacts in reflection UCT images has shown that small, highly attenuating structures, known to cause shadowing in conventional B-scans, are not a major problem in reflection UCT images because of the multiple angles of view. Significant image degradation was shown to arise, however, from a difference in average acoustic speed between the target and the coupling medium. A simple adaption to the reconstruction algorithm, to allow different values of the average acoustic speed to be assigned to the water and the target respectively, was shown to be effective in considerably reducing the axial mis-registration component of the acoustic speed artifact in these cases.

The reflection UCT images from some targets still possess significant artifacts, however. In particular acoustic speed variations within the target itself, and refraction arising from a difference in acoustic speed between the coupling medium and the target, can cause artifacts in the reflection UCT images which cannot be corrected by adjusting the average acoustic speed for the whole target. Correction of these artifacts would require detailed knowledge of the acoustic speed distribution within the target, information which can be provided in principle by a transmission-mode UCT system. In addition, attenuation of the ultrasound from some scan directions for thick or highly attenuating targets can cause some parts of a target to be poorly visualised. One way of overcoming this problem would be to scan the target over a complete 360°, thus ensuring that all parts of the target receive ultrasound over at least 180° even if the ultrasound can only penetrate half-way through the target.

In conclusion, a 180° reflection only UCT system without compensation for acoustic speed variations is capable of producing images of some targets that are superior to conventional real-time B-scans, but is unlikely to show worthwhile advantages in tissues showing considerable attenuation and acoustic speed variations, such as the human breast. It may be possible to overcome some of the problems of 180° scanning using techniques for estimating acoustic speed which do not rely on transmission measurements. Some possibilities along these lines will be discussed in Chapter 7. The alternative is to develop a UCT system for combined reflection and transmission imaging that can scan through 360 degrees in a horizontal plane. Such a system has been built and will be described in the next Chapter.

6 Development of a system for combined acoustic speed and reflection UCT

6.1 Introduction

One of the main conclusions of the study into reflection UCT, reported in Chapter 5, was that the quality of the images is limited when there are significant ($> 5\%$) acoustic speed variations within the target. The reason for this loss of quality is that the acoustic speed variations cause misregistration of the echoes when reconstructing the reflection UCT image. It seems reasonable to assume that if knowledge of the acoustic speed distribution within a target section were available, the quality of a reflection UCT image of the same target could be improved by some appropriate processing of the reflectivity data. Indeed this approach has been suggested by other researchers into ultrasound CT (see section 3.2), although only a few have attempted it experimentally (Kim et al 1984, Bartelt 1988). These attempts were also limited, mainly by the poor quantitative or geometrical accuracy of the acoustic speed images produced. Specifically, Bartelt used a pulse-echo method for the reconstruction of acoustic speed images, the quality of which were very dependent on accurate time-gain compensation. Kim et al used the established transmission UCT technique to obtain acoustic speed images (see section 3.3.2), but both their reflection and transmission measurements were made using stepped single element transducers which inevitably introduced mechanical inaccuracies.

Considering the encouraging results obtained with the linear array based reflection-only system described in Chapter 5, it was hoped that a system incorporating linear arrays with their inherently greater mechanical accuracy, for both reflection and transmission measurements, would be capable of producing reflectivity and acoustic speed images of sufficient quality to make compensation for the affects of varying acoustic speed in the reflection images worthwhile. Consequently a second scanning system based on linear arrays and intended for both reflection and transmission UCT was developed and is described in this chapter.

The chapter will start by introducing the principles of acoustic speed compensation of reflection UCT images (6.2). This will include a discussion of the relative importance of the axial and lateral components of refraction in contributing to artifacts in reflection UCT images, and ways in which these effects can be compensated for. Then the design and construction of a practical combined reflection and transmission UCT system will be described (6.3 and 6.4). Since the technical requirements for reflection UCT have already been discussed in connection with the reflection only vertical scan-plane system, this chapter will emphasise only the additional technical requirements pertaining to transmission UCT and specifically acoustic speed imaging. Various methods for acoustic speed reconstruction will be discussed and compared (6.5). Finally, results of a practical implementation of acoustic speed compensation of reflection UCT images will be given (6.6).

6.2 Theoretical basis of acoustic speed compensation

The basic aim of acoustic speed compensation is to attempt to eliminate, or reduce, those artifacts in reflection UCT images caused by the assumption of a single acoustic speed for an object having an unknown and spatially varying acoustic speed. These artifacts may be considered as consisting of two separable components; (i) displacement of echoes axially, ie along the assumed straight line propagation path of an ultrasound pulse, due to an incorrect acoustic speed being assumed in calculating the position of the target, and (ii) displacement of echoes laterally due to the ultrasound beam being refracted away from the assumed straight path. The purpose of this section is to examine the relative importance and magnitude of these two affects in determining the quality of a reflection UCT image, and to discuss various means of compensating for them.

The simplest case of acoustic speed artifacts in pulse-echo imaging occurs when an ultrasound beam crosses a discrete boundary between two media with different acoustic speeds. Figure 6.1 shows how an echo from a point target can be displacement both axially and laterally due to a change an acoustic speed across a boundary. In many real soft tissues acoustic speed is also likely to vary in a continuous way. However by considering only finite elements of distance and TOF (Smith at al 1980), such a continuous model can be approximated by the discrete interface model discussed below.

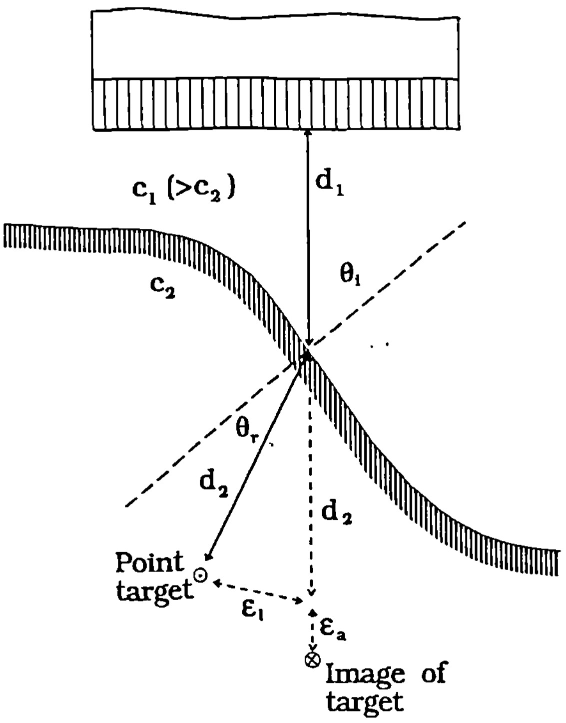

Figure 6.1 Axial and lateral mis-registration due to a change in acoustic speed across a boundary.

6.2.1 Relative magnitudes of axial and lateral displacement errors

The axial range (d) of an echo on a B-scan image is given by the measured TOF (T) of a pulse to and from the scatterer giving rise to the echo and the assumed acoustic speed in the intervening medium. If the acoustic speed (c_2) in the target is assumed (by the reconstruction algorithm) to be equal to the acoustic speed (c_1) in the coupling medium between the transducer and the target, then

$$d = \frac{c_1 T}{2}$$

where T is the actual measured TOF given by

$$T = \frac{2d_1}{c_1} + \frac{2d_2}{c_2}$$

Hence

$$d = d_1 + \frac{c_1 d_2}{c_2}$$

The axial displacement error (ϵ_a) is the difference between the calculated range (d) and the true range ($d_1 + d_2$).

$$\begin{aligned} \varepsilon_a &= \frac{c_1 d_2}{c_2} - d_2 \\ &= \frac{d_2 (c_1 - c_2)}{c_2} \end{aligned} \qquad (6.1)$$

Hence the axial displacement error is due solely to the fractional change in acoustic speed across the boundary and the distance of the target from the boundary.

The lateral displacement error (ϵ_l) is governed by the distance of the target from the boundary and the angles of incidence (θ_i) and refraction (θ_r) of the ultrasound beam.

$$\varepsilon_l = 2\, d_2 \sin\left[\frac{\theta_i - \theta_r}{2}\right]$$

Since the angles of incidence and refraction are related by Snell's Law, this equation becomes

$$\varepsilon_l = 2\, d_2 \sin\left[\frac{\theta_i - \sin^{-1}\left[\frac{c_2 \sin \theta_i}{c_1}\right]}{2}\right] \tag{6.2}$$

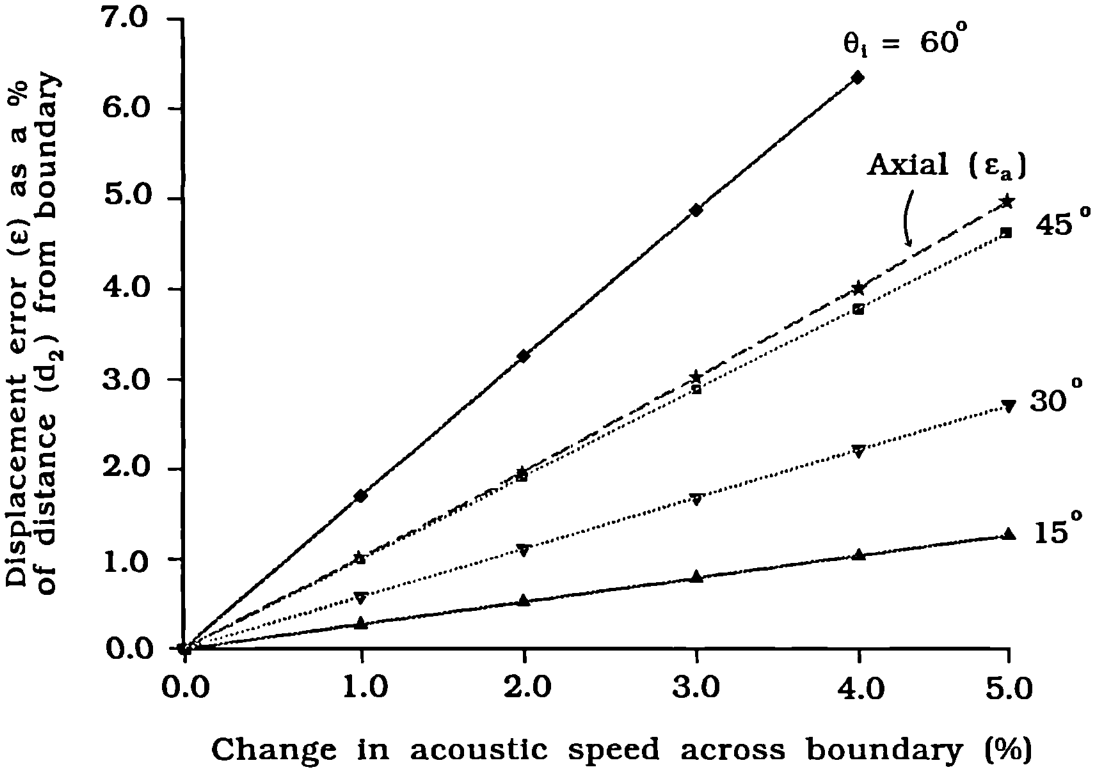

Figure 6.2 Axial and lateral displacement errors as a function of acoustic speed contrast and angle of incidence.

Since there is no simple equation relating ϵ_l to ϵ_a, it is more informative to plot these two quantities against percentage change in acoustic speed, assuming an acoustic speed in the coupling medium (c_l) of 1500 ms^{-1}, for various incident angles (Figure 6.2). This graph shows that the axial displacement error will always exceed the lateral displacement error for incident angles up to about 45°, while for larger incident angles the lateral displacement error is always highest. The relative importance of axial and lateral displacement errors in any real situation will therefore depend on the exact shape and orientation of the boundary. Considering that any segment of an arbitrary boundary may have an arbitrary orientation, the incident angles of beams backscattered from a point scatterer on the other side of the boundary may vary from 0° to ± 90°. This implies that the "average" incident angle for all possible boundaries between the ultrasound source and a scatterer will be 45°. Thus for a target containing many boundaries at different orientations (such as a breast), and where all scatterers within the target are insonified with ultrasound beams over a large range of angles (as in UCT), the average incident angle for all scatterers will be around 45° and the average axial and lateral displacement errors are likely to be similar to each other.

6.2.2 Methods of compensating for displacement errors

Most methods of correcting or compensating for reflection UCT image artifacts due to acoustic speed variations naturally rely on knowledge of the acoustic speed distribution. However some attempts have been made to "focus" images which have been distorted by unknown acoustic speed variations using a technique sometimes called 'wavefront reconstruction' (Hirama et al 1982, Zhao and Trahey 1992). This technique originated from the astronomical field (Muller and Buffington, 1974), where images of distant stars obtained by ground based telescopes are distorted by refraction (lateral displacement) and phase retardation (axial displacement) of light by the atmosphere. The technique however relies on the fact that the star or stars are known to be incoherent point sources, and hence the technique is not in general suitable for ultrasonic imaging where echoes from multiple scatterers interfere coherently. The exception is the situation where the tissue contains a recognisable target, such as a fluid filled vessel, which can be used to focus on (Chen et al, 1987). Since this situation can not always be anticipated in the human breast, knowledge of the acoustic speed distribution is required. One fairly well established technique for obtaining acoustic speed distributions in-vivo is transmission UCT (see 3.3). This is the technique pursued in this thesis.

Axial Displacement Errors

Correction for the axial component of the displacement errors is relatively easy in principle since the targets are assumed to lie along the straight line path of the incident ultrasound beams. Information about the acoustic speed distribution along the path of each ultrasound beam of a reflection image is used to calculate all the axial displacement errors for that beam. This information is then used to correctly register the echoes returned by each beam (ie for each scan line of a reflection image).

For the incorporation of acoustic speed information into the reconstruction of a reflection UCT image to be worthwhile, the estimates of axial displacement derived from the acoustic speed image should be considerably more accurate than the anticipated final resolution of the reflection images (ie better than 0.75 mm). Hence a figure of 0.4mm for the required accuracy in the estimate of the displacement error would be reasonable. Equation 6.1 shows that inaccuracies in the axial displacement estimates will arise from two components of the acoustic speed image: errors in d_2 (ie geometric accuracy) and errors in c_2 (ie quantitative accuracy). The relative importance of geometric and quantitative accuracy in determining the error ($\Delta\epsilon_a$) in the estimate of the axial displacement is given from 6.1 by partial differentiation, so that

$$\Delta\varepsilon_a = \frac{\Delta d_2\,(c_1 - c_2)}{c_2} \qquad for \;\; \Delta c_2 = 0 \qquad (6.3)$$

$$\Delta\varepsilon_a = \frac{-\Delta c_2\, d_2\, c_1}{c_2^2} \qquad for \;\; \Delta d_2 = 0 \qquad (6.4)$$

Hence the geometric accuracy of the acoustic speed image required to achieve a given accuracy in ϵ_a depends on the fractional change in acoustic speed across the boundary. If the maximum likely (ie worst case) change in acoustic speed at a soft tissue boundary is 10% (e.g. Duck 1990), then d_2 must be known to an accuracy of 4 mm to achieve an accuracy of 0.4 mm in the estimate of ϵ_a.

The quantitative accuracy required depends on d_2 and on the absolute values of acoustic speeds on each side of the boundary. For an object with a maximum diameter of 105mm (ie the field width of the ultrasound probe used in Chapter 5), and assuming the acoustic speed in the coupling medium c_1 to be about 1500 ms^{-1} with a change in acoustic speed across the boundary of -10% (ie c_2 = 1364 ms^{-1}), the accuracy required in c_2 to achieve an accuracy of 0.4 mm in ϵ_a is 4.7 ms^{-1}.

Although geometric accuracies of ±4 mm and quantitative accuracies of ± 5 ms^{-1} are theoretically achievable in acoustic speed imaging (see 4.3.3 and later in 6.3.3), whether they will be achievable in practice will depend on the degree of artifacts appearing in acoustic speed images of real targets (section 6.5). Note also that for the majority of acoustic paths within a soft tissue target, the acoustic speed change across a boundary will be less than 10% and the relevant target will be closer than 105 mm to the boundary, under which circumstances the accuracies required of d_2 and c_2 may be considerably less than those quoted above.

Lateral Displacement Errors

Correction for the lateral component of the displacement error is rather more difficult because it requires, from equation 6.2, knowledge of the refraction angles of the ultrasound beams. Calculation of these refraction angles requires accurate information about the orientation of the boundaries (or vectors in the case of continuous transitions) between regions of different acoustic speed as well as the acoustic speed values themselves. If such information was available, corrections to reflection UCT images could in principle be implemented using the ray-tracing or perturbation methods which have been used by various workers for refraction correction in transmission UCT (see 3.3.3). As was the case for the axial corrections, the value or otherwise of lateral corrections will depend on how accurate, in terms of both geometric and quantitative accuracy, the acoustic speed image needs to be.

Since equation 6.2 is not easy to differentiate analytically, it is more informative to assess the affects of geometric accuracy (ie in d_2) and quantitative accuracy (in c_2) graphically. Figure 6.2 suggests that, for an average incident angle of about 45°, the accuracy of the lateral displacement estimates will have a dependence on the accuracy of d_2 and c_2 which is similar to the dependence of the axial displacement estimate on these quantities. Thus, under worst case conditions, d_2 should be known to an accuracy of about 4 mm and c_2 should be known to an accuracy of about 5 ms^{-1}. Unfortunately there is an additional geometric factor that must be considered when estimating the lateral displacement error. This factor is the angle of incidence of the acoustic beam at the boundary, and it will be postulated below that it is the accuracy required of this factor that provides the main limitation to lateral displacement correction.

Any complex boundary can be considered as a set of short (ie considerably less than the beamwidth) linear segments, the orientations of which are required to calculate the incident and refracted angles of an ultrasound beam incident on the boundary. Figure 6.2 showed that the lateral displacement error varies rapidly with incident angle, particularly if the acoustic speed change across the boundary is high. Figure 6.3 shows this dependence explicitly by plotting equation 6.2 for the worst case conditions of an acoustic speed change across a boundary of 10% (c_2 = 1364ms^{-1}) and a path difference (d_2) between target and boundary of 105 mm. By fitting a 4th order polynomial to this

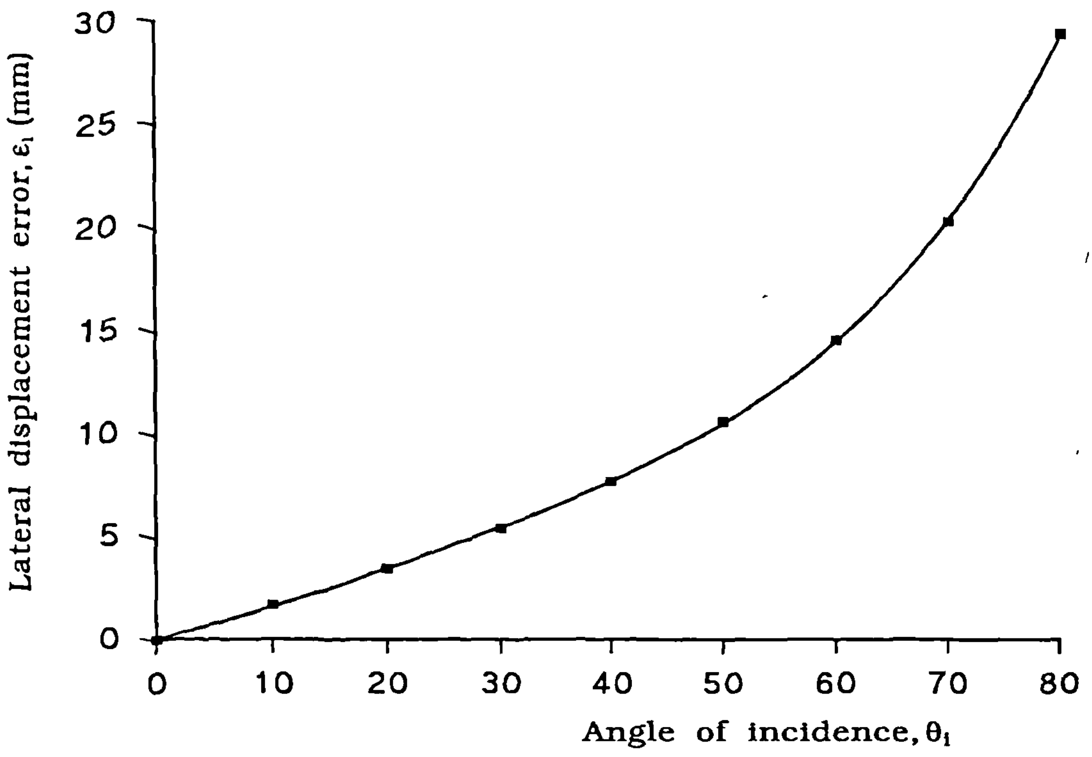

Figure 6.3 **Dependence of lateral displacement error on angle of incidence, for a worst case acoustic speed contrast of 10%.**

data, and differentiating using the coefficients of the polynomial, the error in ε_l per degree of error in the incident angle can be plotted (Figure 6.4) for various angles. It is clear from Figure 6.4 that the incident angles (and hence the orientations of the boundary segments) should be known to within 2 or 3 degrees (or less for angles greater than 45°) if the estimated lateral displacement is to be accurate to 0.4mm. This implies that, for worthwhile lateral displacement corrections, the geometric accuracy of the acoustic speed image must be very high (ie better than about 1/20th of the beamwidth).

The problems of determining refraction angles accurately have been encountered by workers attempting to implement ray-tracing techniques for the correction of refraction artifacts in the transmission acoustic speed images themselves (see 3.3.3). Probably the main reason why such correction were considered even theoretically possible is because the ultimate resolution expected of a transmission acoustic speed image, about 3 mm, is considerably less than that expected of a reflection UCT image (less than 1 mm), so that the orientation of the refracting boundaries also need not be known to the same accuracy.

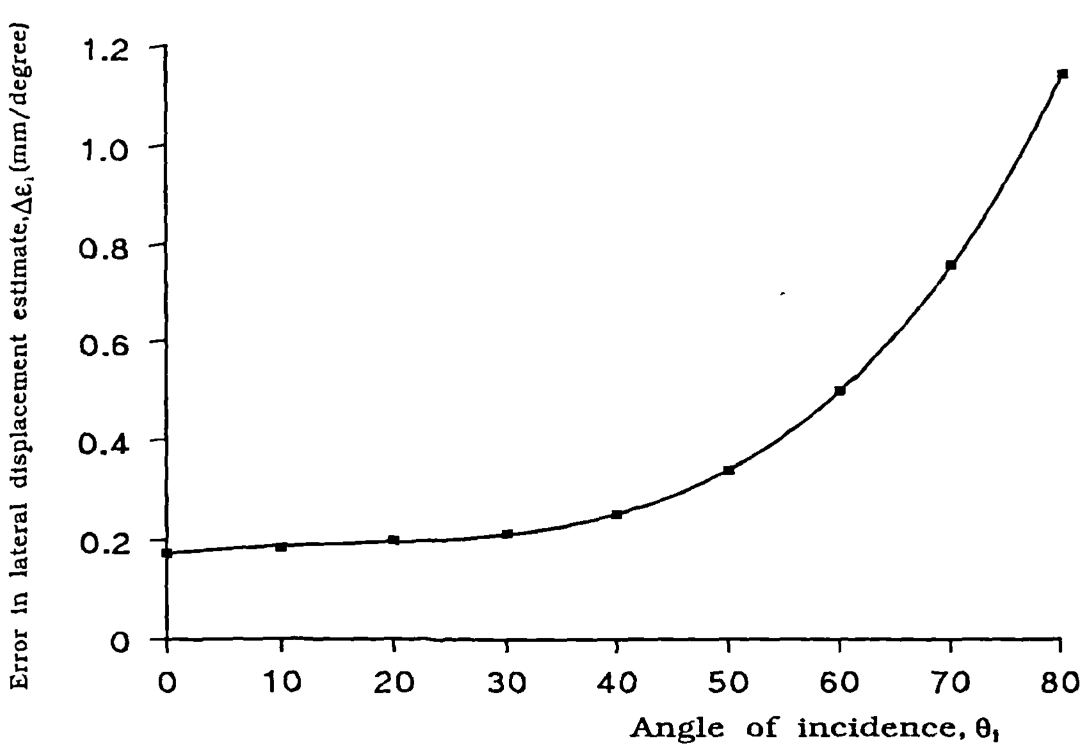

Figure 6.4 **Error in the estimate of lateral displacement caused by a one degree error in the angle of incidence, as a function of incident angle.**

Even if acoustic speed images could be produced that were totally free of artifacts, images produced by transmission UCT (the technique used here) have a resolution that is limited by the acoustic beam width (typically 6-7 times the wavelength). Hence the acoustic speed images at best represent a heavily smoothed version of the "true" acoustic speed distribution, with a resolution that is unlikely to be sufficient for worthwhile lateral displacement corrections. For this reason, only axial displacement corrections will be implemented in this study, with the consequence that the reflection UCT images will rarely be totally free of acoustic speed artifacts. Whether axial corrections alone will show a worthwhile improvement to the resolution of reflection UCT images can only be established by experiment (see section 6.6). The algorithm for performing the axial displacement corrections will be discussed in detail in section 6.6.2.

6.3 Requirements and specifications for acoustic speed CT

6.3.1 General requirements

The basic requirement for transmission (ie acoustic speed) UCT is similar to that for reflection UCT in that measurements are required over many directions about the target. One of the many differences however is that, for transmission UCT, two co-planar ultrasound transducers are required: one to act as a source or transmitter of ultrasonic pulses and another on the opposite side of the target to receive them. This also means that in order to make transmission measurements over the full 180° required for a CT reconstruction, the target must be accessible to ultrasound over a full 360°. This requirement for 360° scanning effectively excludes the possibility of a vertical plane scanning system within a water tank, so this system was designed to scan in a horizontal plane. The choice of a horizontal scan plane actually allows for easier access for most targets, including in-vivo ones, but as will be shown later (section 6.3.4) does create some problems for system design. Scanning over a full 360° should also improve the quality of reflection UCT images, particularly in targets that are highly attenuating.

Similarly to the narrow beam method of reflection UCT, the measurements for transmission UCT must be made at many lateral positions with respect to the target as well as at many angles around it. Using linear arrays as the ultrasonic transducers allows the lateral scanning action to be performed electronically, whilst the rotational movement must still be performed mechanically and preferably under computer control. The linear arrays must therefore be rigidly mounted so that they can rotate together about a constant centre of rotation. The combined transmission and reflection system could again be conveniently broken down into various sub-systems (Figure 6.5) which were designed and constructed separately.

6.3.2 Ultrasound generation and detection

As for the reflection only system, it was decided to base the ultrasound generation and detection on the Hitachi EUB-24F scanner. Accordingly a second identical 3 MHz linear array probe was obtained from the manufacturer. Since the EUB-24 is designed to drive only a single probe in pulse-echo mode, considerable modifications were required to allow one probe to be driven purely as a transmitter with the other was acting purely as a receiver. These modifications will be discussed in detail after the ideal specifications for ultrasonic generation and detection have been considered.

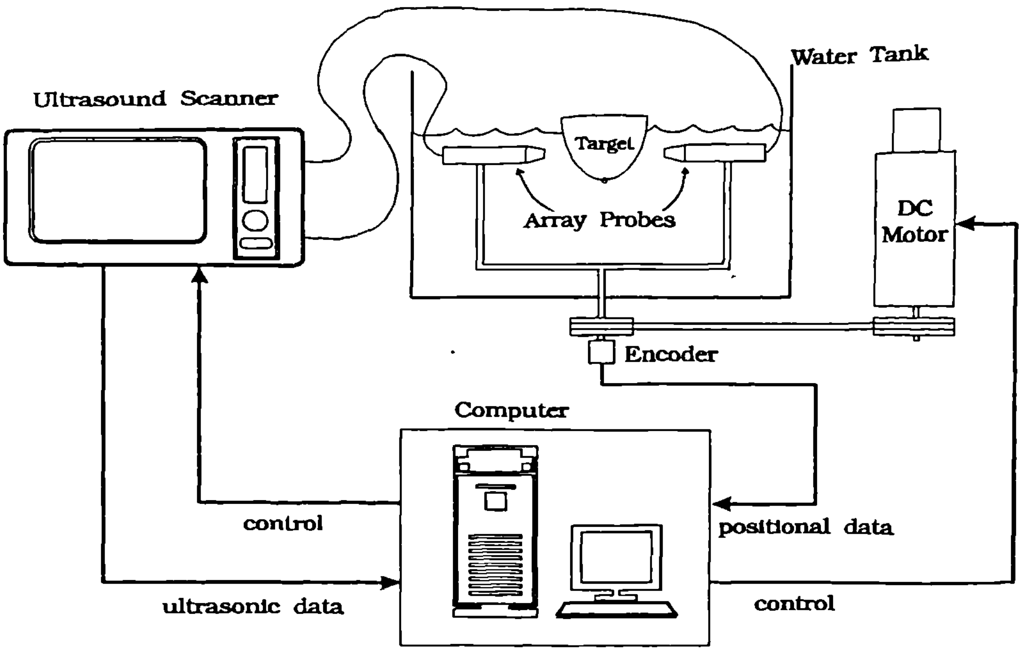

Figure 6.5 **Schematic diagram of the combined reflection and transmission UCT system.**

Ultrasound frequency and pulse length

For transmission measurements, unlike pulse-echo measurements, the ultrasound has to travel only one way through any part of the target being scanned. This would imply that attenuation is less of a problem for transmission UCT than for reflection UCT, but it must be remembered that all transmission measurements involve the passage of an ultrasound pulse through the whole thickness of target, whereas a proportion of the pulse echo data comes from the periphery of the target and thus experiences less attenuation. In particular, for a 360° system the pulse echo measurements need never penetrate more than half way through the target, and hence never suffer from more attenuation than the worst case transmission measurements. Hence attenuation of the ultrasonic pulses is at least as big a problem for transmission UCT as it is for reflection UCT.

The exact consequences of attenuation, and hence a reduction in amplitude, of the transmitted pulses on the quality of the reconstructed acoustic speed image depend partially on the particular method used for measuring the time of flight (TOF) of the pulses. These methods will be discussed fully in section 6.4.5.2. However it can be said that all of the various methods of TOF measurement show decreasing reliability and accuracy with increasing attenuation of the transmitted pulses. This argument suggests that low frequencies should be used for transmission UCT. Opposing this argument is that, for all the TOF measurement methods a lower pulse rise-time, which is an inevitable consequence of using lower frequencies, will limit the sensitivity of the measurements to small TOF differences and hence to small acoustic speed differences. Another justification for higher frequencies is that they allow shorter wavelengths and hence narrower beams, which has important consequences for the spatial resolution of the acoustic speed images (as shown theoretically in 4.4.4).

Weighing up these conflicting requirements, a frequency of around 2 MHz would probably represent the best compromise for the targets of interest. Hence the EUB 24's frequency of 3 MHz, although a little higher than the ideal, was considered acceptable.

The factors dictating the ideal pulse length are much more straight forward. The ultrasound pulse should not be too short, in other words it should not have too wide a bandwidth, since frequency dependent attenuation will distort the pulse shape and make the TOF measurements less accurate. The only upper limit on the ideal length of the pulses is that standing wave affects (ie reverberation), which will only be appreciable for very long pulses, are very undesirable. With these points in mind the EUB 24, with a pulse length of about 3 cycles (or 1.5mm, see Figure 5.4), appears to have rather a wide bandwidth for transmission UCT. The consequences of these limitations of the EUB 24 will become evident when the results of acoustic speed imaging are presented in section 6.5.

Ultrasound beam width

As shown in section 4.4.4, for transmission UCT it is the width of the ultrasound beam that provides the fundamental limit on the potential resolution of the images. Hence for an ideal system the ultrasound beam should be as narrow as possible over as great a range as possible. Unlike reflection UCT where the pulse-echo nature of the measurements allows dynamic focusing to be used (if available) to minimise the beam width over a large range, in a transmission system only one focal zone per transmitted pulse is possible. The obvious way of achieving a narrow beam in the focal zone is to use a large aperture transducer that is strongly focused, but this is undesirable because strong focusing implies a short focal zone with wide beams both before and after it. These factors imply that the transducer should be weakly focused, with the centre of focal zone located as closely as possible to the centre of the target. For targets up to 10 cm in diameter, this implies a focal length of about 7 cm when allowing for a 2 cm standoff between the transducer and the surface of the target.

A transmitted beam plot for the EUB 24 linear array probe, measured in water using a PZT needle hydrophone, is shown in Figure 6.6. The focus is about 60 mm from the probe face, with a 6dB beam width at the focus of 3.6 mm. The 6dB widths of the beam at 2 cm and 12 cm from the probe face (ie at the approximate limits of the largest target) are 10 mm and 4.5 mm respectively.

Hence the potential resolution of the acoustic speed image will lie somewhere between about 3 mm and 10 mm. Given these beam width characteristics this probe fits the requirements for transmission UCT quite well.

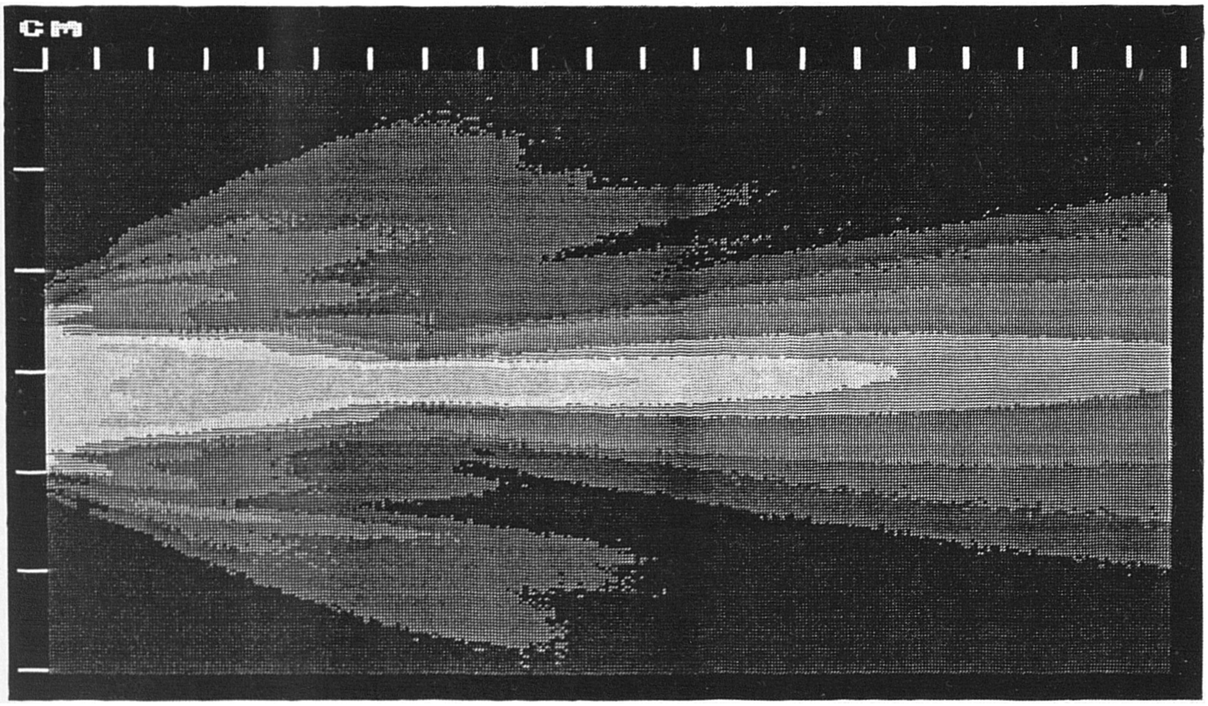

Figure 6.6 **Transmission beam plot of the 3 MHz linear array. Each grey level represents a 6 dB change in peak negative acoustic pressure.**

Scanned field width and beam spacing

As was the case for reflection UCT, the width of the linear array probe (10.5 cm for the EUB 24) limits the maximum dimension of a target to be scanned to about 10 cm. The distance between beam positions in the lateral scan is determined by the inherent resolution of the measured projections, which for transmission UCT is the beam width itself. Thus sampling theory dictates that the beam spacing should be less than half the minimum 6 dB beam width, as was the case for reflection UCT (section 5.3.1).

For the EUB 24, the distance between effective aperture positions, and hence samples of the projection, is 1.5mm. This is, as required, less than the half the minimum 6dB transmission beam width of 3.6 mm. The number of aperture positions is 70, giving 70 samples per projection.

Signal processing

In transmission UCT, whether it be for the reconstruction of acoustic speed or attenuation images, it is preferable that the received pulse is not distorted by any non-linear processing. In the case of acoustic speed imaging non-linear processing such as logarithmic compression or signal demodulation will distort the shape of the pulses differently depending on their amplitude. However, it is also true that varying attenuation leading to pulses of varying amplitude will affect the accuracy of TOF measurements, as mentioned earlier. Indeed the range of amplitudes of the pulses transmitted through a large (10 cm diameter) highly attenuating (1 dB/cm/MHz) target could be as high as 30 dB. Consequently the choice of whether or not to apply logarithmic compression to the received pulses depends largely on the particular method of TOF measurement being used. For example, in methods where the shape of the acoustic pulse is important in determining the TOF (such as the correlation method, see later) logarithmic compression will obviously affect the accuracy, whereas TOF measurements based on threshold methods will be largely unaffected.

Linear amplification of the received signal may be acceptable and indeed is probably desirable for acoustic speed imaging, for the reasons discussed above. Ideally it would be desirable to linearly amplify all of the received pulses to compensate exactly for the attenuation they have received so that they all have the same amplitude, ie a form of automatic gain control (AGC).

The need for excessively large amounts of data storage was one of the reasons quoted for why the demodulated rather than the raw RF signal is used for reflection UCT. In transmission UCT this is less of a problem because only a relatively short segment of received signal, just long enough to include the transmitted pulse, need be digitised and recorded for each transmission.

Modifications to Hitachi EUB 24 required for transmission UCT

Since the EUB 24 is designed to operate a single probe in pulse-echo mode, several modifications and additions were required to allow two probes to scan their apertures synchronously, with one probe transmitting only and the other receiving only. It was necessary that the modifications should inflict minimal disturbance to the integrity of the original circuits, so that the EUB 24 could be restored easily (ie with a flick of a switch) to its normal pulse-echo mode of operation. The basic principles of operation of the Hitachi EUB-24, and the modifications made for transmission imaging, are shown schematically in Figure 6.7.

a) Normal pulse-echo operation

With the EUB 24 in its normal pulse-echo mode, the position at any given time of the active transmit/receive aperture along the probe array is determined by a set of 16 control lines (CNT1 to CNT16). Each of the these lines, of which only three are active (held high) at any one time, are permanently attached via diode switches to sets of five adjacent transducer elements in the probe. Hence at any one time 15 adjacent elements are connected, through CNT switched diodes, to 15 signal lines (HP1 to HP15) which carry both transmit and receive pulses. However of these 15 signal lines only 10 are selected to link up with transducer drive circuits and receiver pre-amplifiers, giving an active aperture of 10 elements (or 15mm). Since the HP signal lines carry both transmission pulses and echoes, the sensitive receiver pre-amplifiers permanently connected to the signal lines must be protected from the large amplitude transmission pulses. This was achieved by applying, for less than 30 μs, a negative bias to a common TGC line attached to the FET input stage of the amplifiers which affectively turns-off these amplifiers.

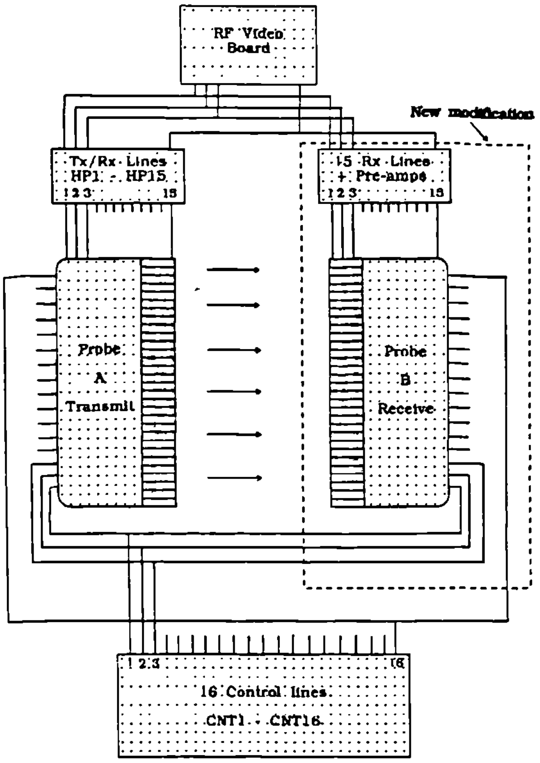

Figure 6.7 **Modifications made to the Hitachi EUB 24F for twin probe transmit/receive operation.**

b) Twin probe operation

Modifying the EUB 24 to force its original probe to operate in transmission only, ie to inhibit reception completely, can be achieved relatively easily by applying a permanent negative bias to the common TGC line. Attaching a second probe to act as a receiver is rather more complicated. Since the position of the active aperture on the receiver probe must always coincide with the position of the aperture on the transmitter, 16 extra CNT lines (which control aperture position) were tapped off from the original lines and taken to an edge connector designed to accept a second probe. Trials were performed to confirm that loading of the CNT lines by the addition of the second probe did not prevent the correct operation of the diode switches. The easiest way to provide amplification for the transmitted pulses received by the second probe would be to connect the receiver probe directly to

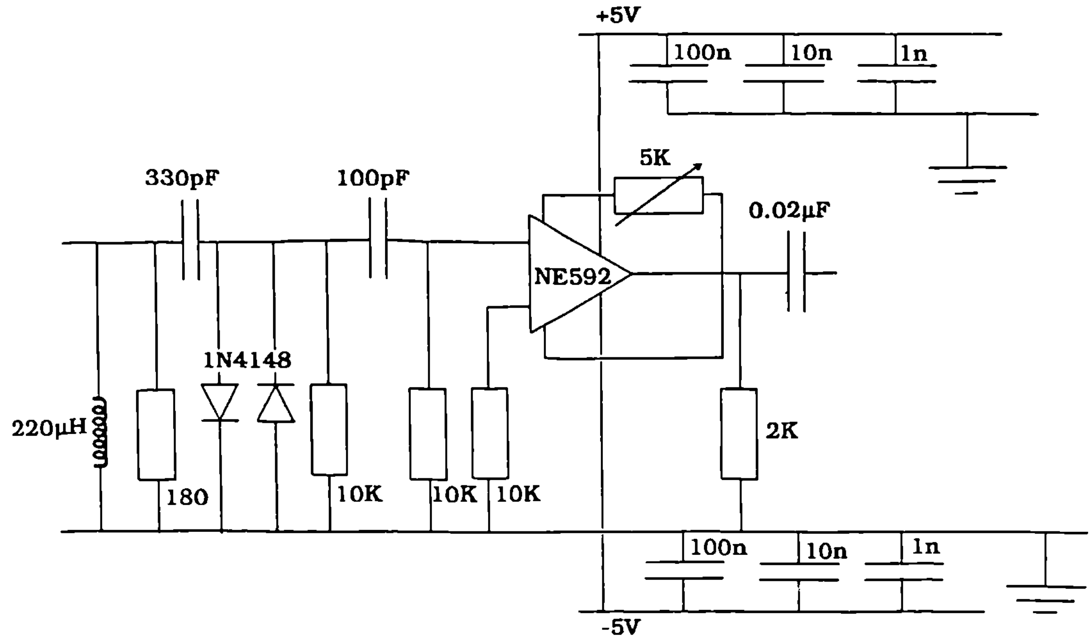

Figure 6.8 **RF pre-amplifier circuit for the received signals.**

the HP signal lines in the EUB 24. Unfortunately this was not possible because a) the EUB 24's receiver pre-amplifiers are already inhibited to prevent the transmitter probe receiving, and b) there would be no way to prevent transmission pulses being sent to the receiver probe. Consequently a batch of 15 identical pre-amplifier circuits (Figure 6.8), designed to have the same input impedance, gain and bandwidth characteristics as the EUB 24's pre-amplifiers, were built by the Electronics Department to provide amplification of the pulses received by the second probe. The outputs of these amplifiers were then connected to the outputs of the corresponding pre-amplifier circuits of the EUB 24.

The modifications required to allow the raw RF signal to be extracted from the EUB 24 after the pre-amplifiers and summing circuits, had already been made for the reflection only system. This RF signal receives some amplification within the EUB 24 via its TGC and overall gain controls, but does not receive automatic gain (AGC) at this stage. Additional amplification, if required, can be provided by the input amplifier of the LeCroy transient recorder, but since no attempt has been made to implement AGC all the signals receive the same amplification.

6.3.3 Digitisation and data transfer

Digitisation rates and implications for contrast-detail resolution

The transmitted pulse (Figure 5.4) from the EUB 24F's linear array possesses no significant signal, in water, above about 6 MHz. Allowing for some wideband noise in the signal, sampling requirements would suggest a digitisation rate of about 24 MHz. In practice, the digitisation rate should be as high as possible for transmission UCT since the sampling interval represents the best possible precision in the measurement of pulse TOF. The precision of the TOF measurement directly determines the potential contrast-detail resolution of the reconstructed acoustic speed image. To appreciate this, consider a small region of diameter d_1 and acoustic speed c_1 imbedded in a uniform background region of acoustic speed c_0. The difference (Δt) in TOF between a pulse traversing the centre of the imbedded region and one just missing it will be given by (see also 4.3.3.4),

$$\Delta t \quad = \quad d_1 \left[\frac{1}{c_1} - \frac{1}{c_0} \right]$$

Defining the acoustic speed contrast (C) as a percentage

$$C \quad = \quad 100 \; * \; \frac{(c_0 - c_1)}{c_1}$$

implies that the product of the contrast and size of the imbedded region is given by

$$C \; . \; d_1 \quad = \quad 100 \; * \; c_0 \; * \; \Delta t$$

Now the product $C.d_1$ will be minimised by the smallest value for Δt, which is simply the precision in the measurement of pulse TOF or the inverse of the digitisation rate (R).

$$ie \quad Min \left[C \; . \; d_1 \right] \quad = \quad 100 \; * \; \frac{c_0}{R} \tag{6.5}$$

This hyperbola is plotted in Figure 6.9 for various values of the digitisation rate, and assuming an acoustic speed (c_0) in the background medium of 1500 m/s. The minimum potential resolution of an acoustic speed image, as defined by the 6dB beam width, is about 3 mm. Hence at a digitisation rate of 25 MHz a target of this size would need to have an acoustic speed contrast of at least 2% (or 30 m/s different to its surroundings) to be detected. At 50 MHz the same target need only show a

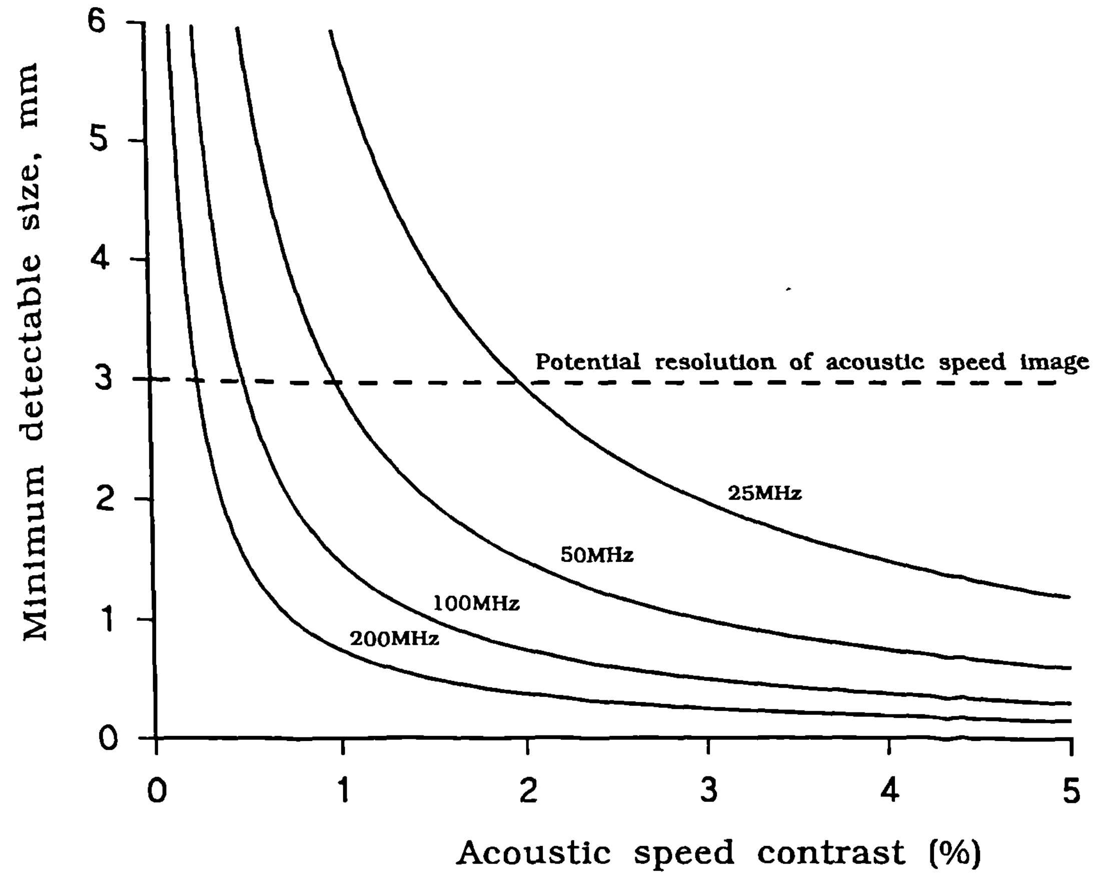

Figure 6.9 **Theoretical contrast-detail diagrams for acoustic speed imaging, for various digitisation rates.**

contrast of 1% (15 m/s). Perhaps more revealing is that for a target of 1% contrast to be detected with a digitisation rate of 25 MHz, it must be at least 6 mm across.

The arguments put forward in section 6.2.1.2 indicated that, for an acoustic speed image to accurate enough to provide worthwhile acoustic speed compensation, the boundary of a region having an acoustic speed contrast of 10% should be represented on the acoustic speed image to an accuracy of better than 4 mm. This geometric accuracy is thus theoretically achievable with a transmission UCT technique. The required quantitative accuracy was ±5 m/s for a circular region of contrast 10% and diameter 105 mm. With a digitisation rate of 50 MHz the theoretical contrast resolution (from equation 6.5) is 0.03%, which is equivalent to a potential accuracy in estimation of the acoustic speed in the region of 0.5 m/s.

In practice many other factors further limit the contrast/detail resolution, but the sampling rate defines its lower boundary. Clearly a digitisation rate of 50 MHz would be desirable to achieve excellent potential contrast/detail resolution. The upper limit on the digitisation rate is ultimately defined by the speed of the digitiser, but in practice also by the problems of data storage (see below).

Dynamic range

The dynamic range of the digitiser (ie the number of bits) must be able to cope with the possible 30 dB range of pulse amplitudes to be digitised. This implies that a minimum of 5 bits is required. The effect of the number of additional digitisation bits on the accuracy of TOF measurements really depends on the particular method of TOF measurement used. For threshold based methods, where the rapidly rising leading edge of the received pulse is used, the precession in the vertical (ie amplitude) axis is not as critical as that in the horizontal (ie time) axis, and a relatively small number of bits would suffice. In the TOF measurement methods that use all the information in the transmitted pulse, and especially when AGC and logarithmic amplification is not provided to reduce the range of pulse amplitudes, amplitude measurement precession is more critical and more digitisation bits are required for good accuracy. The LeCroy digitiser has a dynamic range of 48 dB (8 bits), which is probably only just sufficient for good accuracy in TOF measurements.

Amount of data

The total amount of data required for the reconstruction of a complete acoustic speed image of a single plane will depend on the following factors:-

(1) The number (N_p) of TOF projections (ie the number of probe positions around the target.

(2) The number (l) of beam positions making up a projection.

(3) The time (dt) for which the digitiser must be sampling in order to guarantee that the transmitted pulse has been digitised (ie the digitisation 'window').

(4) The digitisation rate (R).

(5) The dynamic range (Nb) of the digitiser in bytes (1 byte = 8 bits) per sample.

$$\text{Amount of data required (bytes)} = N_p * l * dt * R * Nb \qquad (6.6)$$

It was shown in section 4.4.4 that, to obtain an adequately sampled transmission UCT reconstruction, the number of projections required within a total angle of 180° is given by

$$N_p = \frac{\pi D}{2w}$$

where D is the length of the projection (ie the scanned field width) and w is the 6 dB beam width. For the EUB 24, the beam width (w) is about 3mm at the focus, and the scanning width (a) is 105mm. From equation (3), this implies that we need a minimum of 110 projections for a 360° scan.

Hence amount of data = 110 * 70 * 10E-06 * R * 1

= 0.077 * R (bytes)

The Le-Croy transient recorder and buffer has already been described in section 5.3.2. Using a digitisation rate of 50 MHz results, from equation 6.6, in a total amount of data for a single acoustic speed image of 3,850,000 bytes or just under 4 MBytes. This is four times the LeCroy's buffer storage, so that during a scan the data acquisition must be interrupted to allow the data to be transferred from the LeCroy to the computer. This takes just under a second per transfer and so adds about 4 seconds to the total scan time (see 6.4.3).

6.3.4 Mechanical scanning system

a) Lateral scanning

The requirements for accurate positioning of the transmitting and receiving apertures are even more stringent for transmission acoustic speed CT than they are for reflection UCT. This is because the fundamental quantity used to reconstruct an acoustic speed image is the difference in TOF measured, at each lateral position, with the target in the scan plane and when only the water is present (see 4.3.3.4). These TOF difference values therefore constitute what is known as the projection data. As shown in section 6.3.3 above, for sufficient accuracy in the reconstructed acoustic speed image these TOF differences should be known to an accuracy of 20 ns or better. Since the with-target and the without-target TOF measurements are made on separate scans, the separation between transmitter and receiver probes must change as little as possible between scans. Assuming an average acoustic speed of about 1500 m/s, an error of 20 ns in the TOF measurement corresponds to an acceptable change in the transmitter-receiver separation of only 30 μm. This consistency in separation would be almost impossible to achieve if the lateral movement of the transmitting and receiving apertures was performed mechanically and partly accounts for the poor results of Kim et al (1984).

In the system described here the lateral movement of the transmitter and receiver apertures is performed electronically as part of the normal scanning operation of a multi-element probe. Since the probes are rigid there is no opportunity for the probe separation, at any particular scan angle, to change significantly between scans.

b) Rotational scanning

For this combined transmission and reflection UCT system an angular positional accuracy of better than 0.1 degrees (equivalent to 0.2 mm) is still required, being determined by the potential resolution of a reflection UCT image since this is better than the potential resolution of a transmission UCT image. The requirement for minimum mechanical inertia in the probe support structure, consistent with sufficient rigidity to maintain positional accuracy, also still applies.

Despite these similar requirements, the design considerations for the combined transmission and reflection UCT system are in many ways different from those for the reflection only system. The main reasons for these differences are (i) the need for two diametrically opposed probes and (ii) the decision to scan in a horizontal plane. The vertical scan plane, chosen for the reflection only system, suggested a relatively simple probe support structure based on a horizontal bar which was pivoted at both ends via flat end-plates. This is an inherently strong and stable structure with a centre of rotation defined by the common axis of the pivot points. For a transmission system two bars would be needed, one to support each probe. Also, because a horizontal plane system would need to be accessible from above, each bar could only be pivoted at one end (ie at a common centre of rotation for both). Hence these bars, and their corresponding end-plates, would have to be very strong to provide sufficient rigidity to maintain a constant circle to better than 0.2 mm runout.

Rather than attempting to define a circular motion by rotation around a fixed pivot, it was decided that a more reliable and practical solution in this case would be to base the system around an inherently rigid circular structure with known tolerances. A commercially available system with which there was already some experience within the Department, called the Hepco Slide System, was found to meet the requirements. The Hepco system consists of linear and circular precision steel slideways, with sealed low-friction journals and lightweight carriages, all of various sizes, that can be used as building blocks to construct very complex systems.

The main component of the system purchased for the UCT scanner is a 0.35 m diameter stainless steel slide ring (shown schematically in Figure 6.10) which defines, to a precision of better than 0.1mm, the plane and axis of rotation. One option that was considered, in consultation with the

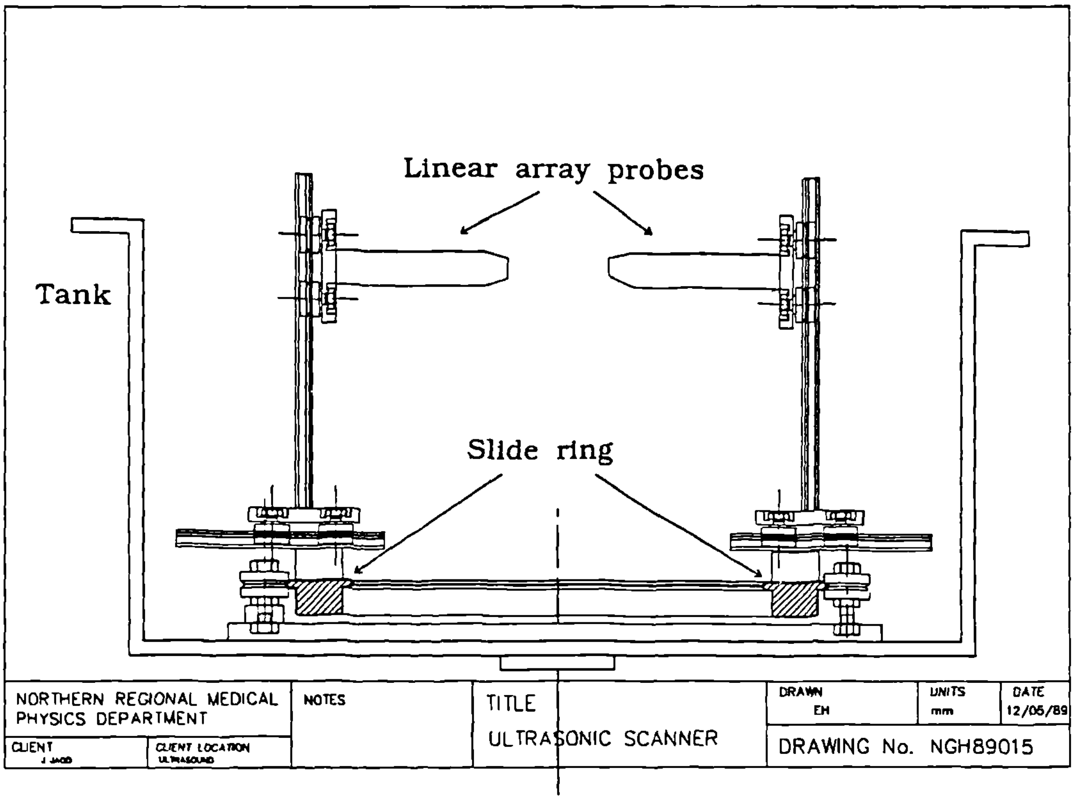

Figure 6.10 **Schematic diagram of the mechanical parts of the combined transmission and reflection system.**

Bioengineering Department, was to attach the ultrasound probes to Hepco carriages which could simply run along the ring. The main problem with this approach is that, since the carriages must be driven together but on opposite sides of the ring, they must be connected in some way across centre of ring. This connection would have to be very strong to maintain the required accuracy and would restricts access.

A potentially better solution is to rigidly mount the probes onto opposite sides of the ring and rotate the ring itself, guided by 5 fixed journals, as in Figure 6.10. The main disadvantage now is that there is considerably more mass to move than with the alternative approach (because the ring is quite heavy), but with the advantage of much greater inherent rigidity. This effectively means that better positional accuracy can be obtained at the expensive of scanning speed. Since it had already been decided that minimising scan times was not a major requirement, this second approach was adopted.

Hepco linear slideways have been used to provide the other planes of movement required -

namely a) to move the probes in and out in order to change the radius of the scan, and b) to move the probes up and down (on a screw thread for sub-millimetre accuracy) to alter the height of the scan plane.

The main problem with the general approach of a submerged steel ring rotating within precession journals is corrosion of the moving parts - particularly those parts which affect the positional accuracy, namely the edge of the ring and the journals themselves. This problem was minimised by using stainless steel parts, the exposed surfaces of which had also been coated commercially with a thin layer of very hard chrome. Additionally, the tank was emptied and all parts dried and sprayed with water-repellent oil when the system was not going to be in use for more than a few days.

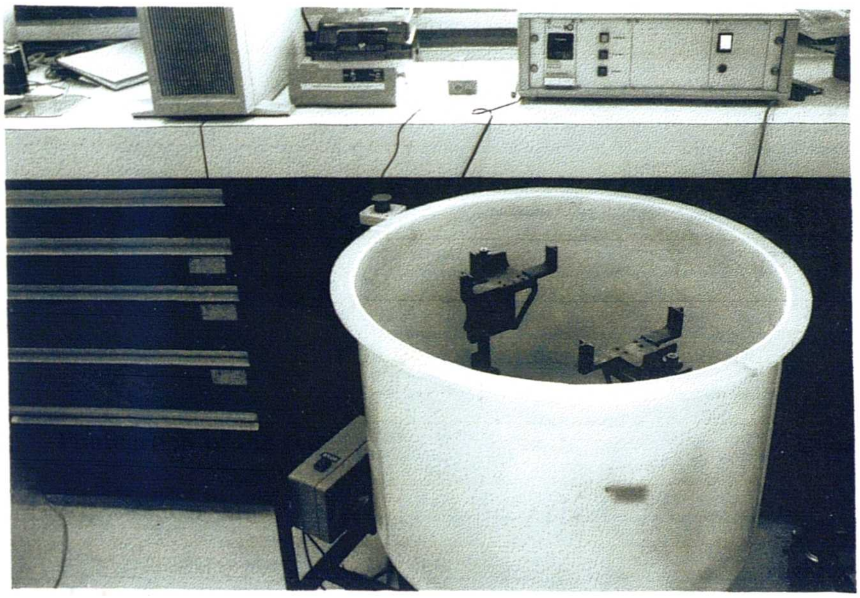

Figure 6.11 Photograph of the combined reflection and transmission UCT system.

c) Scanning tank

Due to the very different requirements of a horizontal plane scanner, it was decided that for the combined transmission and reflection system a cylindrical scanning tank would be more appropriate than a rectangular one. To again allow for a scan diameter of up to 20 cm, with 30 cm allowed for the two probes, a polypropylene tank of diameter 60 cm and height 60 cm was commissioned from a local manufacturer. The positions of the five journals were adjusted until they were all in contact with the ring, and then bolted securely onto a metal plate directly beneath the tank. Hence the rigidity of the system was again made to be independent of the strength of the tank itself. A Photograph of the complete mechanical system is shown in Figure 6.11.

6.3.5 Motor drive system

The positioning requirements of a drive system for the combined transmission and reflection scanner are essentially similar to those for the reflection-only scanner, specifically being able to position the probes with an angular resolution of 0.1 degrees, but over a full 360 degrees instead of 180. Since the servo-motor, tacho and control system used in the other system had been very successful, it was decided to duplicate this system. However because of the considerably greater inertia of the load (ie the slideways and probes) in the combined scanner (0.8 kg m^2 compared to 0.08 kg m^2 for the reflection-only system), a gearing ratio of 150:1 was required to achieve adequate torque at the load. This increase in gearing was provided by using a 50:1 gearbox instead of the 20:1 gearbox.

6.4 Acquisition of the data for an acoustic speed image

6.4.1 Introduction

The sequence of procedures involved in acquiring transmission time of flight data and reconstructing an acoustic speed image will now be described.

6.4.2 Measurement of the centre of rotation

For this system it was again necessary to accurately determine the common centre of rotation of the two probes so that information acquired from different directions may be combined correctly. The same test-object that was developed for the reflection-only system (see 5.4.2) can be used to give the centre of rotation in terms of axial and lateral distances with respect to each probe independently. The lateral distance information can also be used to ensure that the two probes are aligned correctly, ie so that the central axis of both probes lie as close as possible (to within 1/4 of the beam width or 0.8mm) to the centre of rotation.

The axial distance or range information can be used to calculate the separation of probes. Although this information is not actually needed for transmission UCT, it is useful in helping to decide when to start digitising the receiver signal as described in the next section.

6.4.3 Definition of the acquisition parameters

a) Scan parameters:

The scan acquisition parameters define the number of angular positions in the scan and the time allowed for the scan. Since TOF measurements are required both with and without the target present, these parameters must be defined for both circumstances, ie separately for the reference "water" scan and for the "target" scan.

If it were possible to set up the transmitter and receiver probes to be exactly parallel, then clearly only a single measurement of pulse TOF in water would be required and all the TOF measurements obtained with the target could be compared to this constant value. However a deviation in the probe separation of only 0.2 mm would result in a TOF error of about 0.13 μs, which is equivalent (see equation 6.5) to the increase in TOF experienced by a pulse passing through a 10 mm wide region having an acoustic speed 2% higher than the background. For this reason the reference TOF measurements are obtained, in water, across the whole length of the probes (ie utilising all 70 pulse transmissions), and the "target" measurements are compared only to the reference measurement obtained at the corresponding position on the probes.

Following a similar argument, the possibility that the probe separation might change slightly (by < 0.1 mm) as the probes rotate implies that the reference TOF measurements must also be obtained at the same probe positions as are acquired for the target measurements. In practice an experimental investigation, the results of which are presented in section 6.5.4.1, has demonstrated that ten probe positions within the full 180 degrees are usually sufficient for the reference measurements. During reconstruction, the TOF measurements from each probe position in the target scan are compared to those from the nearest available probe position in the reference scan.

b) Data acquisition parameters:

The parameters defining the data acquisition procedure are necessarily somewhat different to those for the reflection-only system. These parameters are the following:-

i. The time delays after each pulse initiation to start and to stop digitising the signals at the receiver, ie the digitisation window, must be defined. The pulse initiation is assumed to coincide with the leading edge of the line sync signals from the EUB 24, which are used to trigger the LeCroy digitiser. Knowing the separation of the probes from the centre of rotation measurements, and the acoustic speed in the coupling medium (e.g. water at a measured temperature), it is then possible to calculate the time after its initiation that a pulse is expected to arrive at the receiver probe *with no target present.* A ten microsecond digitisation window is then calculated, starting 5 μs before and ending 5 μs after the expected arrival time. This length of window is expected to be adequate to catch pulses transmitted through most potential targets. Note that it is not essential for the reconstruction of accurate acoustic speed images that pulse initiation coincides exactly with the line sync signal, since it is the difference in TOF measured with and without the target which is used in the reconstruction. It is essential however that the line sync signals do have a constant time relationship to pulse initiation, which of course they must have for the EUB 24 scanner to operate correctly.

ii. The digitisation rate, which is normally set at 50 MHz for transmission TOF measurements.

iii. The maximum amplitude of the received signal. It is particularly important in TOF measurements to make full use of the available dynamic range of the digitiser (ie 48 dB).

iv. The choice of whether or not to apply logarithmic compression to the received signal before digitisation. As discussed above in section 6.3.1, this choice is determined by which method of TOF measurement is to be used.

6.4.4 Performing the scan

If the probes have not suffered and disturbance since the last time a reference (ie no target) scan has been performed, and the temperature of the water has not changed significantly, then repeating the reference scan is not necessary and only the target scan need be acquired. Since acquisition of a 110 view transmission scan takes about 4 minutes, the target must be fixed as securely as possible. The major proportion of the scan time is taken up by movement of the probes.

6.4.5 Reconstruction of the acoustic speed image

The stages involved in the reconstruction of an acoustic speed image are summarised in Figure 6.12.

6.4.5.1 Pre-filtering

Any high frequency noise or low frequency baseline fluctuations present in the received rf signals can reduce the reliability of pulse TOF measurement, irrespective of the method used. Hence all the received signal (water and target) were optionally smoothed with a digital (ie in software) band-pass filter with a centre frequency at the 3 MHz carrier.

6.4.5.2 Calculation of time of flight profiles

As shown in 4.3.3.2, the measurement of the time of flight of ultrasonic pulses is fundamental to the reconstruction of an acoustic speed image. These measurements need to made to a high degree of accuracy and reliability if significant image artifacts are to be avoided. Several methods for measuring TOF have been considered for this experimental system but two in particular, one based on a threshold approach and the other on a pulse shape approach, have been investigated in detail.

The simplest method to understand, and to implement, is the so-called 'threshold method' (Figure 6.13a). As the name implies, a fixed threshold is set just above the signal noise level and a pulse is assumed to have arrived when the rectified signal first crosses this threshold. To calculate T - T_w, this measurement must be made both for pulses which have travelled through water only, and hence have experienced only minimal attenuation, and for pulses which have become attenuated after travelling through the target. Since the threshold method relies on detecting the leading edge of the transmitted pulses it would be expected to work best when all the transmitted pulses (target or water only) are saturated. This was confirmed by preliminary experiments and hence when using this method the amplifier gain was set high.

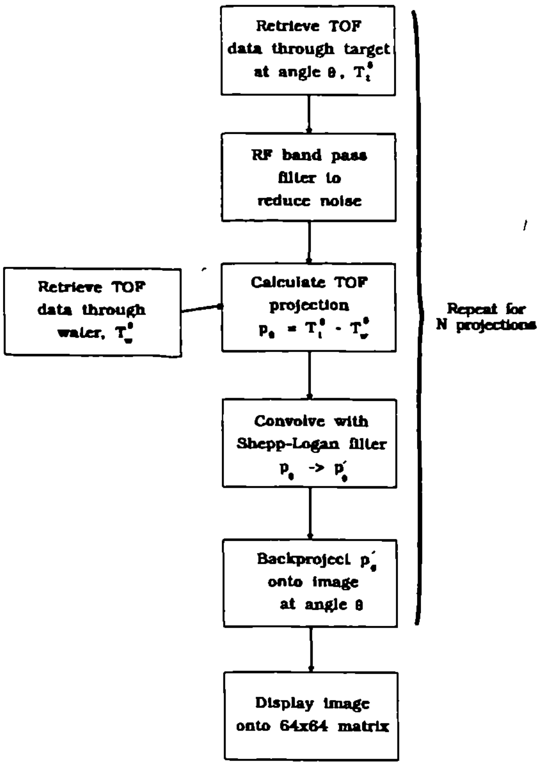

Figure 6.12 **Stages in the reconstruction of an acoustic speed image.**

The other method investigated in detail was the so-called 'correlation method' (Figure 6.13b). In this case a cross-correlation is performed between the reference signal and the signal obtained with the target present. The maximum value of this cross-correlation function then automatically yields T - T_w. The correlation method works best when the transmitted pulses show minimal distortion, and hence saturation of the receiver amplifiers is undesirable.

An experimental comparison of these two methods is presented in section 6.5.3.

6.4.5.3 Backprojection

It was shown in section 2.3 that various methods exist for reconstructing an object from the set of its projections. Of these, the filtered backprojection method (Ramachandran and

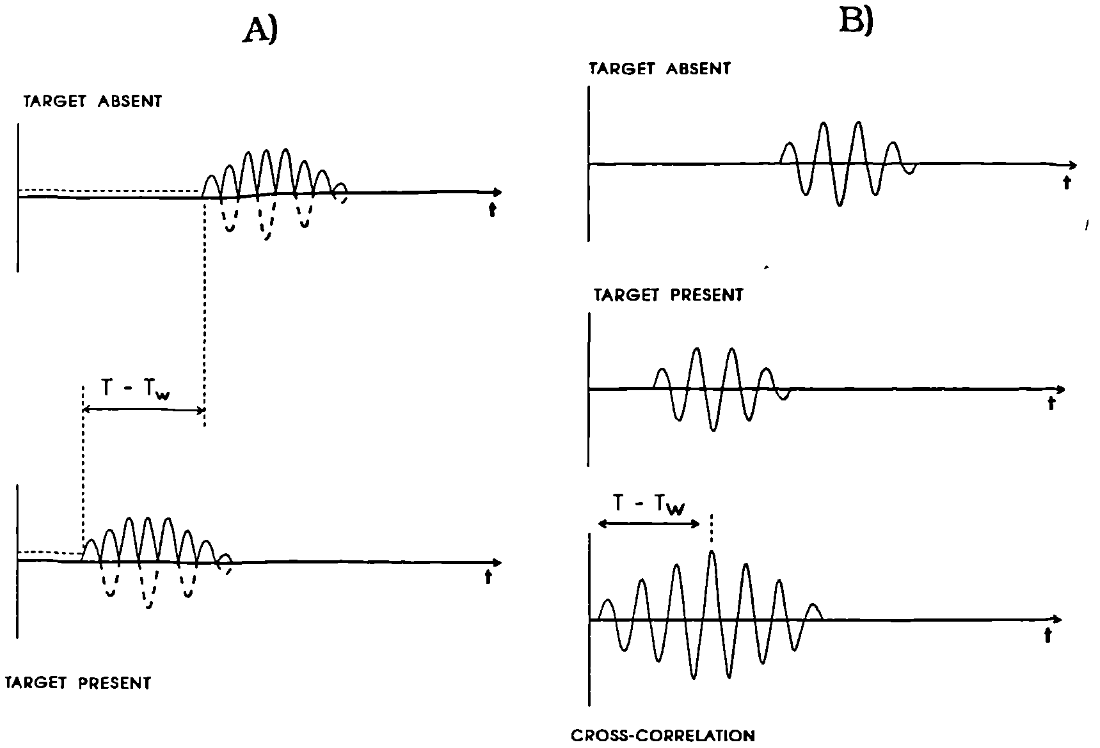

Figure 6.13 **Two methods for measuring pulse TOF: a) threshold method and b) correlation method.**

Lakshminarayanan 1971) has been chosen because it is relatively simple to implement, gives reasonably short processing times, and allows some flexibility in the reconstruction (e.g. for optimisation of resolution or signal/noise) via the choice of the projection filter. The process of backprojection simply involves taking a TOF projection and 'dragging' each value across image space in the same direction along which the projection was obtained. By repeating this operation for every projection, an image is obtained which turns out to be a blurred version of the original object. This blurring can be prevented by first convolving each projection with an appropriate filter before backprojection. Various forms of the well known Shepp-Logan filter (Shepp and Logan 1974) have been used in this system. The particular form of the Shepp-Logan filter determines the resolution of the final acoustic speed image. The filter may be modified, effectively by 'smoothing' it, to generate images showing reduced resolution but also less noise. An investigation of this approach is presented in section 6.5.4.3.

6.4.6 Displaying the acoustic speed image

The reconstructed acoustic speed images are displayed on a 64 by 64 matrix with a linear 256 level grey-scale look-up table. For an object of 10.5 cm diameter this gives a pixel size of 1.6 mm. These pixels are larger than those used for the reflection images (0.4 mm in a 256 by 256 matrix) because of the inherently lower resolution of the acoustic speed images, limited as they are by the ultrasound beam width to about 3 mm.

6.5 Results of acoustic speed imaging

6.5.1 Introduction

When assessing the accuracy of acoustic speed imaging there are essentially two characteristics of the images that must be considered: (i) the geometric or structural accuracy (as in reflection imaging), and (ii) the quantitative accuracy (ie how accurate are the acoustic speed values for a particular region). Hence to adequately test these characteristics phantoms and test objects are required for which both the structure and acoustic speed distributions are known as accurately as possible.

The reconstruction algorithm itself can be tested separately from the rest of the system by using 'perfect' noise-free projection data calculated from a computer simulated object (section 6.5.2). Then the complete system, ie including the acquisition stage, can be tested by measuring projection data from a very simple object having a simple structure and very accurately known acoustic speed variations (sections 6.5.3 and 6.5.4).

Targets showing more complicated structure and greater acoustic speed variations can be provided by phantoms (6.5.5 and 6.5.6) and in-vitro tissues (6.5.7). In order to assess the geometrical accuracy of the acoustic speed images of these targets, information is required about their internal structure. This structural information can be provided by reflection UCT since this has already been shown to be capable of providing acceptable images of the internal structure of such targets. Hence reflection UCT images, obtained using the combined reflection and transmission system described in this chapter, will often be shown alongside the acoustic speed images to aid in their interpretation.

Finally, compensation for acoustic speed artifacts in 360° reflection UCT images generated by this system will be assessed using both phantoms and soft tissues (section 6.6).

6.5.2 Simulated projection data

The objective of this experiment was to test the operation of the filtered backprojection algorithm, ie to check that it generated a 'perfect' acoustic speed image when provided with exact noise-free data. This data was obtained by calculating 110 TOF profiles from the simulated target shown in Figure 6.14a. This target contains four circular regions of different sizes, two having higher acoustic speed and two lower acoustic speed than the background. In calculating the TOF data straight-path propagation has been assumed, ie refraction is ignored.

Figure 6.14b shows the image reconstructed using simple backprojection, ie without prior filtering of the projections. Clearly the image is a reasonable representation of the target, except that the edges of the regions are blurred and the acoustic speed values are totally incorrect. This is because without the appropriate filtering the backprojected image suffers from '1/r' blurring and is not correctly normalised. Figure 6.14c shows the image reconstructed using a standard Shepp and Logan projection filter as described in 2.3.2. The regions are now the correct size with accurate values for the acoustic speed. Note the "pixelation" effect, due to the relatively large pixel size of these acoustic speed images.

6.5.3 A comparison of two methods for calculating TOF profiles

Having established the correct operation of the reconstruction algorithm, the next stage was to test various methods for the calculation of TOF profiles using real measured data. To test TOF measurement adequately a target was needed for which the true TOF values could be calculated. Thus the acoustic speed and thickness of this target had to be known to a high accuracy.

An rectangular block of lexan plastic was chosen as an appropriate target. The thickness (D) of the lexan was measured by digital calipers to be 9.1 ± 0.1 mm. The time of flight of an ultrasound pulse through the block, minus the TOF through the same thickness of water, is given by

$$T - T_w = D \left[\frac{1}{c_l} - \frac{1}{c_w} \right]$$

According to Selfridge (1985) the acoustic speed in lexan is 2300 ± 10 m/s, while the acoustic speed in water at 25°C (the temperature of the water when the data was acquired) is 1498 m/s. Therefore the difference in TOF between the two probes when the lexan is present and when it is not should be 2.12 ± 0.06 μs.

To check this result for two methods of TOF calculation, pulses that had propagated between the probes in water (ie the reference data) were digitised at 50 MHz and stored in the computer. Then the lexan block was placed approximately mid-way between the probes and parallel to the probe

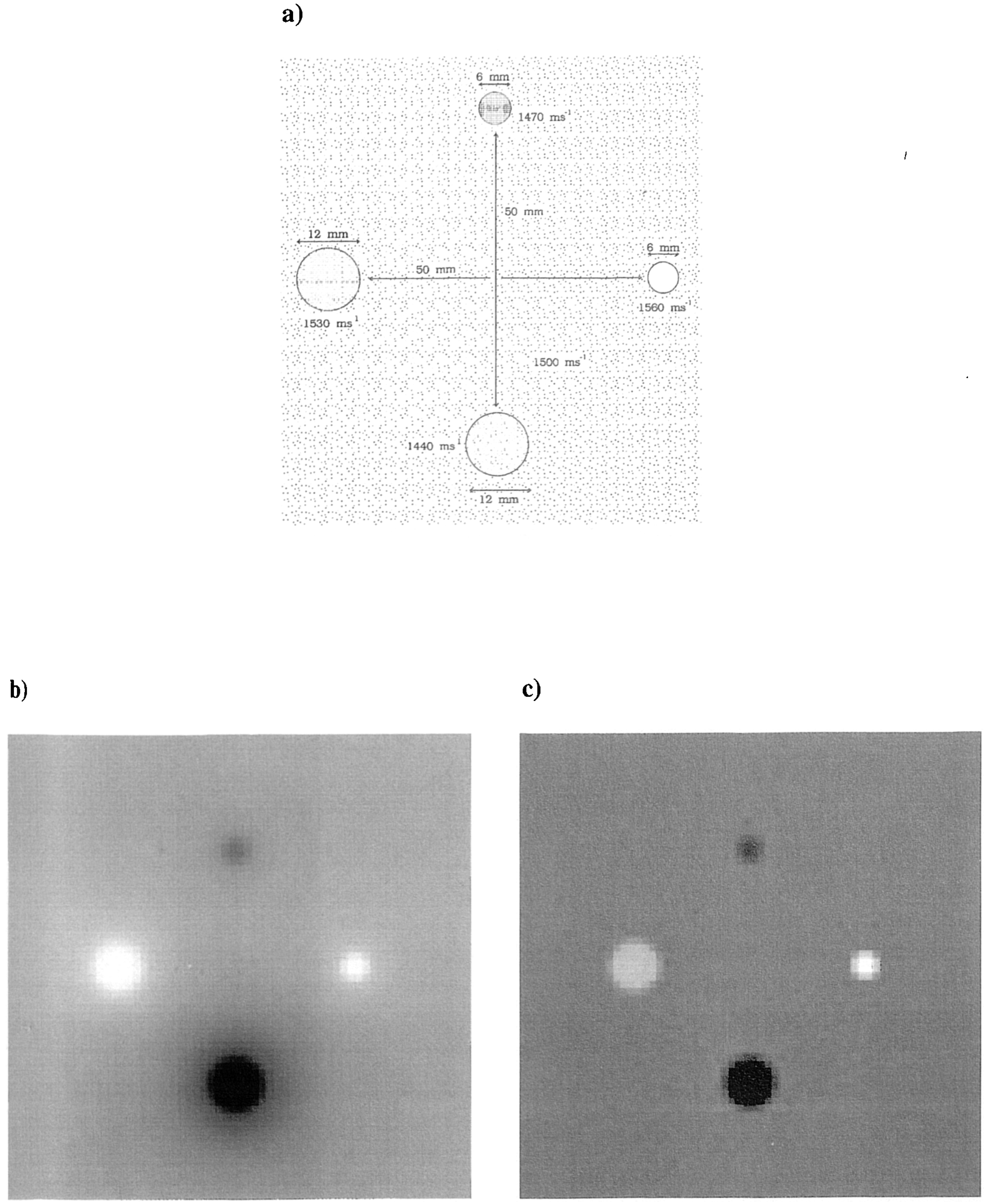

Figure 6.14 Tests of the reconstruction algorithm; a) simulated data, and images reconstructed using b) unfiltered backprojection (white =1640 m/s and black = 1250 m/s) and c) Shepp-Logan filtered backprojection (white = 1560 m/s, black = 1440 m/s).

faces (ie perpendicular to the ultrasound beam). When correct alignment had been confirmed by careful inspection of the pulse-echo image of the lexan surface, the transmitted pulses were digitised and stored. Two methods of calculating the TOF difference from this data were then investigated.

a) <u>Threshold method</u>

Experiments where performed in which one or both of the amplifier gain and threshold level were adjusted. These experiments have shown that the main problems with the threshold method arise from the choice of the threshold level itself. A level set too high risks missing the first half-cycle of the pulse, particularly for attenuated pulses, resulting in an overestimate of the TOF of about 160 ns. A level set too low risks triggering on noise and possibly drastically underestimating the TOF. Figure 6.15a shows a plot of $T - T_w$ against scan-line number (or lateral position) for the optimum combination of gain and threshold level. The 'correct' value of $T - T_w$, and the lateral extent of the lexan block (about 73 mm), are shown by dotted lines. The first half cycle of the through target pulses appears to have been missed on lines 42-44 of Figure 6.15a, resulting in an over-estimate of TOF and hence an under-estimation in $T - T_w$. Another problem with this method, evident in Figure 6.15a from the significant values of $T-T_w$ in lines 9-11 and lines 61-63, is that there is a tendency to overestimate the size of regions, such as the lexan block, with a higher speed of sound than their surroundings. This is because the method always detects the first pulse to arrive, so that a high speed region will be detected even if it intersects only a small portion of the ultrasonic beam. Similarly, the size of a low speed region will be underestimated or may not be detected at all if it is narrower than the beam width, since pulses traversing such regions may appear after the arrival of energy traversing surrounding areas.

b) <u>Correlation method</u>

The results for the correlation method (Figure 6.15b) with this target show better accuracy and consistency than results from the threshold method. The correlation method also has the advantage that, because it tends to 'lock' onto the largest amplitude pulse when multiple pulses have been received, the sizes of high and low speed regions should be correctly represented. This is borne out by Figure 6.15b which shows that the size of the lexan block has been reconstructed correctly. The main problem with the correlation method is that it is likely to become unreliable when the amplitudes of the two signals being correlated is very different, for example after attenuation by the target, or when the pulse shapes become significantly distorted. Pulse shape distortion can occur as a result of attenuation, non-linear propagation in water, non-linear processing such as log-compression, or phase cancellation at the receiver arising from refraction of the beam. In these circumstances the method can be in error by one or more pulse cycles (ie > 330 ns). Since the lexan block is thin and hence not particularly highly attenuating, and has parallel sides which are perpendicular to the beam, these problems are not so evident in Figure 6.15b. However, experiments in which the amplitudes of the through target pulses have been artificially reduced in the computer show (Figure 6.15c) that these problems do occur.

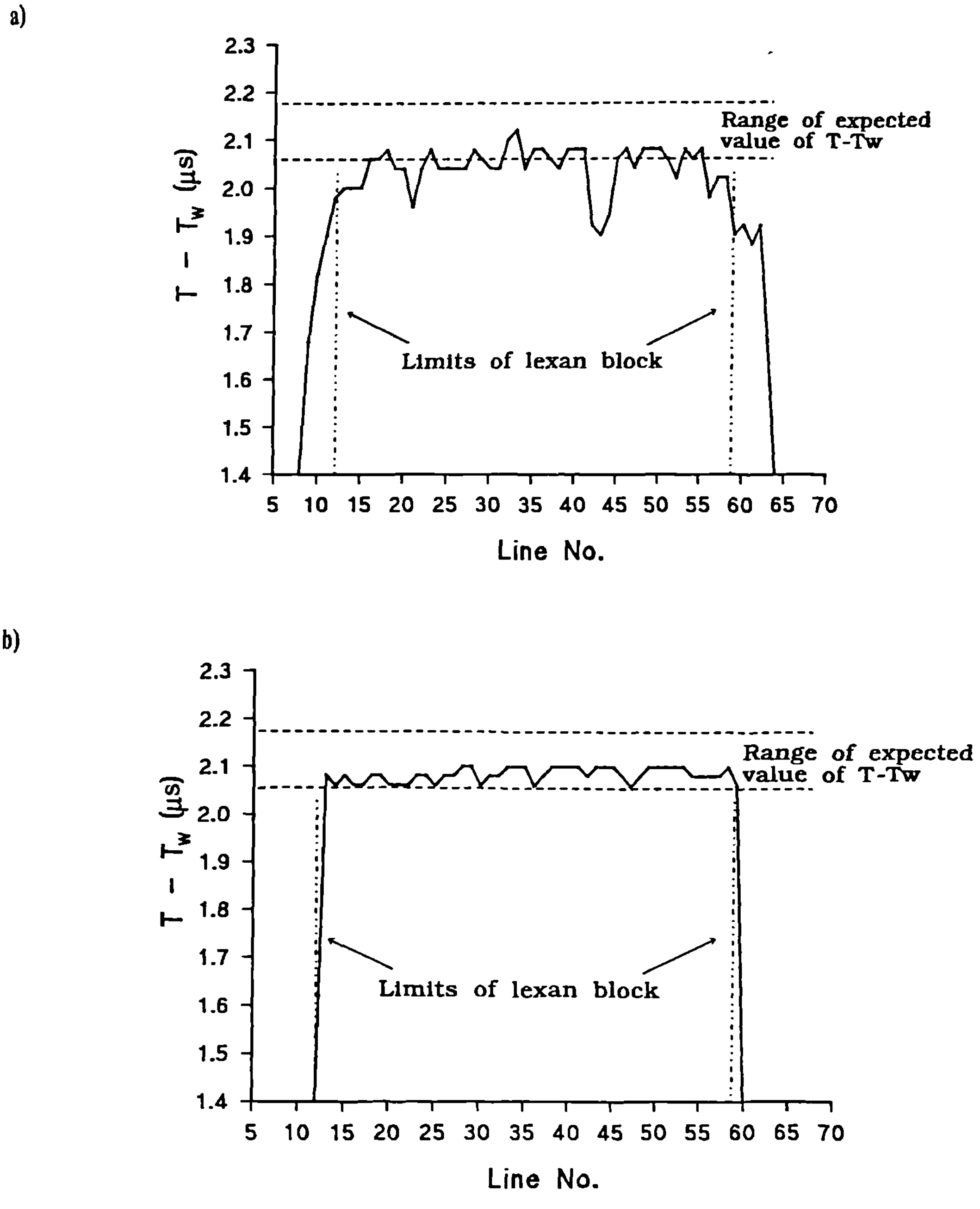

Figure 6.15 TOF measurements from a lexan block: a) threshold method, b) correlation method and c) correlation method with attenuated signals.

c)

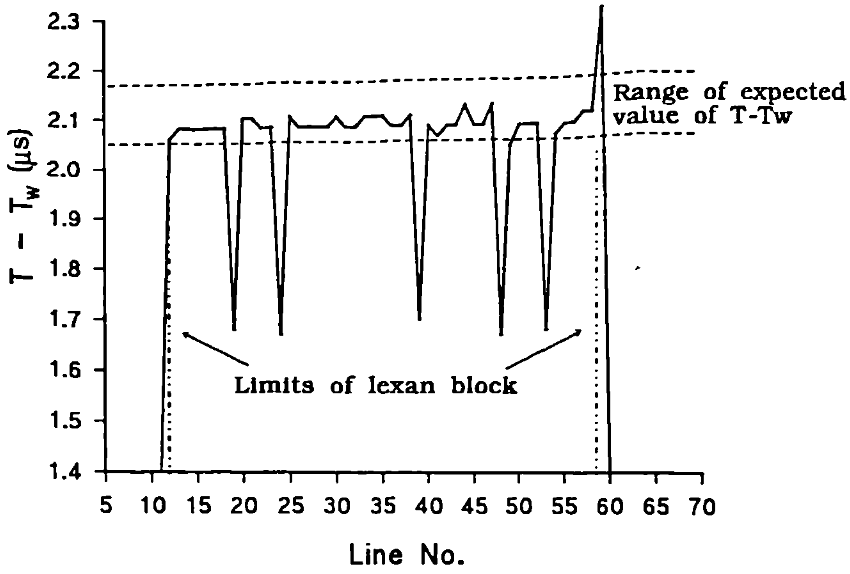

In conclusion, although the correlation method can be very accurate in some circumstance, when attenuation or refraction within the target is significant it tends to become unreliable. The threshold method never achieves the potential accuracy of the correlation method, but is much less badly affected by attenuation and refraction. Hence the method of TOF measurement used should depend on the nature of the particular target being scanned.

6.5.4 Images of a simple phantom - an evaluation of acquisition and processing options

Data obtained from some simple phantoms with known speed of sound distributions was used to evaluate the complete system, from acquisition of the TOF projections to reconstruction of the image. One of these phantoms consisted of three fingers of a latex surgical glove filled with vegetable oil (speed of sound = 1450 m/s), suspended in distilled water (speed of sound = 1480 m/s at 20°C). The target TOF measurements consisted of 110 projections over 180°. The reference through-water TOF measurements were obtained from a single probe position only. Due to the low attenuation of the target, logarithmic compression of the received signal was not required and the correlation method of TOF measurement could be used.

Figure 6.16a shows the acoustic speed reconstruction obtained by simple backprojection (ie no filtering). Peak white represents the highest speed of sound and black the lowest. Although the structure of the target is recognisable, the acoustic speed values obtained by simple backprojection are again clearly incorrect. This image also possesses significant "streak" artifacts which emanate from the edges of the fingers. These are probably due to inconsistencies in the TOF projections caused by errors in the reference TOF data, or by refraction of the acoustic beam for the target data. Several procedures were investigated to see if this image could be improved upon.

6.5.4.1 Number of reference projections required

It was felt that changes in the distance between the probes for different probe positions might be contributing to errors in the TOF projections. One solution to this problem would be to obtain reference TOF data, ie without the target present, for more than one probe position. By varying the number of reference probe positions and observing the affects on the images, it was discovered that little improvement was obtained by having more than 10 reference positions (ie one every 18° for a 180° scan). The acoustic speed image obtained using 10 positions (Figure 6.16b) clearly shows a significant reduction in streak artifacts.

6.5.4.2 Use of median filters to remove 'glitches' in profiles

Refraction is probably the other main cause of streak artifact. This problem is demonstrated in Figure 6.17. When the beam is near to the edge of a region with a different speed of sound than it's surroundings, it will inevitably be refracted to some extent. This will result in less energy (and hence a lower amplitude pulse) reaching the receiver. All the TOF measurement methods will tend to overestimate the TOF when the pulse amplitude is low, causing a positive spike in the $T - T_w$ projection. This so-called 'glitch' noise is not amenable to linear smoothing filters because of it's wide band-width. However, a non-linear filtering operation known as median filtering can be effective in reducing glitch noise (Crawford and Kak, 1982). A 3-point median filter would operate as follows. For each point in the projection, compare it's value to the points on either side and find the point with the median

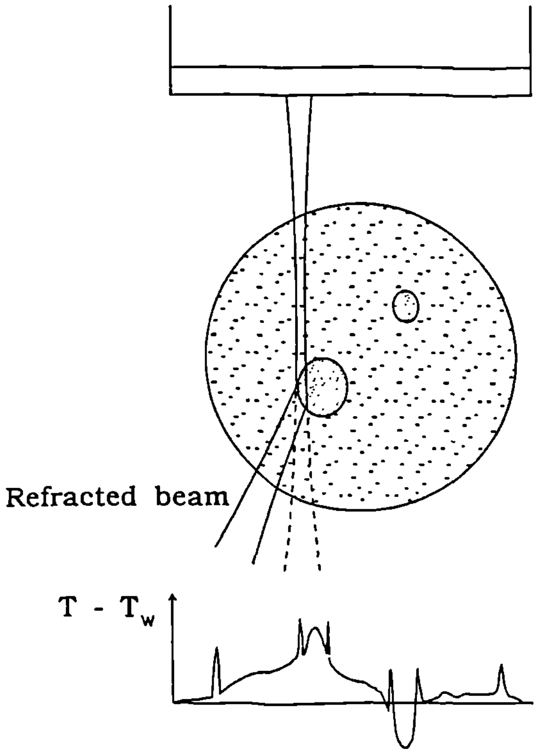

Figure 6.17 **Refraction as a cause of glitch noise in TOF profiles.**

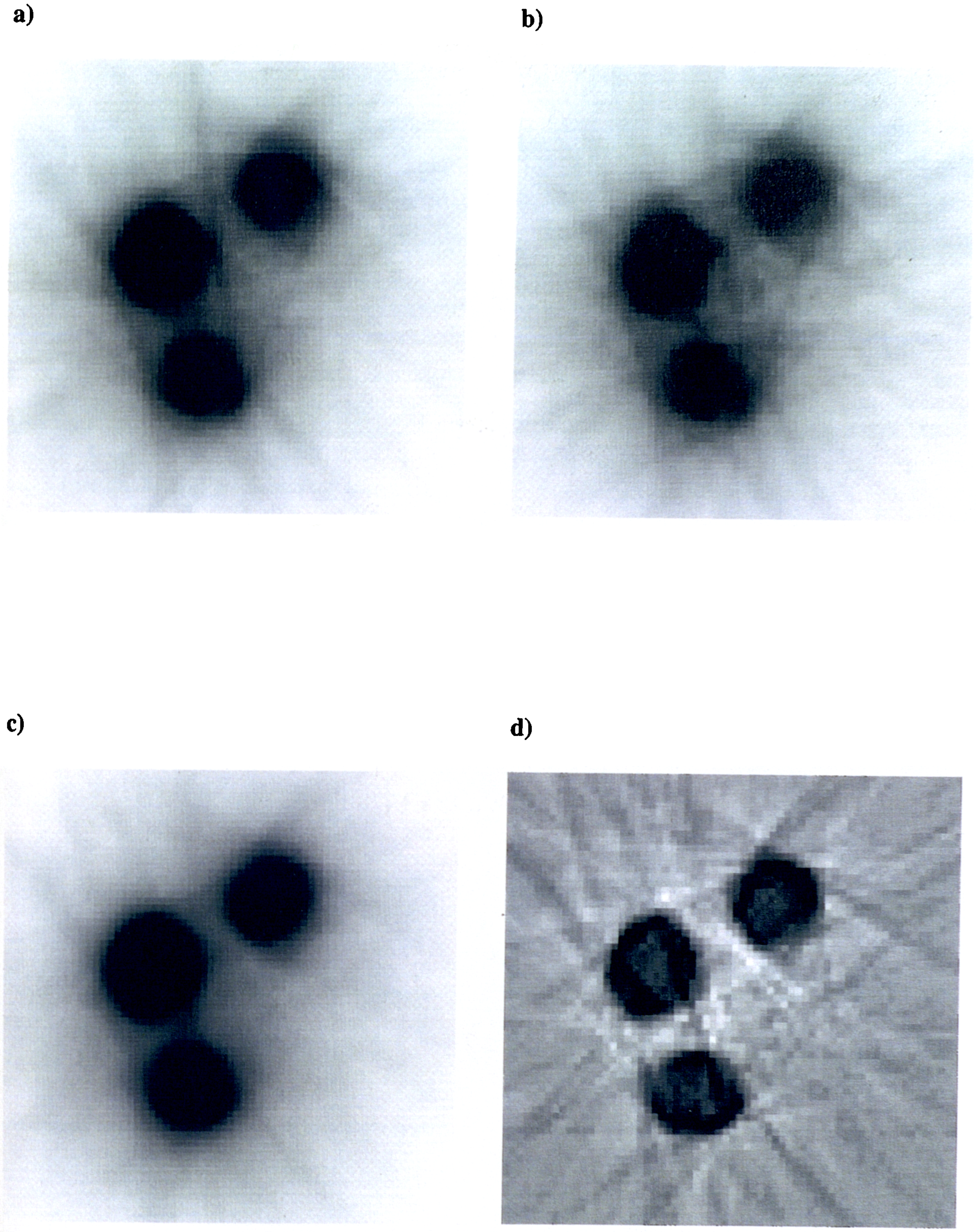

Figure 6.16 Acoustic speed images of a surgical glove filled with vegetable oil; a) unfiltered backprojection (peak white = 1580 m/s and black = 1260 m/s); b) as (a) but with 10 reference positions; c) as (b) but with median filtering; d) as (c) but with Shepp-Logan filtering (white = 1510 m/s and black = 1430 m/s).

value If the central point has the median value, leave it unchanged. If one of the neighbours has the median value, give this value to the central point. This filter will remove glitches which are 1 point wide. A 5-point median filter will remove glitches up to 3 points wide. The only undesirable affect on the projections is to flatten the tops of peaks the bottoms of troughs. Figure 6.16c shows the result of applying a 5-point median filter to the projections used to reconstruct the image shown in Figure 6.16a.

6.5.4.3 Use of Shepp-Logan filters

In Figure 6.16d the same TOF data has been used to reconstruct the image using Shepp-Logan filtered backprojection. The acoustic speed values are now more accurate and the respective regions are the right size. However the image now appears noisier, suggesting that inconsistencies in the projections that have not been completely removed by additional reference TOF data or median filtering are being emphasised by the Shepp-Logan filter. This might be expected since glitch noise extends up to high spatial frequencies. Figure 6.16e shows that affect of applying a modified Shepp-Logan filter with a smoother high frequency roll-off.

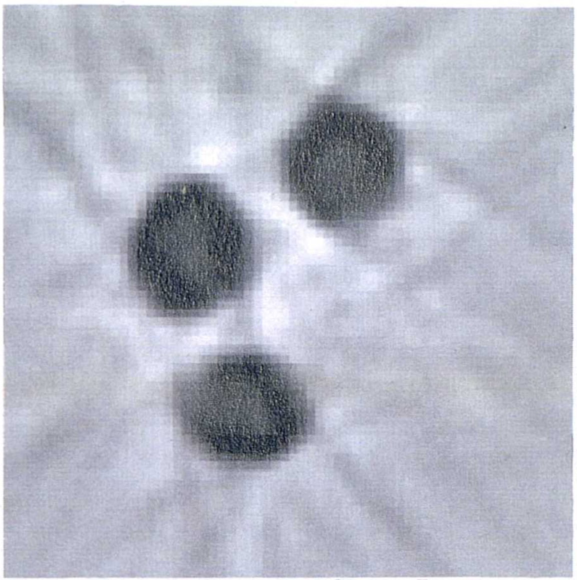

Figure 6.16e Smoothed Shepp-Logan filtered backprojection

6.5.5 Image of a more complicated phantom

Another phantom, shown schematically in Figure 6.18a, consisted of a natural sponge immersed in a latex bag of distilled water (c = 1485 m/s), which was itself immersed in a latex bag full of vegetable oil (c = 1450 m/s). The whole phantom was then suspended in the water bath. Figure 6.18b shows the acoustic speed reconstruction obtained with the correlation method and smoothed Shepp-Logan filtered backprojection. The geometric accuracy of the image appears to be good, with the outline of the bag and the separate regions of vegetable oil (dark grey) and water (light grey) being clearly discernable. Apparent detail can also be seen of the sponge, even though its effective acoustic speed appears to be only about 15 m/s above that of the water.

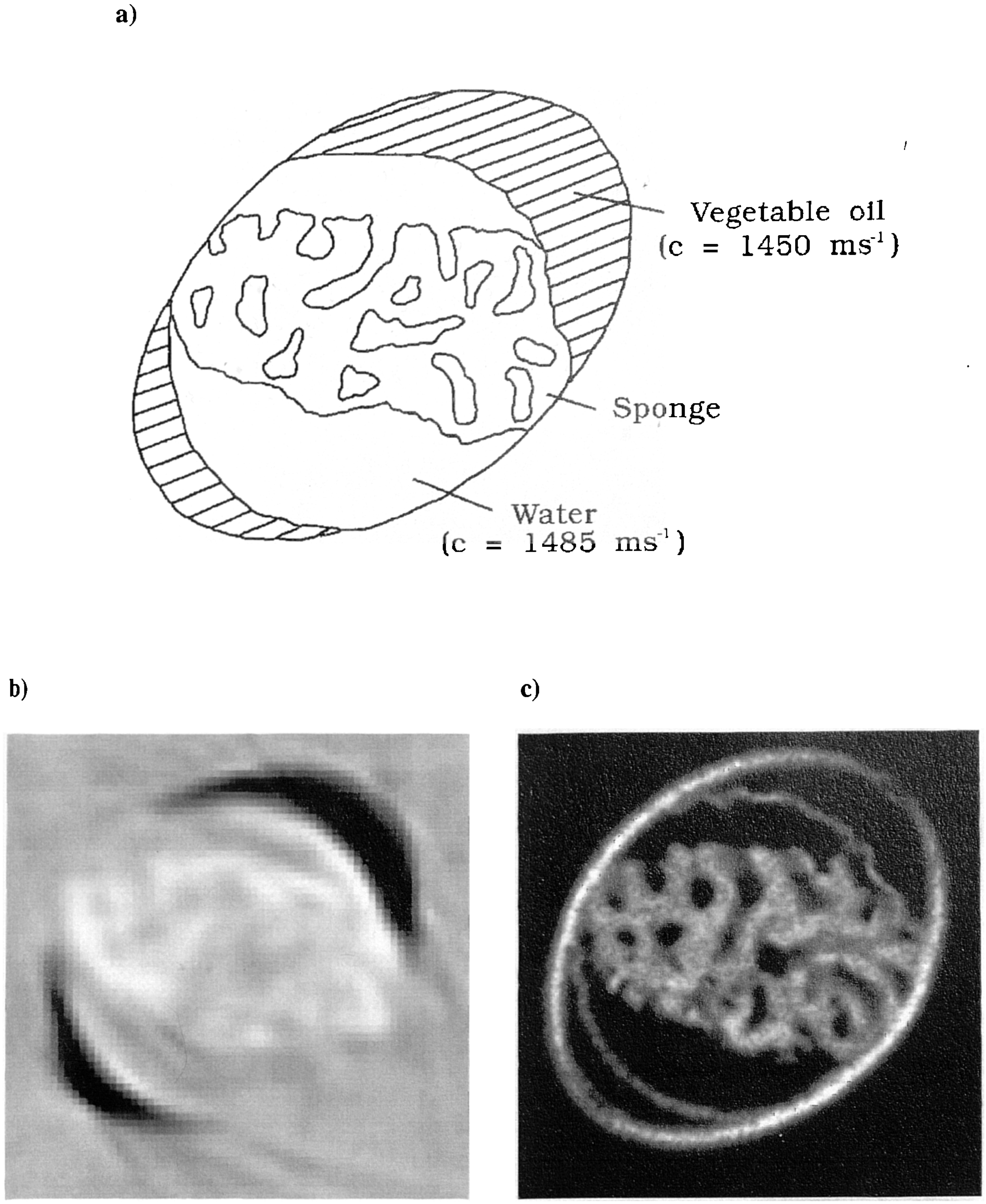

Figure 6.18 Images of a sponge phantom; a) phantom, b) acoustic speed image (white = 1505 m/s, black = 1440 m/s) and c) reflection UCT image.

A reflection mode UCT image was also obtained, and reconstructed assuming a constant acoustic speed in the target of 1485 m/s (Figure 6.18c). As expected the resolution of the reflection UCT image is superior, since it is governed by the ultrasonic pulse length rather than the beam width as is the case with the acoustic speed image. However there is much identifiable structure in common, and the reflection image generally confirms that the detail in the acoustic speed image is not artifactual. Note also that, since the acoustic speed variation in this target is only about 3%, distortion of the reflection UCT image is minimal.

The quantitative accuracy of the acoustic speed image must also be assessed. This was done by calculating the average value of acoustic speed for all the pixels within a particular region, the boundaries of which were defined by the reflection image. The portion of the image representing vegetable oil was calculated at 1451 ± 6 m/s. The average value of acoustic speed in the water was 1484 ± 2 m/s. Hence the average reconstructed values of acoustic speed within these regions agree with the known acoustic speeds to an accuracy of better than 0.4%.

6.5.6 Image artifacts from a phantom having large acoustic speed variations

It is possible that such good results were obtained for the phantom discussed in the previous section because the range of acoustic speed within the phantom was only about 3%. The degree of refraction within this target is likely to have been quite low, and probably lower than that encountered in a typical breast. A phantom similar to this but showing the larger acoustic speed variations more typical of a breast is shown in Figure 6.19a. This phantom consisted of a natural sponge inside a bag containing a solution of water and ethyl alcohol, giving a speed of sound of 1540 m/s. This bag was itself inserted into another bag containing vegetable oil (c = 1450 m/s), giving a total range of acoustic speed of 6%.

The acoustic speed image of this phantom, obtained using the correlation method of TOF measurement, is shown in Figure 6.19b. By comparing this image with the equivalent reflection UCT image shown in Figure 6.19c (reconstructed assuming an acoustic speed of 1485 m/s), it can be seen that the structural detail in the acoustic speed image is poorer and it contains more artifacts than the image of Figure 6.18b. This loss in geometric accuracy may be accounted for by increased refraction causing the paths of some ultrasonic beams through the target to be significantly different to the straight-path assumed in reconstruction. Using the threshold method of TOF measurement results in a better image (Figure 6.19d), although artifacts are still present. These persistent artifacts are presumably due to the extreme cases of refraction where some transmitted pulses may miss the receiver completely, creating 'gaps' in the TOF projection data. Although these gaps can be "filled

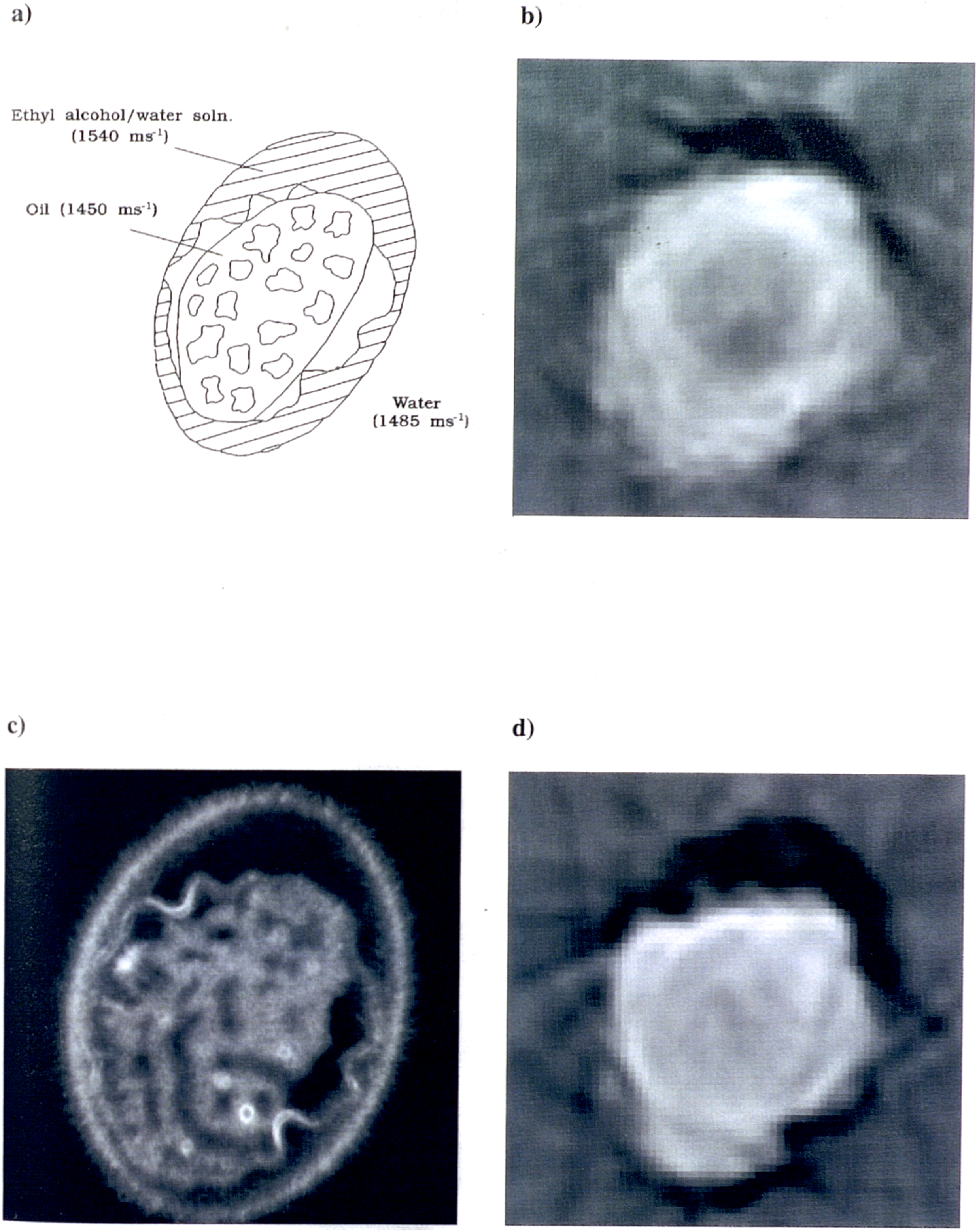

Figure 6.19 Images of a sponge phantom (a) having a large spatial variation in acoustic speed; b) acoustic speed image using correlation method (white = 1540 m/s, black = 1440 m/s); c) reflection UCT image (reconstructed assuming c_{av} = 1485 m/s); d) acoustic speed image using threshold method.

in" by median filtering, all knowledge of the true acoustic speed along that path is lost.

Refraction is also likely to affect the quantitative accuracy of the images, particularly at the boundaries between regions of different acoustic speed. However an analysis of the average acoustic speed values in the water (1483 ± 4 m/s) and in the vegetable oil (1455 ± 6 m/s) has revealed that the quantitative accuracy of the bulk regions is not significantly poorer than for the previous phantom. The reconstructed speed in the water/ethyl alcohol solution (1511 ± 12 m/s) is rather lower than expected, but this may be due to the sponge which has a lower acoustic speed than the solution. Thus these results are encouraging, bearing in mind that the quantitative accuracy required (see section 6.2.2) for effective compensation of reflection images depends on the size of the regions, and for large regions should be better than 5 m/s, whilst the geometric accuracy need only be ± 4mm.

The affects of acoustic speed variations on the reflection UCT image (Figure 6.19c) are very evident for this target, as revealed by the double boundaries of the bag and by tiny air bubbles within the sponge appearing as circles instead of points. Hence this confirms observations made by previous workers (see 3.2), that acoustic speed variations of greater than 5% have a significant effect on the quality of reflection UCT images reconstructed assuming a constant acoustic speed within the target.

6.5.7 Images of animal organs in-vitro

In order to test the ability of this UCT system to produce acoustic speed images of real tissue, several animal organs were obtained from a local abattoir. One such in-vitro target was a sheep's kidney, which was placed inside a bag of saline having an acoustic speed of 1540 m/s. The acoustic speed image (threshold method) and reflection UCT image (1540 m/s) of this target are shown in Figures 6.20a and b respectively. Although acoustic speed artifacts are apparent in the double membranes and general blurring, this reflection UCT image clearly shows the advantage of 360° over 180° scanning (c.f. Figure 5.31), since the resolution and general image quality is now roughly uniform over the whole image.

The acoustic speed image shows similar gross structure to the reflection image, although as usual at considerably reduced resolution. Note for example that the fatty areas in the central pelvis of the kidney have a lower acoustic speed (average 1495 m/s) than the surrounding medulla (average speed 1568 m/s). The quality of the acoustic speed image is again not as high as obtained from some of the phantoms because of the combined affects of considerable attenuation and acoustic speed variations. However the average acoustic speed values are consistent with those reported for fat and for kidney tissue (Duck 1990).

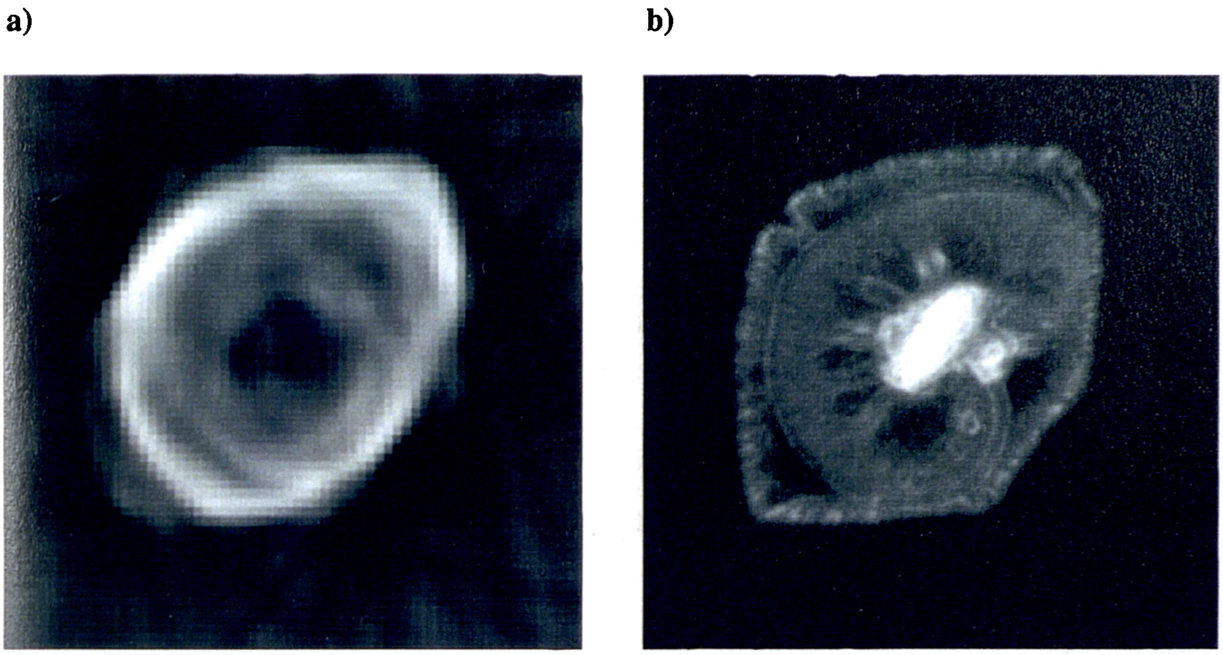

Figure 6.20 **Images of a sheep's kidney in-vitro; a) acoustic speed image (white = 1670 m/s, black = 1450 m/s); b) reflection UCT image (cav = 1540 m/s).**

Figure 6.21a shows an acoustic speed image of a transverse section of a sheep's heart which has been placed in a latex bag containing isotonic saline (c ≈ 1500 m/s). Figure 6.21b shows the reflection UCT image (assuming 1540 m/s). Both images show the affects of the relatively high attenuation of this target (muscle is more highly attenuating than fat or adipose tissue), although the 360° reflection image is again considerably better than a 180° image (Figure 6.21c) reconstructed using only half the data, because each B-scan need only penetrate half way through the target. The high attenuation also causes large errors in the TOF measurements, even when using the threshold method. Although this acoustic speed image is of similar quality than those obtained by other workers, it is debateable whether the resolution and geometric accuracy of these images would be sufficient for diagnosis in their own right. However, such images may still be of sufficient quality to reduce the artifacts and improve the resolution of reflection UCT images. This will be established in the next section.

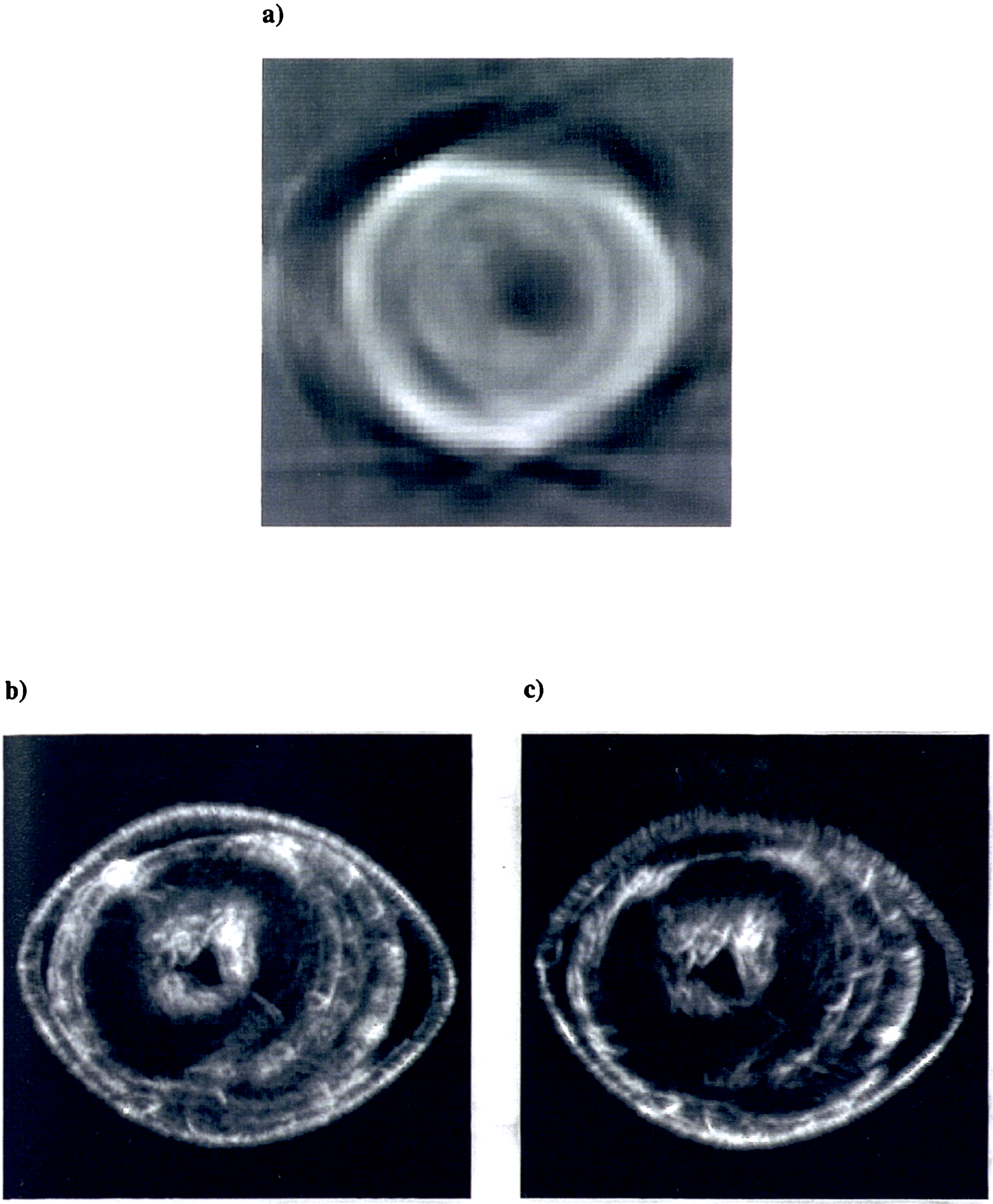

Figure 6.21 Images of a sheep's heart in-vitro; a) acoustic speed image (white = 1690 m/s, black = 1380 m/s); b) reflection UCT image (c_{av} = 1540 m/s); c) reflection UCT image using data from 180^{o}.

6.6 Results for acoustic speed compensation of reflection UCT images

6.6.1 Introduction

It has been shown in the previous section that a transmission UCT system, based on linear arrays, can produce accurate acoustic speed images under certain circumstances. The quality of these images, and especially their geometric accuracy, deteriorates when the acoustic speed variations are large or when the attenuation is high. Since the acoustic speed images were not in general felt to have sufficient geometric accuracy for worthwhile lateral displacement (refraction) corrections, only axial displacement correction has been attempted in this study.

It will now be investigated whether these images are sufficiently accurate to provide worthwhile axial displacement corrections of reflection UCT images obtained from the same target sections. As before simple phantoms will be considered before moving onto animal and human tissues in-vitro.

6.6.2 A practical implementation of acoustic speed compensation

The transmission data for the acoustic speed image was obtained first, and then immediately afterwards (ie before reconstruction of the acoustic speed image) the data for the reflection image was obtained. In this way movement of the target between scans was kept to a minimum.

After reconstruction of the acoustic speed image, reflection UCT images were reconstructed: a) assuming a single acoustic speed in the target (the "uncompensated" image) and b) incorporating information from the acoustic speed image (the "compensated" image). The algorithm for axial displacement corrections operates as follows:-

1) Each scan line of each B-scan comprising the reflection UCT data is taken in turn. Starting from a sample point in the scan line known to lie before the target (ie in the surrounding water), this first sample value is written to the reflection UCT image matrix at a position calculated using the known centre of rotation of the probes.

2) The point at the equivalent position on the acoustic speed image (ie at the known distance from the centre of rotation) is then also identified.

3) The next and subsequent scan line values are then written to the reflection UCT image matrix at

a position advanced from the previous point by the distance

$$\frac{c_i \cdot \delta t}{2}$$

where c_i is the value at the equivalent point (ie advanced by the same distance) in the acoustic speed image, and δt is the time between consecutive samples in the scan line data (ie 1/6.5 MHz or 0.154 μs).

4) This operation is repeated for all scan lines in all B-scans of the reflection UCT data.

6.6.3 Simple wire and cyst phantoms

Figure 6.22a shows the acoustic speed image corresponding to the same section of the cyst phantom shown in Figure 5.27a. There seems to be more artifacts in this image than in the previous acoustic speed images shown. These artifacts are probably caused by the large difference in acoustic speed between the high speed region (1659 ± 16 m/s) and its surroundings (1524 ± 24 m/s), and by the relatively high attenuation of this phantom. However despite these artifacts, when this acoustic speed image is used to compensate the reflection UCT data obtained from the same section through the phantom, the image obtained (Figure 6.22b) is a considerable improvement on the uncorrected reflection UCT image of Figure 5.27b. Note in particular that the boundaries around the cyst and high speed regions are now much sharper and continuous.

Figure 6.23a shows the acoustic speed image corresponding to the uncorrected reflection UCT image of Figure 5.28, and Figure 6.23b is the compensated reflection image. Despite the fact that the acoustic speed image again has artifacts, the blurred image of the nearest wire has now become re-focused into a single point. Thus this result would seem to confirm that, at least for the purpose of correcting a reflection UCT image, good geometric accuracy in the acoustic speed image is less important than a reasonable representation of gross structure with accurate acoustic speed values.

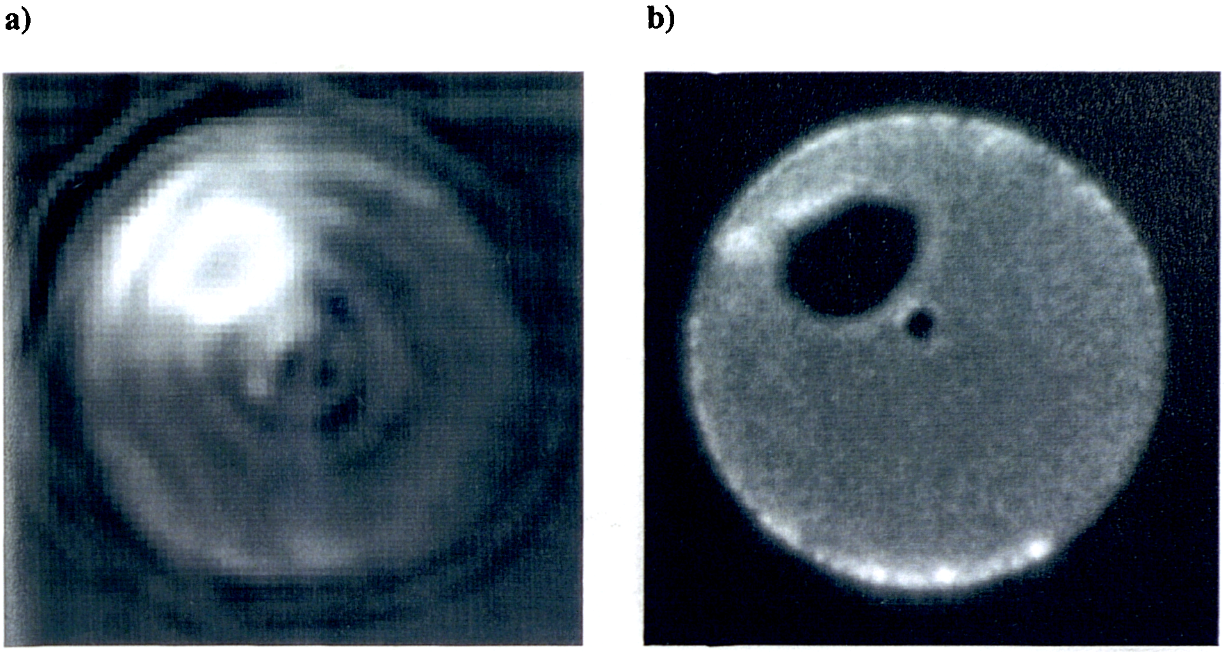

Figure 6.22 Images of the cyst phantom of Figure 6.27; a) acoustic speed image (white = 1680 m/s, black = 1410 m/s); b) reflection UCT image with acoustic speed compensation.

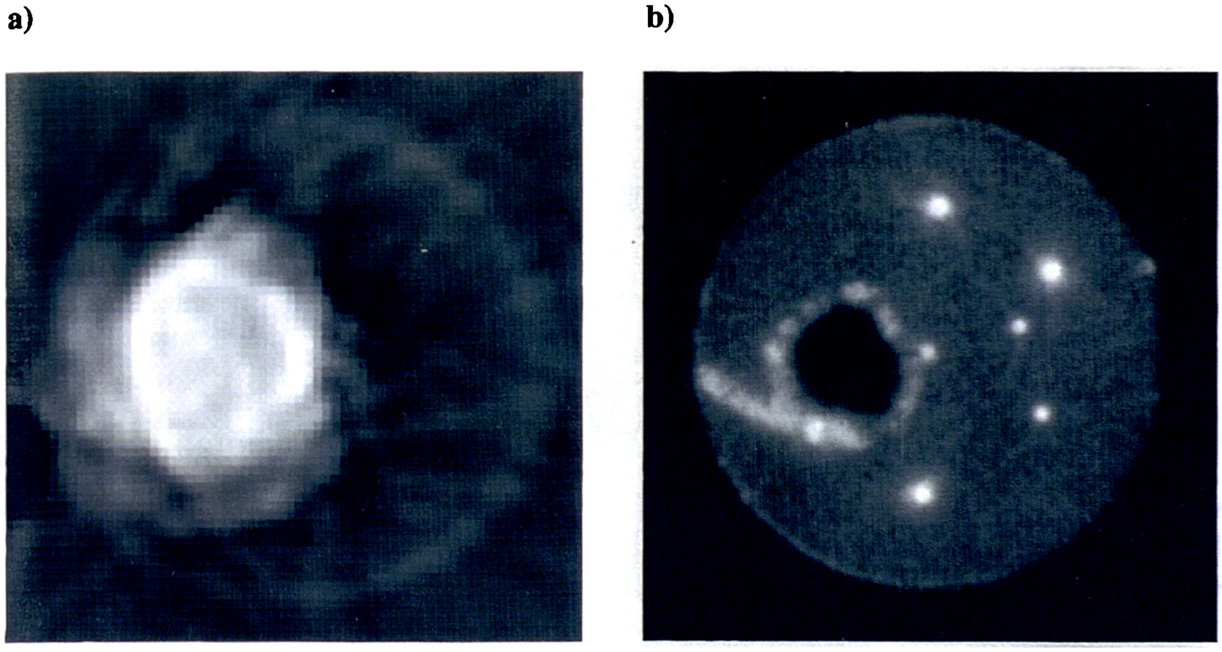

Figure 6.23 Images of the wire phantom of Figure 6.28; a) acoustic speed image (white = 1660 m/s, black = 1420 m/s); b) reflection UCT image with acoustic speed compensation.

6.6.4 More complex sponge phantoms

In a more sophisticated test, acoustic speed data from the sponge phantom image shown in Figure 6.19d was used to improve on the reflection UCT image (Figure 6.19c) obtained assuming a single acoustic speed for the whole target. The result is shown in Figure 6.24a. For this target it is instructive to show an original B-scan image (Figure 6.24b) to emphasise the degree of improvement in image quality obtained by reflection UCT with acoustic speed compensation. The corrected reflection UCT image is clearly sharper than the uncorrected one, although both are a vast improvement on the B-scan image. In particular, the walls of the inner bag have merged from being a double line into a single one. Also, the small air bubbles trapped in the sponge have become sharp points, and the lobes of the sponge itself are more clearly defined. Hence, in this target, acoustic speed compensation has been shown to be effective in restoring those improvements in image quality, obtained by reflection UCT, which are compromised in a target having acoustic speed variations of greater than 5%.

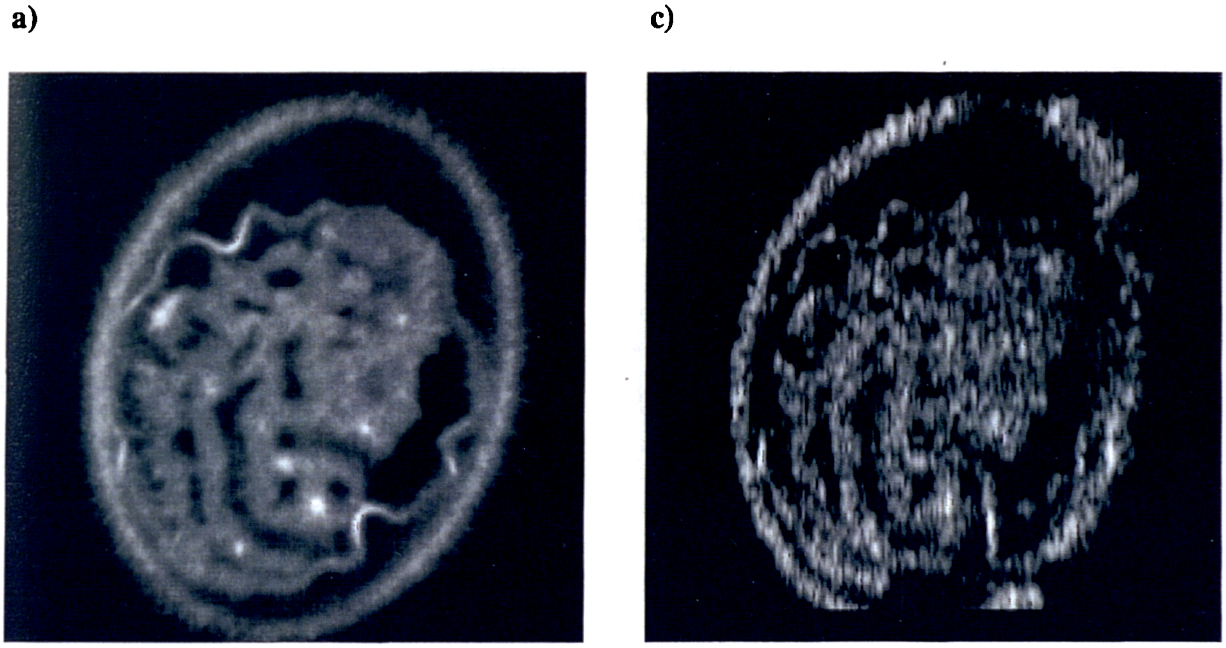

Figure 6.24 Images of the sponge phantom of Figure 6.19; a) acoustic speed compensated reflection UCT image, and b) single B-scan.

6.6.5 Animal organs in-vitro

The acoustic speed images of the in-vitro animal organs shown in 6.5.7 were also used to compensate for acoustic speed artifacts in the equivalent reflection images. Figure 6.25b shows a single B-scan, with the probe viewing from the left, of the sheep's kidney. The acoustic speed and uncorrected reflection UCT images of this target were shown in Figures 6.20a and b respectively. A reflection UCT image reconstructed using values from the acoustic speed image is shown in Figure 6.25a. Specularly reflecting boundaries are now complete, speckle is virtually eliminated and resolution is much improved and isotropic. There is very little evidence of the multiple or dispersed registration of targets seen in Figure 6.20b. All these factors lead to much easier interpretation of the structure. Note for example the radial fibres now visible in the cortical tissue in the compensated reflection UCT image, and which are virtually undetectable in the B-scan image.

Figure 6.26b shows a B-scan of the sheep's heart. Figure 6.21a shows the acoustic speed image and Figure 6.21b the uncompensated reflection UCT image. Despite the apparently poor geometric accuracy of the acoustic speed image, the reflection UCT image reconstructed using these acoustic speed values (Figure 6.26a) is still a considerable improvement on the uncorrected reflection UCT image. For example the left and right ventricles are now clearly defined, whereas in the B-scan the right ventricle is barely visible at all because of the attenuation of the ultrasound signal.

6.6.6 In-vitro human breast

Some studies have also been performed with in-vitro human tissues. A post mastectomy breast, known to possess a cancerous tumour, was obtained from Pathology and placed in a latex bag with isotonic saline (c = 1500 m/s). Figures 6.27a to 6.27d show the B-scan, acoustic speed, uncompensated and compensated reflection UCT images respectively.

This set of images probably demonstrate most dramatically the vast improvement in image quality obtained with reflection UCT compared to conventional B-scanning, and are an indication of the possibilities of combined acoustic and reflection UCT for breast imaging. The main problem with B-scanning in the breast is the large number of interfaces and fibres which permeate typical breast tissue, most of which cannot be seen from a single view direction making interpretation of the B-scans very difficult. In the reflection UCT image all of the fibrous structure is visible and the encapsulated kidney-shaped structure at 4 o'clock, identified by the pathologist as the tumour, is now easily identified. Indeed a section obtained through the tumour showed a remarkable resemblance to the reflection UCT image.

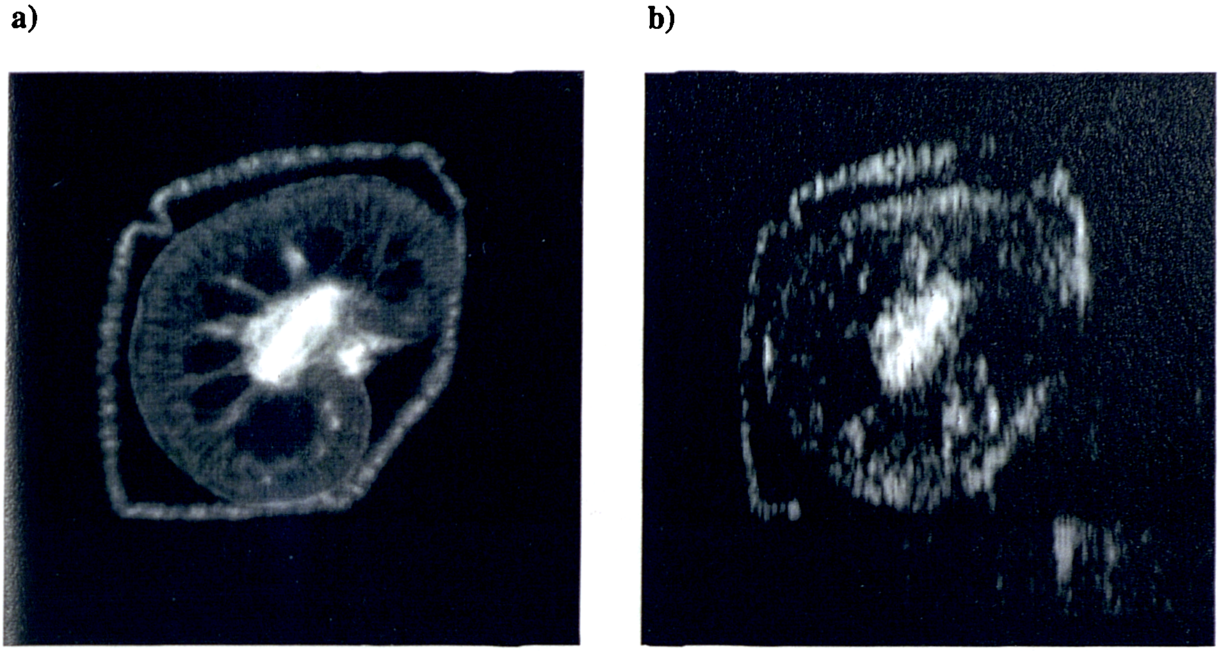

Figure 6.25 Images of the sheep's kidney of Figure 6.20; a) acoustic speed compensated reflection UCT image; b) single B-scan.

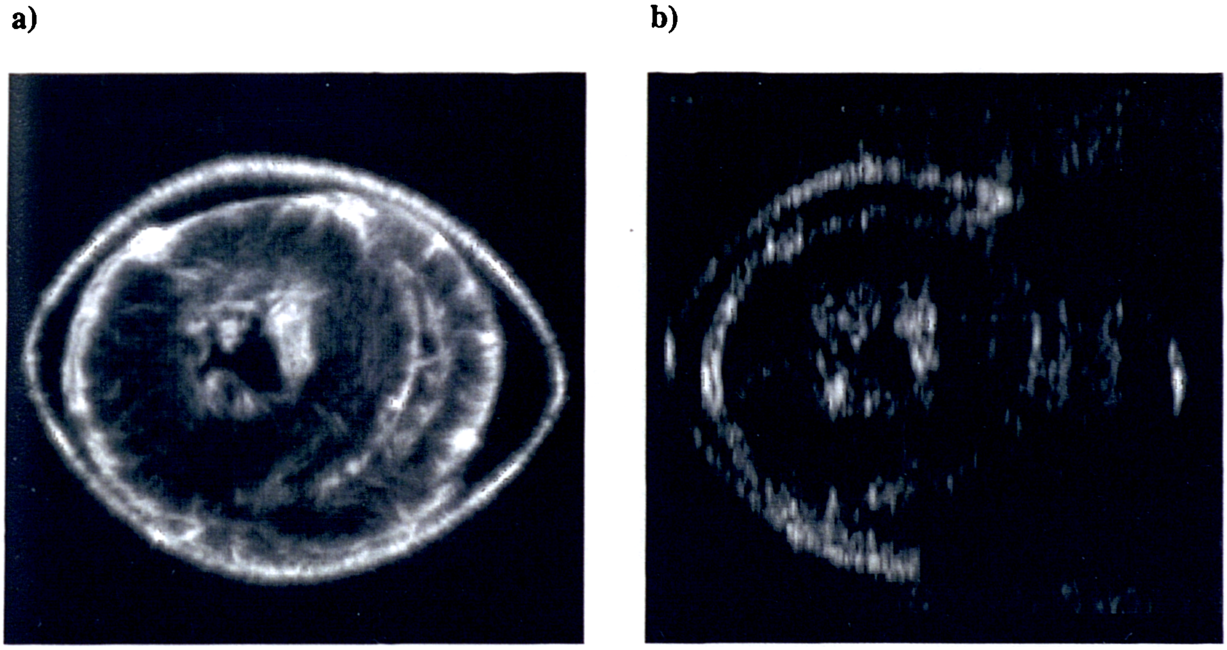

Figure 6.26 Images of the sheep's heart of Figure 6.21; a) acoustic speed compensated reflection UCT image; b) single B-scan.

It is also interesting to note the correspondence between structures in the acoustic speed and reflection images. In particular, the region in the reflection images identified as the tumour is shown in the acoustic speed image to have a noticeably higher acoustic speed then its surroundings. However, the average acoustic speed value in this region (1484 ± 5 m/s) is not significantly higher than average values for "normal" tissue (Greenleaf and Bahn, 1981), making a diagnosis on the basis of the acoustic speed image alone rather unreliable. Similar results to this have been observed by other researchers into transmission UCT (e.g. Glover 1977, Greenleaf and Bahn 1981, see also Chapter 3).

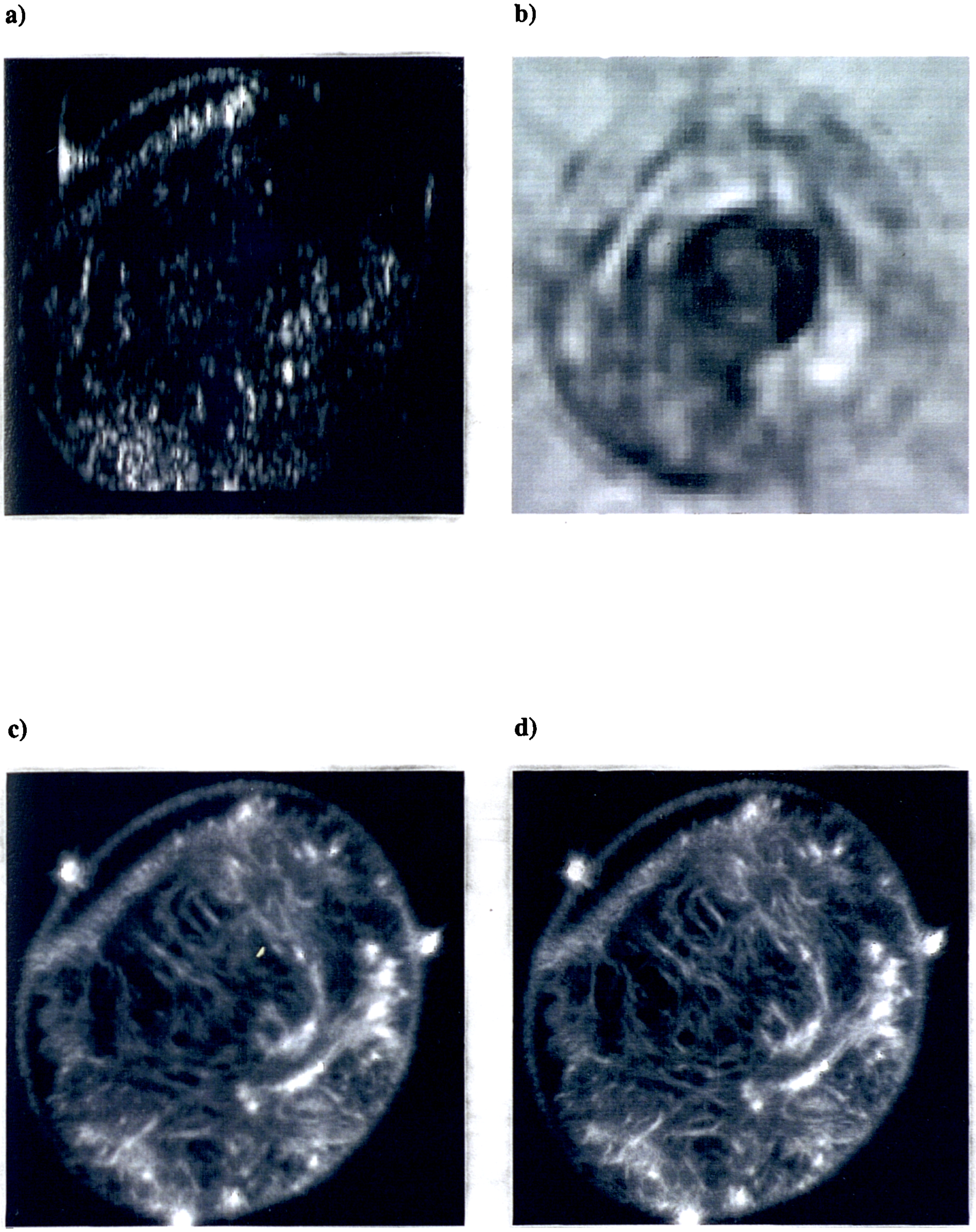

Figure 6.27 Images of a human post-mastectomy breast in-vitro; a) B-scan; b) acoustic speed image (white = 1500 m/s, black = 1450 m/s); c) reflection UCT image (assuming c_{av} = 1480 m/s); d) acoustic speed compensated reflection UCT image.

6.7 Discussion of combined acoustic speed and reflection UCT

This chapter has described the construction of and results from a combined reflection and transmission UCT system. The system is based on conventional linear arrays and scans through 360° in a horizontal plane.

The ability to scan though a complete 360° has, as expected, resulted in the reflection UCT images showing fewer artifacts due to attenuation and far field beam divergence than images obtained from the 180° reflection UCT system described in Chapter 5. Although these advantages are worthwhile, the main reason for developing this system was to attempt to reduce the artifacts in reflection UCT images caused by a varying acoustic speed. Compensating for these artifacts requires knowledge of the spatial distribution of acoustic speeds within the target. Previous workers have shown that images of acoustic speed distributions can be obtained using a transmission UCT system, so this system was constructed to allow transmission measurements to be obtained using the same basic equipment as used for the reflection UCT measurements.

Acoustic speed images of targets having relatively low attenuation and acoustic speed variations, have been reconstructed using a correlation method for time of flight (TOF) measurement and a straight-path CT reconstruction algorithm. The images obtained from these phantoms appear to show very good geometric and quantitative accuracy. One reason for the quality of these images, which appears to be comparable to or better than that obtained by previous workers, may be the use in this system of linear arrays for the transmission measurements. It has been argued here that, to obtain accurate acoustic speed images, the distance between the transmitter and receiver apertures should remain very constant (ideally to within 30 μm) during lateral scanning of the apertures. This constant separation is much easier to achieve using a mechanically fixed electronically stepped system than with the mechanically stepped systems used by all previous workers.

In targets showing relatively high attenuation or acoustic speed variations (e.g. $> 5\%$), such as might be expected in real breast tissue, the geometric accuracy of the images is significantly reduced while the quantitative accuracy seems to be relatively uneffected. The affect of high attenuation is to change the shape and reduce the amplitude of the transmitted acoustic pulse reaching the receiver, resulting in a poorer accuracy in the estimate of the pulse time of flight. It is possible to at least partially overcome this problem by using methods for calculating TOF which are not so dependent on preserving the shape of the pulse envelope, such as threshold methods. Unfortunately these threshold methods tend to introduce there own geometric distortions: specifically the size of regions of low acoustic speed is underestimated whereas the size of regions of high acoustic speed is overestimated. Another possibility, not investigated in this work, would be to use a correlation method while applying some form of automatic gain to the received pulses (or even better to the transmitted pulses) to reduce the variations in pulse amplitude. It might also be possible to send specialised pulse sequences, such as "chirps", designed to optimise the "peakyness" of the cross-correlation function. However, bearing in mind that the linear arrays used in this system generate pulses with a peak amplitude that is about one tenth that generated by modern arrays, probably the simplest solution to the attenuation problem would be to use linear arrays with a higher acoustic output.

The main affect of large acoustic speed variations is probably to cause significant refraction of the transmitted acoustic beam. As well as violating the assumption of straight path propagation inherent in the CT reconstruction algorithm, refraction will also cause less energy to reach the receiver aperture resulting in a pulse of reduced amplitude and poorer accuracy in the estimate of TOF. Although the effect of pulse amplitude loss can again be minimised by using appropriate methods for TOF measurement (see below), it is likely to be much more difficult to correct for the violation of the assumption of straight-path propagation. As discussed in Chapter 3 (section 3.3), some workers have investigated reconstruction algorithms for transmission UCT that do not rely upon the assumption of straight-path propagation. The most successful of these techniques applied ray-tracing to calculate the curved acoustic paths, combined with an iterative reconstruction algorithm (e.g. Anderson 1990). Although some improvements in image quality were reported for phantoms, few results have been presented from real tissues. However there may be some scope in using similar techniques to improve the acoustic speed images obtained from this system.

It has been shown here that by using a threshold method for calculating the pulse TOF, the error in the TOF measurement due to attenuation or refraction is minimised even if the pulses have not taken the assumed straight path through the target. This may explain why the acoustic speed images show better quantitative accuracy, which depends mainly on the accuracy of the TOF estimates, than they do geometric accuracy which depends mainly on the degree of deviation from a straight line of the pulse's paths.

In this work no serious attempt has been made to establish whether the acoustic speed images are of sufficient quality to provide diagnostic information in there own right. This is because the main reason for obtaining these images was to establish whether they could be used to provide worthwhile compensation for the artifacts in reflection UCT images caused by a varying acoustic speed in the target. It was argued in section 6.2.2 that the resolution of the acoustic speed images, limited as they are in a transmission UCT system by the ultrasound beam width, is insufficient to correct for the lateral displacement component of these artifacts. Possible ways of producing acoustic speed images with the required accuracy will be discussed in Chapter 7.

Since no attempt has been made to correct for the lateral component of the reflection UCT artifacts, the existence of geometric distortion in the acoustic speed images is only of importance if it affects the ability to compensate for the axial component of these artifacts. Previous results from Chapter 5 have suggested that only large regions, with a relatively high acoustic speed difference between themselves and their surroundings, cause significant artifacts in reflection UCT images. Theoretical arguments (section 6.2.1) suggest that in these cases the quantitative accuracy of the acoustic speed image is more important than the geometric accuracy. This prediction seems to have been borne out by the results of this study, since even acoustic speed images showing considerable geometric distortion have been used to provide worthwhile compensation for axial displacement artifacts in reflection UCT images obtained from the same targets.

To conclude, the results of this study have shown that images of tissue structure at high resolution, and quantitative images of tissue acoustic speed at lower resolution, can be obtained by combining the principles of reflection and transmission UCT within a single system. This system uses linear arrays for both reflection and transmission measurements and thus restricts the mechanical movement required during data acquisition to a rotational movement only. The elimination of the lateral movement (required when using single element transducers for transmission measurements) is particularly important in improving the quality of acoustic speed images. The main limitations of this combined reflection and transmission system are the remaining rotational movement of the probes, which increases the data acquisition times and consequent subject movement, and the need for the targets and the probes to be entirely immersed in a water bath. These limitations have restricted the practical application of this prototype system mainly to in-vitro targets.

Although some in-vivo studies of the female breast have been performed, the results have been disappointing and have not been reported here. While movement of the subject during data acquisition has been a factor, probably the main reason for these disappointing results in-vivo has been due to excessive attenuation of the ultrasound signals, both in reflection and transmission, due to the large size and relatively high attenuation of the breasts studied. This problem is being addressed by modifying the system to accept more modern linear arrays with a considerably higher acoustic output. The problems of subject movement and general patient acceptability are more difficult to solve, requiring the construction of systems designed specifically for the particular clinical application. Some possible approaches to clinically viable systems will be discussed in chapter 7.

7 Conclusions and future developments

7.1 Introduction

The purpose of this chapter is to summarise the main results and conclusions of the previous chapters, and in the light of these findings to consider possibilities for the future development of ultrasound CT techniques. Of particular importance in this consideration is the need to develop systems with which these techniques can be applied effectively to patients in-vivo.

7.2 Main experimental findings of this study

These may be summarised as follows:-

1) It was shown in Chapter 5 that, by simply combining reflectivity (or backscatter) data from many directions and assuming a constant acoustic speed for the whole target, images can be generated that show considerably better resolution (approximately 1mm) and fewer artifacts than conventional B-scan images generated with the same equipment, provided that acoustic speed variations within the target do not exceed about 5%. An important requirement for achieving such good resolution is high mechanical accuracy in the scanning system. This has been achieved by the use of a) a linear array for lateral scanning, b) a very rigid rotational scanning arrangement and c) an accurate and automatic method of calculating the centre of rotation of the system.

2) In situations where the acoustic speed variations are greater than 5%, such as is likely to occur in many female breasts, it has been shown that the quality of reflection UCT images is significantly reduced due to incorrect registration of echoes in the composite B-scan images. It has been suggested by previous workers that this problem could be alleviated by using the "true" acoustic speed distribution in the reconstruction of the reflection UCT image.

3) It has already been shown by several workers (see Chapter 3) that acoustic speed distributions can be obtained by the technique of transmission UCT. Since a transmission UCT technique requires 360° scanning, a 180° reflection-only system (as described in Chapter 5) is not suitable for transmission measurements. Hence such a system is likely to find clinical applications only in targets having relatively low acoustic speed inhomogeneity (the neck or lower limb may be possibilities), unless non-transmission methods of acoustic speed imaging can be developed (see 7.4.2).

4) The 360° system described in Chapter 6 has demonstrated that both reflection and transmission UCT can be implemented using identical linear arrays in a single system. Use of linear arrays allows for much greater positional accuracy than is possible with mechanically scanned systems. This appears to be the first system to be described that uses linear arrays for transmission measurements, which may explain why the acoustic speed compensated reflection UCT images obtained from this system appear to be superior than others reported to date.

5) The acoustic speed compensated reflection images of in-vitro targets produced by this system are also superior to those available from conventional "state-of-the-art" real-time ultrasonic imaging systems, despite the fact that this system uses linear arrays which are about 13 years old.

6) The low acoustic output of these linear arrays does cause problems when imaging large or highly attenuating targets. It is expected that these problems will be reduced or eliminated by using more modern arrays with higher outputs.

7.3 Limitations of the present systems for clinical applications

Possibly the main potential clinical application of these systems is in breast cancer screening, due to the accessibility of breast tissue, the absence of bone or gas and the need for alternative tests using non-ionising radiation. Although conventional ultrasound has already found widespread use in breast cancer diagnosis, particularly for differentiating between tumours and cysts, it is not generally considered to be suitable for mass screening for many of the reasons discussed in Chapter 1 (eg poor lateral resolution and high operator dependence). However it has been shown in this work that techniques involving reflection ultrasound CT combined with acoustic speed imaging can overcome mast of these problems. In addition ultrasound has some significant advantages over X-ray mammography such as the low risk to patients and the fact that the procedure is painless.

With the application to breast cancer screening in mind, the main limitations of the systems described in this thesis will be discussed and suggestions for ways of overcoming these limitations considered.

7.3.1 Scan times and movement artifacts

Very few in-vivo studies have been performed as part of this study. One of the main reasons for this is the long scan times required (about 30 seconds for a single reflection UCT slice and about 2 minutes for transmission UCT), resulting in inevitable subject movement and movement induced artifacts. If this subject movement could be eliminated then images obtained in-vivo should be as good as those that have been obtained in-vitro. However since it is unrealistic to expect the subject to remain completely immobilised (ie prevent breathing) for more than about 20 to 30 seconds, the only way to minimise movement induced artifacts is to reduce the scan times.

In the present system the fraction of the scan time spent transmitting and receiving ultrasonic data is small compared to the time spent mechanically moving the probes and in transferring data between the digitiser and the computer's hard disc. In fact, the data for a single reflection image (15 frames by 70 pulse-echo scan lines) could in theory be obtained in about 0.2 seconds, while that for a transmission acoustic speed image (110 frames by 70 transmission lines) would require about 0.8 seconds, giving a total scan time (per slice) of approximately 1 second. If reflection and transmission data could be collected simultaneously the total scan time for both would only be about 0.8 seconds.

The time spent moving the probes around the target, which in the present system is by far the major component of the scan time, could in principle be eliminated completely. This could be achieved by using a mechanically fixed system which acquires data around the target by electronic switching of active transducer elements, analogous to the way in which the linear arrays perform a lateral scan of the target. Various possible configurations are shown in Figure 7.1. These will be discussed more fully in section 7.4

The time required to transfer and store the ultrasonic data depends on various aspects of the transient recorder, computer and their interface. In the present system there is insufficient memory in the transient recorder to store all of the data for a transmission UCT image, so some of that data must be transferred to the computer for storage onto disc and this is relatively time consuming. However, the cost of computer memory is decreasing rapidly and it is not difficult to imagine a digitiser with a 5 MByte buffer which would be able to store all of the data (reflection and transmission) for one slice. In this case the data for a single slice could be transferred to the computer for longer term storage while the system was being prepared for the acquisition of subsequent slices. A small amount of subject movement between slices is likely to be more acceptable than movement occurring during acquisition of a slice.

The times required for reconstructing the images from the measured data are of less importance. For this system the reconstruction times are about 30 minutes for an acoustic speed compensated reflection UCT image, and about two hours for an acoustic speed image. However, little attempt has been made to optimise the software for speed, and the computer used is considerably slower than more modern systems or a dedicated processor would be. It is not unrealistic to anticipate total reconstruction times of less than 2 minutes per slice for relatively little additional cost.

7.3.2 Patient acceptability

Another disadvantage of these systems, especially for any in-vivo clinical studies, is the relatively poor patient acceptability of water-bath scanning. The main problem is the necessity for total emersion of the target being scanned because of the requirement of transmission UCT for 360° access. The method adopted here for in-vivo studies of the breast has been to make a 15 cm diameter hole in an adjustable height couch, with the breast protruding through the hole and into the water. Although relatively comfortable for the subject, this approach is only suitable for sagittal sections of the breast and there are difficulties in obtaining sections close to the chest wall. Coronal and transverse sections, which would give information close to the chest wall, only allow scanning over at most 180° and are thus unsuitable for transmission UCT. This problem would be eliminated if acoustic speed information could be obtained using methods that do not require transmission measurements. This possibility will be considered further in section 7.4.2.

If the requirement for the mechanical movement of the probes can be eliminated, it is possible to envisage systems which do not require total emersion in a water bath. One possibility is a fixed ring of transducers in direct contact with the skin. Other possibilities are discussed in section 7.4. As well as being more convenient for the patient, these approaches should allow sections close to the chest wall to be obtained more easily.

7.3.3 Refraction artifacts

Acoustic speed images, and reflection UCT images with acoustic speed compensation, both suffer from the affects of ultrasound beam refraction. To achieve the full potential resolution of reflection UCT, refraction must be compensated for in both the reflection and acoustic speed images. If such compensation were possible it may also then be worthwhile using RF data for the reconstruction of the reflection UCT images, with a potential resolution of less than the ultrasound wavelength (eg less than 0.5mm at 3MHz).

To account for refraction requires more sophisticated reconstruction algorithms than have been used in this study. As discussed in section 6.2.2, one of the problems with incorporating refraction into the reconstruction of acoustic speed images, for example by ray-tracing methods, is that the images have inherently insufficient resolution to calculate refraction angles accurately. One possibility that appears not to have been explored previously would be to use the corresponding reflection UCT image, which shows interfaces between discrete regions of different acoustic speed at inherently greater resolution, to define the refraction angles in the reconstruction of the acoustic speed image. This reconstruction approach could proceed in four stages:-

(1) First reconstruct an acoustic speed image using a conventional straight-path algorithm.

(2) Then reconstruct a reflection UCT image with axial acoustic speed compensation but not refraction correction. Hence steps (1) and (2) are already performed in the system described in Chapter 6.

(3) Use a ray-tracing technique with data from the acoustic speed image, and with refraction angles defined by the reflection UCT image, to map the acoustic beam paths through the target and hence reconstruct an improved acoustic speed image.

(4) Reconstruct an improved reflection image using ray-tracing on the previous reflection image and acoustic speed information from the latest acoustic speed image.

Stages (3) and (4) could be iterated as necessary, although a thorough mathematical analysis, which is beyond the scope of this thesis, would be required to establish whether such an iteration would converge.

7.4 Alternative data acquisition systems

In this section, a general discussion is presented of the ways in which the improvements to UCT introduced in the previous section could be implemented in practical systems.

7.4.1 Totally enclosing arrays

Both reflection and transmission UCT require the acquisition of data from many directions around the target. In the mechanically scanned systems described here this has been achieved by moving linear arrays around the target (Figure 7.1a). Clearly a UCT system in which mechanical movement was eliminated completely would have great advantages, particularly in terms of scan times (and hence image quality) and patient acceptability. It is possible to envisage systems that could obtain these view directions by having a large number of transducer elements distributed around the target to be scanned. Several configurations are possible.

1) Circular Ring Array

One possibility is a ring of evenly distributed elements (Figure 7.1b), having a diameter that is larger than the maximum scan diameter required (eg 12 cm). Circular ring arrays for reflection measurements have already been described by several workers (Johnson et al 1978, Norton and Linzer 1981, Devaney and Belykin 1984, Feron and Saniie 1987, and Witten et al 1988), although most have only looked at backscatter measurements using a co-incident single element source and receiver - this approach has occasionally been called synthetic aperture imaging instead of reflection UCT.

Backscatter measurements, particularly when using a small receive aperture, only utilise a tiny fraction of the ultrasonic energy entering and scattered from a target. A more efficient approach would be to collect data at all scattering angles, for example by transmitting with one element at a time and receiving simultaneously with all the other elements in the ring. Note that for this configuration the elements must be small enough to insonate the entire object as in broad-beam reflection UCT. If the RF signal at each receiving element is digitised and stored it is then possible to focus, in the computer, at all points in the target - ie digitally synthesising a 360° aperture. This can be achieved by calculating, for each point in the image, the appropriate times of flight to every element and summing the outputs corresponding to these times. A backprojection approach may be more efficient since, for each pair of transmitter and receiver elements and assuming a constant acoustic speed in the target, the signal at the receiver is the sum of the scattered waves from points lying on a set of ellipses with foci at the transmitter and receiver. Hence an image could be reconstructed by backprojecting the signals at each receiver along elliptical paths. Note that in the

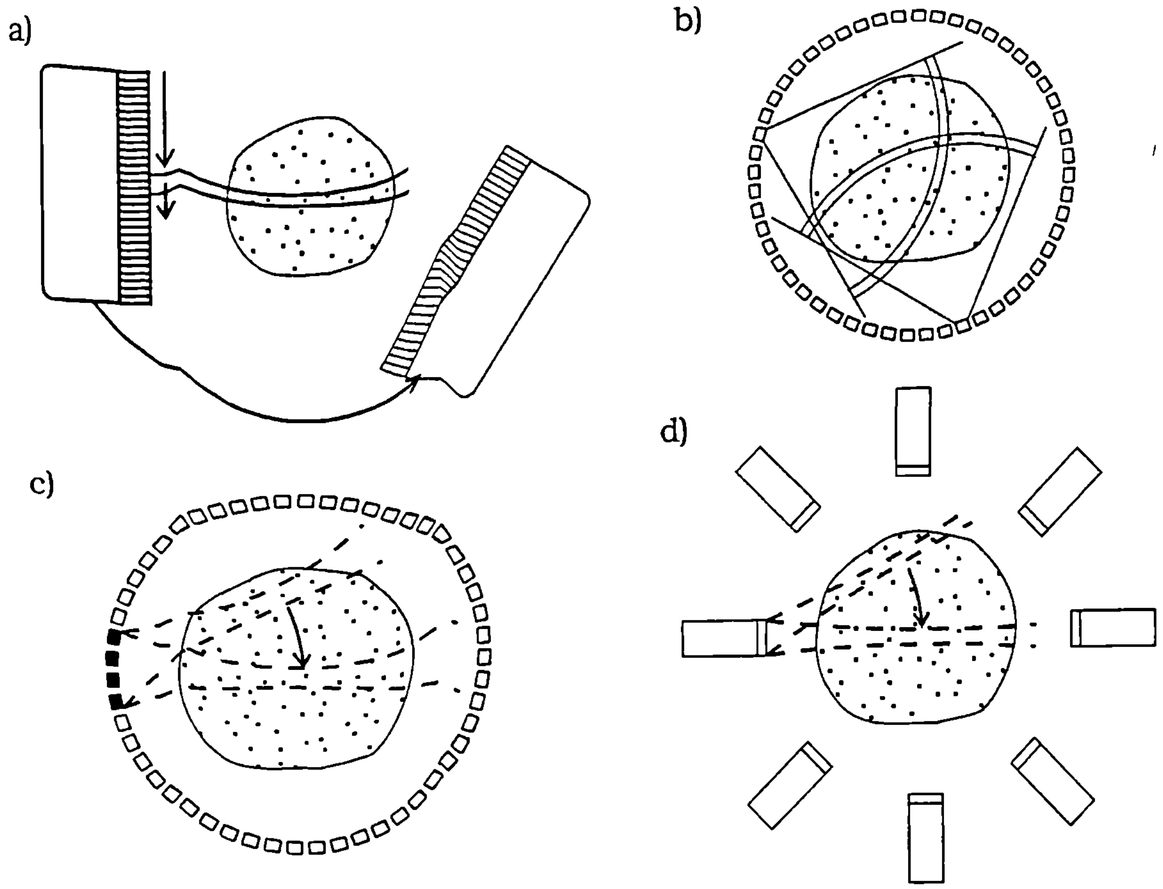

Figure 7.1 **Various possible configurations for ultrasound CT: a) mechanically rotated linear arrays; b) fixed circular ring array; c) ring array with sub-grouping in transmission; d) fixed phased arrays.**

case of a co-incident transmitter and receiver the ellipses simplify to concentric circles, as observed by Norton (1979). In common with other backprojection techniques the image would be degraded by a blurring function, although it should be possible to de-convolve this. Although the blurring function in this case would not be given simply by (1/r), if data from a sufficiently large number of element is used the function should be very close to (1/r) in the near vicinity of an image point.

Regardless of which reconstruction method is used, to enable focusing at points near the edge of the target and to avoid grating lobes in receive, the element spacing p must be chosen such that (Whittingham 1991)

$$p < \frac{\lambda}{2\sin\theta_{max}} \qquad (7.1)$$

where θ_{max} is the angle between the line joining an element to the centre of the array and a line tangential to the maximum target diameter. Consider an array of diameter 16cm with elements having a beam divergence angle of 90°, thus giving a maximum target diameter of 11.3cm. From equation 6.1 the maximum element pitch should be 0.35mm, giving a minimum of 1422 elements in the array which would be rather expensive. This should be compared to the theoretical requirement for CT of $\pi l/dl$ elements, which for a pulse length of 1mm is only about 350 elements. By using short acoustic pulses it may be possible to avoid grating lobes and hence have a larger element pitch and fewer elements, but the elements would still need to be small enough to give 90° irradiation (ie less than 0.8mm wide).

An interesting point is that these multi-angle scattering measurements are likely to result in images showing less emphasis on specular reflectors than do images obtained solely from backscatter measurements, since these would only be detected by relatively few elements at each transmission, whereas isotropic scatterers would be detected by all elements. Also note that the data acquisition time for such a system (350 transmissions) would be less than 0.1 seconds per slice, thus opening up the possibility of nearly real-time data acquisition. Whether the images could be reconstructed quickly enough to achieve near real time frame rates is less certain.

Clearly the problem of varying acoustic speed can not be ignored, any more than it could be for reflection UCT using linear arrays. Hence a method for obtaining acoustic speed images is essential. Bearing in mind that all the elements are receiving simultaneously in this system, the information for a transmission UCT approach to acoustic speed imaging should already be available. To a first approximation, the minimum time taken for acoustic energy to arrive at any one element after transmission from another element should represent the minimum path (ie a straight path) between the two elements. Assuming a beam divergence angle of 90°, each element can only transmit directly to one half of the array. In this case the number of independent straight-line transmission paths linking N transmitters and receivers is given by

$$\frac{N}{2}\left[1+\frac{N}{2}\right]$$

which for 350 elements gives 30,800 lines of transmission data. Comparing this to the 7,700 lines used to reconstruct an acoustic speed image for the system described in Chapter 6 shows that this approach is potentially viable. Note that the reconstruction of an acoustic speed image from this data would require a fan-beam algorithm - these have already been developed for X-ray CT.

One disadvantage of this broad-beam approach to transmission UCT is that, since there are now many possible paths linking each transmitter to each receiver, the likelihood is reduced that the first acoustic energy to arrive has followed the straight path. In conventional transmission UCT the beam is confined to be relatively narrow (by using larger transmitting apertures and focusing), thus restricting the number of potential paths linking transmitter and receiver. Another problem may be that the acoustic energy reaching each receiver will be much lower than in the conventional technique, making detection of the leading edge of the pulse less accurate.

To achieve higher transmission energy the elements could be grouped in transmission (Figure 7.1c). However in this case the beam divergence angle would be reduced, necessitating steering of the transmit beam across the target (as in a conventional phased array). However there is now a problem with transmission grating lobes and, for transmission UCT, fewer independent scan lines. Also the scan time would be increased significantly. Another option involving element grouping on transmission, which does not require increased scan times, would be to apply delays to the elements so that they form a convex (ie a divergent) beam, thus insonating the entire object without the need for beam steering and hence multiple transmissions. Clearly for either of these configurations complex multiplexing arrangements would be required.

2) Multiple Phased Arrays

Another configuration, which could be realised with equipment that is already commercially available, would have a number of identical phased array probes (e.g. 8 or 16) distributed in a fixed arrangement around the target (Figure 7.1d). Unlike the ring-array, the transducer elements would no longer be distributed evenly around the target because of the relatively large gaps between probes, so that less of the available scattered energy could be received.

However such a system could incorporate the same number of total elements as the ring array because the elements are more densely packed within the phased arrays themselves (modern probes typically have element sizes of about 0.2mm or less). Hence in principle the same amount of positional information could be obtained. If only backscatter data were available (as in a conventional phased array), a reflection UCT image could be reconstructed in a similar way to that described in Chapter 6 for linear arrays. Ideally however it would again be preferable to have full control over the elements in transmission and reception - ie to transmit a divergent beam and to receive simultaneously on all elements of all the phased arrays and do the receiver beam-forming in software. In this way all the scattered data can be obtained from one transmission resulting in a faster scan and more efficient use of the scattered energy.

The main problem with the use of phased arrays in the configuration of Figure 7.1e is that, when using a transmission UCT method for acoustic speed imaging, there would now be an insufficient number of possible paths joining any two probes for the reconstruction of a useful image. Hence to make this approach viable for breast scanning, a method is required for acoustic speed imaging that does not rely on transmission measurements.

7.4.2 Acoustic speed imaging using side scatter measurements

The ability to measure ultrasound which has been scattered at angles other than 0° (transmission imaging) and 180° (reflection imaging) opens up possibilities for alternative methods of acoustic speed imaging. Several such techniques have already been investigated by other workers. Robinson et al (1982) suggested a method involving cross-correlation of overlapping regions from two sector scans obtained from different transducer positions. The maximum of the cross-correlation function (ie the mean spatial shift in the image) is then related to the average acoustic speed in the region. Experiments on liver tissue in-vivo suggested a repeatability of +/- 15 ms^{-1} (about 1%) in the estimate of acoustic speed, although this was in a rather large region of interest (at least 3 cm in diameter) so the technique as described is probably not suitable for imaging.

Another technique that has attracted some interest in recent years is the beam-tracking method (or the similar crossed-beam method), first proposed by Ophir (1986). In this method two co-planar transducers (one transmitting and one receiving) are arranged so that their beam axes intersect at right angles (Figure 7.2). The TOF between the transmitter and the receiver, via side scatter in the cross-over region, is the total path length divided by the average acoustic speed along the path. By moving the receiving transducer a small distance (dx) laterally, the average acoustic speed (c) along a short segment of the transmission path is related to the difference in TOF (dt) obtained at the two receiver positions (ie c=dx/dt). Clearly this estimate will be contaminated if the TOF from the cross-over region to the receiver is different at the two positions, ie because of a difference in acoustic speed along these paths. However a more accurate estimate of average acoustic speed can

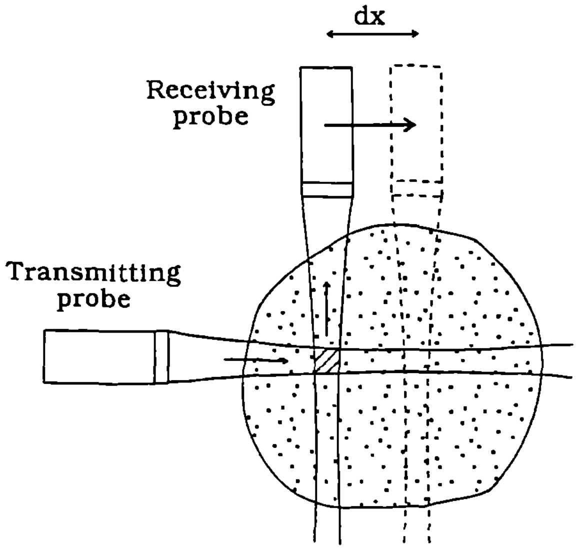

Figure 7.2 **Principle of the beam-tracking method for the in-vivo measurement of acoustic speed (Ophir 1986).**

be obtained, at the expense of increased sample size, by taking measurements of TOF at many (eg 10 to 100) receiver positions and plotting dt against dx. The slope of this graph then gives c_{av}, with any variation in acoustic speed between the transmission path and the receivers contributing "noise" to this linear regression.

The size of the sample region from which a reasonably accurate estimate of acoustic speed can be obtained is the limiting factor in using this technique for in-vivo acoustic speed imaging. Cespedes et al (1992) have predicted, by computer simulation, that a minimum sample size of 10mm by 10mm is required for an accuracy of 1% in acoustic speed. One way of potentially improving the accuracy of the acoustic speed estimate, and reducing the sample size, is to average measurements taken at angles other than 90°. This could be achieved by having many transducers distributed around the target, as in the configurations shown in Figure 7.1. Since measurements over a range of angle *up to* 90° may be sufficient for acceptable accuracy in some targets, this opens up the possibility of limited-angle reflection and acoustic speed imaging in targets that would not otherwise be suitable (such as the neck and limbs).

The arrangement of Figure 7.2 can also be thought of as a "right-angle" transmission CT problem, since the TOF along this path is determined by the integrated refractive index along the path. A set of TOF measurements along "x" then represent a projection of refractive index for bent paths, and other projection could be obtained by rotating the transducers (or by having multiple transducers). Clearly the reconstruction algorithm required would be rather different to that for straight-path CT, but there seems no reason why such an algorithm could not be developed. This connection between cross-beam acoustic speed imaging and CT has apparently not been made by other workers.

Perhaps the most exciting prospect of all is a technique combining all the positive aspects of reflection UCT, side-scatter imaging and transmission CT techniques. This could involve initially obtaining a high resolution reflection image of the boundaries of the target. Acoustic speed estimates would then be made using side-scatter measurements, starting from the edges of the target (outside which the acoustic speed is known exactly) and working-in towards the centre of the target. The side-scatter data could then be reconstructed into a conventional reflection or scatter image with accurate acoustic speed compensation. It would even be possible in this model to make accurate corrections for refraction at the target boundary, one of the main problems in the conventional crossed-beam technique.

8 References

Abbott JG and Thurstone FL 1979 Acoustic speckle: Theory and experimental analysis
Ultrasonic Imaging 1, 303-324

Adams MF and Anderson AP 1980 Tomography from multiview ultrasonic diffraction data: Comparison with image reconstruction from projections
Acoustical Imaging 10, 365-380

Anderson AH 1990 A ray tracing approach to restoration and resolution enhancement in experimental ultrasound tomography
Ultrasonic Imaging 12, 268-291

Anderson AP and Adams MF 1982 Synthetic aperture tomographic imaging for ultrasonic diagnostics
Acoustical Imaging 12, 565-578

Ball J, Johnson SA and Stenger F 1980 Explicit inversion of the Helmholtz equation for ultra-sound insonification and spherical detection
Acoustical Imaging 8, 451-461

Bamber JC and Dickinson RJ 1980 Ultrasonic B-scanning: A computer simulation
Phys. Med. Biol. 25, 463-479

Bartelt H 1988 Computation of local directivity, speed of sound and attenuation from ultrasonic reflection tomography data
Ultrasonic Imaging 10(2), 110-120

Born M and Wolf E Principles of Optics
Fifth Edition, Pergamon Press, 1975

Bracewell RN and Riddle AC 1967 Inversion of radioisotope scans in radio astronomy
Astrophys. J. 150(2), 427-434

Brandenburger GH, Klepper JR, Miller JB and Synder DL 1981 Effects of anisotropy in the ultrasonic attenuation of tissue on computed tomography
Ultrasonic Imaging 3, 113-143

Burlew MM, Madsen EL, Zagzebski JA, Banjavic RA and Sum SW 1980 A new ultrasound tissue-equivalent material
Radiology 134(2), 517-520

Carson PL, Meyer CR, Scherzinger AL and Oughton TV 1981 Breast imaging in coronal planes with simultaneous pulse echo and transmission ultrasound
Science 214, 1141-1143

Carson PL, Scherzinger AL, Meyer CR, Moore GE, Jobe W and
Samuels B 1988 Lesion detectability in ultrasonic computed tomography in symptomatic breast patients.
Invest. Radiol. 23, 421-427

Carson PL and Scherzinger A L 1979 Ultrasonic computed tomography
in New Tachniques and Instrumentation in Ultrasonography, pp 144-166

Cespedes I, Ophir J and Huang Y 1992 On the feasibility of pulse-echo speed of sound estimation in small regions: simulation studies
Ultrasound Med. Biol. 18(3), 283-291

Chen CF, Robinson DE, Wilson LS, Griffiths KA, Manoharan A and Doust BD 1987 Clinical sound speed measurement in liver and spleen in vivo
Ultrasonic Imaging 9, 221-235

Chenevert TL, Bylski DI, Carson PL, Meyer CR, Bland PH, Adler DD and Schmitt RM 1984 Ultrasonic computed tomography of the breast
Radiology 152, 155-159

Crawford CR and Kak AC 1982 Multipath artifact corrections in ultrasonic transmission tomography
Ultrasonic Imaging 4, 234-266

Crowther RA, De Rosier DJ and Klug A 1970 The reconstruction of a three-dimensional structure from projections and its application to electron microscopy
Proc. Roy. Soc. Lond. A. 317, 319-340

De Rosier DJ and Klug A 1968 Reconstruction of three dimensional structures from electron micrographs
Nature 217, 130-134

Devaney AJ 1982 A filtered backpropagation algorithm for diffraction tomography
Ultrasonic Imaging 4, 336-350

Devaney AJ and Beylkin G 1984 Diffraction tomography using arbitary transmitter and receiver surfaces
Ultrasonic Imaging 6, 181-193

Dickinson RJ 1986 Reflection and scattering
in Physical Principles of Medical Ultrasonics, Ed. CR Hill, Ellis Horwood Ltd., Chichester, England

Dines KA and Kak AC 1979 Ultrasonic attenuation tomography in soft tissues
Ultrasonic Imaging 1(1), 18-33

Dines KA, Fry FJ, Patrick JT and Gilmor RL 1981 Computerised ultrasound tomography of the human head: experimental results
Ultrasonic Imaging 3, 342-351

Duck F, Johnson S, Greenleaf J and Samayoa W 1977 Digital image focussing in the near field of a sampled acoustic aperture
Ultrasonics 15, 83-88

Duck FA and Hill CR 1979 Acoustic attenuation reconstruction from back-scattered ultrasound
in Computer Aided Tomography and Ultrasonics in Medicine, Ed. Raviv et al. pp 137-148 (North Holland Publishing Company).

Duck FA 1990 Physical Properties of Tissue
Academic Press, London, England

Ermert H and Roehrlein G 1986 Ultrasound reflection-mode computerised tomography for in-vivo imaging of small organs
1986 IEEE Ultrasonics Symposium Proceedings, IEEE Cat. No. 86, pp 825-828

Farrell EJ 1981 Tomographic imaging of attenuation with simulation correction for refraction
Ultrasonic Imaging 3, 144-163

Fatemi M and Kak AC 1980 Ultrasonic B-scan imaging: Theory of image formation and a technique for restoration
Ultrasonic Imaging 2, 1-47

Feron ML and Saniie J 1987 Diffraction tomography using the total scattered field
Acoustical Imaging 16, 237-248

Friedrich M, Hundt E and Maderlechner G 1982 Computerised ultrasound echo tomography of the breast
Eur. J. Radiol. 2, 78-87

Gilbert P 1972 Iterative methods for the three-dimensional reconstruction of an object from projections
J. Theor. Biol. 36, 105-117

Glover GH and Sharp JC 1977 Reconstruction of ultrasound propogation speed distributions in soft tissue: time of flight tomography
IEEE Trans. Sonics & Ultrason. 24, 229-334

Glover GH 1977 Computerised time-of-flight ultrasonic tomography for breast examination
Ultrasound Med. Biol. 3, 117-127

Gordon R, Bender R and Herman GT 1970 Algebraic reconstruction techniques (ART) for three-dimensional electron microscopy and X-ray photography
J. Theor. Biol. 29, 471-481

Gordon R and Herman GT 1974 Three-dimensional reconstruction from projections: A review of algorithms
Int. Rev. Cytol. 38, 111-151

Greenleaf JF, Johnson SA, Lee SL, Herman GT and Wood EH 1974 Algebraic reconstruction of spatial distributions of acoustic absorption with tissues from their two-dimensional acoustic projections
Acoustical Holography 5, 591-603

Greenleaf JF, Johnson SA, Samayoa, WF and Duck FA 1975 Algebraic reconstruction of spatial distributions of acoustic velocities in tissue from their time-of-flight profiles
Acoustical Holography 6, 71-90

Greenleaf JF, Johnson SA, Samayoa WF and Hansen CR 1977 Refractive index by reconstruction: use to improve compound B-scan resolution
Acoustical Holography 7, 263-273

Greenleaf JF, Johnson SA and Lent AH 1978 Measurement of spatial distribution of refractive index in tissues by ultrasonic computer assisted tomography
Ultrasound Med. Biol. 3, 327-339

Greenleaf JF, Johnson SA, Bahn RC, Rajagopalan B and Kenue S 1979 Introduction to computed ultrasound tomography
in Computer Aided Tomography and Ultrasonics in Medicine (ed Raviv et al) pp 151-164 (North-Holland Publishing Co.)

Greenleaf JF, Surender KK, Rajagopalan B, Bahn RC and Johnson SA 1980 Breast imaging by ultrasonic computer-assisted tomography
Acoustical Imaging 8, 599-614

Greenleaf JF and Bahn RC 1981 Clinical imaging with transmission ultrasonic computerised tomography
IEEE Trans. Biomed. Eng. 28(2), 177-185

Greenleaf JF, Thomas PJ and Rajagopalan B 1981 Effects of diffraction on ultrasonic computer-assisted tomography
Acoustical Imaging 11, 351-362

Herman GT and Rowland S 1973 Three methods for reconstructing objects from X-rays: A comparative study
Comput. Graphics Image Process. 2,, 151-178

Herment A, Guglielmi JP, Peronneau P and Dumee Ph 1989a High-resolution, reflection mode tomographic imaging. Part I : Principles and methods
Ultrasonic Imaging 11, 1-21

Herment A, Guglielmi JP, Peronneau P and Dumee Ph 1989b High-resolution, reflection mode tomographic imaging. Part II : Application to echography
Ultrasonic Imaging 11, 22-41

Hill CR, Bamber JC, Crawford DC, Lowe HJ and Webb S 1991 What might echography learn from image science?
Ultrasound Med. Biol. 17(6), 559-575

Hiller D and Ermert H 1980 Tomographic reconstruction of B-scan images
Acoustical Imaging 10, 347-364

Hiller D and Ermert H 1982 Ultrasound computerised tomography using transmission and reflection mode: application to medical diagnosis
Acoustical Imaging 12, 553-564

Hiller D and Ermert H 1984 System analysis of ultrasound reflection mode computerised tomography
IEEE Trans. Sonics & Ultrason. 31(4), 240-250

Hirama M, Ikedo O and Sato T 1982 Adaptive ultrasonic array imaging system through an inhomogeneous layer
J. Acoust. Soc. Amer. 71, 100-109

Jellins J and Kossoff G 1973 Velocity compensation in water-coupled breast echography
Ultrasonics 11, 223-226

Johnson SA, Greenleaf JF, Samayoa WF, Duck FA and Sjostrand JD 1975 Reconstruction of three-dimensional velocity fields and other parameters by acoustic ray tracing
1975 Ultrasonic Symposium Proceedings, IEEE Cat. No. 75, CHP994-1SU

Johnson SA, Greenleaf JF, Tunaka M, Rajagopolan, R and Bahn RC 1977 Reflection and transmission techniques for high resolution quantitative synthesis of ultrasound parameter images
IEEE Ultrasonic Symposium Proceedings, IEEE Cat. No. 77 CH1264-1SU

Johnson SA, Greenleaf JF, Rajagopalan B and Tanaka M 1978 Algebraic and analytic inversion of acoustic data from partially or fully enclosing apertures
Acoustical Imaging 8, 577-598

Jones HW and Meng JS 1988 Algorithm comparison and parameter consideration in tof tomography
Acoustical Imaging 17, 639-646

Kim JH, Park SB and Johnson SA 1984 Tomographic imaging of ultrasonic reflectivity with correction for acoustic speed variations
Ultrasonic Imaging 6, 304-312

Klepper JR, Brandenburger GH, Mimbs, JW, Sobel BE and Miller JG 1981 Application of phase-insensitive detection and frequency-dependent measurements to computed ultrasonic attenuation tomography
IEEE Trans. Biomed. Eng. 28(2), 186-200

Kondo M, Takamizawa K, Hirama M, Okazaki K, Iinuma K and Takehara Y 1990 An evaluation of an in-vivo local sound speed estimation technique by the crossed beam method
Ultrasound Med. Biol. 16(1), 65-72

Kuhl DE and Edwards RQ 1963 Image separation radioisotope scanning.
Radiology 80(4), 653-662

Lopez H, Loew MH, Butler PF, Hill MC and Allman RM 1990 A clinical evaluation of contrast-detail analysis for ultrasound images
Med. Phys. 17(1), 48-57

Maderlechner G, Hundt E, Kronmuller E and Trautenberg E 1980 Experimental results of computerised ultrasound echo tomography
Acoustical Imaging 10, 415-425

Madsen EL, Zagzebski JA and Banjavic RA 1978 Tissue mimicking materials for ultrasound phantoms
Med. Phys. 5, 391-394

Martin K 1986 Portable equipment and techniques for measurement of ultrasonic power and intensity
In Physics in Medical Ultrasound, IPSM Report No. 47 (ed J A Evans), pp 20-29

McKinnon GC and Bates RHT 1980 A limitation of ultrasonic transmission tomography
Ultrasonic Imaging 2, 291-301

Miller JG, Klepper JR, Brandenburger GH, Busse LJ, O'Donnell M and Mimbs JW 1979
Reconstructive tomography based on ultrasonic attenuation
in Computer Aided Tomography and Ultrasonics in Medicine (ed Raviv et al) pp 151-164 (North-Holland Publishing Co.)

Morse PM and Ingard KU 1968 Theoretical Acoustics
McGraw-Hill Book Company, New York

Mueller RK, Kaveh M and Iverson RD 1978 A new approach to acoustic tomography using diffraction techniques
Acoustical Imaging 8, 615-628

Mueller RK, Kaveh M and Wade G 1979 Reconstructive tomography and applications to ultrasonics
Proceedings of the IEEE, 67(4), 567-587

Mueller RK 1980 Diffraction tomography I: The wave equation
Ultrasonic Imaging 2, 213-222

Muller RA and Buffington A 1974 Real-time correction of atmospherically degraded telescope images through image sharpening
J. Opt. Soc. Amer. 64(9), 1200-1209

Norton SJ and Linzer M 1979 Ultrasonic reflectivity tomography: reconstruction with circular transducer arrays
Ultrasonic Imaging 1, 154-184

Norton SJ and Linzer M 1981 Ultrasonic reflectivity imaging in three dimensions: exact inverse scattering solutions for plane, cylindrical and spherical apertures
IEEE Trans. Biomed. Eng. 28(2), 202-220

Norton SJ and Linzer M 1982 Correcting for ray refraction in velocity and attenuation tomography: a perturbation approach
Ultrasonic Imaging 4, 201-233

Norton SJ 1983 Generation of separate density and compressibility images in tissue
Ultrasonic Imaging 5, 240-252 (1983)

O'Donnell M 1982 Phase-insensitive pulse-echo imaging
Ultrasonic Imaging 4, 321-335

Ophir J 1986 Estimation of the speed of ultrasound propagation in biological tissues: A beam-tracking method
IEEE Trans. Ultrason. Ferro. Freq. 33(4), 359-368

Ramachandran GN and Lakshminarayanan AV 1971 Three-dimensional reconstructions from radiographs and electron micrographs: Application of convolutions instead of Fourier Transforms
Proc. Nat. Acad. Sci. USA, 68(9), 2236-2240

Robinson DE, Chen F and Wilson LS 1982 Measurement of velocity of propagation from ultrasonic pulse-echo data
Ultrasound Med. Biol. 8(4), 413-420

Robinson BS and Greenleaf JF 1986 The scattering of ultrasound by cylinders: Implications for diffraction tomography
J. Acoust. Soc. Am. 80(1), 40-49

Robinson BS and Greenleaf JF 1989 An experimental study of diffraction tomography under the Born approximation
Acoustical Imaging 18, 392-400

Roehrlein G and Ermert H 1985 Limited angle reflection mode computerised tomography
Acoustical Imaging 14, 413-424

Roehrlein G and Ermert H 1986 Speckle in ultrasound computerised reflection mode tomography
Acoustical Imaging 15, 341-357

Rosenfeld A and Kak AC 1976 Digital Picture Processing
Academic Press, New York

Rouseff D, Tsang L and Porter RP 1988 Diffraction tomography by a method of image projections
Ultrasonic Imaging 10, 204-219

Scherzinger AL, Belgam RA, Carson PL, Meyer CR, Sutherland JV, Bookstein FL and Silver TM 1989 Assessment of ultrasonic computed tomography in symptomatic breast patients by discriminant analysis
Ultrasound in Med. Biol. 15(1), 21-28

Schomberg H 1978 An improved approach to reconstructive ultrasound tomography
J. Phys. D: Appl. Phys. 11, 181-185

Schreiman JS, Gisvold JJ, Greenleaf JF and Bahn RC 1984 Ultrasound transmission computed tomography of the breast
Radiology 150, 523-530

Shepp LA and Logan BF 1974 The Fourier reconstruction of a head section
IEEE Trans. Nucl. Sci. NS-21, 21-43

Smith AM, Goldberg M and Liu ESK 1980 Numerical ray tracing in media involving continuous and discrete refractive boundaries
Ultrasonic Imaging 2, 291-301

Smith SW and Lopez H 1981 A contrast-detail analysis of diagnostic ultrasound imaging
Med. Phys. 9(1), 4-12

Sponheim N and Johansen I 1991 Experimental results in ultrasonic tomography using a filtered backpropagation algorithm
Ultrasonic Imaging 13, 56-70

Vezzetti DJ and Aks SO 1979 Reconstructions from scattering data: analysis and improvements of the inverse Born approximation
Ultrasonic Imaging 1, 333-345

Vezzetti DJ and Aks SO 1980 Ultrasonic scattering theory II: Scattering from composites
Ultrasonic Imaging 2, 195-212

Wade G, Elliot S, Khogeer I, Flesher G, Eisler J, Mensa D, Ramesh NS and Heidbreder G 1978
Acoustic echo computer tomography
Acoustical Imaging 8, 565-576

Wade G 1979 A survey of techniques for ultrasonic tomography
in Computer Aided Tomography and Ultrasonics in Medicine, Ed. Raviv et al, pp 165-215 (North Holland Publishing Company)

Whittingham TA 1991 Resolution and information limitations from transducer arrays
Phys. Med. Biol. 36(11), 1503-1514

Witten A, Tuggle J and Waag RC 1988 A practical approach to ultrasonic imaging using diffraction tomography
J. Acoust. Soc. Am. 83(4), 1645-1652

Zhao D and Trahey GE 1992 A statistical analysis of phase aberration correction using image quality factors in coherent imaging systems
IEEE Trans. Med. Imag. 11(3), 446-452

9 Appendices

I: The Wiener Inverse Filter

For a linear imaging system the relationship between the image s′(x,y) and the original object s(x,y) can be given by

$$s'(x,y) \quad = \quad s(x,y) \; * \; h(x,y) \; + \; n(x,y)$$

where h(x,y) is the system point spread function and n(x,y) is the noise generated in the image (from whatever source). The equivalent expression in the spatial frequency domain is

$$S'(X,Y) \quad = \quad S(X,Y) \, . \, H(X,Y) \; + \; N(X,Y)$$

In order to generate a faithful (ie unblurred) image of the original object, it is necessary to process the image with a filter derived by inverting this equation. In the case of a noise-free image where n(x,y) (and N(X,Y)) is zero this filter takes the simple form

$$F(X,Y) \quad = \quad \frac{S'(X,Y)}{H(X,Y)}$$

Hence, provided that H(X,Y) is known and that it has no zeros, the original object can be restored from the blurred image by multiplying S′(X,Y) by F(X,Y), or equivalently by convolving s′(x,y) with the filter's Fourier Transform, f(x,y).

In almost any real image some noise will be present, and its amplitude will typically fall-off less quickly in the frequency domain than will the signal in S′(X,Y) determined by the OTF, H(X,Y). Hence this filter runs into problems at higher frequencies when H(X,Y) becomes small, because F(X,Y) becomes large leading to amplification of high frequency noise.

A filter which overcomes these limitations is the well known Wiener filter (see e.g. Rosenfeld and Kak, 1976). This filter seeks the least-squares estimate of S′(X,Y), and allows F(X,Y) to fall smoothly to zero for spatial frequencies where H(X,Y) is not significantly above the noise level. It is defined as

$$F(X,Y) \quad = \quad \frac{H^{*}(X,Y)}{|H(X,Y)|^{2} \, + \, \Phi(X,Y)}$$

where * denotes a complex conjugate and Φ is a measure of the noise-to-signal ratio (explicitly N^2/S^2).

Although it may occasionally be possible to measure $\Phi(X,Y)$, this has not been done in these studies. In any case, it is usually adequate to represent Φ by a single constant value, say K, in other words assume that the signal and noise spectra are 'white',

$$ie \quad F(X,Y) = \frac{H^{*}(X,Y)}{|H(X,Y)|^{2} + K}$$

The value of K can be varied to achieve the best compromise between maximum frequency content in the image (ie detail) and the level of noise in the image. For reflection UCT it has been found that the best results are obtained for values of K between 0.001 and 0.01. Note that when K is zero (ie no noise) the Wiener filter reduces to the simple inverse filter.

II: The Production of Phantoms

Material requirements

To adequately compare the image quality of B-scanning, reflection UCT and transmission UCT, phantoms were required which had predictable bulk acoustic speed, attenuation and scattering properties that were closely equivalent to those found in soft tissues. A predictable internal and external structure was also desirable.

Gelatine based phantoms: Various materials for mimicking soft tissue (called tissue mimicking TM or tissue equivalent TE materials) have been proposed over the years. The most commonly used material has probably been a gelatine and distilled water base with variable quantities of graphite powder added to provide scattering (Madsen et al 1978). Varying quantities of alcohol may also added to modify the acoustic speed of the material from approx 1500 m/s (no alcohol) to approx 1600 m/s (20% alcohol). To make the material, water is heated to near boiling point and gelatine added and thoroughly melted. Graphite powder and alcohol are then added as the material cools but before it starts to set.

Although phantoms for this project were initially made with gelatine, these phantoms had a tendency to rot over a period of weeks and when higher quantities of alcohol were added they tended to be rather soft.

Agar based phantoms: Phantoms which use agar instead of gelatine (Burlew et al, 1980) as the base materials have advantages because (1) agar contains no nitrogen and hence is less prone to bacterial invasion, and (2) the phantoms produced seem to be inherently stiffer than gelatine based ones. Hence all of the results from TEM phantoms presented in this thesis are from agar based phantoms.

Structural requirements

The TEM phantoms had to meet the following requirements for UCT imaging:-

(a) They needed to be submergible in water.
(b) They had to be accessible from 360°.
(c) They had to be relatively long lasting (ie useable for a few months).

In addition it was found that the phantom material could not be left in direct contact with water, because this caused leeching of the alcohol out of phantom. Also the material could not be exposed to air for long periods because it tended to dry out. Hence it was decided to make the phantoms inside air-tight polythene bags. The polythene was thin enough to not significantly attenuate the ultrasound entering the phantom.

A mould in which to make phantom was also needed to give it some convenient external shape. Accordingly plastic jars of diameter 9.2 cm were used. These were first coated with grease before being lined with a polythene bag. The molten agar was then poured in and allowed to set. Once set, a nylon cap was placed on top of the phantom, within the polythene bag, into which was screwed a plastic rod for securing the phantom in a fixed position for scanning. The open top of the polythene bag was then wrapped securely around the rod, and the bag with agar material inside carefully removed from the plastic jar.

Phantom inserts (ie for introducing regions of different acoustic speed or attenuation) where made by inserting greased and heated metal rods of various sizes into the previously set phantom. After a few minutes, ie long enough for the phantom to partially re-set around the rods, the rods were carefully removed. The material for the insert was then poured into the holes. If the insert material was another TE material, this was allowed to cool such that it was just about to set before being poured into the holes.